

© 2006

MATTHEW J. PANZNER

ALL RIGHTS RESERVED

SILVER N-HETEROCYCLIC CARBENES AND SUBSTITUTED
CYCLOTRIPHOSPHAZENES

A Dissertation

Presented to

The Graduate Faculty of The University of Akron

In Partial Fulfillment

of the Requirements for the Degree

Doctor of Philosophy

Matthew J. Panzner

December, 2006

SILVER N-HETEROCYCLIC CARBENES AND SUBSTITUTED
CYCLOTRIPHOSPHAZENES

Matthew J. Panzner

Dissertation

Approved:

Accepted:

Advisor
Dr. Wiley J. Youngs

Department Chair
Dr. Kim C. Calvo

Co-Advisor
Dr. Claire A. Tessier

Dean of the College
Dr. Ronald F. Levant

Committee Member
Dr. Christopher Ziegler

Dean of Graduate School
Dr. George R. Newkome

Committee Member
Dr. Peter Rinaldi

Date

Committee Member
Dr. Judit Puskas

ABSTRACT

It has been nearly four decades since the synthesis of the first transition metal complexes of N-Heterocyclic carbenes (NHCs) by Öfele and Wanzlick. During this time Arduengo isolated the first free NHC, numerous NHC transition metal complexes have been studied for their catalytic properties, and NHC metal complexes are currently being investigated for their use as potential pharmaceuticals. It is the medicinal applications of NHCs that will be discussed in first portion of this dissertation.

Chapter 1 provides a review of recent investigations and results of potential metal NHC pharmaceuticals. The discussion focuses on NHC complexes of silver, gold, and rhodium. In Chapter 2 the challenge of increasing silver NHC stability by ligand modification is discussed. Chapter 3 focuses on the syntheses of several macrocyclic imidazolium salts which serve as precursors for the formation of NHCs.

The second portion of this dissertation investigates the Lewis acid-base chemistry and nucleophilic substitution of phosphazenes. Cyclophosphazenes have been studied for well over a century and are of particular interest because of their ability to form high weight inorganic polymers via ring opening polymerization. Chapter 4 provides a background on cyclophosphazenes and their polymerization as well as a discussion of the Lewis acid chemistry of chlorophosphazene trimer. In Chapter 5 the nucleophilic substitution of $[\text{N}(\text{PCl}_2)_3]$ with imidazole is discussed.

DEDICATION

To my loving wife and best friend,

Kathleen Panzner

To my parents and brother,

Steve Panzner, Barbara Panzner, Steven Panzner

ACKNOWLEDGEMENTS

It seems nearly impossible to express the amount of gratitude that I have for so many who made this dissertation possible. First I would like to thank Professors Wiley J. Youngs and Claire A. Tessier for their guidance, humor and friendship. Their creativity and passion for chemistry will continue to serve as an ideal example for my own chemical endeavors.

I would like to thank the members of both the Youngs and Tessier groups: Semih Durmus, Doug Medvetz, Aysegul Kascatan-Nebioglu, Khadijah Hindi, Samittichai Seeyangnok, Tatiana Eliseeva and Sarah Walton. Their friendship helped to make graduate life more enjoyable. I would also like to thank Dr. Jered Garrison for all his help in teaching me X-ray crystallography.

I would especially like to thank my parents Steve and Barbara Panzner. They gave me love, encouragement, and taught me the value of hard work. I would also like to thank my brother Steven Panzner. It is a blessing to have such a good friend to share my successes with and to have someone to help me through hardships. I could not wish for a better family.

Finally I would like to thank my beautiful wife Kathleen Panzner. She has shown me the truest meaning of love. She has never ceased to encourage and support me and her patience has been instrumental in the completion of this dissertation.

TABLE OF CONTENTS

	Page
LIST OF TABLES	xi
LIST OF FIGURES	xii
LIST OF SCHEMES.....	xvi
LIST OF EQUATIONS	xvii
CHAPTER	
I. N-HETEROCYCLIC CARBENE METAL COMPLEXES: POTENTIAL USES AS PHARMACEUTICALS	1
1.1 Introduction.....	1
1.2 N-heterocyclic Carbenes.....	1
1.3 Silver NHC Complexes.....	3
1.3.1. Silver Antimicrobials.....	4
1.3.2. Synthesis of Silver NHC-Pincer Complexes	5
1.3.4. Synthesis of Silver NHC Complexes for Encapsulation in Electrospun Nanofibers.....	10
1.3.5. Antimicrobial Testing of Nanofiber Encapsulated Silver NHC complexes ...	13
1.3.6. Synthesis of Caffeine Based Silver NHC Complexes	18
1.3.7. Antimicrobial Studies of Methylated Caffeine Silver Acetate	19
1.4. Gold NHC Complexes	22
1.4.1. Rationale and Synthesis of Gold NHC Antimicrobials	24

1.4.2. Antimicrobial Testing of Gold NHC Complexes	26
1.4.3. Gold NHC Antitumor Complexes	28
1.4.4. Synthesis of and Testing of Gold NHC Antitumor Complexes.....	28
1.5. Rhodium NHC Model Complexes.....	30
1.5.1. Synthesis of Rhodium NHC Complexes.....	31
1.5.2. Ligand Modification for Targeting	33
1.6 Conclusions.....	36
II. SYNTHESIS OF STERICALLY SHIELDED AND ELECTRONICALLY STABILIZED SILVER N-HETEROCYCLIC CARBENE COMPLEXS.....	37
2.1 Introduction.....	37
2.2 Synthesis and Characterization of a Sterically Shielded Silver N-Heterocyclic Carbene Complex.....	38
2.3 Synthesis and Characterization of an Electronically Stabilized Silver N- Heterocyclic Carbene Complexes.....	51
2.4 Conclusion	643
2.5 Experimental Section.....	645
2.5.1 General Considerations.....	65
2.5.2 X-ray Structure Determination Details	65
2.5.3 Synthesis of 1,1'-methylene bis(imidazole) (C ₇ H ₈ N ₄).....	66
2.5.4 Synthesis of 1 [Br] ₂ (C ₂₉ H ₂₆ N ₄ Br ₂).....	66
2.5.5 Synthesis of 2 [PF ₆] (C ₅₈ H ₄₈ N ₈ Ag ₂ P ₂ F ₁₂).....	67
2.5.6 Synthesis of 1-hydroxyethyl-3,7-dimethylxanthine 3 (C ₉ H ₁₂ N ₄ O ₃).....	68
2.5.7 Synthesis of 4 [I] (C ₁₀ H ₁₅ N ₄ O ₃ I).....	69
2.5.8 Synthesis of silver complex 5 (C ₁₂ H ₁₇ N ₄ O ₅ Ag)	70

III. BISIMIDAZOLE BASED CYCLOPHANES	71
3.1 Introduction	71
3.2 Synthesis and Characterization of Bisimidazole Based Cyclophanes	73
3.3 Conclusion	82
3.4 Experimental Section	84
3.4.1 General Considerations	84
3.4.2 X-ray Structure Determination Details	84
3.4.3 Synthesis of 3 [PF ₆] ₂ (C ₂₁ H ₁₈ N ₆ P ₂ F ₁₂)	85
3.4.4 Synthesis of 5 [Br] ₄ (C ₁₈ H ₂₄ N ₈ Br ₄)	86
3.4.5 Synthesis of 6 [Br] ₄ (C ₂₀ H ₂₈ N ₈ Br ₄) and 6 [PF ₆] ₄ (C ₂₀ H ₂₈ N ₈ P ₄ F ₂₄)	86
IV. CYCLO AND POLYPHOSPHAZENES	88
4.1 Introduction	88
4.2 Polyphosphazenes	89
4.2.1 Polymerization of Cyclophosphazenes	90
4.3 Bonding Structure of Cyclophosphazenes	92
4.4 Lewis Acid-Base Chemistry of [NPCl ₂] ₃	95
4.5 Experimental Section	102
4.5.1 General Considerations	102
4.5.2 X-ray Structure Determination Details	102
4.5.3 X-ray Details for [NPCl ₂] ₃ · AlCl ₃	103
4.5.4 X-ray Details for [NPCl ₂] ₃ · GaCl ₃	103
4.5.5 X-ray Details for H[NPCl ₂] ₃ ⁺ AlBr ₄ ⁻	104

4.5.6 X-ray Details for $\text{H}[\text{NPCl}_2]_3^+\text{SbCl}_6^-$	104
V. AN IMDAZOLE SUBSTITUTED CYCLOTRIPHOSHAZENE.....	105
5.1 Introduction.....	105
5.2 Synthesis of Hexakis(imidazolyl)cyclotriphosphazene	106
5.2.1 Initial Synthetic Approaches.....	106
5.2.2 Improved Synthetic Procedure.....	111
5.3 Experimental Section	116
5.3.1 General Considerations.....	116
5.3.2 X-ray Structure Determination Details	116
5.3.3 Synthesis of 2 $[\text{NP}(\text{C}_3\text{H}_3\text{N}_2)_2]_3$	117
BIBLIOGRAPHY	118
APPENDICES	126
APPENDIX A: SUPPLEMENTTARY MATERIAL FOR THE X-RAY CRYSTAL STRUCTURE OF $\text{C}_{29}\text{H}_{26}\text{N}_4\text{P}_2\text{F}_{12}$ (II- 1 $[\text{PF}_6]_2$)	127
APPENDIX B: SUPPLEMENTTARY MATERIAL FOR THE X-RAY CRYSTAL STRUCTURE OF $\text{C}_{58}\text{H}_{48}\text{N}_8\text{Ag}_2\text{P}_2\text{F}_{12}$ (II- 2 $[\text{PF}_6]$)	133
APPENDIX C: SUPPLEMENTTARY MATERIAL FOR THE X-RAY CRYSTAL STRUCTURE OF $\text{C}_{10}\text{H}_{15}\text{N}_4\text{O}_3\text{I}$ (II- 4 $[\text{I}]$).....	149
APPENDIX D: SUPPLEMENTTARY MATERIAL FOR THE X-RAY CRYSTAL STRUCTURE OF $\text{C}_{12}\text{H}_{17}\text{N}_4\text{O}_5\text{Ag}$ (II- 5)	154
APPENDIX E: SUPPLEMENTTARY MATERIAL FOR THE X-RAY CRYSTAL STRUCTURE O $\text{FC}_{21}\text{H}_{18}\text{N}_6\text{2}(\text{P}_1\text{F}_6) \cdot 4(\text{C}_2\text{H}_6\text{SO})$ (III- 3 $[\text{PF}_6]_2$)	161
APPENDIX F: SUPPLEMENTTARY MATERIAL FOR THE X-RAY CRYSTAL STRUCTURE OF $\text{C}_{18}\text{H}_{24}\text{N}_8\text{Br}_4$ (III- 5 $[\text{Br}]_4$).....	172
APPENDIX G: SUPPLEMENTTARY MATERIAL FOR THE X-RAY CRYSTAL STRUCTURE OF $\text{C}_{20}\text{H}_{28}\text{N}_8\text{P}_4\text{F}_{24}$ (III- 6 $[\text{PF}_6]_4$).....	177

APPENDIX H: SUPPLEMENTTARY MATERIAL FOR THE X-RAY CRYSTAL STRUCTURE OF $[\text{NPCl}_2]_3 \cdot \text{AlCl}_3$ (IV)	186
APPENDIX I: SUPPLEMENTTARY MATERIAL FOR THE X-RAY CRYSTAL STRUCTURE OF $[\text{NPCl}_2]_3 \cdot \text{GaCl}_3$ (IV).....	192
APPENDIX J: SUPPLEMENTTARY MATERIAL FOR THE X-RAY CRYSTAL STRUCTURE OF $\text{H}[\text{NPCl}_2]_3^+ \text{AlBr}_4^-$ (IV)	199
APPENDIX K: SUPPLEMENTTARY MATERIAL FOR THE X-RAY CRYSTAL STRUCTURE OF $\text{H}[\text{NPCl}_2]_3^+ \text{SbCl}_6^-$ (IV)	204
APPENDIX L: SUPPLEMENTTARY MATERIAL FOR THE X-RAY CRYSTAL STRUCTURE OF $[\text{NP}(\text{C}_3\text{H}_3\text{N}_2)_2]_3$ (V-2).....	209
APPENDIX M: ABBREVIATIONS AND ACCRONYMS	218

LIST OF TABLES

Table	Page
1-1 Efficacy of Silver Complexes for Inhibiting Bacterial Growth	9
1-2 MIC Results for Silver Complexes (AgCl removed).....	11
1-3 MIC results for AgNO ₃ and Silver NHC Complex 12	15
1-4 MIC results for silver complex 17	21
1-5 MIC values for tested Au NHC compounds	27
4-1 Comparison of bond lengths of neutral Lewis acid adducts with [NPCl ₂] ₃	98
4-2 Comparison of bond lengths of Brønsted acid adducts with [NPCl ₂] ₃	100

LIST OF FIGURES

Figure	Page
1-1 Resonance structures for NHCs.....	2
1-2 Orbital diagrams for Fischer (VI) and N-heterocyclic carbene (VII).	3
1-3 Silver sulphadiazine.....	4
1-4 Crystal structure of polymeric 6a	6
1-5 Thermal ellipsoid plot of trinuclear silver complex 10 with the pyridine carbon atoms removed.....	7
1-6 Kirby-Bauer diffusion method compared on <i>E-coli</i> for 6a compared to AgNO ₃	9
1-7 Agar plate showing N (AgNO ₃) compared to E (6a) from high (1) to low (5) concentration.....	11
1-8. a) As-spun fiber of 12 and Tecophilic. b) Formation of silver particles after exposure to water.....	14
1-9 Modified Kirby Bauer test results. a. 25% 12 /Tecophilic, b. Tecophilic, c. 75% 12 /Tecophilic.	16
1-10 Zones of inhibition of 15b encapsulated fibers. a) 33% 15b /Tecophilic.	17
1-11 TEM image of protruding silver particles from the surface of an as-spun fiber.....	17
1-12 FE-SEM image of encapsulated 15b . XEDS spectrum shows the composition of the aggregated particles as Ag and Br.....	18
1-13 a) Synthetic route to the formation of methylated caffeine silver acetate NHC. b) Thermal ellipsoid plot of the silver acetate NHC complex 17	19
1-14 A TEM of untreated <i>B. dolosa</i> . B TEM of <i>B. dolosa</i> treated with silver complex 17	22

1-15 Gold complexes with AuSP and AuNP cores studied for antimicrobial effectiveness.....	24
1-16 Gold NHC MMP agents.	29
1-17 Thermal ellipsoid plots of rhodium NHC-pincer complexes 39 and 40b	32
1-18 Targeted radiopharmaceutical assembly.	34
2-1 The ¹ H NMR spectrum of 1,1'-methylene bis(imidazole) in D ₂ O.....	40
2-2 ¹ H NMR spectrum of 1 [Br] ₂ in d ₆ -DMSO.....	41
2-3 ¹ H NMR spectrum of 1 [Br] ₂ in d ₆ -DMSO. Expansion of aromatic region.	42
2-4 Thermal ellipsoid plot of the dicationic portion of 1 [PF ₆] ₂ with thermal ellipsoids drawn at 50% probability.	43
2-5 Thermal ellipsoid plot depicting the hydrogen bonding of 1 [PF ₆] ₂ with thermal ellipsoids shown at 50% probability.....	44
2-6 ¹ H NMR spectrum of 2 [PF ₆] ₂ in d ₃ -acetonitrile.....	46
2-7 ¹ H NMR spectrum of 2 [PF ₆] ₂ in d ₃ -acetonitrile. Expansion of aromatic region.	47
2-8 Thermal ellipsoid plots of 2 [PF ₆] with hydrogen atoms removed for clarity. Thermal ellipsoids shown at 50% probability. a) top view, b) side view.....	49
2-9 Space filling model of depicting the shielding of the silver core of complex 2 [PF ₆].	50
2-10 Structure and numbering scheme for theobromine.	51
2-11 ¹ H NMR spectrum of 3 in D ₂ O.....	53
2-12 ¹ H NMR spectrum of 4 [I] in D ₂ O.....	54
2-13 Thermal ellipsoid plot of the cationic portion of 4 [I]. Thermal ellipsoids shown at 50% probability.....	55
2-14 Thermal ellipsoid plot depicting the hydrogen bonding of 4 [I]. Thermal ellipsoids shown at 50% probability.	56
2-15 Stack plot of the ¹ H NMR spectra of silver complex 5 in D ₂ O. 1) 9 h 2) 12 h 3) 1.7 d 4) 4 d 5) 7 d.....	58

2-16	Stack plot of ^{13}C NMR spectra of silver complex 5 in D_2O . 1) 9h 2) 7 d.	59
2-17	^1H NMR spectrum of the decomposition product of 5 in D_2O	61
2-18	Proposed structures of the decomposition products of 5 based upon EA-MS.	62
2-19	Thermal ellipsoid plot of silver complex 5 with thermal ellipsoids shown at 50% probability.	62
2-20	Thermal ellipsoid plot of complex 5 depicting the intermolecular Ag-Ag interaction. Thermal ellipsoids shown at 50% probability.	63
3-1	Porphyrim and porphyrim like molecules.	72
3-2	^1H NMR spectrum of $\mathbf{3}[\text{PF}_6]_2$ in $d_3\text{-CD}_3\text{CN}$	75
3-3	^1H NMR spectrum of $\mathbf{3}[\text{PF}_6]_2$ in $d_3\text{-CD}_3\text{CN}$. Expansion of aromatic region.	76
3-4	Thermal ellipsoid plot of the dicationic portion of $\mathbf{3}[\text{PF}_6]_2$ with hydrogen atoms removed for clarity. Thermal ellipsoids shown at 50% probability.	77
3-5	Thermal ellipsoid plot of the tetracationic portion of $\mathbf{5}[\text{Br}]_4$ with hydrogen atoms omitted for clarity. Thermal ellipsoids shown at 50% probability.	78
3-6	Thermal ellipsoid plot depicting the hydrogen bonding of $\mathbf{5}[\text{Br}]_4$. Thermal ellipsoids shown at 50% probability.	79
3-7	^1H NMR ^1H NMR spectrum of $\mathbf{6}[\text{Br}]_4$ in D_2O . Unlabeled peaks correspond to residual butyl alcohol and D_2O	80
3-8	Thermal ellipsoid plot of the tetracationic portion of $\mathbf{6}[\text{PF}_6]_4$ with hydrogen atoms omitted for clarity. Thermal ellipsoids shown at 50% probability.	81
3-9	Thermal ellipsoid plot depicting the hydrogen bonding of $\mathbf{6}[\text{PF}_6]_4$. Thermal ellipsoids shown at 30% probability.	82
4-1	Illustration of <i>cis-trans</i> planar conformation of polyphosphazenes.	89
4-2	Pairing of electrons in $[\text{NPR}_2]_3$. ¹⁰⁹	93
4-3	Depiction of the orbital mismatch in the $d\pi\text{-}p\pi$ bonding structure of $[\text{NPR}_2]_3$	93
4-4	“Island” bonding in cyclophosphazenes.	94

4-5	Zwitterionic structure of $[\text{NPR}_2]_3$. ¹⁰⁹	94
4-6	Proposed structures for the reaction of Lewis acids with $[\text{NPCl}_2]_3$. ¹¹⁴	95
4-7	Thermal ellipsoid plot of the neutral adduct of AlCl_3 with $[\text{NPCl}_2]_3$	97
4-8	Thermal ellipsoid plot of the neutral adduct of GaCl_3 with $[\text{NPCl}_2]_3$	97
4-9	Thermal ellipsoid plot of $[\text{NPCl}_2]_3\text{H}^+ \text{AlBr}_4^-$ adduct.	99
4-10	Thermal ellipsoid plot of $[\text{NPCl}_2]_3\text{H}^+ \text{SbCl}_6^-$ adduct.	100
5-1	^{31}P NMR spectrum of 3 in D_2O	107
5-2	Penta substituted product of 1	108
5-3	^{31}P spectrum of a mixture of 2 and 3 in D_2O	109
5-4	^{31}P NMR spectrum of phosphazene oligomers in d_6 -DMSO.	110
5-5	^{31}P NMR spectrum of 2 and 3 in d_6 -DMSO. Isolated from the reaction of six equivalents of potassium imidazole with 1	112
5-6	^{31}P NMR spectrum of 2 in d_6 -DMSO.	113
5-7	Top: thermal ellipsoid plot of 2 with hydrogen atoms removed for clarity and thermal ellipsoids shown at 50 % probability. Bottom: side view of the ring distortion of 2 with only the bonding nitrogen atoms of the imidazole rings shown. Thermal ellipsoids shown at 50 % probability.	115

LIST OF SCHEMES

Scheme	Page
1-1 General synthesis for pyridine based NHC-pincer complexes.	5
1-2 Synthetic route for the formation of trinuclear silver NHC-pincer complex.....	7
1-3 Synthetic route for the formation silver NHC Cyclophane <i>gem</i> -Diol.	12
1-4 Synthetic route for the formation of tripodal silver NHC complexes.....	13
1-5 Synthesis of Au(I)-NHCs from a) olefins, b) free NHCs, c) Ag(I)-NHCs via transmetallation, d) Group 6 carbonyl complexes.	23
1-6 Synthetic route to Au-NHCs for antimicrobial testing.	26
1-7 Synthetic route for the formation rhodium NHC-pincer complexes.	32
1-8 General synthesis for the formation of targeted pyridine based NHC-pincer complexes.	35
3-1 Synthesis of imidazolium cyclophanes 3[PF ₆] ₂	73
4-1 Ionization mechanism for ROP of [NPCl ₂] ₃	92
4-2 Protonation mechanism for ROP of [NPCl ₂] ₃	92
4-3 Rationale for the formation of protonated [NPCl ₂] ₃ Lewis acid adducts.....	99
5-1 Reaction of six equivalents of potassium imidazole with 1.....	111

LIST OF EQUATIONS

Equation	Page
1-1 Synthesis of a bisimidazole precursor for targeting.....	36
2-1 Synthesis of 1,1'-methylene bis(imidazole).....	38
2-2 Synthesis of the sterically shielded imidazolium salt 1[Br] ₂	39
2-3 Synthesis of the sterically shielded silver NHC complex 2[PF ₆] ₂	45
2-4 Synthesis of 1-hydroxyethyl-3,7-dimethylxanthine 3.....	52
2-5 Synthesis of xanthinium salt 4[I].....	52
2-6 Synthesis of silver NHC 5.....	56
3-1 Synthesis of tetraimidazolium salt 5[Br] ₄	74
3-2 Synthesis of tetraimidazolium salt 6[Br] ₄	81
4-1 Synthesis of hexachlorocyclotriphosphazene, [PCl ₂ N] ₃	88
4-2 Synthesis of chloropolyphosphazene from [PCl ₂ N] ₃ . ¹⁰⁶	90
4-3 Synthesis of neutral [NPCl ₂] ₃ Lewis acid adducts. ¹¹⁴	96
5-1 Hydrolysis of medicinally substituted phosphazene.....	105
5-2 Synthesis of Hexakis(imidazolyl)cyclotriphosphazene.....	106

CHAPTER I
N-HETEROCYCLIC CARBENE METAL COMPLEXES:
POTENTIAL USES AS PHARMACEUTICALS

1.1 Introduction

The purpose of this chapter will be to review the present research of N-heterocyclic carbene (NHC) metal complexes currently being investigated for their potential uses as pharmaceuticals. In particular, the discussion will focus on NHC complexes of silver, gold, and rhodium. Silver and gold complexes will be explored for their antimicrobial efficacy, gold complexes for their anticancer properties, and rhodium complexes as models for ^{105}Rh based anticancer agents.

1.2 N-heterocyclic Carbenes

The past decade has been marked by a continually growing interest in the research of NHC metal complexes. Although the first transition metal complexes of NHCs were synthesized by Öfele¹ and Wanzlick² in 1968, it was Arduengo's discovery of the first isolable free NHC in 1991 that brought this area to the forefront of chemical research.³ NHCs have been used to bind nearly every transition metal, and have also been shown to complex a variety of main group and lanthanide metals.¹⁻¹⁷ Several reviews have been published on the subject, and NHCs and their metal complexes remain actively studied in the area in catalytic chemistry.⁷⁻¹³

NHCs are most typically obtained by the deprotonation of imidazolium salt precursors. Their enhanced stability is derived from the π donation of the lone pair electrons of the two adjacent nitrogen atoms into the empty p_z orbital of the carbene carbon. This synergistic effect gives rise to a stabilization energy of approximately 70 kcal/mol.⁸ An additional 25 kcal/mol of stabilization is gained from aromaticity. The various resonance forms of NHCs are illustrated in Figure 1-1. Resonance structures **II** and **III** illustrate the multiple bond character of the nitrogen to carbene carbon bond and are summarized by **IV**. The overall aromatic structure is depicted by **V**.

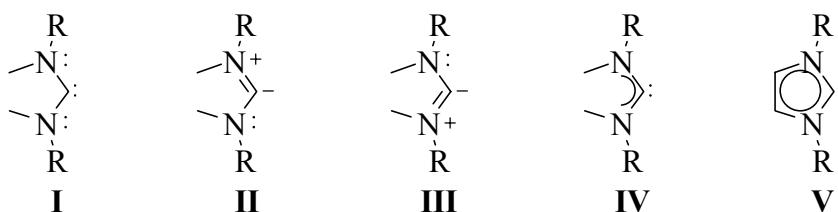


Figure 1-1. Resonance structures for NHCs.

NHCs bind to metals (**VII**) via strong σ -donation with π -back-donation contributing to a lesser extent. Some degree of π -back-donation, depending on the type of the metal, has been recently suggested by several theoretical and structural studies.¹⁴⁻²¹ In this way NHCs are very similar to more classically well known Fischer carbenes (**VI**), although the degree of π -back-donation of these carbenes is much greater, Figure 1-2.

The high stability of NHC metal complexes makes them very attractive for use as metal based therapeutic agents. This stability could prove extremely important, especially when using NHC ligands for therapeutic radiopharmaceuticals. One of the most frequent problems of potential radiopharmaceuticals is dissociation of the radioisotope from the chelating ligand due to poor kinetic stability.²² This results in an increased probability of

accumulating radioactive materials in healthy tissues injuring the patient or potentially causing fatal harm. NHCs bind tightly to metals and may avoid this major problem.

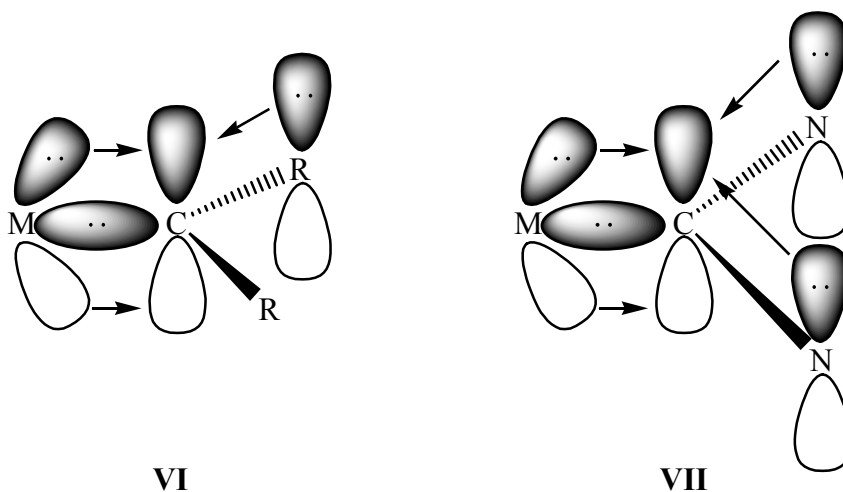


Figure 1-2. Orbital diagrams for Fischer (VI) and N-heterocyclic carbene (VII).

1.3 Silver NHC Complexes

The first characterized silver NHC was synthesized by the reaction of a free NHC with a silver salt.²³ It has since been shown that such complexes can be easily generated *in situ* from the reaction of an imidazolium salt with a silver base. Examples of such reactions are well documented using AgOAc, Ag₂O and Ag₂CO₃.²⁴⁻²⁶ The ability to make silver NHC complexes without first generating the free carbene is a major synthetic advantage over many other transition metals. This enables reactions to be carried out in aqueous solvents and avoids the need for inert atmospheres.

1.3.1. Silver Antimicrobials

The effective use of silver in various forms for its antimicrobial properties has been well known throughout history.²⁷ It was most likely first used to maintain water purity by the Greeks and Romans,^{28,29} a practice which is also employed by NASA.^{30,31} Silver nitrate was first employed in medicine prior to the 1800's. More recently, the application of 1% silver nitrate solution to newborns eyes was used as an effective treatment for the prevention of gonorrheal ophthalmia.³² In the 1960's silver sulphadiazine was developed, shown in Figure 1-3. Marketed as Silvadene® Cream 1%, this silver complex still remains one of the most successful and widely used antimicrobial treatments for burn wounds.

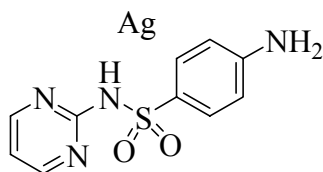


Figure 1-3. Silver sulphadiazine.³³

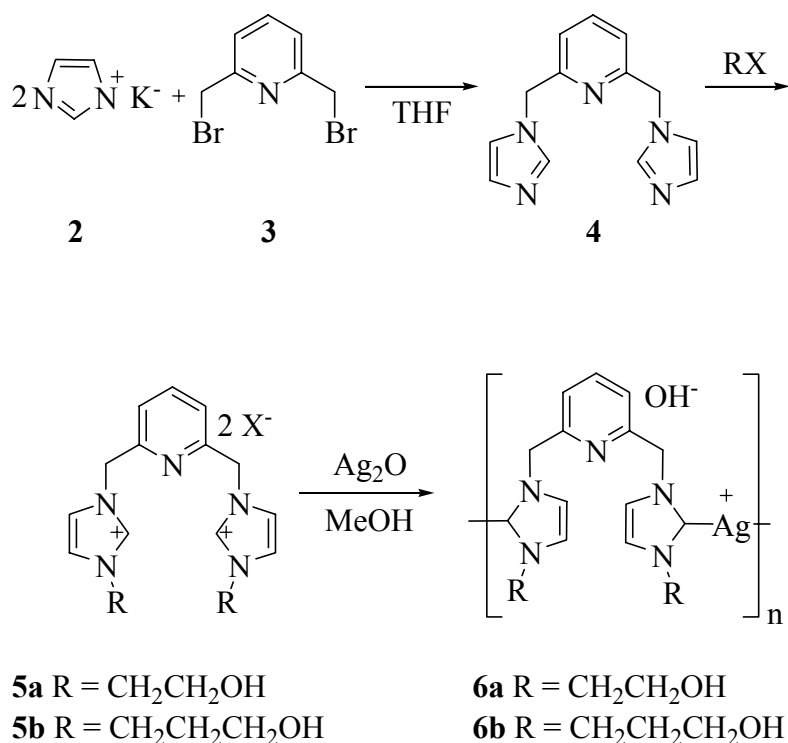
In studies strips of metallic silver have been shown to cause zones of inhibition on lawns of bacteria.³⁴ If the tarnish is removed from the surface of the strips no inhibition is observed. Molten silver cooled in the presence of air also shows activity in contrast to being cooled in an inert atmosphere which displays no antimicrobial activity.³⁴ These observations highlight the necessity of surface oxidization for efficacy, and that silver cations are responsible for the antimicrobial activity.³⁴

1.3.2. Synthesis of Silver NHC-Pincer Complexes

A variety of NHC-pincer precursors can be generated from imidazole and pyridine starting materials. A large selection of alkyl imidazoles is commercially available which makes them convenient reagents for one step synthesis of imidazolium salt precursors. Alternatively, precursors with one of the ring nitrogen atoms unsubstituted can also be prepared. This enables the synthesis of imidazolium salts functionalized with substituents currently unavailable commercially.

A general synthesis for NHC-pincer complexes is depicted in Scheme 1-1.

Precursor **4** can be synthesized by the reaction of two equivalents of potassium imidazole **2** with 2,6-bis(bromomethyl)pyridine **3** in dry THF.³⁵



Scheme 1-1. General synthesis for pyridine based NHC-pincer complexes.³⁶

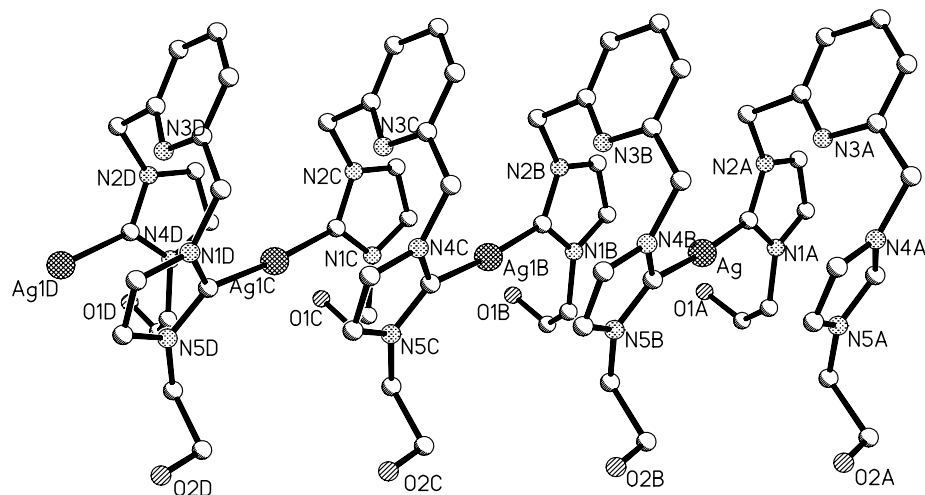
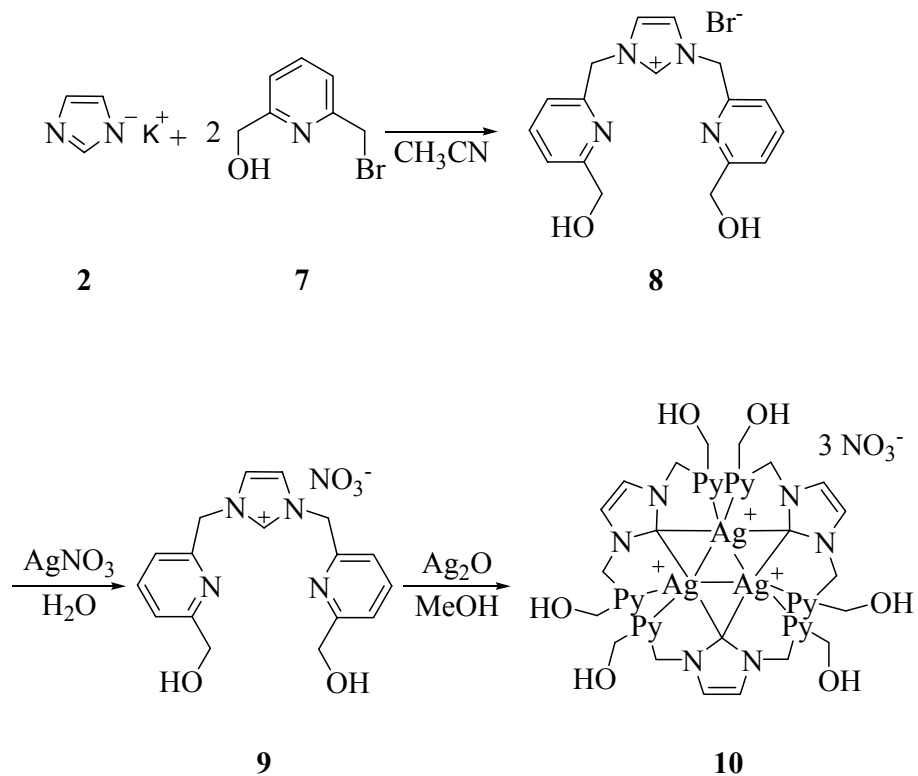


Figure 1-4. Crystal structure of polymeric **6a**.³⁶

The condensation of **4** with either 2-iodoethanol or 3-bromopropanol gives imidazolium salts **5a** and **5b** with corresponding halide anions.³⁶ The halide salts can be reacted with an equivalent of Ag_2O to afford polymeric biscarbenes **6a** and **6b**. The alcohol functional groups give these complexes exceptionally good water solubility. Compounds **6a** and **6b** decompose slowly, in water gradually releasing silver cations. The crystal structure of **6a** is given in Figure 1-4 with atoms shown isotropically.

NHC-pincer complexes containing only one NHC unit are also attainable as shown in Figure 1-6. The reaction of potassium imidazole **2** with two equivalents of (6-bromomethyl-pyridin-2-yl)-methanol **7** affords imidazolium precursor **8** as the bromide salt.³⁷ The nitrate salt **9** is readily generated by the addition of an equimolar amount of AgNO_3 to **8** in water. When nitrate salt **9** is combined with 0.6 equivalents of Ag_2O in methanol a trinuclear silver NHC-pincer complex **10** is formed. This complex gains stability not only from the NHC units but also from six coordinating pyridines. A thermal ellipsoid plot of **10**, with the pyridine carbons removed, is shown in Figure 1-5.



Scheme 1-2. Synthetic route for the formation of trinuclear silver NHC-pincer complex.³⁷

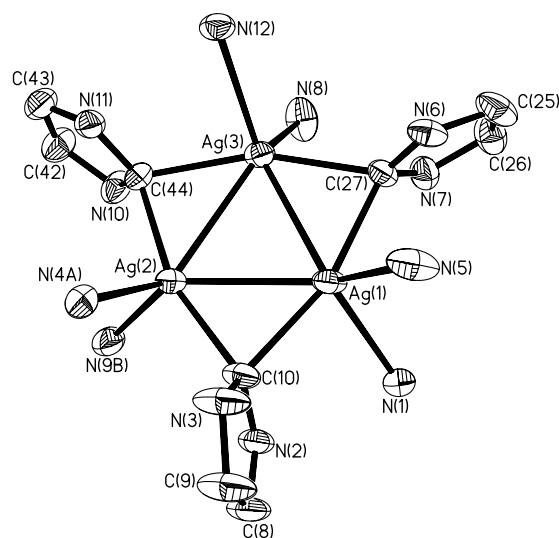


Figure 1-5. Thermal ellipsoid plot of trinuclear silver complex **10** with the pyridine carbon atoms removed.³⁷

1.3.3. Antimicrobial Activity of Silver NHC-Pincer Complexes

Silver NHC-pincer complexes **6a** and **6b** have been tested for their antimicrobial efficacy against several strains of bacteria.³⁶ Laboratory strains of *Escherichia coli*, *Staphylococcus aureus*, and *Pseudomonas aeruginosa* were chosen because of their common association with chronic wound infections. Both compounds were tested for their ability to inhibit growth of the organisms (results shown in Table 1-1) and for their minimum inhibitory concentrations (MIC) (results shown in Table 1-2). In all tests, silver nitrate was used for comparison and the imidazolium salt precursors were used as controls.

A constant volume of the bacteria was spread over a nutrient rich agar plate and a lawn of bacteria was established. Filter paper disks (6 mm) were bathed in 20 μ L of the silver complexes at known concentrations. The plates were incubated overnight with the filter disks, and the activity of the silver compounds was determined by measuring the diameter of the clear zone of growth inhibition around the disks, Figure 1-6. The zone of inhibition for the imidazolium salt precursors remained constant throughout the study. The 6 mm diameter observed during testing coincides with the diameter of the filter paper disks and shows that the ligands have no antimicrobial activity by themselves.

The MIC values were determined using the same three types of bacteria, however the MICs were based upon the amount of silver available instead of the concentration of silver ions.³⁸ Upon adding silver compounds to the growth medium (LB broth) AgCl



Figure 1-6. Kirby-Bauer diffusion method compared on *E-coli* for **6a** compared to AgNO_3 .³⁹

Table 1-1

Efficacy of Silver Complexes for Inhibiting Bacterial Growth³⁶

Tested Compds (w/v)	Ag ($\mu\text{g/mL}$) ^a	Diameter of the zone of inhibition (mm)		
		E. coli	S. aureus	P. aeruginosa
AgNO_3 (0.50%)	3176	11.38	10.88	11.00
6a (1.31%)	3130	11.50	11.00	12.00
6b (1.42%)	3195	11.58	10.67	10.25
6a (0.50%)	1195	10.13	10.00	11.13
6b (0.50%)	1125	10.00	9.00	12.00
5a (0.50%)		6.00	6.00	6.00
5b (0.50%)		6.00	6.00	6.00

a. The amount of silver $\mu\text{g/mL}$ for each complex was calculated as (molecular mass of Ag/formula weight of the compound) x weight %.

began to precipitate in all samples. The AgCl was removed and a dilution series of the Ag complexes in LB broth were prepared. Freshly grown organisms (20 μ L) were added daily. MIC values were determined by visual inspection of the solutions turbidity.²⁶

Both compounds **6a** and **6b** showed greatly enhanced activity over silver nitrate even at lower initial concentrations. This is most likely due to the added stability that the NHC-pincer ligand gives to the complexes against the formation of AgCl. The higher stability of these complexes was likely responsible for a greater concentration of silver ions remaining in solution.

Similar tests were also conducted on yeast and fungi (*Candida albicans*, *Aspergillus niger*, *Mucor*, *Saccharomyce cerevisiae*) using complexes **6a** and **6b**. For each organism, a solution of LB broth containing the minimum inhibitory concentration (MIC) for each silver compound was used to inoculate agar plates with active fungal colonies. The absence of viable organisms was observed for **6a** versus silver nitrate at a variety of concentrations. **6a** appears to outperform silver nitrate until very low concentrations of silver complex are used.

1.3.4. Synthesis of Silver NHC Complexes for Encapsulation in Electrospun Nanofibers

Although it is essential for silver NHC complexes to decompose to silver cations to have a microbicidal effect, the rate at which these cations are produced is also exceptionally important. Rapid decomposition leads to a decrease in long term efficacy, a limitation which can severally restrict the usefulness of the complex as a pharmaceutical.⁴⁰ By encapsulating silver NHC complexes inside a polymer fiber, the

Table 1-2

MIC Results for Silver Complexes (AgCl removed)^{a 36}

test comps	Ag (mg/mL)	E. coli		S. aureus		P. aeruginosa	
		day 1	day2	day 1	day2	day 1	day2
6a	1186	-	-	-	-	-	-
1DF		-	+	-	+	-	-
2DF		-	+	+		-	+
3DF		+		+		+	
4DF		+		+		+	
6b	1125	-	-	-	-	-	-
1DF		-	+	-	+	-	+
2DF		-	+	-		-	+
3DF		+		+		+	
4DF		+		+		+	
AgNO ₃	3176	-	+	+		-	+
1DF		+		+		+	
2DF		+		+		+	
3DF		+		+		+	
4DF		+		+		+	

a. 0.5% w/v each of the silver complexes was used. DF is the dilution factor (1mL).
 + = growth, - = no growth.

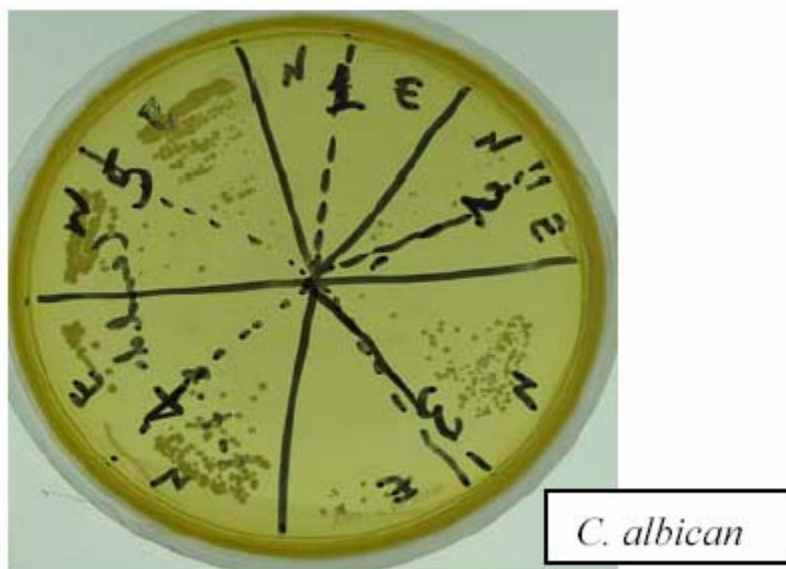
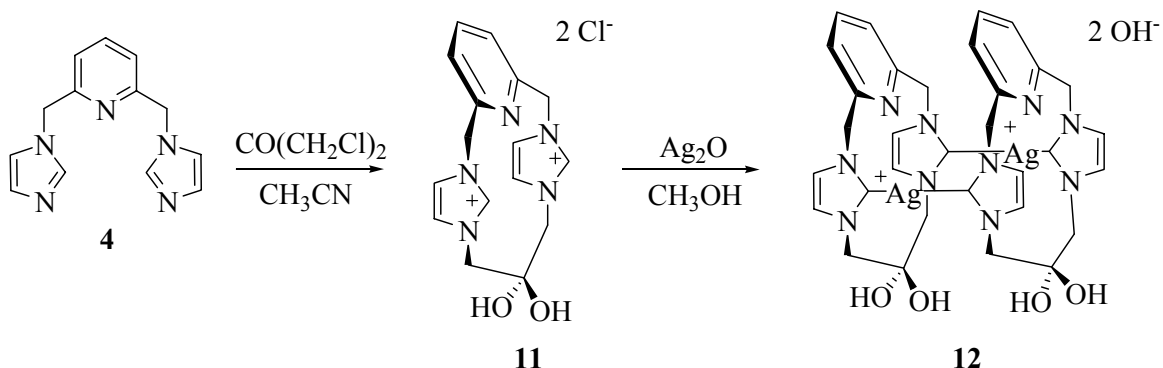


Figure 1-7. Agar plate showing N (AgNO₃) compared to E (**6a**) from high (1) to low (5) concentration.³⁹

rate at which silver cations are released can be retarded leading to an increase in the complexes antimicrobial efficacy. The polymer fiber also serves to retain the resulting ligand byproducts avoiding unnecessary contact with tissues.⁴¹

Electrospinning is a low cost efficient means of producing nonwoven polymer fibers on the nanoscale. Fiber thicknesses can range from less than 3 nm to over 1 μm depending on spinning conditions.^{42, 43} The concepts and instrumentation used in the electrospinning process are simple to apply and use. A polymer solution or melt is held in a syringe or capillary tube which contains an electrode. A grounded collection surface is placed below and a high voltage source is used to apply a charge to the system. When the critical voltage is surpassed the surface tension of the polymer solution is broken and a jet is formed. The solvent is evaporated in the process and a mat of entangled fibers can be collected.^{44- 48}

The synthetic route for the formation of a silver NHC cyclophane *gem*-diol complex is depicted in Scheme 1-3. The condensation of **4** with 1,3 dichloroacetone in acetonitrile affords imidazolium cyclophane **11**. The reaction **11** with Ag_2O in methanol

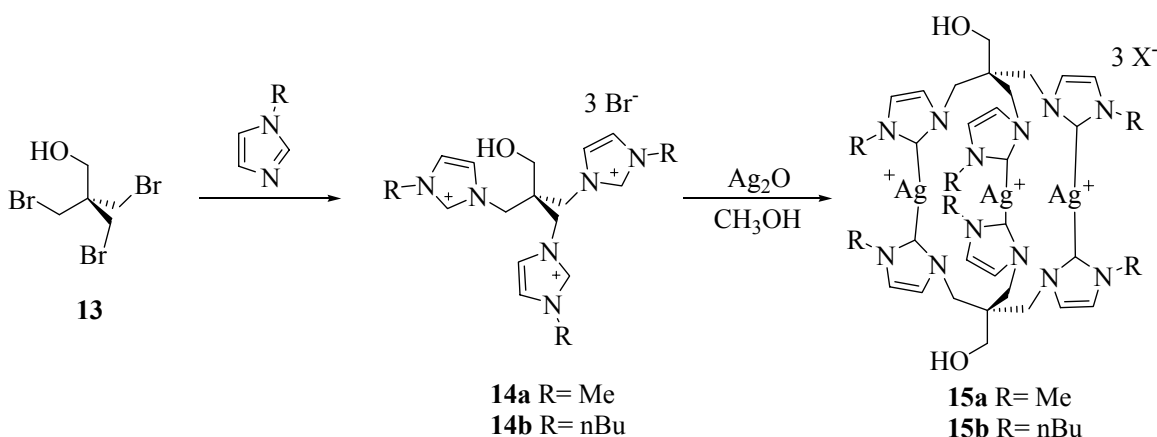


Scheme 1-3. Synthetic route for the formation silver NHC Cyclophane *gem*-Diol.⁴⁰

yields silver NHC cyclophane *gem*-diol complex **12**. It is assumed that the conversion of the carbonyl to the *gem*-diol occurs by some acid catalyzed process in the synthesis.⁴⁰

The synthesis of tripodal silver NHC complexes **15a** and **15b** are shown in Scheme 1-4. The reaction of excess methyl or N-butylimidazole with pentaerythritol **13** results in the formation of imidazolium salt precursors **14a** and **14b**. The reaction of these salts with Ag₂O in methanol gives tripodal silver NHC complexes **15a** and **15b**.⁴¹

Although the X-ray crystal structure has not been determined for either complex, similar complexes have been reported in the literature and the structures are assumed to be analogous.⁴⁹



Scheme 1-4. Synthetic route for the formation of tripodal silver NHC complexes.⁴¹

1.3.5. Antimicrobial Testing of Nanofiber Encapsulated Silver NHC complexes

Silver complexes **12**, **15a**, and **15b** were encapsulated via electrospinning in Tecophilic polymer. Tecophilic is a polyether-based thermoplastic aliphatic polyurethane and was chosen because it is a well known medical grade hydrophilic polymer.⁴⁰

Tecophilic also has the ability to absorb up to 150% of its dry weight in water which is necessary to facilitate the release of silver ions from the polymer matrix. The chosen

silver complex and Tecophilic polymer were dissolved in ethanol and electrospun to give homogeneous as-spun fibers, Figure 1-8.^{40,41}

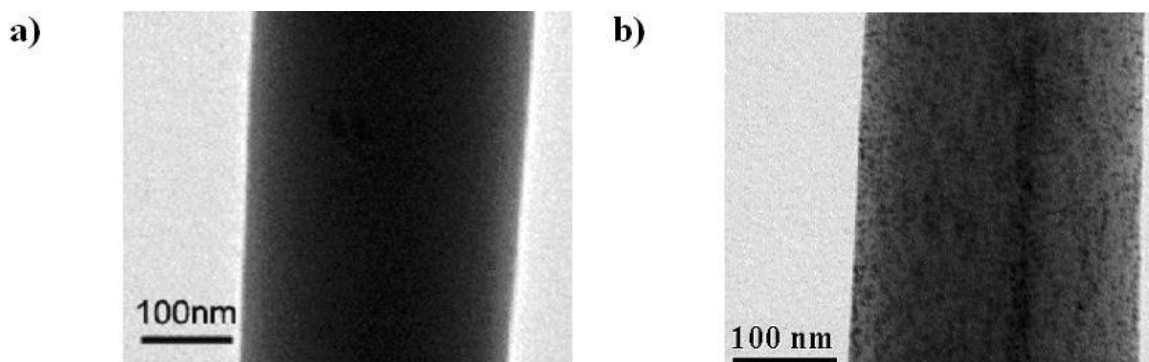


Figure 1-8. a) As-spun fiber of **12** and Tecophilic. b) Formation of silver particles after exposure to water.⁴⁰

Silver complex **12** was tested for its antimicrobial efficacy against bacterial strains of *E. coli*, *P. aeruginosa* and *S. aureus* with silver nitrate used as a standard for comparison. Successive dilutions were performed and the MIC results for the two compounds were observed over 48 h. After the first day, both complexes were equally effective against all test organisms. However, at the end of the 48 h study, silver complex **12** was observed to be less effective than silver nitrate, Table 1-3. This could be attributed to the low water solubility and low stability of complex **12** in aqueous solvents.⁴⁰

Silver complex **12** was encapsulated in Tecophilic polymer in ratios of 25% **12**/Tecophilic and 75% **12**/Tecophilic. A modified Kirby Bauer technique was used to determine the ability of the fiber mats to inhibit growth of *E. coli*, *P. aeruginosa*, *S. aureus*. Small sections of the fiber mats were placed on a lawn of the chosen organism and incubated overnight. Pure Tecophilic was used as a control and showed no inhibition

Table 1-3

MIC results for AgNO₃ and Silver NHC Complex **12**.⁴⁰

sample	conc. (wt/V%)	conc. (μg/mL)	vol. of bacteria (μL)	E. coli		P. aeruginosa		S. aureus	
				day 1	day 2	day 1	day 2	day 1	day 2
AgNO ₃	0.50	3462	100	-	-	-	-	-	-
	1DF	1731	100	-	-	-	-	-	-
	2DF	866	100	-	-	-	-	-	-
	3DF	433	100	-	-	-	-	-	-
	4DF	216	100	-	+	-	-	-	+
12	1.38	3341	100	-	-	-	-	-	-
	1DF	1676	100	-	-	-	-	-	-
	2DF	838	100	-	-	-	-	-	-
	3DF	419	100	-	+	-	+	-	+
	4DF	209	100	-	+	-	+	-	+

of organism growth. The 75% **12**/Tecophilic showed a zone of inhibition of 4 mm around the mat where as the 25% **12**/Tecophilic showed only a 2 mm zone of inhibition, Figure 1-9.

After a week of daily additions of 25 μL of fresh organism, fibers of **12**/Tecophilic continued to show antimicrobial efficacy. The 75% **12**/Tecophilic continued its antimicrobial activity for over two weeks. In fact the fiber mat of 75% **12**/Tecophilic was as effective as AgNO₃ at concentrations 8 fold lower. The results clearly show the enhanced antimicrobial properties of silver complex **12** when it is encapsulated in Tecophilic polymer.⁴⁰

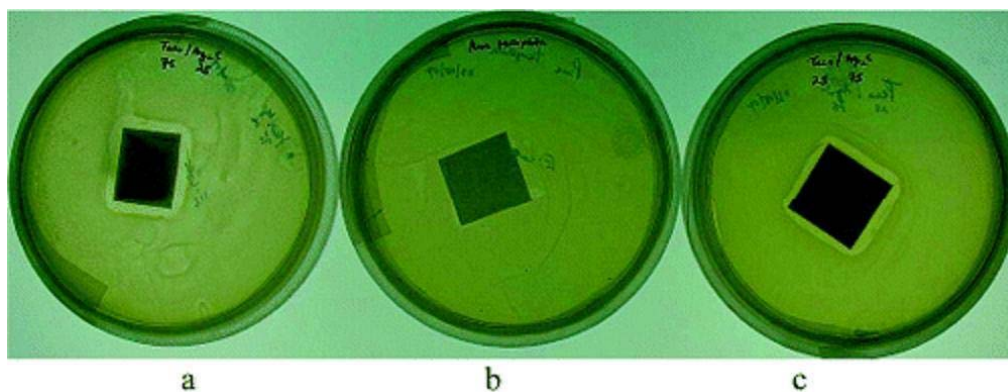


Figure 1-9. Modified Kirby Bauer test results. a. 25% **12**/Tecophilic, b. Tecophilic, c. 75% **12**/Tecophilic.⁴⁰

Fibers containing silver complex **15b** were also tested for their antimicrobial activity against *E. coli*, *P. aeruginosa*, *S. aureus*, *C. albicans*, *A. niger*, and *S. cerevisiae*. Again a modified Kirby Bauer test was used to determine the antimicrobial efficacy of the encapsulated complex. 25 μ L of freshly grown organism was spread on an agar plate to establish a lawn of either bacteria or fungi. Fiber mats of 33% **15b**/Tecophilic and 67% **15b**/Tecophilic were placed on the plates which were then incubated. Clear zones of inhibition were observed on the plates containing both bacterial and fungal colonies, Figure 1-10. Pure Tecophilic showed no inhibition to any of the tested organisms.⁴¹

Transmission electron microscopy (TEM) was used to demonstrate the mechanism of the release of silver particles from the fibers. Figure 1-11 shows the protrusion of silver particles from the surface of the as-spun fibers after exposure to water. Field emission scanning electron microscopy (FE-SEM) and X-ray energy dispersive spectroscopy (XEDS) were used to identify the elemental makeup of the aggregated particles, Figure 1-12.

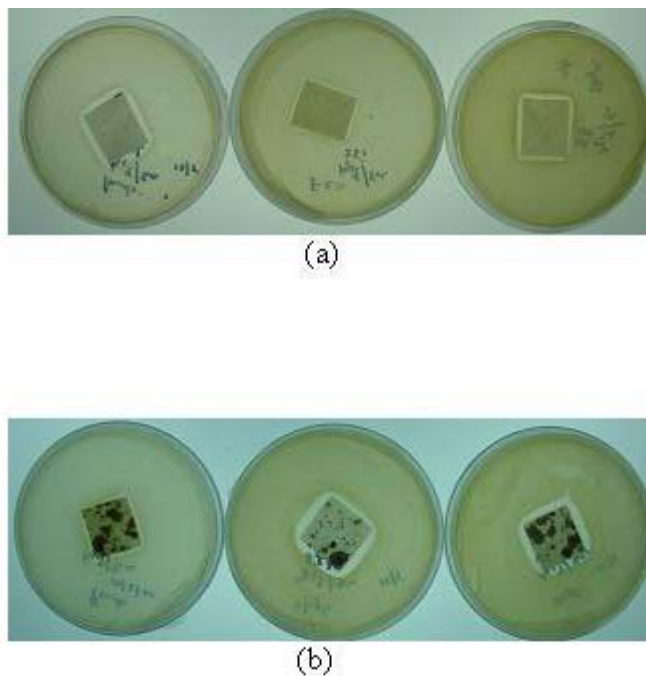


Figure 1-10. Zones of inhibition of **15b** encapsulated fibers. a) 33% **15b**/Tecophilic. b) 66% **15b**/Tecophilic.⁴¹

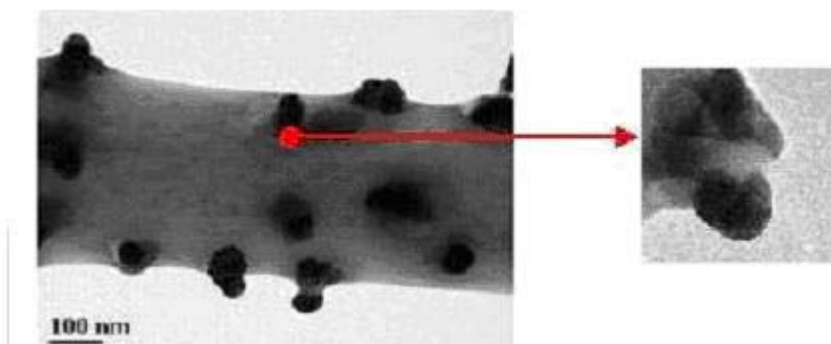


Figure 1-11. TEM image of protruding silver particles from the surface of an as-spun fiber.⁴¹

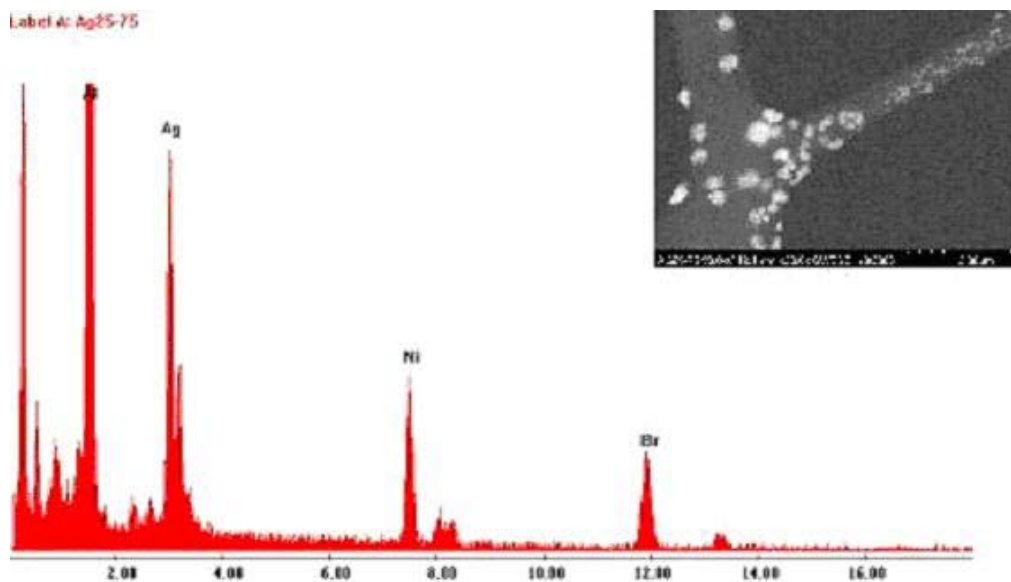


Figure 1-12. FE-SEM image of encapsulated **15b**. XEDS spectrum shows the composition of the aggregated particles as Ag and Br.⁴¹

1.3.6. Synthesis of Caffeine Based Silver NHC Complexes

The use of natural products can be a major advantage when designing new pharmaceuticals. The use of such molecules not only affords the potential to reduce the toxic effect of a new drug, but they can also be readily obtained at low cost. The most relevant biological molecules in the production of new NHC metal complexes are xanthine derivatives. The ring nitrogen atoms of xanthines can be substituted to form new imidazolium salt precursors. The most convenient xanthine derivative to use for this purpose is caffeine because it is available in large quantities, is inexpensive and has very low toxicity to humans.

The reaction of caffeine with excess methyl iodide results in the formation of methylated caffeine iodide, **16**. Excess methylating agent is necessary because the N9 position of caffeine is slightly deactivated by the two carbonyl moieties on the back side

of the molecule. The combination of AgOAc with imidazolium salt **16** in methanol yields silver NHC complex **17** shown in Figure 1-13.^{50, 51}

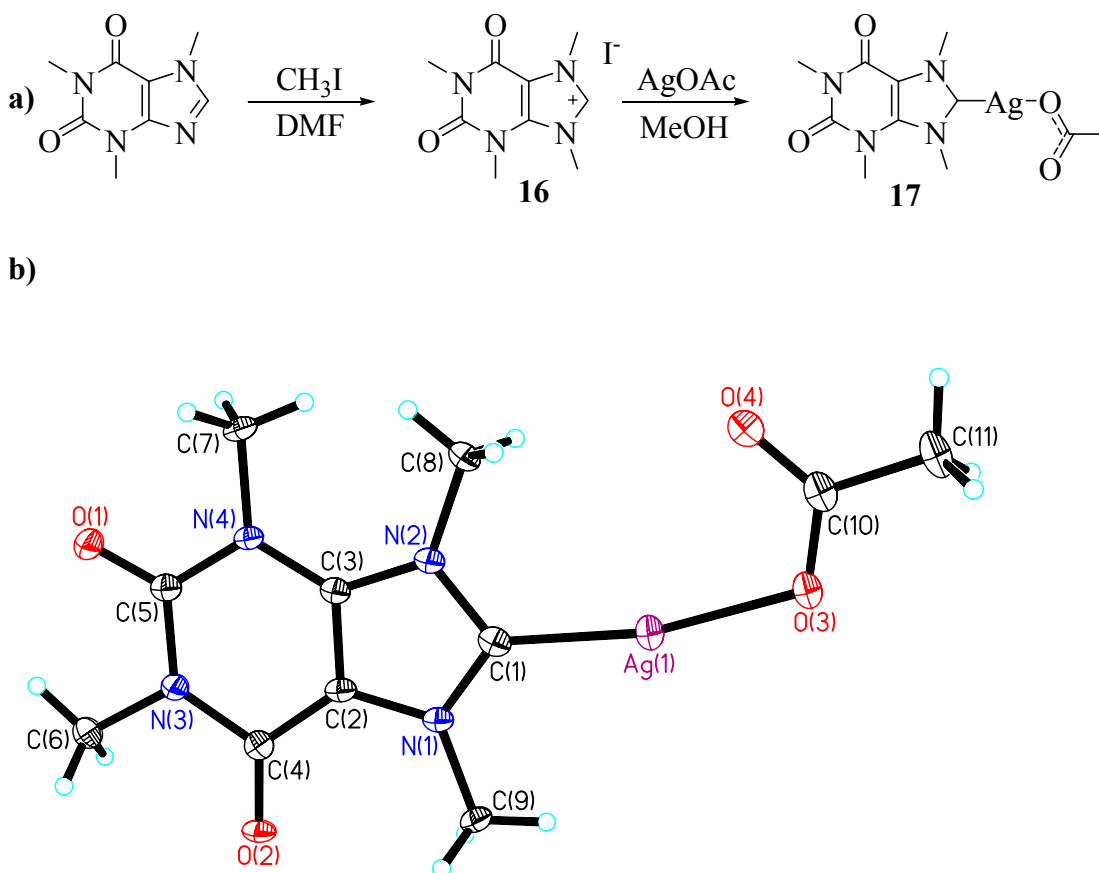


Figure 1-13. a) Synthetic route to the formation of methylated caffeine silver acetate NHC. b) Thermal ellipsoid plot of the silver acetate NHC complex **17**.^{50,51}

1.3.7. Antimicrobial Studies of Methylated Caffeine Silver Acetate

Methylated caffeine iodide **16** and its corresponding silver acetate NHC complex **17** were tested against a panel of bacteria and fungi associated with chronic lung infections in cystic fibrosis (CF) patients. Approximately 60,000 people worldwide are afflicted with this genetic ailment. In CF patients the cystic fibrosis transmembrane regulator (CFTR) is poorly functional or completely nonfunctional leading to the build up

of a thick mucus layer in the lungs. This mucus layer provides an ideal environment for the growth of infectious bacteria. As a result, patients with CF often suffer from chronic lung infections, which ultimately lead to death.^{50,51}

Methylated caffeine iodide **16** was tested for its antimicrobial efficacy against bacterial strains of *E. coli*, *P. aeruginosa*, *S. aureus*. The fungicidal abilities of **16** were also tested against *C. albicans*, *A. niger*, *S. cerevisiae*. The study showed **16** to be most effective against *E. coli* and *P. aeruginosa* with an MIC value of 50 mg/ml and less effective against *S. aureus* 100 mg/ml. The fungal studies demonstrated **16** to be most effective against *A. niger* with an MIC value of 75 mg/ml and less effective against *C. albicans* and *S. cerevisiae* 150 mg/ml.

Silver complex **17** was tested against a wide array of CF relevant bacterial strains. The study includes particularly resistant bacteria mainly recovered from the lungs of CF patients. MIC values were determined using two different types of growth media Luria broth (LB) and Mueller-Hinton (M-H). In general the lowest MIC values were observed in the LB growth media, Table 1-4.

Although the mechanism for the antimicrobial efficacy of complex **17** is unknown, the study does suggest that silver is responsible for the majority of the activity. The MIC value for **17** against *E. coli* J53 strains without silver resistance was found to be 1 µg/ml whereas the J53 strain with silver resistance gave an MIC of 5 mg/ml.

Table 1-4

MIC results for silver complex 17.⁵¹

genomovar	species name	strain	MIC ($\mu\text{g/mL}$)	
			M-H	LB
	<i>P. aeruginosa</i>	27853-ATCC	4	10
		PAO1-V	4	4
		6294	6	6
		2192	4	2
		PAM57-15	2	4
		FRD1	1	10
		324	1	6
		1061	1	8
		N6	1	10
		N8	1	6
		N13	1	6
		PAJG3	1	8
	<i>E. coli</i>	J53	1	4
		J53+pMG101 (silver resistant)	>5000	>5000
<i>Burkholderia cepacia</i> Complex				
I	<i>B. cepacia</i>	PC783	6	6
II	<i>B. multivorans</i>	HI2229	6	10
		AU8170	2	4
		AU5735	8	2
		AU7484	6	2
		AU5248	2	2
III	<i>B. cenocepacia</i>	H12718	6	4
		J2315	1	4
		ATTC BAA-245	1	4
IV	<i>B. stabilis</i>	H12210	2	2
		ATTC BAA-67	1	1
V	<i>B. vientnamiensis</i>	PC259	4	4
VI	<i>B. dolosa</i>	AU0645	4	8
		ATTC BAA-246	1	4
		AU4459	6	4
		AU5404	6	4
		AU4881	1	4
		AU9248	1	2
		AU4894	1	4
VII	<i>B. ambifaria</i>	H12468	6	6
VIII	<i>B. anthina</i>	AU1293	4	4
IX	<i>B. pyrrocinia</i>	BC11	4	4

In an attempt to understand the mechanism of antimicrobial action of complex **17**, *Burkholderia dolosa* was inoculated with the silver complex and both treated and non-treated cells were observed by TEM. The TEM images clearly show a distinct difference between the treated and untreated cell morphologies as shown in Figure 1-14. *B. dolosa* treated with **17** display “ghost” membranes that lack cytoplasm. The cell wall is also visibly disrupted suggesting the complex may be responsible for initiating destruction of the bacterial cell membrane. The “ghost” membranes were also filled with electron dense clusters which appear in black on the images. These dense clusters are best explained by the deposition of silver salts in the cell membrane.⁵¹

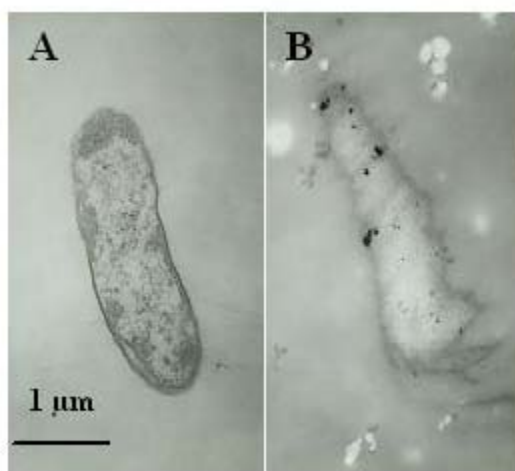


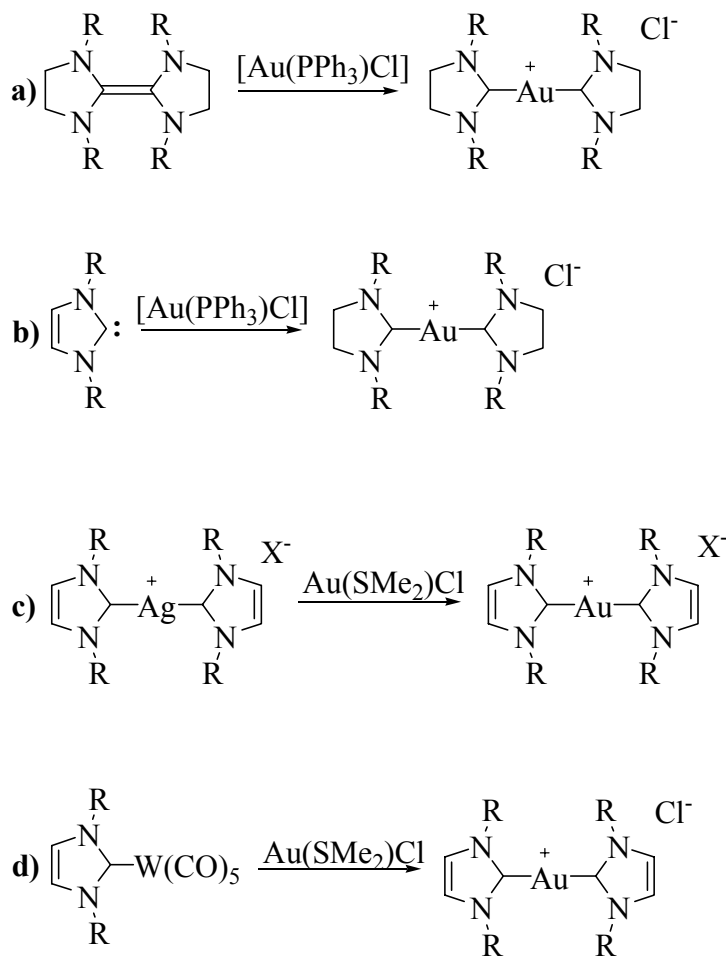
Figure 1-14. A TEM of untreated *B. dolosa*. B TEM of *B. dolosa* treated with silver complex **17**.⁵¹

1.4. Gold NHC Complexes

Unlike their silver counterparts, gold NHC complexes have not received a great deal of chemical investigation. This is also in contrast to the abundant amount of work published on gold complexes of other organic ligand systems such as phosphines and thiolates.⁵²⁻⁵⁶ However, recently research on gold NHCs has begun to yield a number of

very promising results. The latest reports describe the antimicrobial,⁵⁷ antimitochondrial, anticancer,⁵⁸ and catalytic properties of gold NHCs.⁵⁹

A variety of synthetic methods can be employed to produce gold NHC complexes. As with any NHC transition metal complex, the route of synthesis can depend upon the azolium precursor used to generate the NHC, upon the source of the metal being used, or both. Gold NHCs have been synthesized via reaction of gold starting materials directly with free NHCs, azolium salts,⁵⁶ cleavage of electron rich olefins,⁵⁷ transmetallation using silver NHCs, transfer to gold from Group 6 metal carbonyl



Scheme 1-5. Synthesis of Au(I)-NHCs from a) olefins, b) free NHCs, c) Ag(I)-NHCs via transmetallation, d) Group 6 carbonyl complexes.⁶¹

complexes,⁶⁰ and protonation or alkylation of gold azolyl compounds, Scheme 1-5.⁶¹ The most common gold reagents used throughout the literature are $[\text{Au}(\text{PPh}_3)\text{Cl}]$ and $[\text{Au}(\text{SMe}_2)\text{Cl}]$.

1.4.1. Rationale and Synthesis of Gold NHC Antimicrobials

A study focusing on the synthesis and antimicrobial properties of six gold NHC complexes has recently been reported.⁵⁷ The six NHC ligands examined differed only in the substituents on the nitrogen atoms of the imidazoline ring. The rationalization behind this study was the reported antimicrobial effectiveness of gold complexes composed of a variety of AuSP and AuNP cores.⁵²⁻⁵⁶ Previous studies have shown complexes **18** and **19** to have moderate activity against *Bacillus subtilis* and *Staphylococcus aureus*, complex

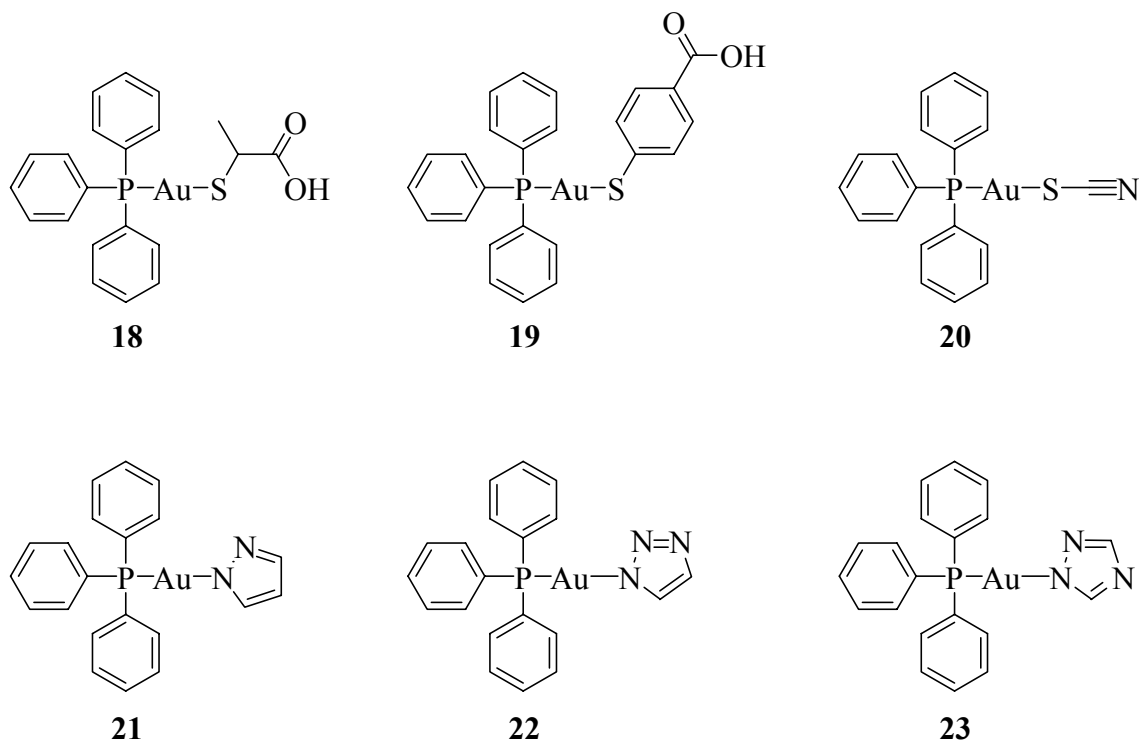
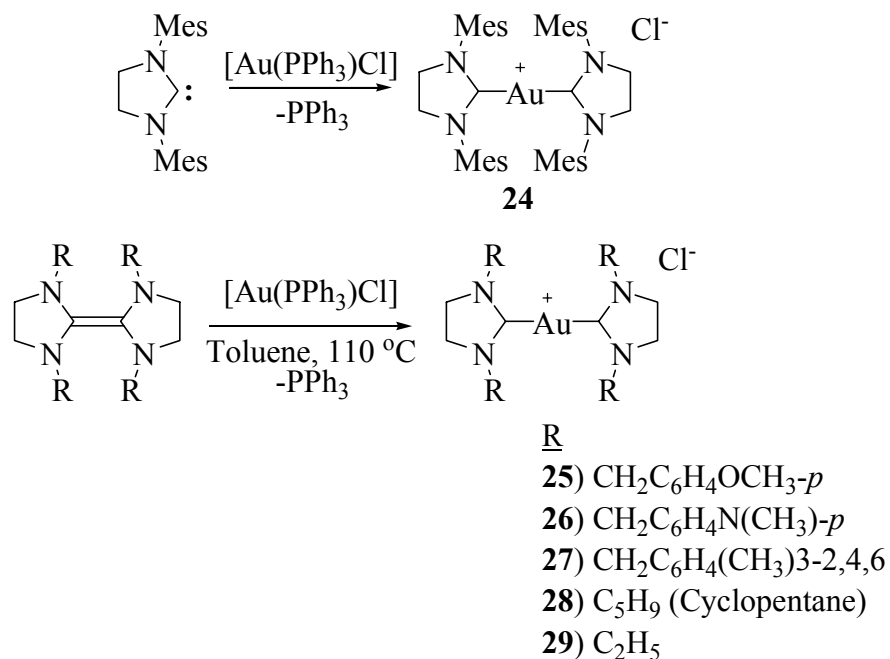


Figure 1-15. Gold complexes with AuSP and AuNP cores studied for antimicrobial effectiveness.

20 to have good activity against *Staphylococcus aureus*, *Enterococcus faecalis*, *Proteus mirabilis*, *Pseudomonas aeruginosa* and *Candida albicans*, and **21-23** to have good activity against *Bacillus subtilis* and *Staphylococcus aureus*.

NHCs are often compared to alkyl phosphines because both are strong σ -donors and possess only weak π -back donation character.^{62, 63} Studies have also shown NHCs to bind more tightly to metals than their phosphine counterparts, and because of this they have been used to substitute or replace phosphines in a variety of substances.^{6,62} It is also assumed that an Au-C bond would be favorable in comparison to an Au-N bond based upon the theory of hard and soft acids and bases.⁵⁷ Based on the strength of the NHC-Au bond along with the favorable soft-soft interaction For these reasons the N, P, and S ligands about the gold center were replaced with NHCs in order to yield new properties and enhance the stability of this type of antimicrobial.⁵⁷

Six gold NHC complexes were prepared by the reaction of the free carbene or corresponding electron rich olefin with $[\text{Au}(\text{PPh}_3)\text{Cl}]$.⁵⁷ The second route required the reaction to take place in boiling toluene, Scheme 1-6. Both synthetic methods made use of dry solvents and inert atmospheres. The resulting Au-NHC complexes were air and light stable. Structures were confirmed by the observation of resonances between 204-207 ppm in the ^{13}C NMR corresponding to the carbene carbon bound to the gold center.



Scheme 1-6. Synthetic route to Au-NHCs for antimicrobial testing.⁵⁷

1.4.2. Antimicrobial Testing of Gold NHC Complexes

The six complexes were tested for antimicrobial activity against seven relevant pathogens: *Escherichia coli*, *Staphylococcus epidermidis*, *Staphylococcus aureus*, *Enterococcus faecalis*, *Enterobacter cloacae*, *Pseudomonas aeruginosa*, *Candida albicans*.⁵⁷ Ampicillin a common antibiotic, Flucytosine an antifungal drug, and the imidazolium salt 1,3-(dimesitylmethylimidazolium) chloride were used as standards for comparison. The organisms were introduced to agar plates and the bacteria were incubated at 37 °C for 24 h and the fungi at 30 °C for 48 h. Samples of the compounds and standards were diluted in a solution of 10% DMSO in water. A sequence of serial dilutions were made from 1600 to 3.12 µg ml⁻¹ and the MIC values were determined, Table 1-5.⁵⁷

Table 1-5

MIC values for tested Au NHC compounds.⁵⁷

Compound	MIC ($\mu\text{g ml}^{-1}$)						
	<i>E. coli</i>	<i>S. epidermidis</i>	<i>S. aureus</i>	<i>E. faecalis</i>	<i>E. cloacae</i>	<i>P. aeruginosa</i>	<i>C. albicans</i>
Ampicillin	< 3.12	< 3.12	< 3.12	6.25	< 3.12	25	-
Flucytosine	-	-	-	-	-	-	6.25
Mmi ^a	400	6.25	3.12	3.12	1600	3.12	200
24	800	800	3.12	800	3.12	1600	800
25	1600	6.25	3.12	3.12	1600	3.12	200
26	3.12	>1600	>1600	>1600	>1600	>1600	>1600
27	200	>1600	200	>1600	100	>1600	>1600
28	1600	>1600	50	800	12.5	>1600	1600
29	400	>1600	50	>1600	800	>1600	>1600

a) Mmi = 1,3-(dimesitylmethylimidazolium) chloride

Of the six gold compounds studied, only **25** showed antimicrobial activity against a wide range of bacteria. Of the remaining complexes only **24** and **26** showed any significant antimicrobial activity. It appears that benzyl substituents give rise to the most active gold complexes, in particular, the *p*-substituted benzyls as is the case with complexes **25** and **26**. Also of note is the excellent antimicrobial activity of the Mmi, which is as effective as the best gold complex **25**. It is interesting that the gold complex with 1,3-(dimesitylmethylimidazolium) chloride, **27**, has almost no activity at all against the panel of bacteria tested.

1.4.3. Gold NHC Antitumor Complexes

A series of cationic gold NHC complexes have been synthesized for the purpose of evaluating their efficacy as mitochondrial membrane permeabilization (MMP) agents.⁶⁴ There has been a recent focus on the study of MMP agents because of their selectivity in targeting carcinomas.^{65,66} Lipophilic cations are readily absorbed by cells and localized in the mitochondria. This phenomenon provides an avenue that can be utilized to induce apoptosis in cancerous cells. A large difference in membrane potentials exists between normal epithelial and carcinoma cells.^{65,66} Due to this distinguishing feature, it is envisioned that certain MMP agents will accumulate more rapidly in carcinoma cells than in surrounding normal tissue. This would provide a mode to selectively target carcinoma, and would limit harmful toxic effects to normal cells.⁶⁵

1.4.4. Synthesis of and Testing of Gold NHC Antitumor Complexes

Gold NHC complexes **30-36**, Figure 1-16, were synthesized via deprotonation of the corresponding imidazolium salts in the presence of Au(SMe₂)Cl.⁵⁸ The salts and the gold starting material were dissolved in hot DMF and the appropriate carboxylate salt (sodium acetate, lithium acetate or lithium butyrate) was added. The products precipitated from solution and were purified by recrystallization.⁵⁸

The ability of complexes **30-36** to induce mitochondrial swelling in vitro was studied. The selected gold NHC complex was introduced to a solution of mitochondria isolated from homogenized rat livers. The amount of mitochondrial swelling was then monitored by a reduction in absorbance at 540 nm using a UV-Vis spectrophotometer.

All of the tested complexes, with the exception of **30**, induced considerable swelling of the mitochondria at concentrations as low as 10 μM . During the course of the experiment it was discovered that μM concentrations of Ca^{2+} were necessary for the gold complexes to achieve their maximum effect.⁵⁸

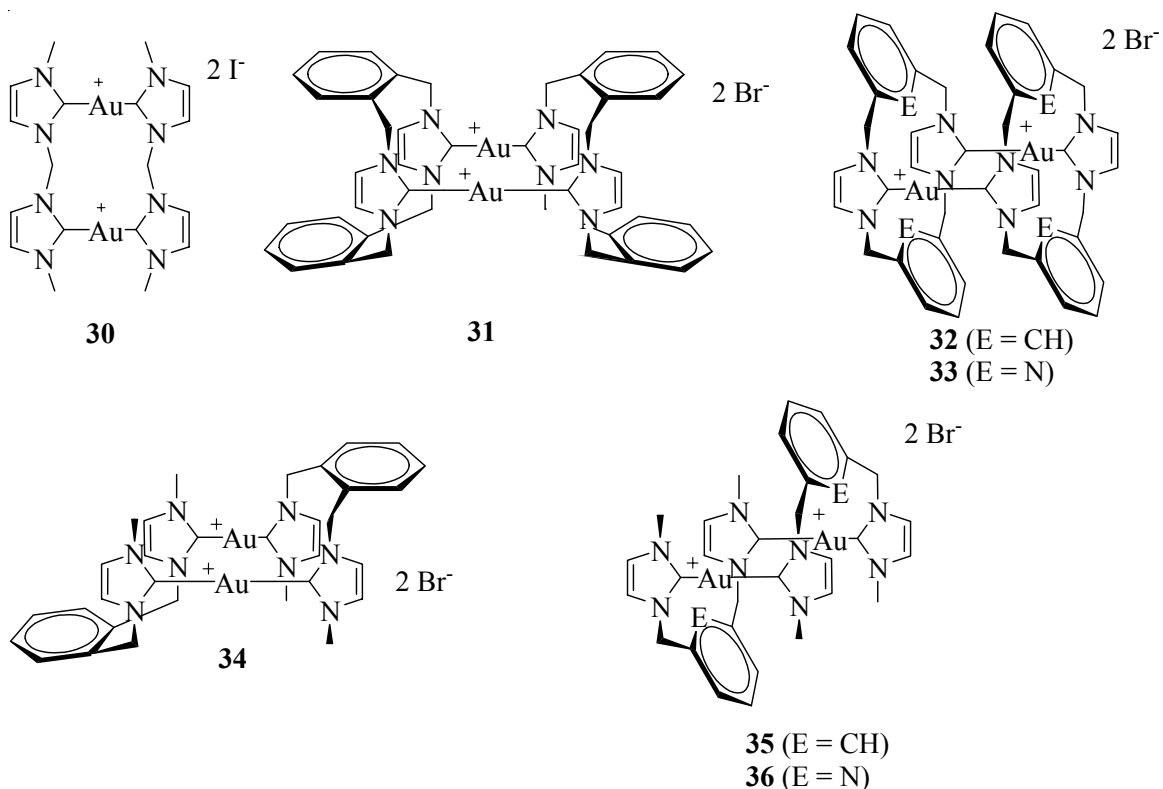


Figure 1-16. Gold NHC MMP agents.⁵⁸

A secondary investigation of this phenomenon was conducted using gold NHC complex **31**. At a concentration of 25 μM CaCl_2 , complex **31** caused significant mitochondrial swelling at concentrations as low as 0.5 μM . When the source of Ca^{2+} was removed, mitochondrial swelling was completely inhibited at that same concentration. In fact a 65% reduction in swelling was observed at concentrations up to 10 μM . At a

40 μM concentration of **31**, significant swelling was observed, although it took nearly three times longer to achieve in comparison to the same concentration in the presence of Ca^{2+} .

The amount of gold complex absorbed by the mitochondria was also observed throughout the study. Complex **30** showed the lowest amount of uptake (1.1 μg of Au/mg of mitochondrial protein). This would seem to correlate to the impotence of **30** in inducing mitochondrial swelling. However, complexes **34-36** all have higher uptake concentrations (4.7-5.2 μg of Au/mg of mitochondrial protein) than **31-33** (2.4-4.5 μg of Au/mg of mitochondrial protein), and there is no direct correlation between these values and the effectiveness of the complexes to induce mitochondrial swelling. This fact seems to suggest that some minimal uptake concentration is necessary, but the true efficacy of the complex is probably due to some unknown interaction with the mitochondria.

1.5. Rhodium NHC Model Complexes

The use of radionuclides for cancer therapy is not a new concept in the field of medicine. $^{99\text{m}}\text{Tc}$ radiotracers were first synthesized in 1964, and $^{99\text{m}}\text{Tc}$ still remains the most widely used radionuclide for diagnostic imaging.⁶⁷ ^{131}I administered in the form of NaI is a common and exceptionally effective treatment for differentiated thyroid carcinoma.⁶⁸

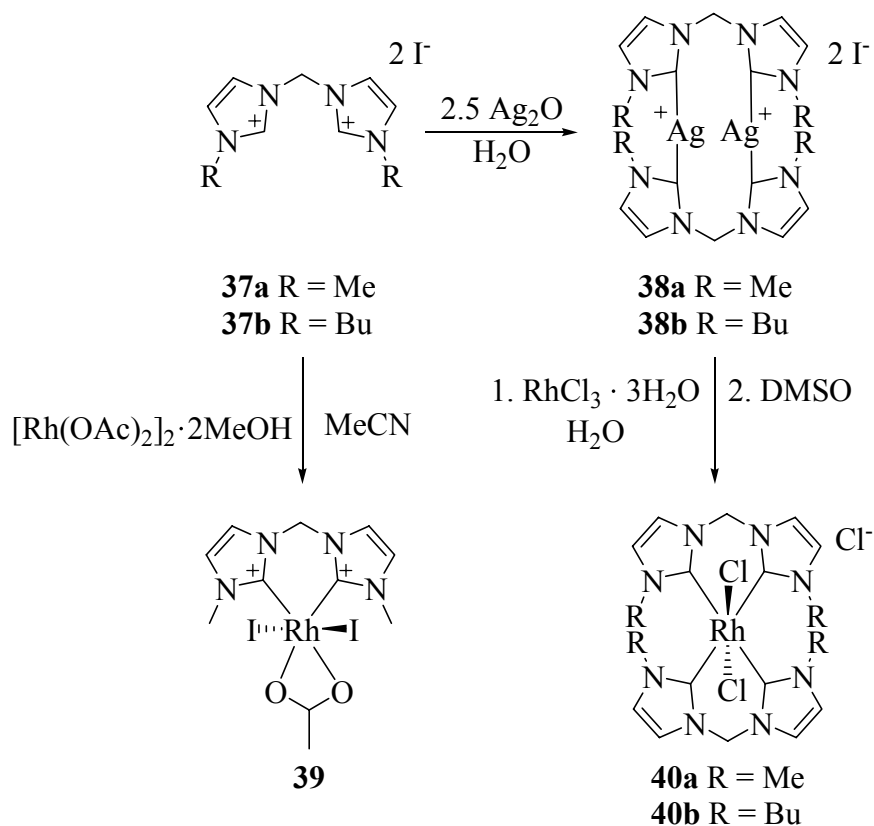
^{105}Rh , like ^{131}I , decays through the emission of β radiation. ^{105}Rh emits beta particles in a ratio of 70% 0.560 MeV and 30% 0.250 MeV that are suitable for radiation therapy as well as a 319 keV gamma particle that is suitable for imaging. Its $t_{1/2}$ of 36.4 hours is advantageous in that it should provide sufficient time to kill large tumors when

appropriately targeted, but it is also short enough to avoid prolonged accumulation of radioactive material in the body.⁶⁹

1.5.1. Synthesis of Rhodium NHC Complexes

The only radioactive ^{105}Rh starting material available for synthesis is $^{105}\text{RhCl}_3 \cdot x\text{H}_2\text{O}$. This presents the challenge of making a robust, chelating rhodium NHC-pincer complex starting with $\text{RhCl}_3 \cdot x\text{H}_2\text{O}$. The synthetic preparation also needs to be relatively simple and performed well within the 36.4 hour half life of the radioisotope. There are several ways to approach these challenges. The first involves rapid transformation of the $\text{RhCl}_3 \cdot x\text{H}_2\text{O}$ into a form that had been previously used to make rhodium carbene complexes.⁷⁰⁻⁷⁴ The second would be direct synthesis of rhodium NHC-pincer complexes from $\text{RhCl}_3 \cdot x\text{H}_2\text{O}$.

When investigating potential radiopharmaceuticals it is always preferable to start with non-radioactive model complexes. Non-radioactive $^{103}\text{RhCl}_3 \cdot x\text{H}_2\text{O}$ was used in the synthesis of rhodium NHC-pincer model complexes. Initial attempts to make rhodium NHC-pincer complexes from $\text{RhCl}_3 \cdot x\text{H}_2\text{O}$ involved a conversion to $(\text{Rh}(\text{OAc})_2)_2 \cdot 2\text{MeOH}$.⁷⁵ The reaction of NHC-pincer precursor **37a** with $(\text{Rh}(\text{OAc})_2)_2 \cdot 2\text{MeOH}$, KI, and sodium acetate in acetonitrile afforded rhodium complex **39**, Scheme 1-7.⁷⁶ Although the complex is a suitable model, its synthetic preparation raises some major problems. Acetonitrile is toxic and not acceptable for medical use, and the reaction requires several subsequent steps that would later involve radioactive materials. These problems all but exclude this approach for practical use.



Scheme 1-7. Synthetic route for the formation of rhodium NHC-pincer complexes.⁷⁷

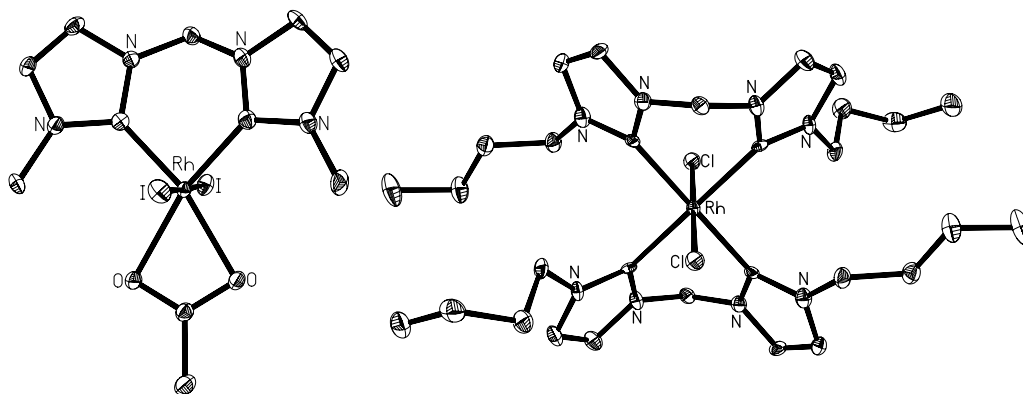


Figure 1-17. Thermal ellipsoid plots of rhodium NHC-pincer complexes 39 and 40b.⁷⁷

Because of the obstacles associated with the first approach, a synthetic route for the formation of a rhodium NHC-pincer complex directly from $\text{RhCl}_3 \cdot x\text{H}_2\text{O}$ was pursued. Silver complexes **38a** and **38b** were obtained by the reaction of Ag_2O with the appropriate imidazolium salt precursors.⁷⁷ Following isolation of the silver complex, an

aqueous solution was prepared, and $\text{RhCl}_3 \cdot 3\text{H}_2\text{O}$ was added. A red solid was isolated from the reaction which was subsequently heated in DMSO at 100 °C for 1 hour to give rhodium complexes **40a** or **40b**.⁷⁸ This synthetic procedure appears to avoid use of medically unacceptable solvents, since DMSO is biologically benign, and only introduces what will be the eventual radioactive material at the final stage of preparation.^{79,80}

1.5.2. Ligand Modification for Targeting

Although successful radiological agents exist for the treatment of cancer their effectiveness is usually limited to one or two specific cancer types. As mentioned previously, ^{131}I in the form of NaI is an effective treatment for differentiated thyroid carcinoma; however, this treatment relies on the body's natural tendency to accumulate iodine in the thyroid.⁶⁸ Another approach involves the use of targeting moieties to localize a radioactive source at the site of a tumor.

The typical assembly for a targeted bioinorganic radiopharmaceutical by use of a bifunctional chelating agent is depicted in Figure 1-18. The desired radioisotope is contained by a strongly chelating ligand which through a linker of desired length is attached to a specific targeting group. This group could be a large monoclonal antibody, a smaller peptide, or non-peptide targeting molecule which would bind to over expressed receptor sites on tumors. In recent years, peptides have become a much more attractive choice because of the advent of peptide synthesizers.⁸¹

A general route for the formation of targeted pyridine based NHC-pincer complexes is shown in Scheme 1-8. The condensation of (6-bromomethyl-pyridin-2-yl)-methanol **7** with an equivalent of substituted imidazole **41** would yield a

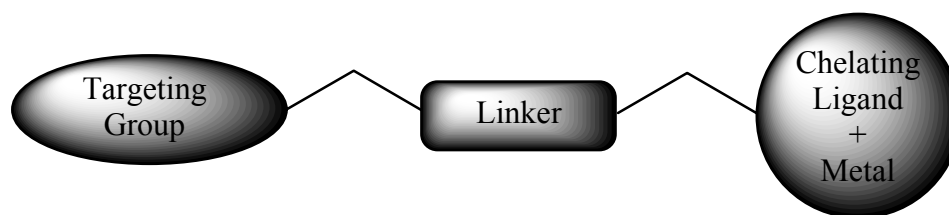
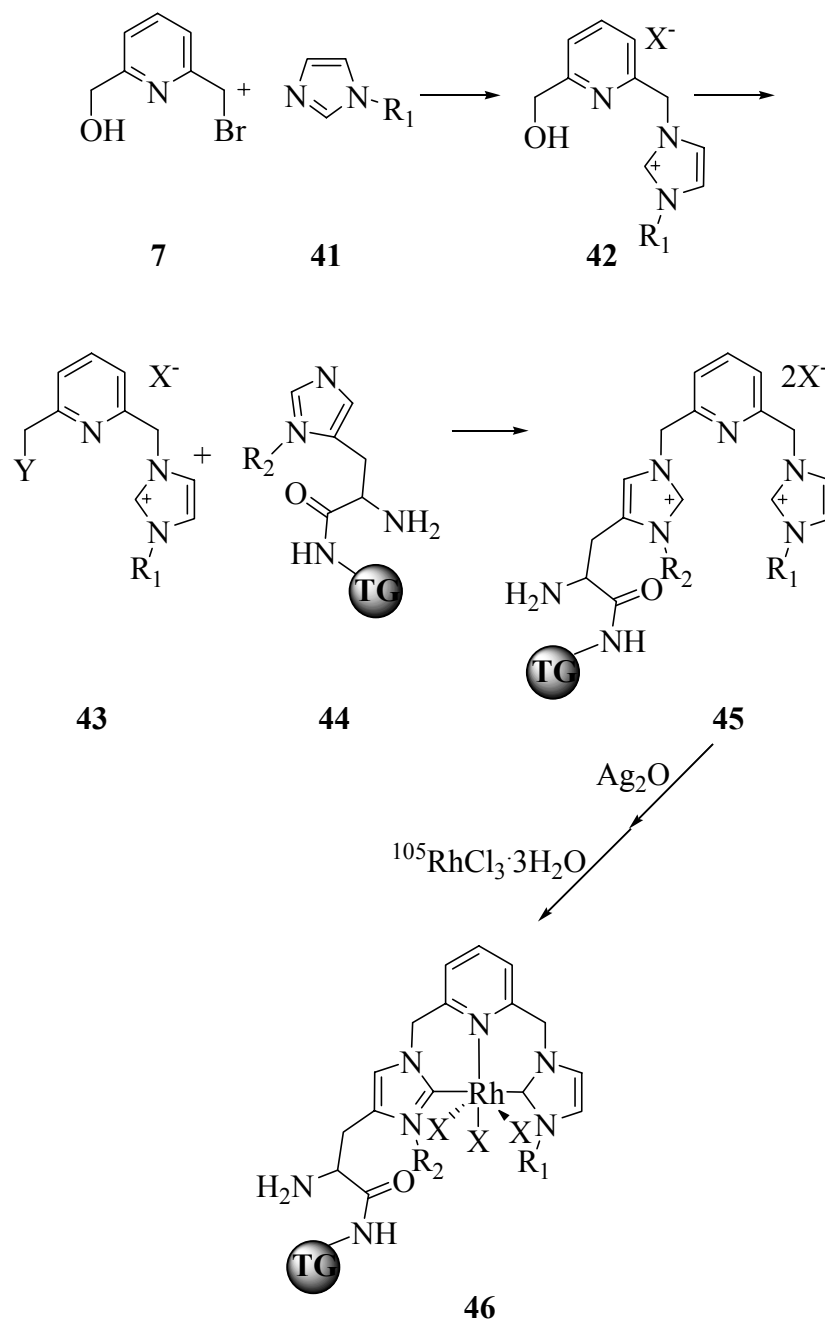


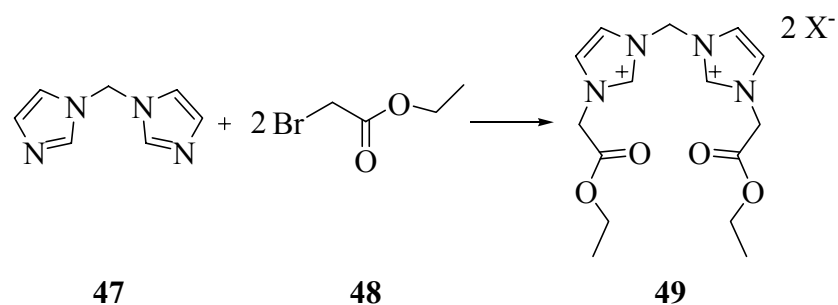
Figure 1-18. Targeted radiopharmaceutical assembly.³⁷

monocationic imidazolium salt **42**. Conversion of the alcohol group to a more readily displaced leaving group, compound **43**, followed by reaction with a targeting peptide terminated by a histidine derivative **44** would yield a targeted NHC-pincer precursor **45**.³⁷ In the final step, this precursor could be used to form a silver complex used for transmetallation to produce the ¹⁰⁵Rh pharmaceutical **46**.³⁷

An alternative precursor could be synthesized starting with 1,1'-methylene bis(imidazole) **47** Equation 1-1. The condensation of **47** with bromoester **48** forms the ester functionalized bisimidazolium salt **49**. Hydrolysis of the ester would give the carboxylic acid functionalized salt. This compound potentially could be used for condensations with small peptides known to have binding affinities to over expressed receptor sites specific tumor cells.



Scheme 1-8. General synthesis for the formation of targeted pyridine based NHC-pincer complexes.³⁷



Equation 1-1. Synthesis of a bisimidazole precursor for targeting.

1.6 Conclusions

NHC complexes show a great deal of promise for use in a variety of medicinal applications. The fact that NHCs form such strong metal complexes should give them a major advantage over current organic ligands. Initial studies of silver NHC complexes show that they have properties important for use as effective antimicrobials. These complexes have better MIC results and bacterial growth inhibitions than silver nitrate against a variety of infectious bacteria and fungi. Also, silver NHC complexes can be easily generated in biologically friendly solvents such as water and alcohols and from biologically relevant subunits.

Alternatively, the synthesis of rhodium complexes of NHCs in water has not yet been achieved. The use of silver NHC-pincer complexes for transmetallation reactions to give rhodium complexes is a major step forward towards this goal. Currently this route requires the use of DMSO as a solvent which, although not ideal, is a medically acceptable solvent. Studies are continuing for improving this synthesis as well as incorporating targeting moieties to form fully functional pharmaceuticals.

CHAPTER II
SYNTHESIS OF STERICALLY SHIELDED AND ELECTRONICALLY STABILIZED
SILVER N-HETEROCYCLIC CARBENE COMPLEXS

2.1 Introduction

The study of silver N-heterocyclic carbene (NHC) complexes for use as effective antimicrobials has become a very active area of interest in recent years.^{35-37,40,41,50,51} The principal challenge in designing such compounds has been the relatively low stability of many silver NHCs in aqueous media.⁷⁸ Although it is essential for these complexes to decompose to silver cations to have a microbicidal effect, the rate at which the cations are produced is important. Weakly coordinating complexes will release silver too quickly generating only short term effects. Finding ways to increase the strength of the silver carbene bond or to diminish the susceptibility of the carbene carbon to attack by protons will allow for a lengthened release of silver cations. Achieving this goal would be a major step towards producing a practical silver NHC antimicrobial.

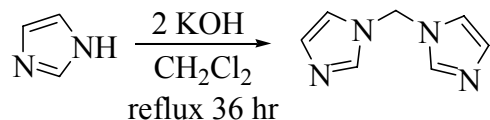
In this research the challenge of increasing silver NHC stability was approached by two methods. The first method made use of sterically bulky substituents in order to shield the silver carbene bond from attack by advantageous halides or protons. The second approach was to use an NHC with electron withdrawing groups as a means of electronically adjusting the carbene silver bond.⁸² The use electron withdrawing groups to

increase the stability of silver NHCs has been demonstrated using xanthine derivatives such as caffeine.^{50,51}

2.2 Synthesis and Characterization of a Sterically Shielded Silver N-Heterocyclic Carbene Complex

The starting material 1,1'-methylene bis(imidazole) was synthesized by a simplified procedure. Reported syntheses of 1,1'-methylene bis(imidazole) involve either a solid state transfer reaction or a liquid-liquid phase transfer reaction using tetrabutylammonium bromide as a phase transfer catalyst.^{83,84} Although reported yields are very high, the procedure is carried out on a small scale affording 10 mmol of product and the work up requires purification by either column chromatography or by sublimation.

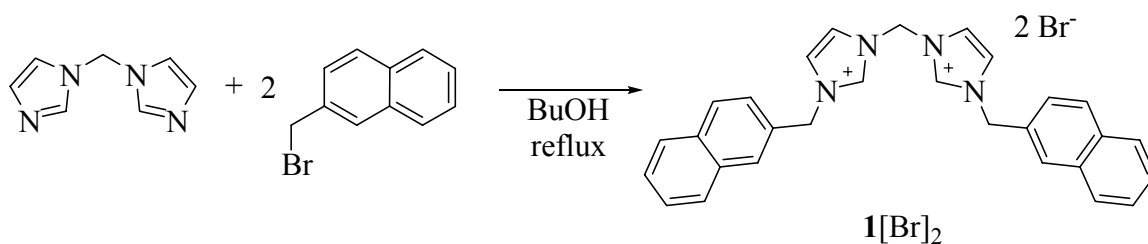
The simplified synthetic route to 1,1'-methylene bis(imidazole) is depicted in Equation 2-1. The condensation of imidazole with dichloromethane can be achieved by refluxing imidazole with two equivalents of potassium hydroxide in a large excess of dichloromethane. The liquid phase can be decanted every 12 hours and the volatiles removed to afford 1,1'-methylene bis(imidazole) as an off white solid. Washing with diethyl ether removes residual imidazole. This process can be repeated several times until yields drop off significantly.



Equation 2-1. Synthesis of 1,1'-methylene bis(imidazole).

The ^1H and ^{13}C NMR spectra of 1,1'-methylene bis(imidazole) are both consistent with the given structure. The ^1H NMR spectrum, shown in Figure 2-1, gives resonances at ca. δ 6.1 (s, 2H, CH_2), 6.9 (s, 2H, CH), 7.12 (d, 2H, $J = 1$ Hz, CH), and 7.8 (s, 2H, CH). Splitting was observed for only one of the two different hydrogen atoms on the backbone of the imidazole rings.

The synthesis of the sterically shielded imidazolium salt **1** $[\text{Br}]_2$ is illustrated in Equation 2-2. The condensation of one equivalent 1,1'-methylene bis(imidazole) with two equivalents 2-bromomethyl naphthalene in butyl alcohol at reflux results in the formation of dicationic imidazolium salt **1** $[\text{Br}]_2$. The product precipitates from the reaction over a course of several hours and is collected as an off white solid in 74% yield.



Equation 2-2. Synthesis of the sterically shielded imidazolium salt **1** $[\text{Br}]_2$.

The ^1H and ^{13}C NMR spectra of **1** $[\text{Br}]_2$ are consistent with the proposed structure. The ^1H NMR spectrum, shown in Figures 2-2 and 2-3, presents resonances at ca. δ 5.7 (s, 4H, N- CH_2 -naphthalene), 6.7 (s, 2H, N- CH_2 -N), 7.6 (m, 6H, CH), 7.9 (m, 8H, CH), 8.0 (s, 2H, CH), 8.2 (s, 2H, CH), 9.7 (s, 2H, C^+ -H). The resonance observed at 9.7 ppm is diagnostic corresponding to the hydrogen bound to C(2) of the imidazole ring. The resonance of the C(2)-H of most imidazolium salts typically ranges between δ 8-10.

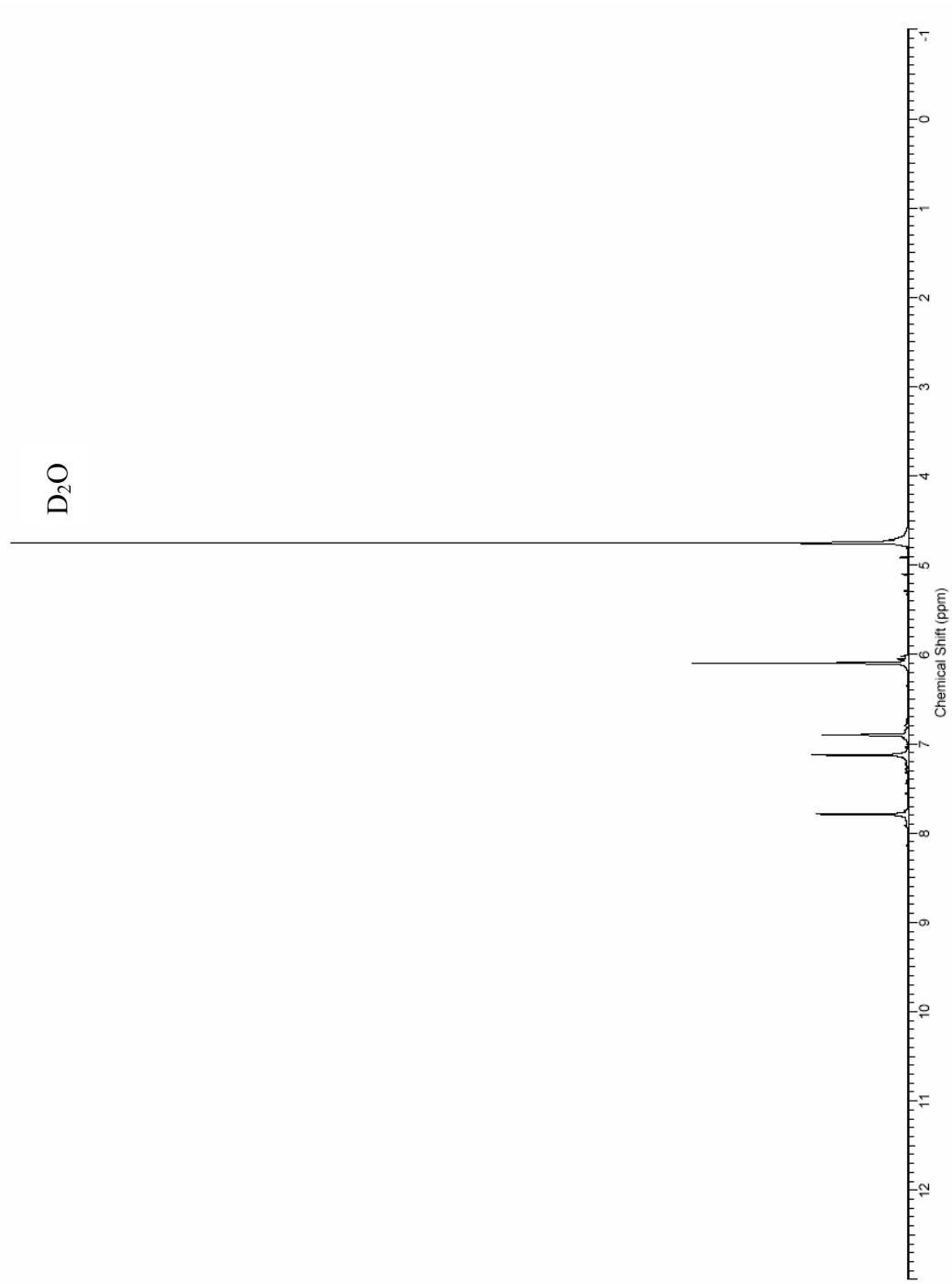


Figure 2-1. The ^1H NMR spectrum of 1,1'-methylene bis(imidazole) in D_2O .

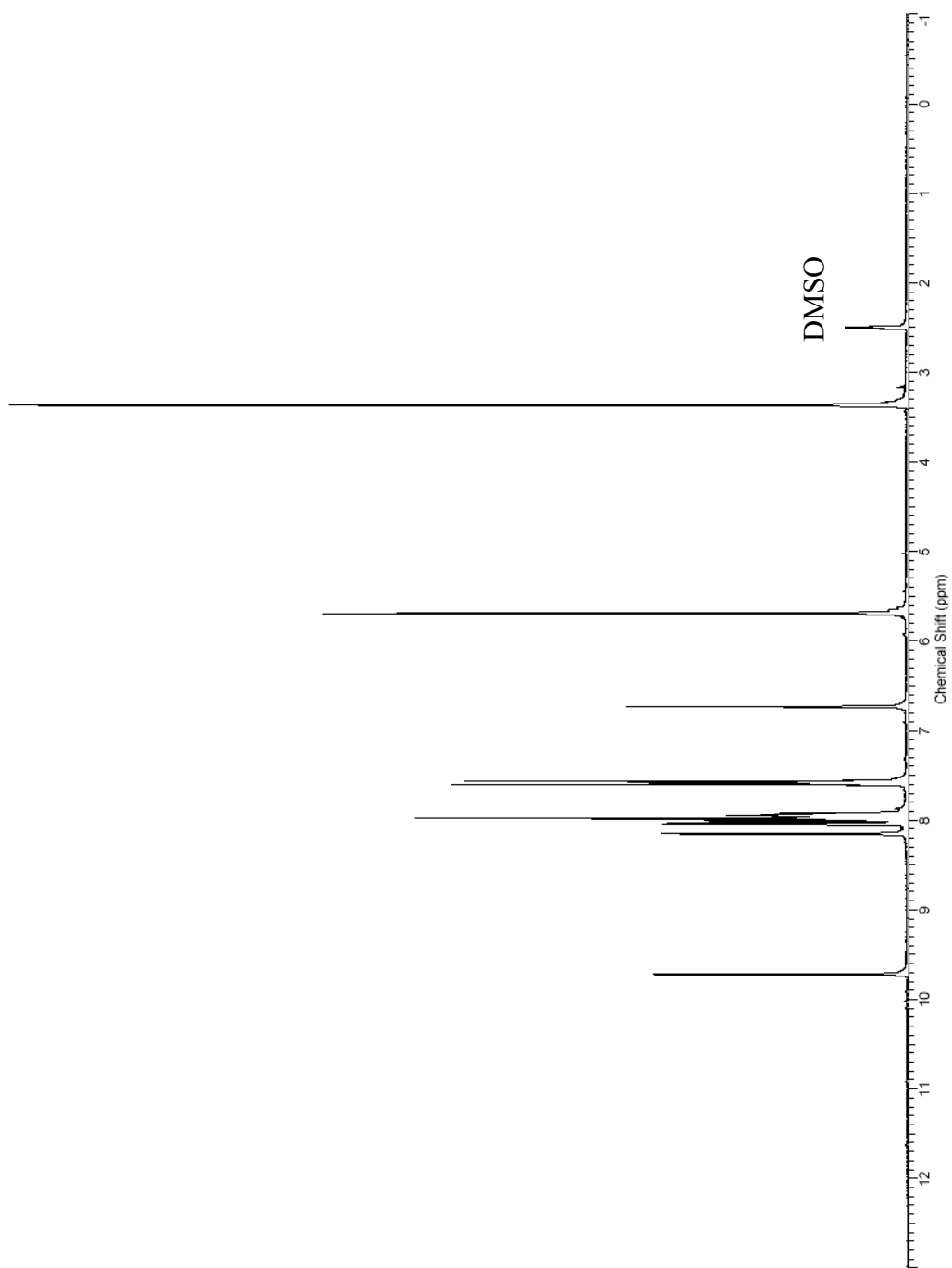


Figure 2-2. ^1H NMR spectrum of $\mathbf{1}[\text{Br}]_2$ in d_6 -DMSO.

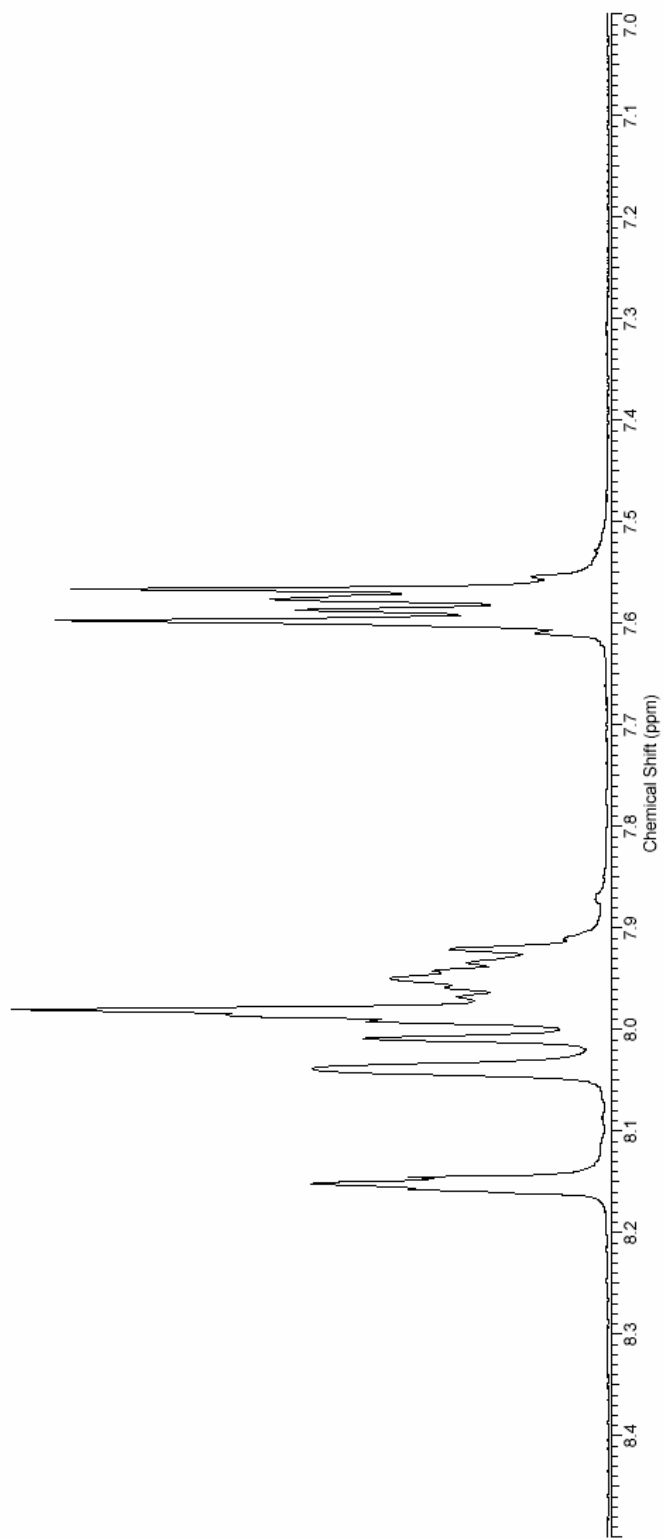


Figure 2-3. ^1H NMR spectrum of **1**[Br]₂ in d_6 -DMSO. Expansion of aromatic region.

Excess ammonium hexafluorophosphate was added to a sample of $\mathbf{1}[\text{Br}]_2$ in water affording a $\mathbf{1}[\text{PF}_6]_2$ as a white solid. Single crystals of $\mathbf{1}[\text{PF}_6]_2$ suitable for X-ray crystallography were grown via slow evaporation from a concentrated sample in acetonitrile. The thermal ellipsoid plot of the dicationic portion of $\mathbf{1}[\text{PF}_6]_2$ is depicted in Figure 2-4. The asymmetric unit contains half of the dicationic portion of $\mathbf{1}[\text{PF}_6]_2$ along with one hexafluorophosphate anion. Carbon atom C1 occupies the special position $(1/2, y, 1/4)$ with 2 fold symmetry. The planes formed by the imidazole rings are nearly orthogonal to those of the naphthalene rings (89.1°).

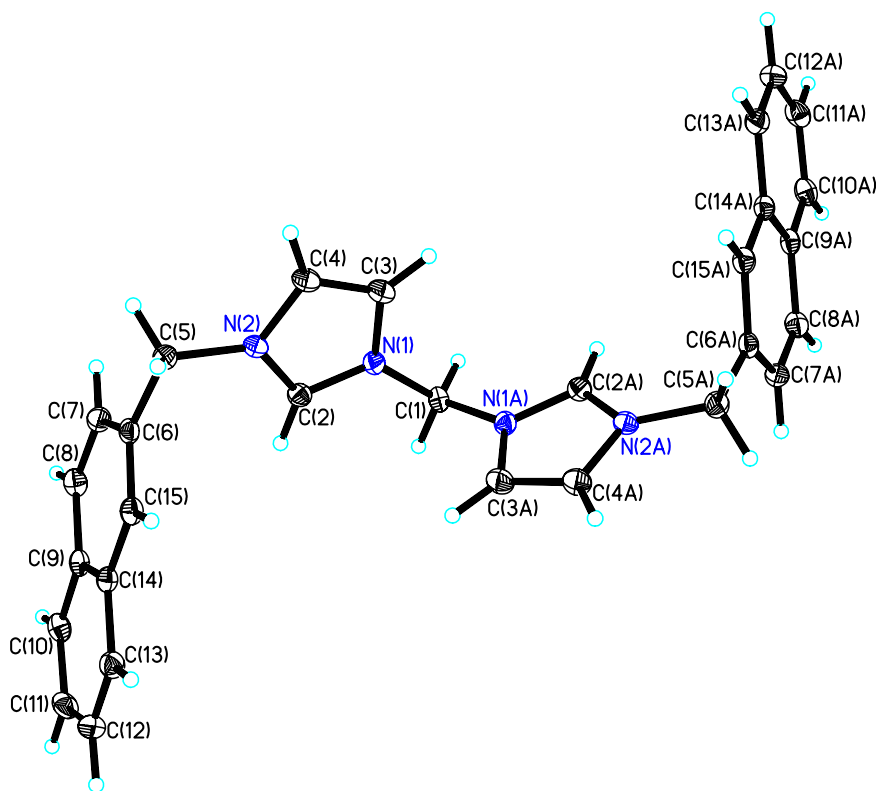


Figure 2-4. Thermal ellipsoid plot of the dicationic portion of $\mathbf{1}[\text{PF}_6]_2$ with thermal ellipsoids drawn at 50% probability.

Bisimidazolium salt **1**[PF₆]₂ shows the presence of a hydrogen-bonding in the solid state crystal structure, shown in Figure 2-5. A short donor acceptor distance exists between the imidazolium carbon of and a fluorine atom of the corresponding PF₆⁻ anion (C...F ≈ 3.18 Å).

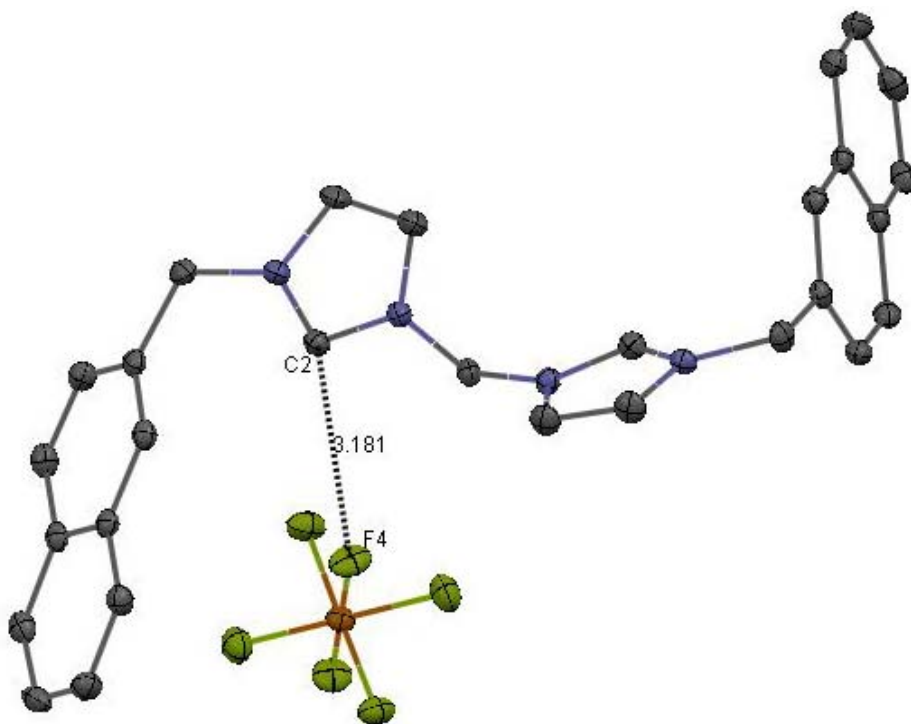
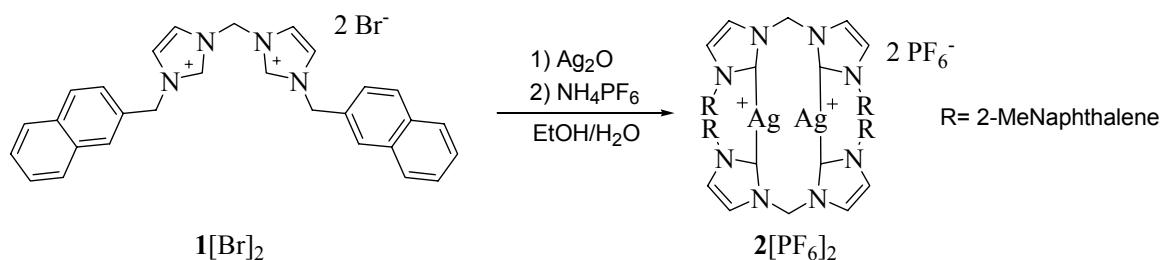


Figure 2-5. Thermal ellipsoid plot depicting the hydrogen bonding of **1**[PF₆]₂ with thermal ellipsoids shown at 50% probability.

The reaction of **1**[Br]₂ with Ag₂O in a mixture of ethanol/water at 60 °C for 3 hours results in the formation of **2**[Br]₂. Following filtration of excess Ag₂O and AgBr an excess amount of NH₄PF₆ can be added to the filtrate to afford silver complex **2**[PF₆]₂ as a white solid in 97% yield, Equation 2-3. Converting to the PF₆ salt of the silver complex appears to increase the complexes stability to light and moisture. The complex is

decomposes in solution but as a solid it is stable for months in the absence of light. This is an attribute previously observed with similar complexes.^{78,85}



Equation 2-3. Synthesis of the sterically shielded silver NHC complex $2[\text{PF}_6]_2$.

The ^1H NMR spectrum of silver complex $2[\text{PF}_6]_2$, shown in Figures 2-6 and 2-7, gives resonances at ca. δ 4.9 (s, 8H, N-CH₂-Naphthalene), 5.8 (s, 4H, N-CH₂-N), 7.0 (d, 4H, $J = 8.4$ Hz naphthalene), 7.2 (s, 4H, CH), 7.3 (s, 4H, CH), 7.4 – 7.5 (m, 12H), 7.5 (d, 4H, $J = 7.8$ Hz naphthalene), 7.6 (d, 4H, 8.4Hz naphthalene), 7.7 (d, 4H, $J = 7.8$ Hz naphthalene). As in the case of the starting salt $1[\text{Br}]_2$ the assignment of all of the imidazole and naphthalene resonances was nearly impossible because of the large amount of overlap in the aromatic region of the spectrum. The most important feature of the ^1H NMR spectrum is the absence of the resonance of the imidazolium hydrogen atoms at ca. 9 ppm. The absence of this resonance can be used as an indication for the formation of a silver carbene.^{9,35,26,37,77,78}

The ^{13}C NMR spectrum shows an absence of the C(2) carbon resonance at ca. 138 ppm. A peak corresponding to the resonance of the carbene carbon atom was not observed. This phenomenon is not without precedence in the literature, and has been observed for chemically similar complexes.^{9,26,78} The absence of this resonance can be explained by the fluxional behavior of the silver carbene bond in solution.

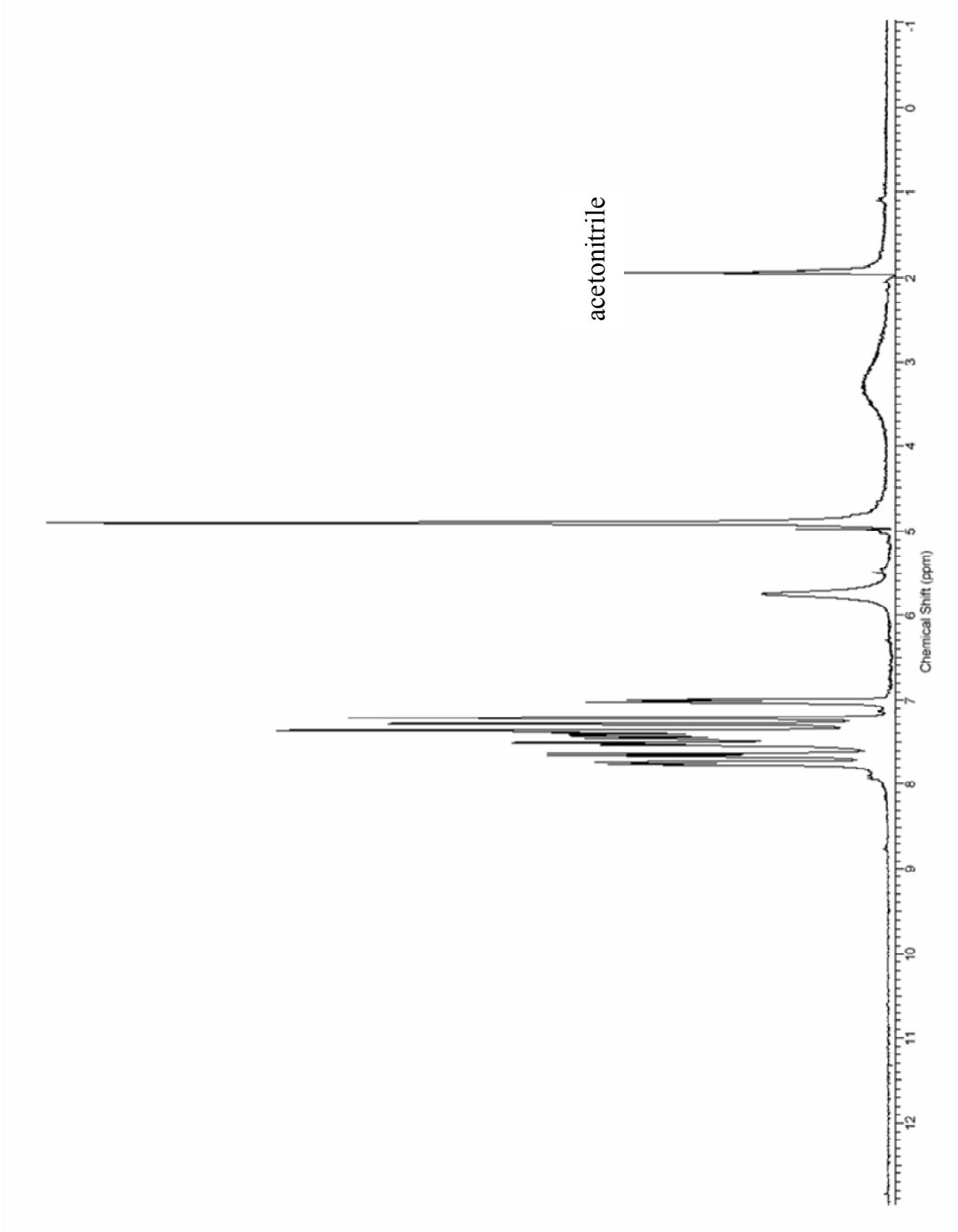


Figure 2-6. ^1H NMR spectrum of $2[\text{PF}_6]_2$ in d_3 -acetonitrile.

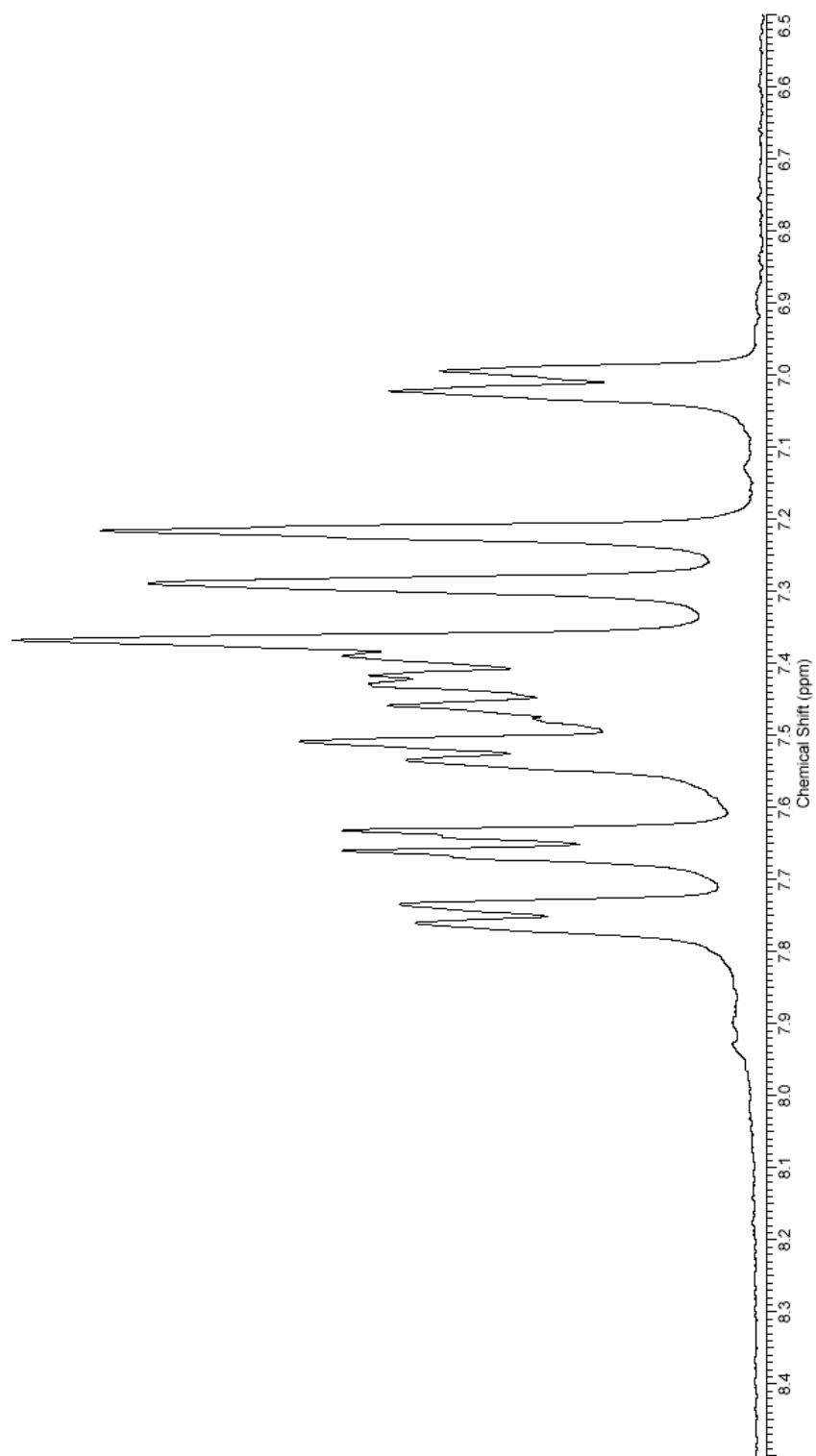
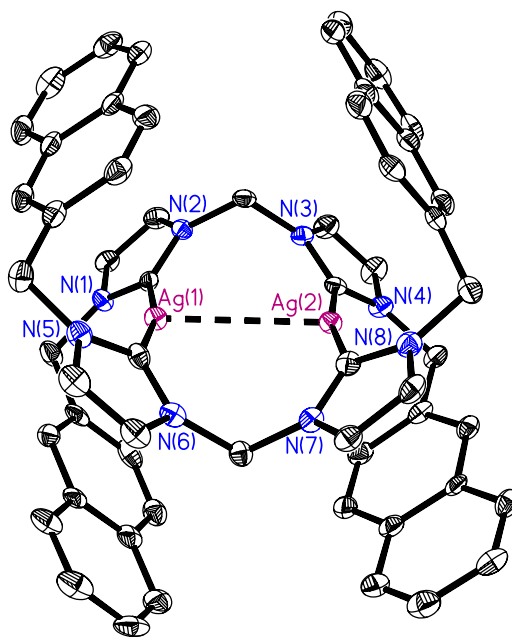


Figure 2-7. ^1H NMR spectrum of $2[\text{PF}_6]_2$ in d_3 -acetonitrile. Expansion of aromatic region.

Crystals of $2[\text{PF}_6]$ suitable for single crystal X-ray diffraction studies were grown from a concentrated sample in a mixture of acetonitrile and water. The asymmetric unit consists of one dicationic silver biscarbene, two hexafluorophosphate anions and two acetonitrile solvent molecules. Compound $2[\text{PF}_6]$, depicted in Figure 2-8, forms a “shell-like” structure with the naphthalene rings shielding the silver core, Figure 2-7. The asymmetric unit has four silver N-heterocyclic carbene bonds ranging from 2.095(4) – 2.100(4) Å. The carbene-Ag-carbene bond angles deviate significantly from linearity with angles ranging from 168.00(15) – 168.67(15)°. The reason for this deviation is likely due to the restriction of the linking methylene group upon the N-heterocyclic carbene rings.

The structure also contains a short intramolecular Ag-Ag interaction of 3.2440(5) Å which is shorter than twice the van der Waals radius (3.40 Å). This distance is consistent with a previously reported bisimidazole based silver complex.⁸⁶ Ag-Ag distances shorter than 3.40 Å are considered to be diagnostic for “argentophilic” interactions.⁸⁷ The exact make up of the orbital contacts for these interactions have not yet been fully determined.

a)



b)

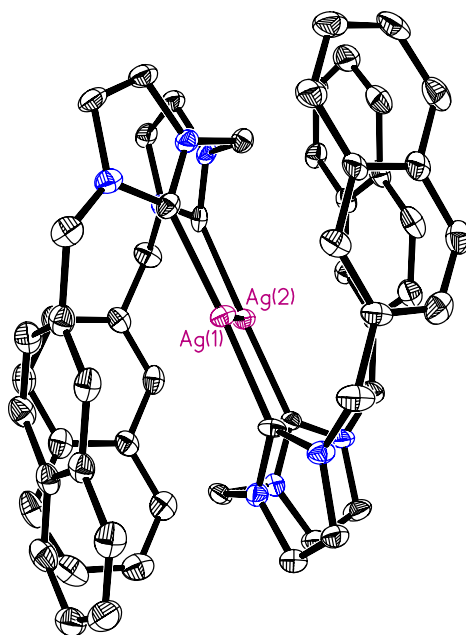


Figure 2-8. Thermal ellipsoid plots of 2[PF₆] with hydrogen atoms removed for clarity. Thermal ellipsoids shown at 50% probability. a) top view, b) side view.

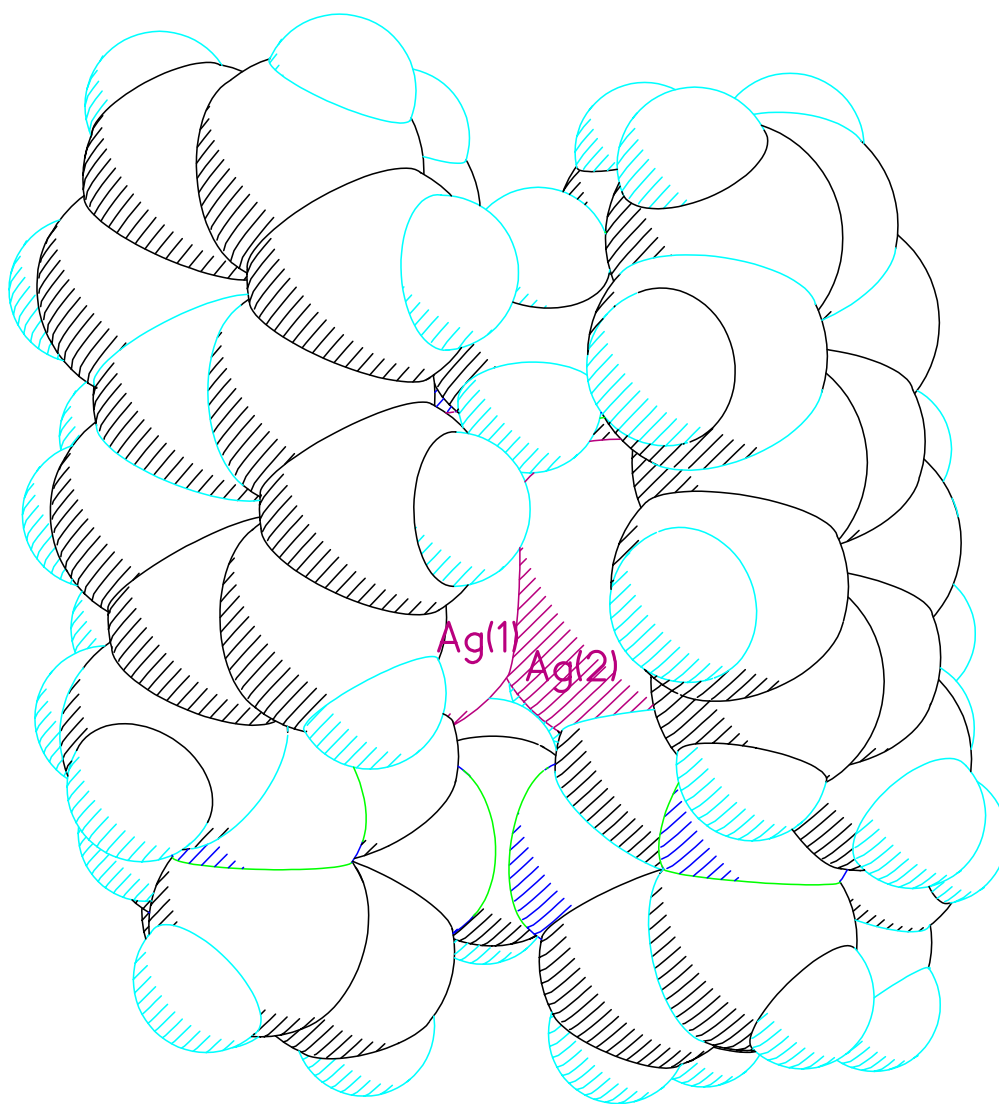


Figure 2-9. Space filling model of depicting the shielding of the silver core of complex $2[PF_6]$.

2.3 Synthesis and Characterization of an Electronically Stabilized Silver N-Heterocyclic Carbene Complexes

The syntheses of electronically stabilized silver NHC complexes of methylated caffeine have recently been reported.^{51,85} Based upon these studies it was determined that xanthine derivatives in general could serve as useful building blocks for such complexes. Theobromine, Figure 2-10, is one such derivative and, like caffeine, is a naturally produced molecule, commonly often found in chocolate. The advantage of using theobromine is the availability of the N(1) position for substitution. When deprotonated the N(1) position of theobromine is a much better nucleophile than the N(9) position which aids in the isolation of singular substitution products.

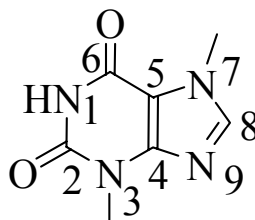
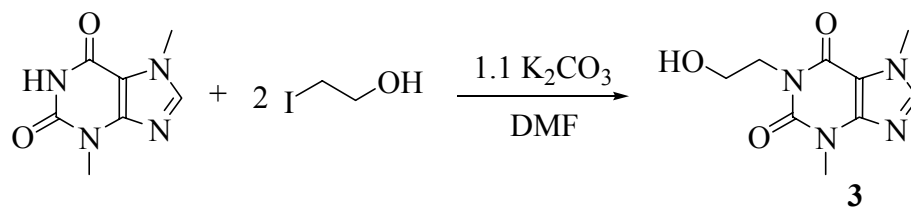


Figure 2-10. Structure and numbering scheme for theobromine.

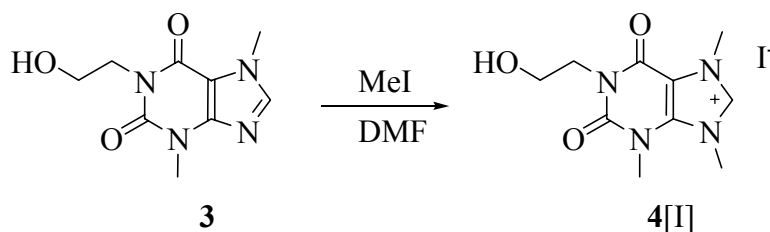
The condensation of 2-iodoethanol with theobromine in refluxing DMF results in the formation of 1-hydroxyethyl-3,7-dimethylxanthine (**3**) in approximately 68% yield, Equation 2-4. It was determined that the use of K_2CO_3 as a base gave the best product yields and eliminated side products generated by the use of stronger bases. The pure compound can be isolated by recrystallization from cold methanol.



Equation 2-4. Synthesis of 1-hydroxyethyl-3,7-dimethylxanthine **3**.

The TOF-MS-EA⁺ spectrum shows **3**[Na]⁺ (C₉H₁₂N₄O₃Na) at m/z 247 (C₉H₁₂N₄O₃Na; calculated m/z 247). The ¹H and ¹³C NMR spectra of **3** are consistent with the proposed structure (the ¹H NMR of **3** is given in Figure 2-9). The ¹H NMR gives resonances at ca. δ 3.4 (s, 3H, CH₃), 3.7 (t, 2H, CH₂), 3.8 (s, 3H, CH₃), 4.0 (t, 2H, CH₂), 7.8 (s, 1H, CH).

The synthesis of 1-hydroxyethyl-3,7,9-trimethylxanthinium iodide **4**[I] is illustrated in Equation 2-5. The reaction of excess iodomethane with **3** at 100 °C in DMF affords **4**[I] as an off white solid. The TOF-MS-EA⁺ spectrum shows **4**⁺ (C₁₀H₁₅N₄O₃) at m/z 239 (C₁₀H₁₅N₄O₃; calculated m/z 239). The ¹H and ¹³C NMR spectra of **4**[I] are consistent with the proposed structure (the ¹H NMR of **3** is given in Figure 2-11). The ¹H NMR consists of resonances at ca. δ 3.8 (m, 5H), 4.0 (s, 3H, CH₃), 4.1 (m, 5H), 8.9 (s, 1H, C⁺-H). The notable features of the ¹H NMR spectrum of **4**[I], shown in Figure 2-12, are the downfield shift of the methyl and ethyl resonances, the addition of a third methyl resonance, and the shift of the C(8) hydrogen to ca. 9 ppm.



Equation 2-5. Synthesis of xanthinium salt **4**[I].

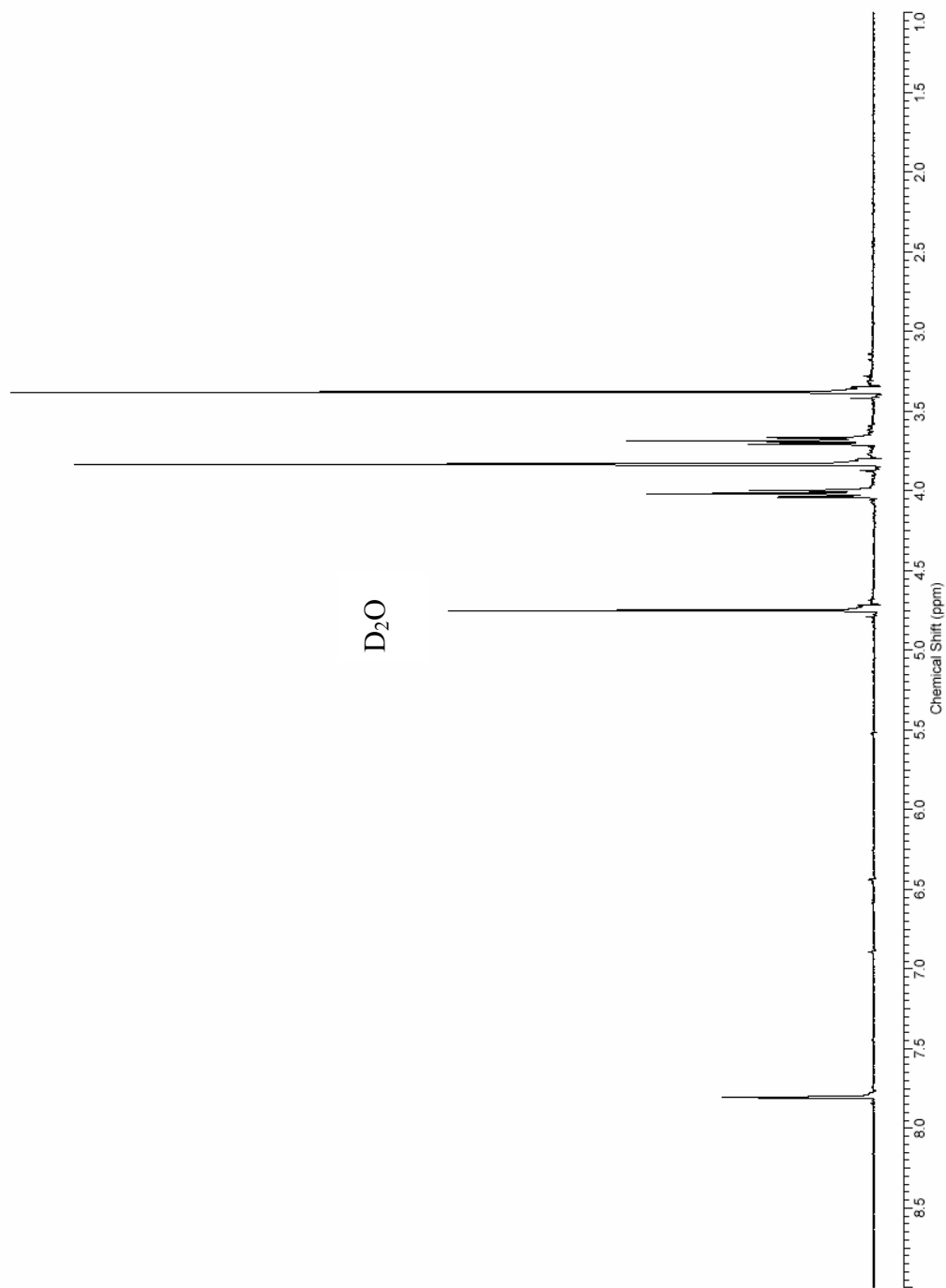


Figure 2-11. ^1H NMR spectrum of **3** in D_2O .

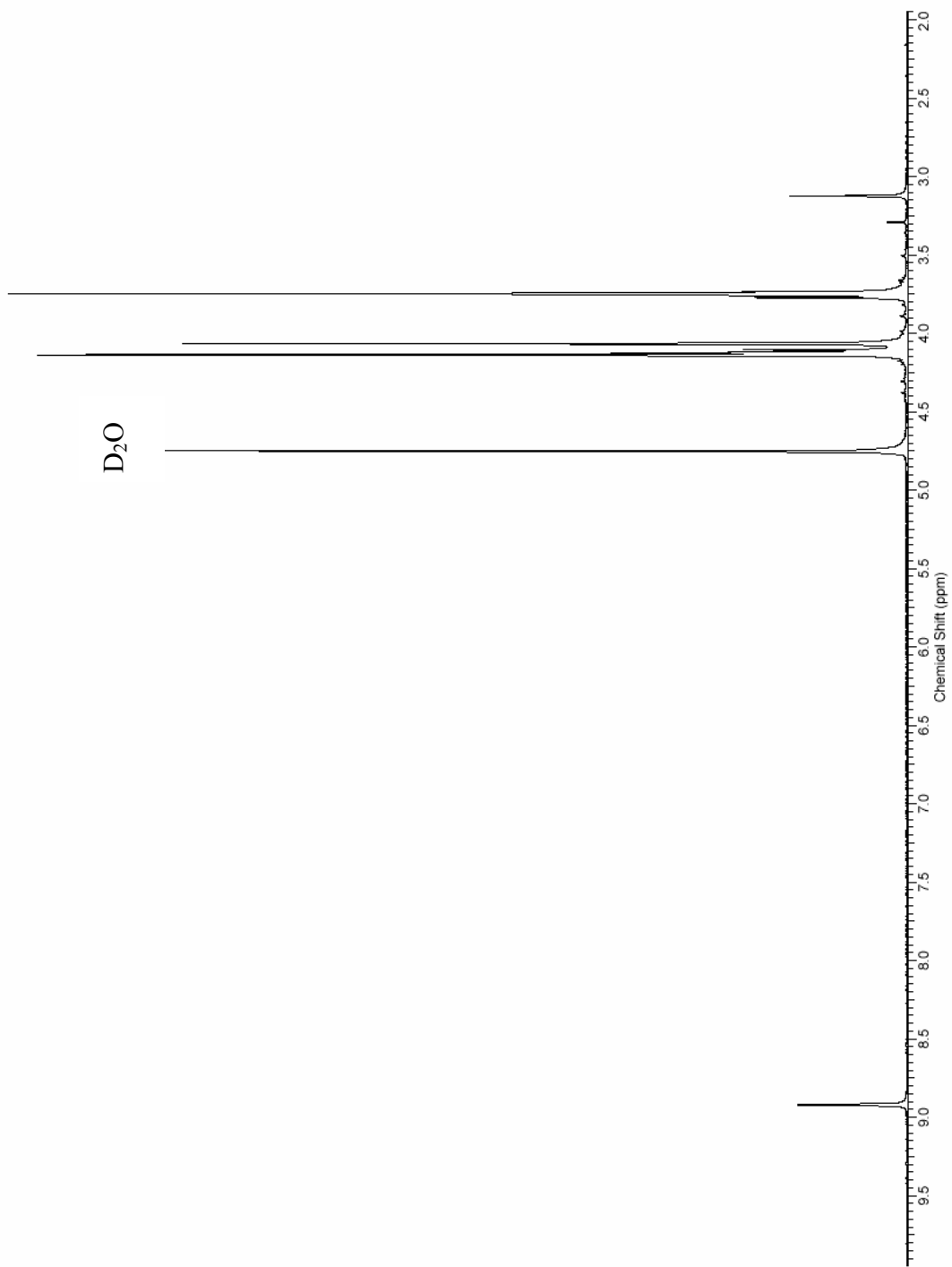


Figure 2-12. ^1H NMR spectrum of 4[I] in D_2O .

Crystals of **4**[I] suitable for single crystal X-ray diffraction studies were grown by slow evaporation from a concentrated sample in methanol. The structure of the cationic portion of **4**[I] is shown in Figure 2-13. The asymmetric unit contains one 1-hydroxyethyl-3,7,9-trimethylxanthinium cation and one iodide anion. Compound **4**[I] packs with intermolecular hydrogen bonds. A short donor acceptor distance exists between the between the xanthinium carbon atom and the iodide anion ($C \cdots I \approx 3.85 \text{ \AA}$) as shown in Figure 2-14.

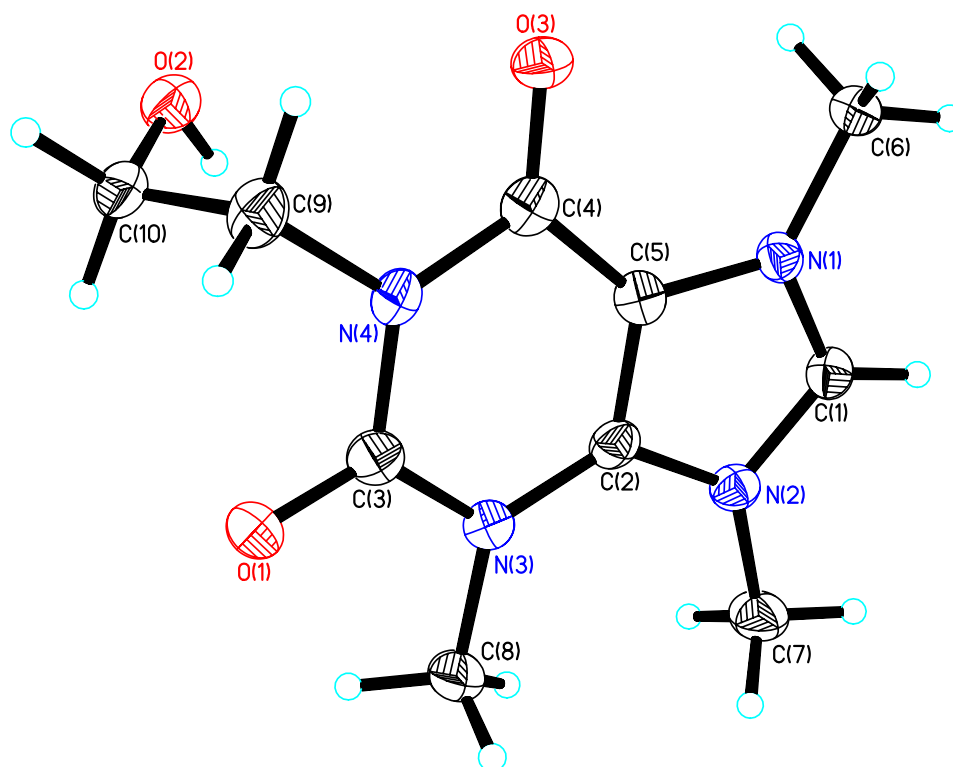


Figure 2-13. Thermal ellipsoid plot of the cationic portion of **4**[I]. Thermal ellipsoids shown at 50% probability.

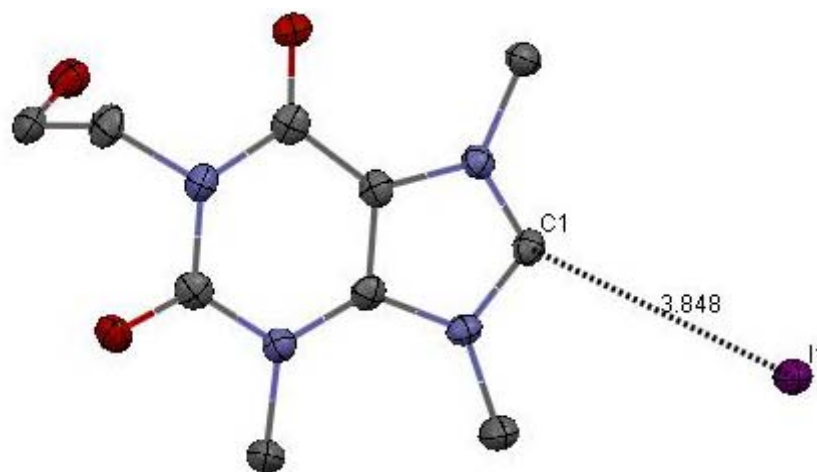
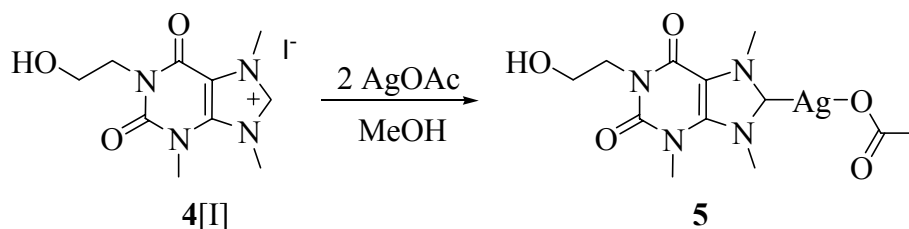


Figure 2-14. Thermal ellipsoid plot depicting the hydrogen bonding of **4**[I]. Thermal ellipsoids shown at 50% probability.

The synthesis of silver NHC complex **5** is illustrated in Equation 2-6. The addition of two equivalents of silver acetate to **4**[I] in methanol affords silver NHC complex **5** as a white solid in moderate yield 40%. Compound **5** generates the cationic silver monocarbene (loss of acetate) as well as the cationic silver biscarbene in the gas phase. The TOF-MS-EA⁺ spectrum of **5** shows the monocarbene (C₁₀H₁₄N₄O₃Ag) at m/z 345/347 (C₁₀H₁₄N₄O₃Ag; calculated m/z 345/347) and the biscarbene at m/z 583/585 (C₂₀H₂₈N₈O₆Ag; calculated m/z 583/585).



Equation 2-6. Synthesis of silver NHC **5**.

The ^1H NMR spectrum of **5** consists of resonances at ca. δ 1.85 (s, 3H, CH_3 acetate), 3.73 (m, 5H), 3.99 (s, 3H, CH_3), 4.08 (m, 2H, CH_2), 4.13 (s, 3H, CH_3). Only very minor upfield shifts are observed when compared to the precursor **4**[I], however the shift is significant enough to give separation between the hydrogen atoms of one of the methyl groups and the methylene hydrogen atoms of the ethanol chain. The most important feature of the ^1H NMR spectrum is the absence of the xanthinium hydrogen resonance at ca. 9 ppm. A resonance corresponding to the resonance of the carbene carbon atom was not observed, which is consistent with structurally similar complexes.⁵¹

The stability of **5** in aqueous media was studied by ^1H and ^{13}C NMR. The decomposition of **5** in D_2O was monitored for one week. From these studies it appears that silver complex **5** decomposes over several days in water in the absence of light. After nine hours, the ^1H NMR spectrum shows several new resonance peaks upfield of those originally observed for **5**. In 4 days nearly all of the silver complex has decomposed and by 7 days is no longer observed in the ^1H (Figure 2-15) or ^{13}C NMR spectrum (Figure 2-16). The most notable features of the ^{13}C NMR spectrum after 7 days are the formation of two resonance peaks at ca. 91 and 95 ppm, the shift of the carbonyl carbon atoms, and the doubling of all of the resonance peaks. From the ^{13}C NMR spectrum it is clear that the decomposition product is not the xanthinium starting compound.

In order to further identify the decomposition product the D_2O was allowed to evaporate from the NMR sample. This resulted in the isolation of a crystalline material and a waxy solid. The crystals were confirmed to be silver acetate by X-ray crystallography. The sample was redissolved in D_2O and NaCl was added to precipitate

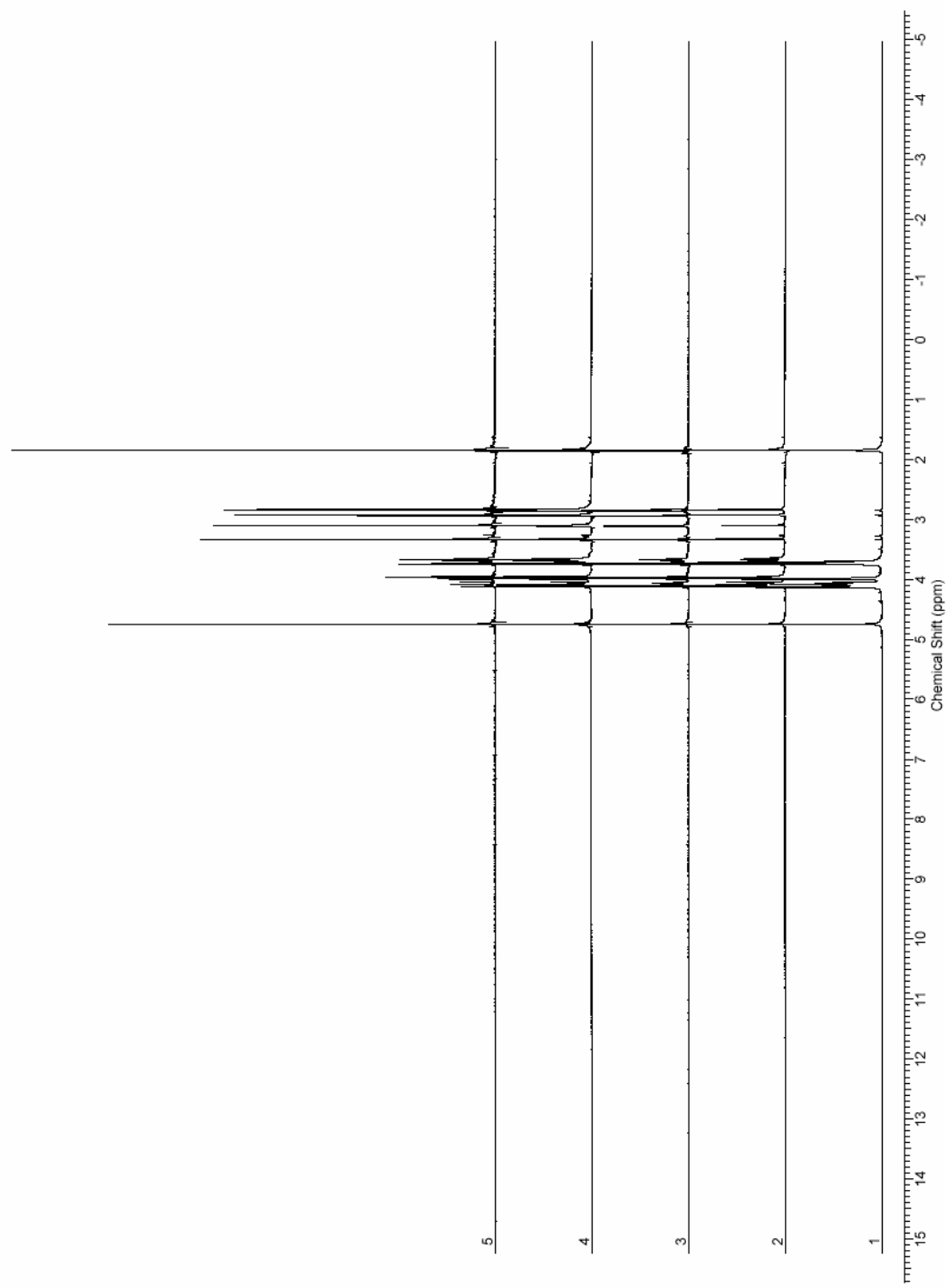


Figure 2-15. Stack plot of the ¹H NMR spectra of silver complex **5** in D₂O. 1) 9 h 2) 12 h 3) 1.7 d 4) 4 d 5) 7 d

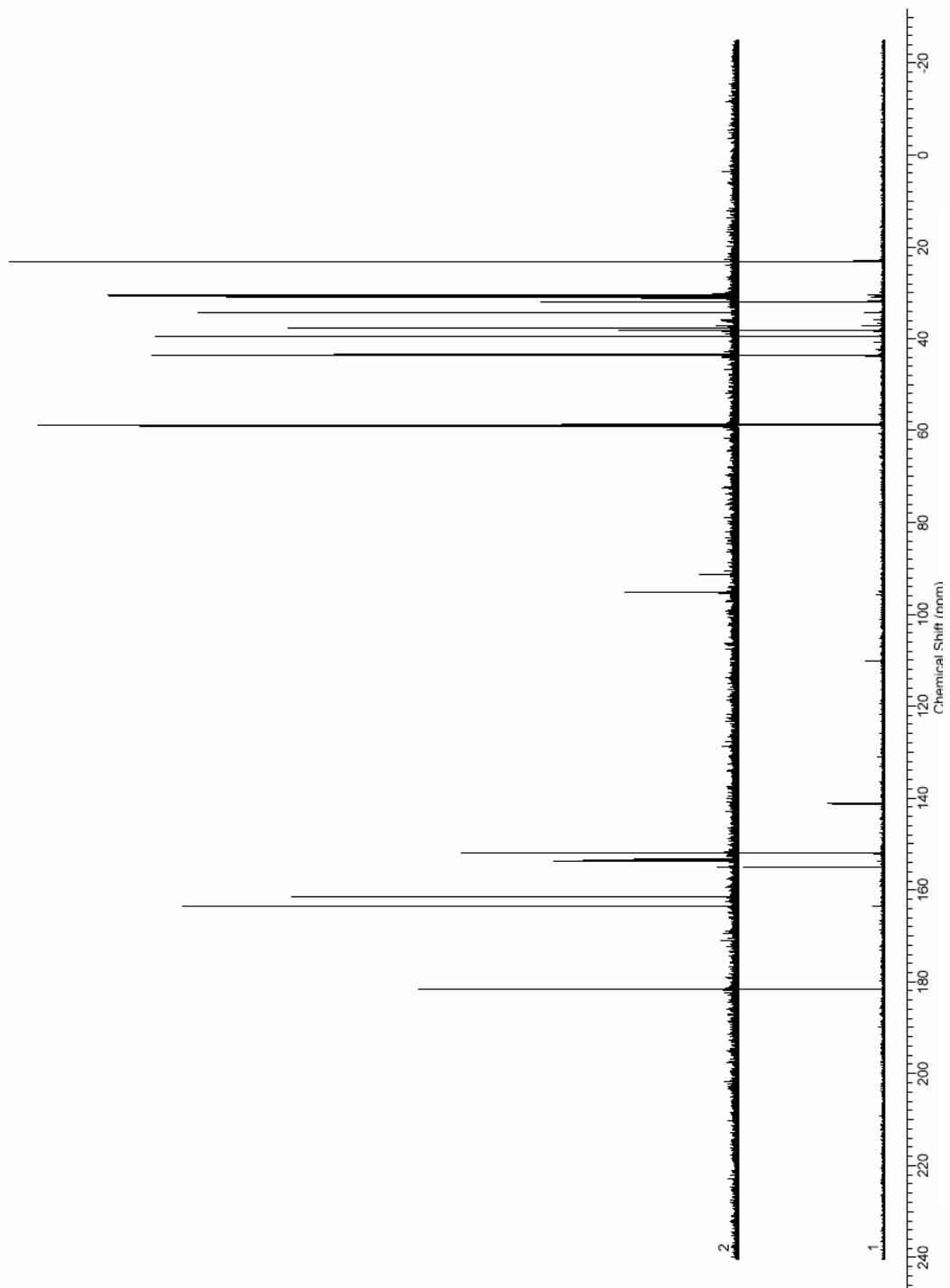


Figure 2-16. Stack plot of ^{13}C NMR spectra of silver complex **5** in D_2O . 1) 9h 2) 7 d.

AgCl from solution. After filtration of AgCl a ^1H NMR spectrum was collected, Figure 2-17. The NMR sample was then analyzed by mass spectrometry. The ES-MS⁺ spectrum shows peaks at m/z 541, 282, and 262. These correspond to the proposed structures given in Figure 2-18.

Crystals of **5** suitable for single crystal X-ray diffraction studies were grown by slow evaporation from a concentrated sample in methanol, Figure 2-19. The asymmetric unit contains one full molecule of silver complex **5**. The silver atom in complex **5** is bonded to the carbene carbon atom (C1-Ag1 = 2.072(4) Å) and one of the oxygen atoms of the acetate counter ion (O4-Ag1 = 2.118(3) Å). The geometry at the silver is nearly linear with a C1-Ag1-O4 bond angle of 175.89(12)°. The solid state structure of complex **5** also shows a short intermolecular Ag-Ag interaction of approximately 3.2 Å, which is shorter than the sum of the two van der Waals radii of the silver atoms, Figure 2-20.

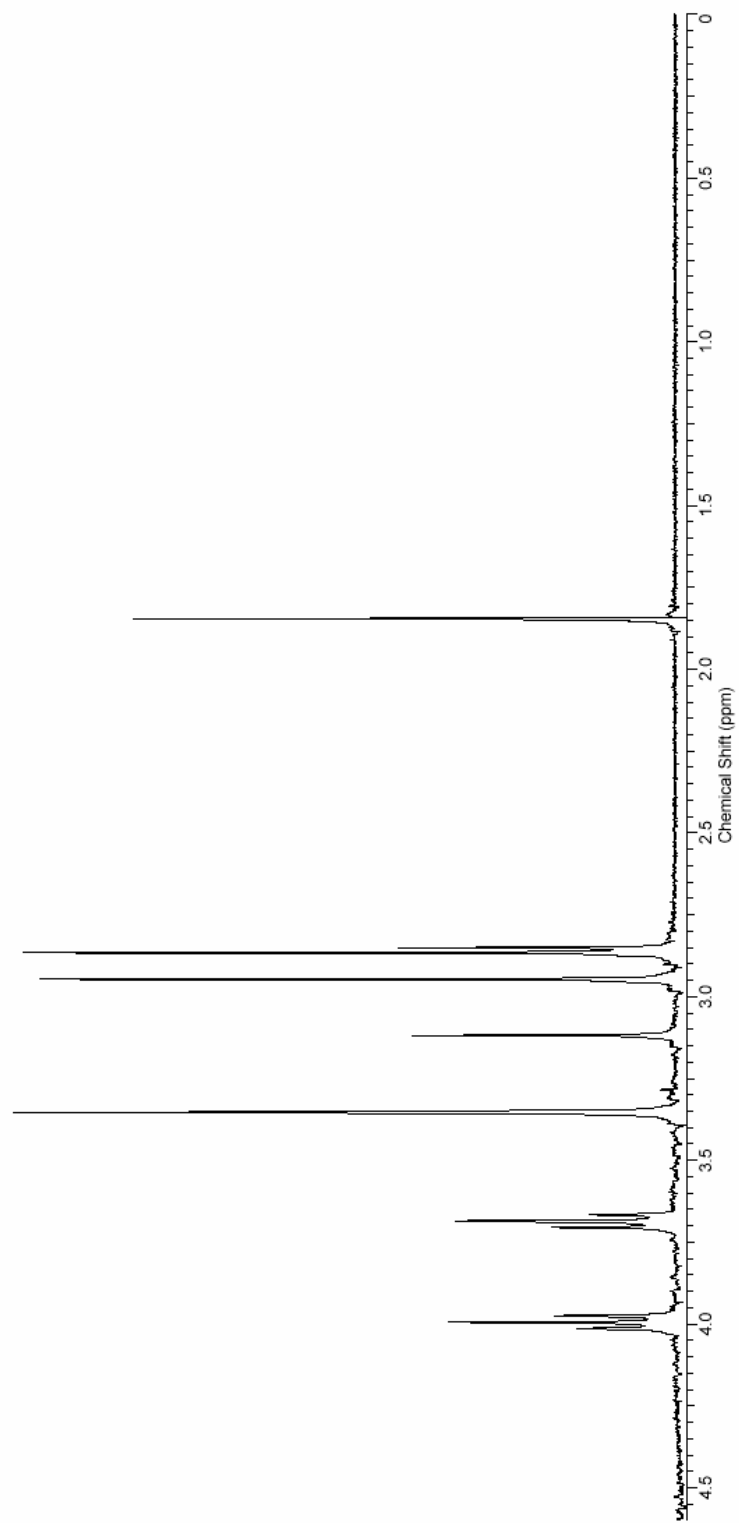


Figure 2-17. ^1H NMR spectrum of the decomposition product of **5** in D_2O .

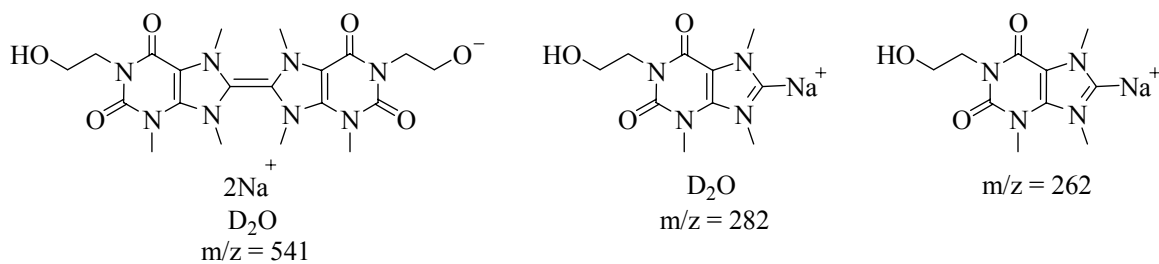


Figure 2-18. Proposed structures of the decomposition products of **5** based upon EA-MS.

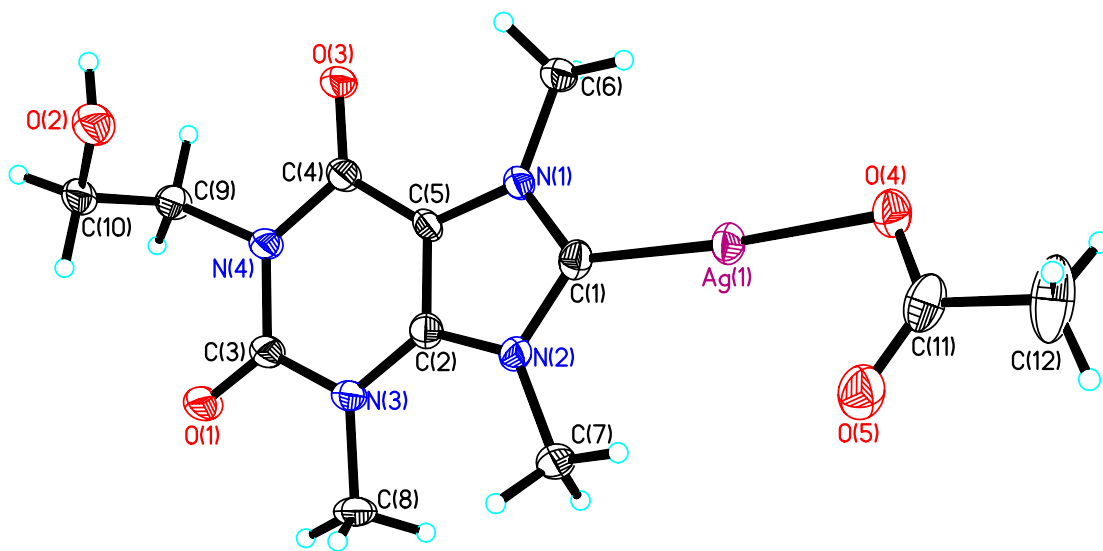


Figure 2-19. Thermal ellipsoid plot of silver complex **5** with thermal ellipsoids shown at 50% probability.

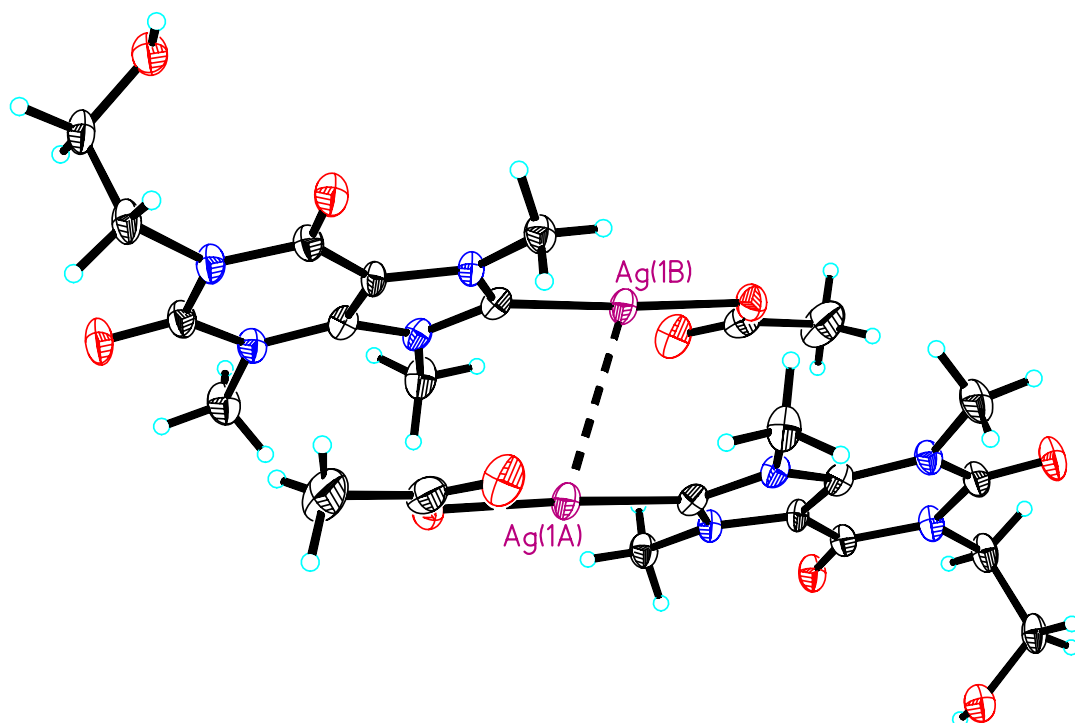


Figure 2-20. Thermal ellipsoid plot of complex **5** depicting the intermolecular Ag-Ag interaction. Thermal ellipsoids shown at 50% probability.

2.4 Conclusions

In order to make silver NHC complexes viable candidates for antimicrobial use their stability must be increased. Silver complex **2**[PF₆]₂ makes use of steric shielding to protect the silver atoms from attack by advantageous halides or protons. In the crystalline form the two silver atoms of **2**[PF₆]₂ have a close interatomic distance of ~ 3.2 Å, which is considered to be an argentophilic interaction. Although stable in the solid state, this silver complex is unstable in solution.

Silver complex **5** is based upon modified theobromine. Theobromine is a naturally occurring xanthine derivative most typically isolated from chocolate. Complex **5** has significantly increased stability to light and aqueous solution. The stability is comparable

to that of the silver NHC complex of methylated caffeine.^{50,51} The major difference between the two complexes is the increased water solubility of **5** due to its incorporation of an alcohol side chain. It is believed that both of these silver complexes are stabilized by the electron withdrawing groups that are covalently bound to the NHC.

2.5 Experimental Section

2.5.1 General Considerations

Imidazole, ammonium hexafluorophosphate, and silver acetate were purchased from Aldrich and used as received. 2-(bromomethyl)naphthalene, iodoethanol, iodomethane, and theobromine were purchased from Alfa Aesar and used as received. All solvents were purchased from Fisher Scientific and used without further purification. All reactions were carried out under aerobic conditions. ^1H and ^{13}C NMR data were obtained using a Varian Mercury 300 MHz instrument. The spectra were referenced to deuterated solvents. Elemental analyses were performed by the University of Illinois microanalysis laboratory. Mass spectrometry analyses were performed by the Ohio State University mass spectrometry and proteomics facility.

2.5.2 X-ray Structure Determination Details

Data sets were collected on a Bruker Apex CCD diffractometer with graphite-monochromated Mo $K\alpha$ radiation ($\lambda = 0.71073 \text{ \AA}$). Unit cell determination was achieved by using reflections from three different orientations. An empirical absorption correction and other corrections were done using multi-scan SADABS. Structure solution, refinement and modeling were accomplished using the Bruker SHELXTL package.⁸⁸ The structure was obtained by full-matrix least-squares refinement of F^2 and the selection of appropriate atoms from the generated difference map.

2.5.3 Synthesis of 1,1'-methylene bis(imidazole) (C₇H₈N₄)

To a 1 L flask was added imidazole (34.04 g, 500 mmol), KOH (56.11 g, 1 mol) in dichloromethane (500 mL). The solution was refluxed for 12 hours after which time the solvent was decanted and the volatiles removed to afford 1,1'-methylene bis(imidazole) as a white solid. The solid was washed with ether and dried. Dichloromethane (500 mL) was then added to the solid crude remaining in the reaction flask and the solution was refluxed. This process was repeated two additional times. Yield: 23.92 g, (64.6%). Mp: 167-168 °C. ¹H NMR (300 MHz, D₂O): δ 6.09 (s, 2H, CH₂), 6.90 (s, 2H, CH), 7.12 (d, 2H, *J* = 1 Hz, CH), and 7.79 (s, 2H, CH). ¹³C{¹H} NMR (75 MHz, D₂O): δ 56.1 (CH₂), 119.4 (CH), 128.9 (CH), 137.8 (CH).

2.5.4 Synthesis of **1**[Br]₂ (C₂₉H₂₆N₄Br₂)

To a 50 mL flask was added 1,1'-methylene bis(imidazole) (0.74 g, 5 mmol) and 2-(bromomethyl)naphthalene (2.21 g, 10 mmol) in butyl alcohol (10 mL). The solution was brought to reflux for 2 hours in which time a precipitate formed. The solid was filtered and washed with THF to afford **1**[Br]₂ as an off white solid. Yield: 2.19 g, (74.2%). Mp: 310-313 °C. Anal. Calcd. for C₂₉H₂₆N₄Br₂: C, 59.18; H, 4.46; N, 9.53. Found: C, 58.58; H, 4.45; N, 9.25. ¹H NMR (300 MHz, *d*₆-DMSO): δ 5.7 (s, 4H, N-CH₂-naphthalene), 6.7 (s, 2H, N-CH₂-N), 7.6 (m, 6H, CH), 7.9 (m, 8H, CH), 8.0 (s, 2H, CH), 8.2 (s, 2H, CH), 9.7 (s, 2H, N-CH-N). ¹³C{¹H} NMR (75 MHz, *d*₆-DMSO): δ 52.5

(CH₂), 58.2 (CH₂), 122.5, 123.3, 126.0, 126.7, 126.8, 127.7, 127.9, 128.0, 128.8, 131.6, 132.7, 132.8, 137.9 (Aromatic). TOF-MS-EA⁺: m/z 511 (M⁺ of C₂₉H₂₆N₄Br).
 X-ray crystal structure analysis of **1**[PF₆]₂: formula C₂₉H₂₆F₁₂N₄P₂, *Mw* = 720.48, colorless crystal 0.28 x 0.20 x 0.07 mm, *a* = 33.719(4) Å, *b* = 5.9540(7) Å, *c* = 14.3469(17) Å, α = 90°, β = 97.050(2)°, γ = 90°, *V* = 2858.6(6) Å³, *D*_{calc} = 1.674 Mg cm⁻³, μ = 0.261 mm⁻¹, *Z* = 4, monoclinic, space group *C2/c* (No. 15), λ = 0.71073 Å, *T* = 100 K, ω and φ scans, 12206 reflections collected, 3444 independent (*R*_{int}) 0.0313, 213 refined parameters, *R*₁/*wR*₂ (*I* ≥ 2σ(*I*)) = 0.0482 / 0.1202 and *R*₁/*wR*₂ (all data) = 0.0603 / 0.1341, maximum (minimum) residual electron density 0.531 (-0.348) e Å⁻³, all hydrogen atoms were calculated and refined as riding atoms.

2.5.5 Synthesis of **2**[PF₆] (C₅₈H₄₈N₈Ag₂P₂F₁₂)

To a 100 mL flask was added **1**[Br]₂ (0.50 g, 0.85 mmol) and Ag₂O (0.21 g, 0.91 mmol) and ethanol/water (40 mL) (50:50). The reaction was heated at 60 °C for 3 hours. The solution was filtered over Celite. Excess NH₄PF₆ was added to the filtrate resulting in the precipitation of **2**[PF₆]₂ as a white solid. Addition of acetonitrile to a concentrated solution of **2**[PF₆]₂ in EtOH/H₂O afforded crystals suitable for X-ray analysis. Yield: 0.56 g, (96.7%). Mp: 190-192 °C. ¹H NMR (300 MHz, *d*₃-CD₃CN): δ 4.92 (s, CH₂), 5.77 (s, CH₂), 7.02 (d, CH), 7.24 (s, CH), 7.31 (s, CH), 7.39-7.48 (m, CH), 7.53 (d, CH), 7.65 (d, CH), 7.78 (d, CH). ¹³C {¹H} NMR (75 MHz, *d*₃-CD₃CN): δ 55.9 (CH₂), 65.3 (CH₂), 122.4, 124.7, 126.3, 127.8, 127.9, 128.1, 128.6, 128.7, 129.8, 133.9, 134.0, 134.6 (Aromatic).

X-ray crystal structure analysis of **2**[PF₆]₂: formula C₆₂H₅₄Ag₂F₁₂N₁₀P₂, *M_w* = 1444.83, colorless crystal 0.22 x 0.16 x 0.09 mm, *a* = 14.6559(12) Å, *b* = 19.6526(16) Å, *c* = 20.5800(16) Å, α = 90°, β = 96.132(2)°, γ = 90°, *V* = 5893.7(8) Å³, *D*_{calc} = 1.628 Mg cm⁻³, μ = 0.808 mm⁻¹, *Z* = 4, monoclinic, space group *P*2₁/*c* (No. 14), λ = 0.71073 Å, *T* = 100 K, ω and φ scans, 52254 reflections collected, 14175 independent (*R*_{int}) 0.0682, 795 refined parameters, *R*₁/*wR*₂ (*I* ≥ 2σ(*I*)) = 0.0594 / 0.1089 and *R*₁/*wR*₂ (all data) = 0.0888 / 0.1185, maximum (minimum) residual electron density 1.163 (-1.193) e Å⁻³, all hydrogen atoms were calculated and refined as riding atoms.

2.5.6 Synthesis of 1-hydroxyethyl-3,7-dimethylxanthine **3** (C₉H₁₂N₄O₃).

To a 500 mL round bottom flask was added theobromine (9.0 g, 50 mmol) and K₂CO₃ (7.6 g, 55mmol) in DMF (150 mL). The solution was brought to reflux at which time 2-iodoethanol (3.9 mL, 50 mmol) was added. The solution was stirred for 1 h and an additional equivalent of 2-iodoethanol (3.9 mL, 50 mmol) was added. The reaction was then stirred at reflux for 17 h. DMF was removed and the crude material dissolved methanol and cooled to give **3** as colorless crystals. Yield: 7.62 g, (67.7%). Mp: 201-203 °C. C₉H₁₂N₄O₃: C, 48.19; H, 5.40; N, 25.00. Found: C, 48.00; H, 5.33; N, 24.25. ¹H NMR (300 MHz, D₂O) δ 3.38 (s, 3H, CH₃), 3.69 (t, 2H, CH₂), 3.83 (s, 3H, CH₃), 4.02 (t, 2H, CH₂), 7.80 (s, 1H, CH). ¹³C {¹H} NMR (75 MHz, D₂O) δ 29.9 (CH₃), 33.6 (CH₃), 43.0 (CH₂), 58.9 (CH₂), 107.7 (C), 143.7 (CH), 148.5 (C), 152.4 (C=O), 156.0 (C=O). TOF-MS-EA⁺: *m/z* 247 (M⁺ of C₉H₁₂N₄O₃Na).

2.5.7 Synthesis of 4[I] (C₁₀H₁₅N₄O₃I)

To a 50 mL round bottom flask was added **3** (3.66 g, 10 mmol) and iodomethane (5 mL, 80 mmol) in DMF (25 mL). The solution was heated at 150 °C for 18h with stirring. When cooled, acetone (200 mL) was added and the solution stirred vigorously. The xanthinium salt **4**[I] precipitated from solution and was collected as an off white solid. Yield: 1.09 g, (29.7%). Mp: 175-176 °C. C₁₀H₁₅N₄O₃I: C, 32.79; H, 4.13; N, 15.30. Found: C, 32.47; H, 4.00; N, 14.53. ¹H NMR (300 MHz, D₂O) δ 3.8 (m, 5H), 4.0 (s, 3H, CH₃), 4.1 (m, 5H), 8.9 (s, 1H, N-CH-N). ¹³C {¹H} NMR (75 MHz, D₂O) δ 32.1 (CH₃), 36.2 (CH₃), 37.6 (CH₃), 44.1 (CH₂), 58.6 (CH₂), 109.2 (C), 140.0 (CH), 151.6 (C=O), 154.8 (C=O). TOF-MS-EA⁺: m/z 239 (M⁺ of C₁₀H₁₅N₄O₃).

X-ray crystal structure analysis of **4**[I]: formula C₁₀H₁₅IN₄O₃, *M_w* = 366.16, colorless crystal 0.37 x 0.29 x 0.19 mm, *a* = 15.0967(18) Å, *b* = 10.4071(13) Å, *c* = 8.7080(10) Å, α = 90°, β = 104.119(2)°, γ = 90°, *V* = 1326.8(3) Å³, *D*_{calc} = 1.833 Mg cm⁻³, μ = 2.421 mm⁻¹, *Z* = 4, monoclinic, space group *P*2₁/*c* (No. 14), λ = 0.71073 Å, *T* = 100 K, ω and φ scans, 11589 reflections collected, 3212 independent (*R*_{int}) 0.0516, 167 refined parameters, *R*₁/*wR*₂ (*I* ≥ 2σ(*I*)) = 0.0448 / 0.1071 and *R*₁/*wR*₂ (all data) = 0.0565 / 0.1133, maximum (minimum) residual electron density 2.389 (-1.410) e Å⁻³, all hydrogen atoms were calculated and refined as riding atoms.

2.5.8 Synthesis of silver complex **5** (C₁₂H₁₇N₄O₅Ag)

Xanthinium salt **4**[I] (0.37 g, 1 mmol) and silver acetate (0.33 g, 2 mmol) were stirred at room temperature in methanol (40 mL) for 1.5h. The reaction was filtered over Celite to remove silver iodide and excess silver acetate. The solvent was removed and a small volume of 2-propanol was added to afford silver complex **5** as a white solid. Yield: 0.24 g, (40.3%). Mp: 212-214 °C. C₁₂H₁₇N₄O₅Ag: C, 35.64; H, 4.24; N, 13.86. Found: C, 35.48; H, 4.14; N, 13.40. ¹H NMR (300 MHz, D₂O) δ 1.85 (s, 3H, CH₃), 3.73 (m, 5H), 3.99 (s, 3H, CH₃), 4.08 (m, 2H, CH₂), 4.13 (s, 3H, CH₃). ¹³C {¹H} NMR (75 MHz, D₂O) δ 23.2 (CH₃), 32.0 (CH₃), 38.3 (CH₃), 39.5 (CH₃), 43.7 (CH₂), 58.7 (CH₂), 110.1 (C), 141.2 (C), 152.0 (C=O), 155.0 (C=O), 181.5 (C=O). TOF-MS-EA⁺: m/z 345/347 (M⁺ of C₁₀H₁₄N₄O₃Ag), m/z 583/585 (M⁺ of C₂₀H₂₈N₈O₆Ag).

X-ray crystal structure analysis of **5**: formula C₁₂H₁₇AgN₄O₅, *M*_w = 405.17, colorless crystal 0.43 x 0.08 x 0.07 mm, *a* = 23.896(3) Å, *b* = 8.2797(11) Å, *c* = 14.8598(19) Å, *α* = 90°, *β* = 94.104(2)°, *γ* = 90°, *V* = 2932.5(6) Å³, *D*_{calc} = 1.835 Mg cm⁻³, *μ* = 1.405 mm⁻¹, *Z* = 8, monoclinic, space group *C*2/*c* (No. 15), *λ* = 0.71073 Å, *T* = 100 K, *ω* and *φ* scans, 12470 reflections collected, 3512 independent (*R*_{int}) 0.0494, 204 refined parameters, *R*₁/*wR*₂ (*I* ≥ 2σ(*I*)) = 0.0447 / 0.0975 and *R*₁/*wR*₂ (all data) = 0.0624 / 0.1061, maximum (minimum) residual electron density 1.335 (-0.794) e Å⁻³, all hydrogen atoms were calculated and refined as riding atoms.

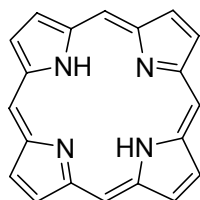
CHAPTER III

BISIMIDAZOLE BASED CYCLOPHANES

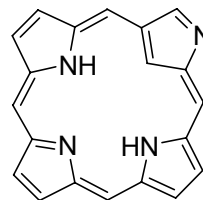
3.1 Introduction

In recent years our group^{35,37,40,89,90} and others^{91,92,93,94,95} have investigated the synthesis of imidazolium linked cyclophanes. Cyclophanes of this type are of interest because of their similarity to macrocycles such as N-confused porphyrins and porphyrinogens, shown in Figure 3-1.^{96,97,98,99} N-confused porphyrins are well known for their ability to complex to transition metals with varying coordination geometries and oxidation states. It is envisioned that the substitution of one or all of the pyrrole units of a porphyrin like molecule with imidazoles substituted at the 1 and 3 positions would serve as precursors to a new category of cyclophanes known as ‘carbene porphyrinoids.’ N-heterocyclic carbenes have been shown to form complexes with nearly every transition metal and many main group elements in a fashion similar to phosphines, however in almost all cases with increased stability.^{6,7,8} It is expected that ‘carbene porphyrinoids’ should combine the metal complexation properties associated with porphyrins, N-confused porphyrins and N-heterocyclic carbenes. Cyclic N-heterocyclic carbenes with a crown ether like structures have also recently been reported.^{100,101} These structures contain four N-heterocyclic carbene units for complexation of metal ions, and have been termed ‘carbacroons’.¹⁰⁰

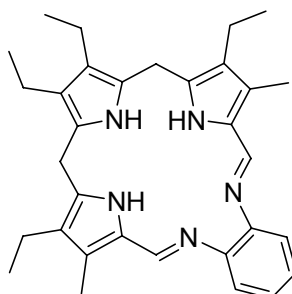
One of the most difficult challenges of designing a metal based pharmaceutical is creating ligand systems that bind strongly enough to the metal to protect it from dissociation in the body. Metal dissociation, especially in the case of radio-pharmaceuticals, can expose patients to serious harm. Tuning the ‘pocket’ size of the ligand is one potential way to increase the kinetic stability of a drug.^{89,102} This has been demonstrated in example by the ability of texaphyrins (expanded porphyrins) to stabilize lanthanides better than conventional porphyrins. Because of the strength of metal N-heterocyclic carbene bonds it is envisioned that cyclophanes containing such units and having varying cavity sizes would possess the properties necessary to avoid this dilemma.



Porphyrin



N-Confused Porphyrin

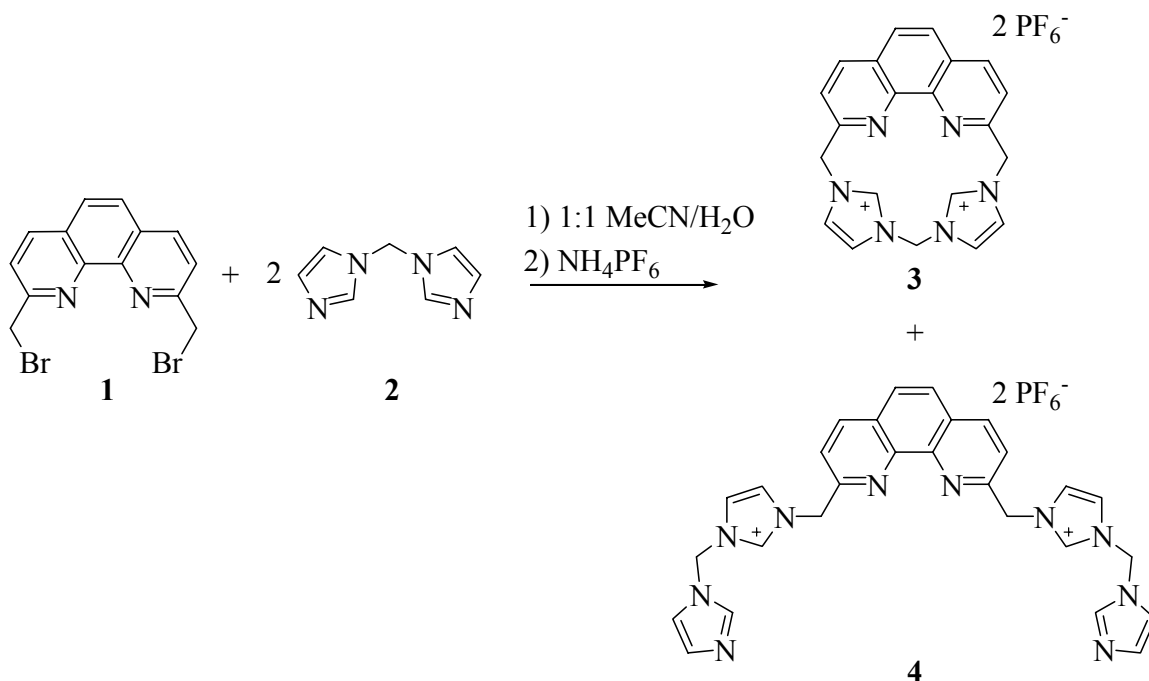


Texaphyrin

Figure 3-1. Porphyrin and porphyrin like molecules.

3.2 Synthesis and Characterization of Bisimidazole Based Cyclophanes

Condensation of 2,9-bis(bromomethyl)-1,10-phenanthroline, **1**, with 1,1'-methylene bis(imidazole), **2**, afforded a mixture of two products by TLC. After anion exchange with ammonium hexafluorophosphate, analysis by ^1H NMR and FAB-MS revealed the presence of cyclophane, **3** $[\text{PF}_6^-]_2$, as well as an open substituted system, **4** $[\text{PF}_6^-]_2$ (Scheme 3-1). The ^1H NMR spectrum revealed two imidazolium cations and two pairs of methylene peaks which suggest two imidazolium species were present. FAB-MS supported the existence of the two species, m/z 499 **3** $[\text{PF}_6^-]_2$ and 648 **4** $[\text{PF}_6^-]_2$. Separation of the mixture was achieved by use of chromatography on alumina with acetonitrile as the eluent. The desired compound **3** $[\text{PF}_6^-]_2$ was obtained as a colorless solid in 17% yield.

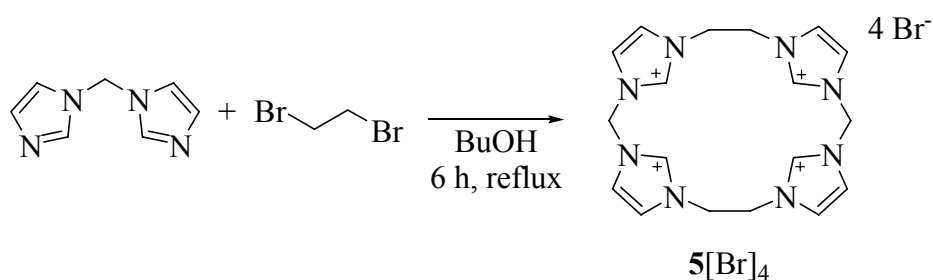


Scheme 3-1. Synthesis of imidazolium cyclophanes **3** $[\text{PF}_6^-]_2$.⁸⁹

The ^1H and ^{13}C NMR spectra of $\mathbf{3}[\text{PF}_6]_2$ are consistent with the proposed structure (the ^1H NMR of $\mathbf{3}[\text{PF}_6]_2$ is given in Figures 3-2 and 3-3). The most notable feature of the ^1H NMR spectrum is the resonance of the C(2) hydrogen atoms at 9.68 ppm.

Crystals of $\mathbf{3}[\text{PF}_6]_2$ suitable for X-ray crystallography were grown from a concentrated solution of acetonitrile and DMSO. The dicationic portion of $\mathbf{3}[\text{PF}_6]_2$ is shown in Figure 3-4. The asymmetric unit contained $\mathbf{3}[\text{PF}_6]_2$ as well as four DMSO solvent molecules. The average pocket size of $\mathbf{3}[\text{PF}_6]_2$ measured from the centroids of the imidazolium rings to the nitrogen atoms of the phenanthroline is approximately 4.81 Å. The dihedral angles of the imidazolium rings are 64.3° to 67.1° from the plane of the phenanthroline (C(1)-C(12) and N(1)-N(2)).

In attempt to synthesize tetracarbene cyclophanes 1,1'-methylene bis(imidazole) was reacted with dihaloalkanes. The reaction of 1,2-dibromoethane with 1,1'-methylene bis(imidazole) resulted in then formation of the cyclic tetraimidazolium salt $\mathbf{5}[\text{Br}]_4$, depicted in Scheme 3-2. ESI-MS results for $\mathbf{5}[\text{PF}_6]_4$ show the formation of the partial polycarbene species in the gas phase. Although the initial monocation peak at m/z 787



Equation 3-1. Synthesis of tetraimidazolium salt $\mathbf{5}[\text{Br}]_4$.

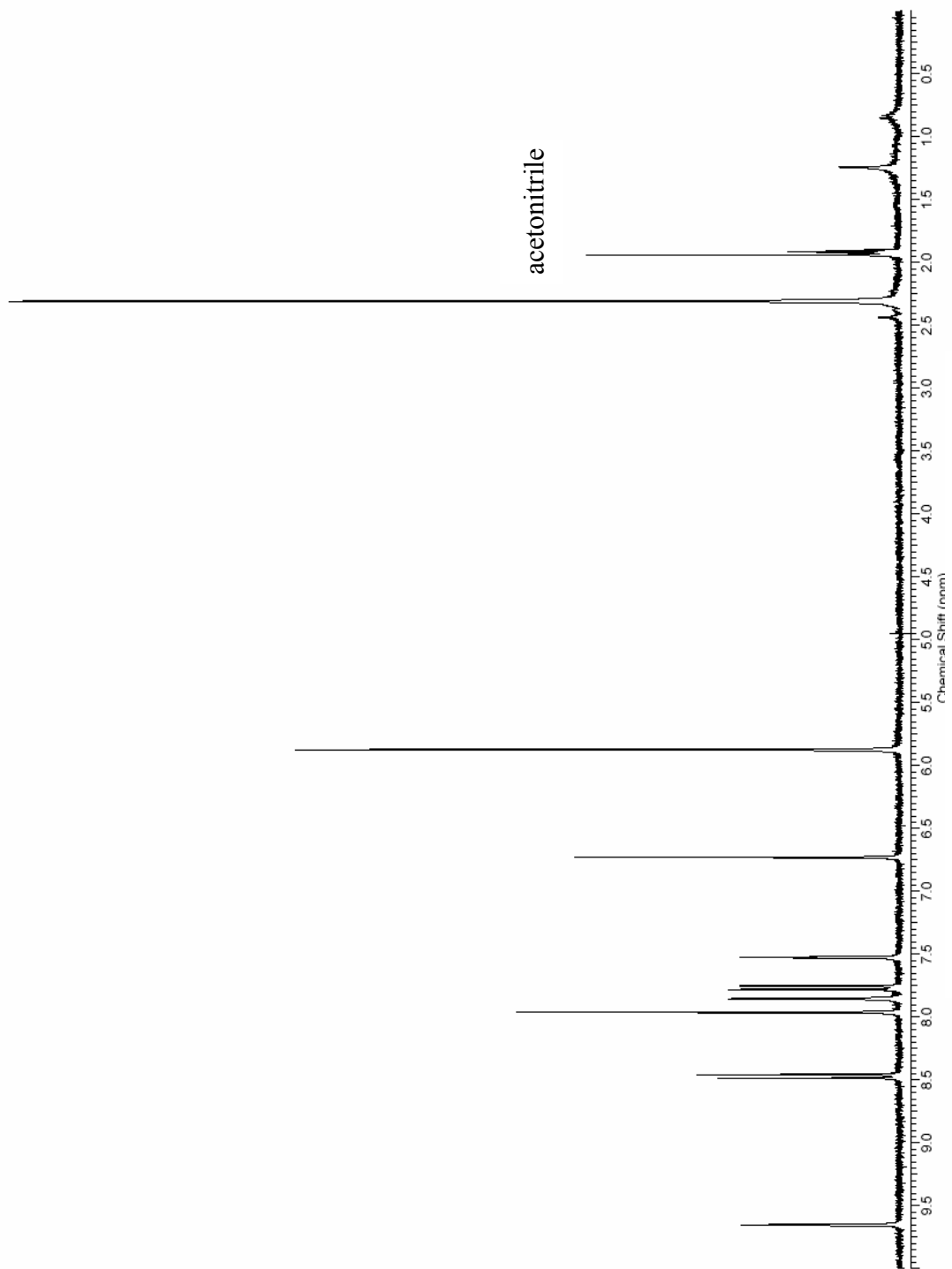


Figure 3-2. ^1H NMR spectrum of $3[\text{PF}_6]_2$ in $d_3\text{-CD}_3\text{CN}$.

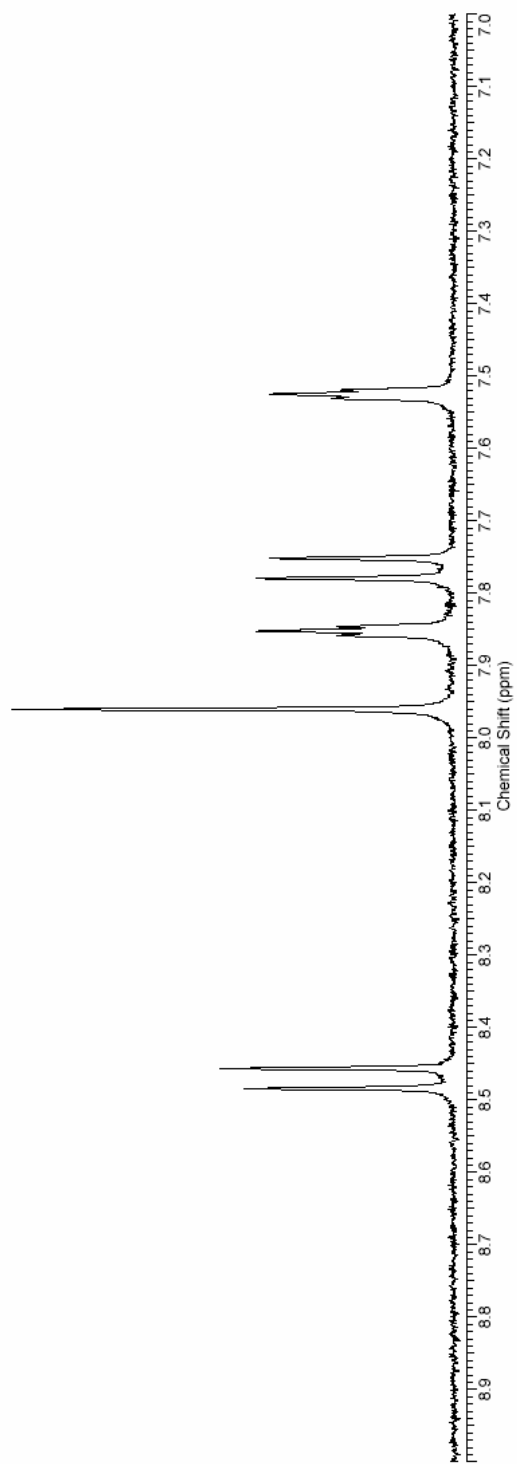


Figure 3-3. ^1H NMR spectrum of $3[\text{PF}_6]_2$ in $d_3\text{-CD}_3\text{CN}$. Expansion of aromatic region.

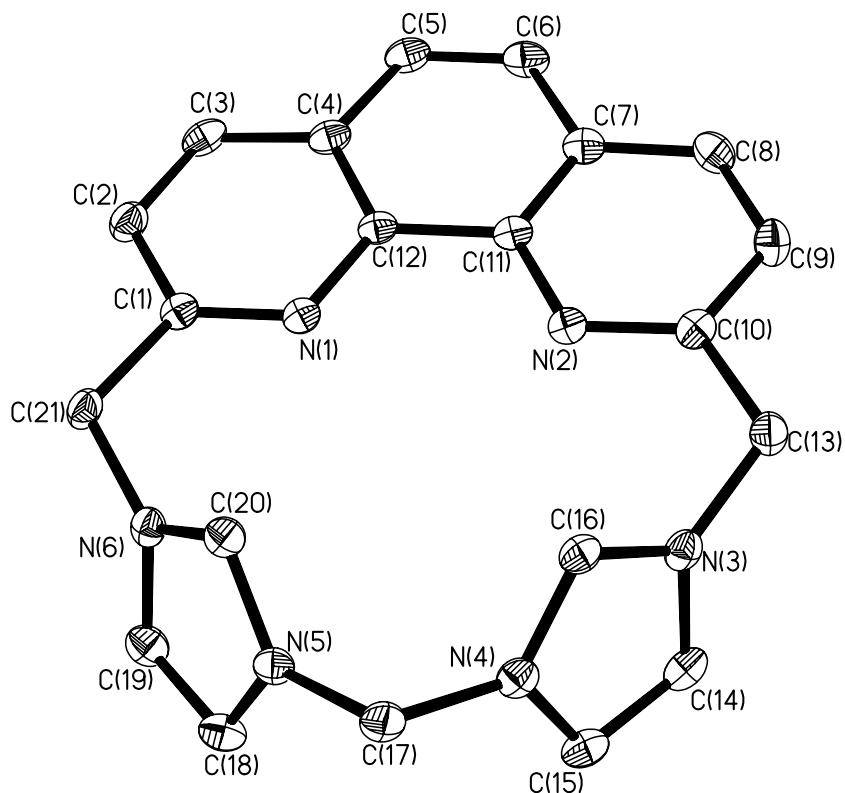


Figure 3-4. Thermal ellipsoid plot of the dicationic portion of $3[PF_6]_2$ with hydrogen atoms removed for clarity. Thermal ellipsoids shown at 50% probability.

is not observed the subsequent peaks at m/z 641, 495, and 349 can be seen. These correspond to the loss of two PF_6^- anions and the formation of the monocarbene, the loss of three PF_6^- anions and the formation of the dicarbene, and the loss of all anions and the formation of the triscarbene.

The 1H and ^{13}C NMR spectra are both consistent with the given structure. The most notable features of the 1H NMR spectrum are the resonances that correspond to the hydrogen atoms of the ethyl linkage and the C(2) hydrogen atoms. The CH_2 hydrogen atoms of the ethyl linkage are equivalent and give a single resonance at ca. 4.7 ppm and

the C(2) hydrogen atoms are shifted upfield to ca. 9.4 ppm, which is diagnostic for the formation of the imidazolium salt.

Crystals of $5[\text{Br}]_4$ suitable for X-ray crystallography were grown from a concentrated sample in water. The tetracationic portion of $5[\text{Br}]_4$ is depicted in Figure 3-5. The asymmetric unit contains half of the tetracationic cyclophane, two bromide anions, and one solvent water molecule. The average pocket size measured from the centroids of the imidazole rings is 6.6 Å. $5[\text{Br}]_4$ packs with intermolecular hydrogen bonds between the imidazolium carbon atoms and two of the bromide anions ($\text{C} \cdots \text{Br} \approx 3.5$ Å) depicted in Figure 3-6.

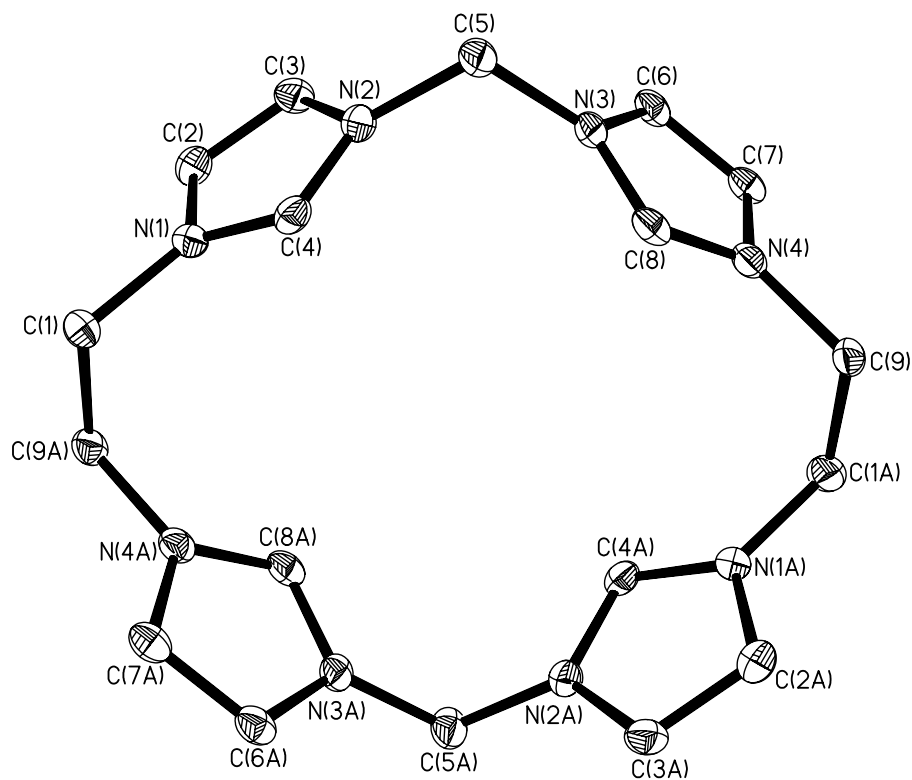


Figure 3-5. Thermal ellipsoid plot of the tetracationic portion of $5[\text{Br}]_4$ with hydrogen atoms omitted for clarity. Thermal ellipsoids shown at 50% probability.

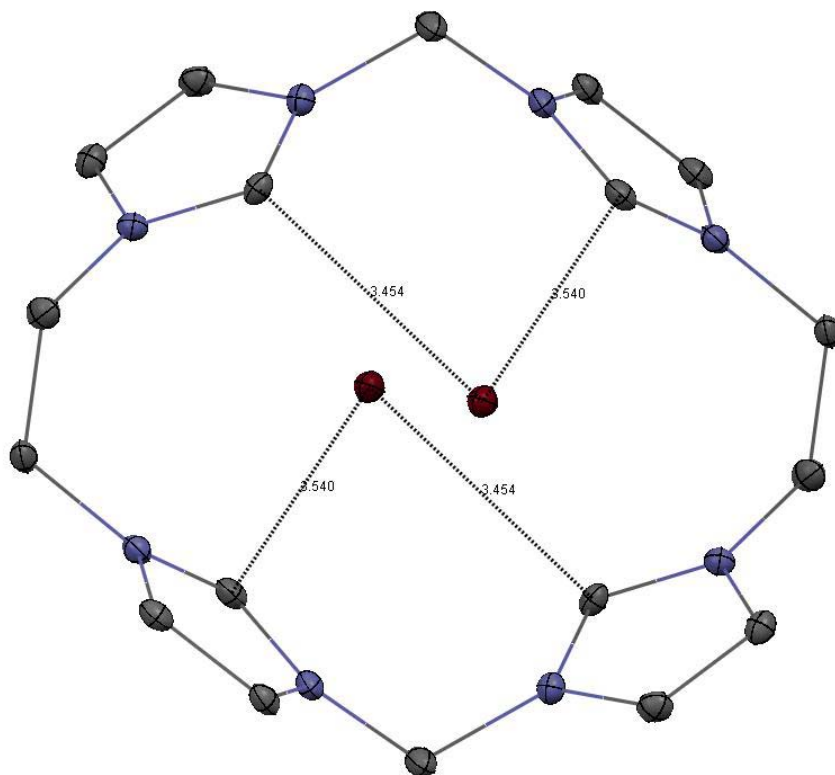


Figure 3-6. Thermal ellipsoid plot depicting the hydrogen bonding of $5[\text{Br}]_4$. Thermal ellipsoids shown at 50% probability.

The reaction of 1,3-dibromopropane with 1,1'-methylene bis(imidazole) resulted in the formation of the cyclic tetraimidazolium salt $6[\text{Br}]_4$, shown in Equation 3-2. The ESI-MS results for $6[\text{PF}_6]_4$ shows the monoanion $6[\text{PF}_6]_5^-$ at m/z 1105. The ^1H and ^{13}C NMR spectra are consistent with the given structure. The most notable features of the ^1H NMR spectrum, shown in Figure 3-7, are the addition of the resonances associated with the hydrogen atoms of the propyl linkage and the upfield shift of the C(2) hydrogen atoms.

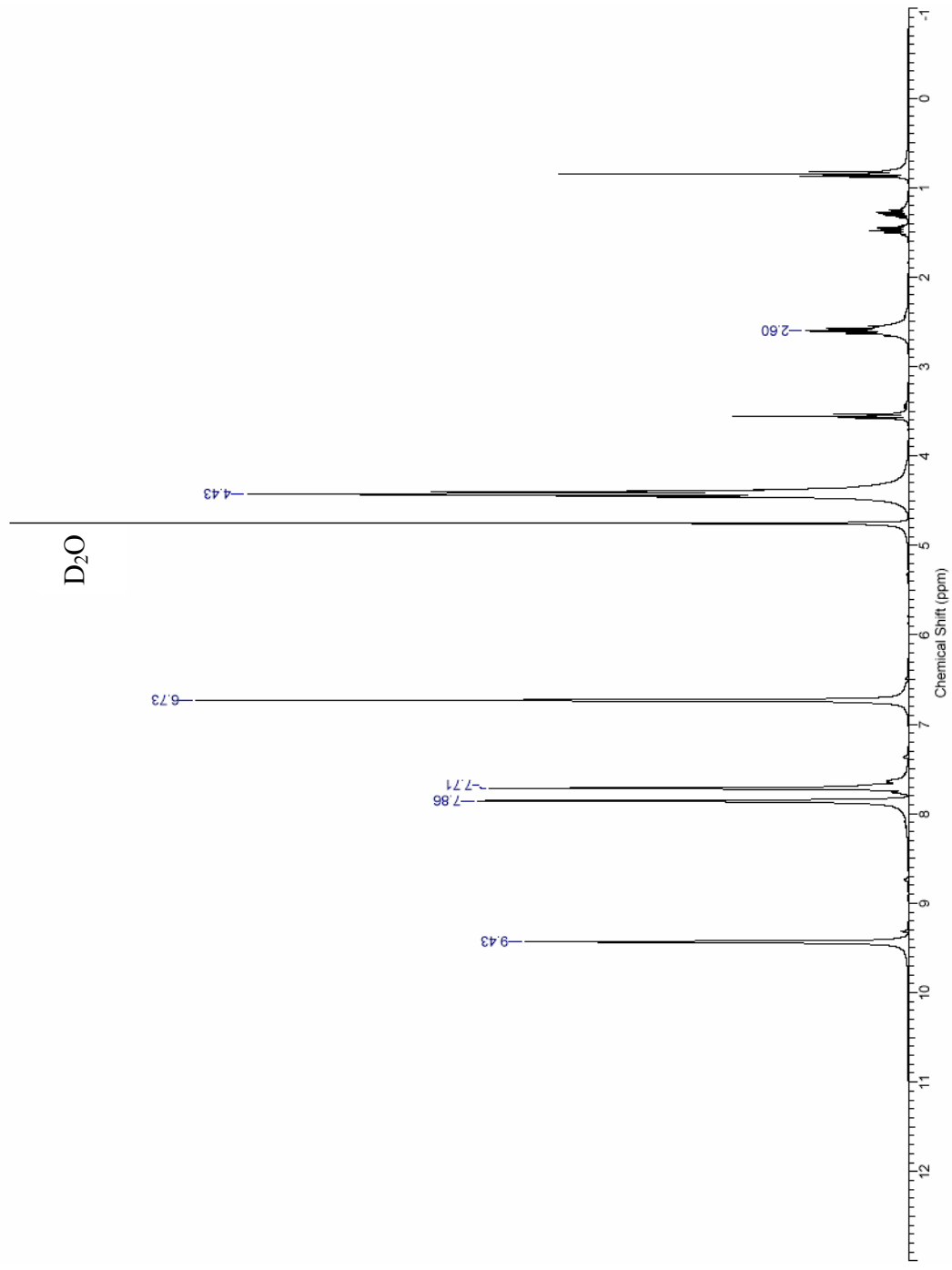
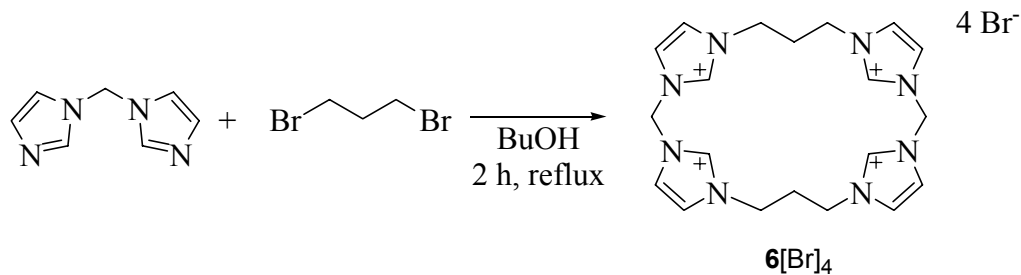


Figure 3-7. ¹H NMR spectrum of 6[Br]₄ in D₂O. Unlabeled peaks correspond to residual butyl alcohol .



Equation 3-2. Synthesis of tetraimidazolium salt **6[Br]₄**.

Excess NH_4PF_6 was added to **6[Br]₄** and crystals of **6[PF₆]₄** suitable for X-ray crystallography were grown from a concentrated sample in acetonitrile and toluene. The tetracationic portion of **6[PF₆]₄** is depicted in Figure 3-8. The asymmetric unit contains half of the tetracationic portion of **6[PF₆]₄**, two PF_6^- anions, and one acetonitrile solvent molecule. One of the PF_6^- anions is disordered in two parts by a simple rotation.

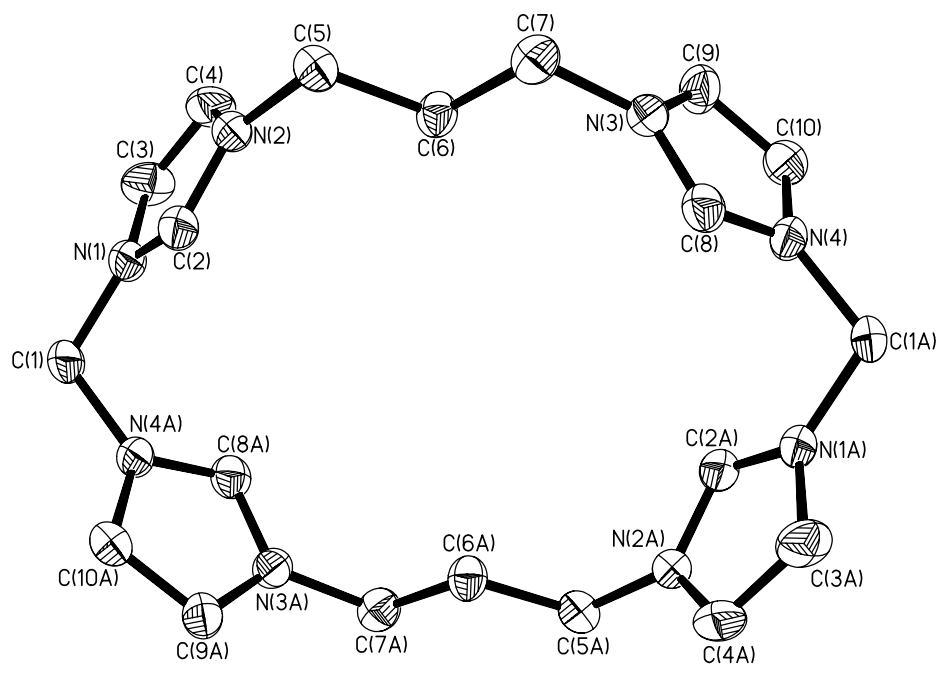


Figure 3-8. Thermal ellipsoid plot of the tetracationic portion of **6[PF₆]₄** with hydrogen atoms omitted for clarity. Thermal ellipsoids shown at 50% probability.

The average pocket size measured from the centroids of the imidazole rings is 7.8 Å. $6[PF_6]_4$ packs with intermolecular hydrogen bonds. Short donor-acceptor distances exist between the imidazolium carbon atoms and the fluorine atoms of the PF_6^- anions (C...F $\approx 2.99 - 3.19$ Å), shown in Figure 3-9.

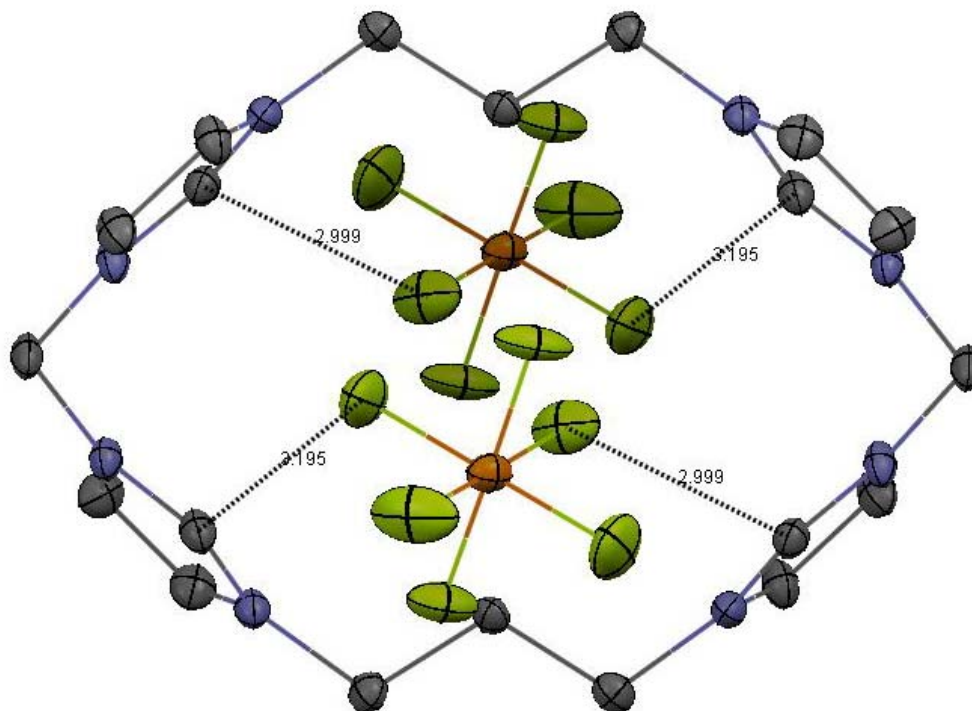


Figure 3-9. Thermal ellipsoid plot depicting the hydrogen bonding of $6[PF_6]_4$. Thermal ellipsoids shown at 30% probability.

3.3 Conclusions

A series of imidazolium cyclophanes have been constructed using 1,1'-methylene bis(imidazole) as a basic building unit. These NHC precursors have been modified by using different linking groups to form cyclophanes with varying pocket sizes. The pocket sizes have been measured based upon the single crystal structures of the individual compounds. The purpose of the varying the internal size of the ligand is to optimize the

core to better accommodate specific transition metals. In this way they are envisioned to form more kinetically stable metal complexes for use in metal based pharmaceutical applications.

3.4 Experimental Section

3.4.1 General Considerations

All reactions were performed under standard aerobic conditions. 1,2-dibromoethane and 1,3-dibromopropane were purchased from Acros and used as received. 1,1'-methylene bis(imidazole) was prepared as reported in section 2.4.3. 2,9-bis(bromomethyl)-1,10-phenanthroline was prepared according to literature procedure.¹⁰³ All solvents were purchased from Fisher Scientific and used without further purification. ¹H and ¹³C NMR data were obtained using a Varian Mercury or Gemini 300 MHz instrument. Mass spectrometric analysis was performed by the mass spectrometry facility at the University of Akron.

3.4.2 X-ray Structure Determination Details

Data sets were collected on a Bruker Apex CCD diffractometer with graphite-monochromated Mo K α radiation ($\lambda = 0.71073 \text{ \AA}$). Unit cell determination was achieved by using reflections from three different orientations. An empirical absorption correction and other corrections were performed using multi-scan SADABS. Structure solution, refinement and modeling were accomplished using the Bruker SHELXTL package.⁸⁸ The structure was obtained by full-matrix least-squares refinement of F² and the selection of appropriate atoms from the generated difference map.

3.4.3 Synthesis of $\mathbf{3}[\text{PF}_6]_2$ ($\text{C}_{21}\text{H}_{18}\text{N}_6\text{P}_2\text{F}_{12}$)

A mixture of 2,9-bis(bromomethyl)-1,10-phenanthroline (0.1 mmol, 0.0384 g) and 1,1'-methylene bis(imidazole) (0.2 mmol, 0.0296 g) was stirred at reflux in acetonitrile/ H_2O (50:50) for 12 h. The volatile components were removed and water and excess NH_4PF_6 was added. The crude product was collected as a yellowish solid 0.0322 g (50%). The crude was purified by column chromatography on alumina using acetonitrile as the eluting solvent. The clean product was collected as a pale yellow solid. Yield: 0.0110 g, 0.017 mmol, 17%. Crystals were obtained from a mixture of acetonitrile and DMSO as colorless plates. ^1H NMR (300 MHz, $\text{CH}_3\text{CN}-d_3$): δ 5.89 (s, 4 H), 6.75 (s, 2 H), 7.55 (s, 2H), 7.78 (d, 2 H), 7.88 (s, 2 H), 7.99 (s, 2 H), 4.48 (d, 2 H), 9.68 (s, 2 H). ^{13}C NMR (75 MHz, $\text{CD}_3\text{CN}-d_3$): δ 54.95 and 60.84 (CH_2), 122.87, 123.26, 125.67, 128.33, 130.35, 139.34, 140.14, 153.18 (aromatic). MS-FAB: m/z 499 (M^+ of $\text{C}_{21}\text{H}_{18}\text{N}_6\text{PF}_6$).

X-ray crystal structure analysis of $\mathbf{3}[\text{PF}_6]_2$: formula $\text{C}_{29}\text{H}_{42}\text{F}_{12}\text{N}_6\text{P}_2\text{O}_4\text{S}_4$, $M_w = 956.87$, colorless crystal 0.41 x 0.13 x 0.06 mm, $a = 14.956(3)$ Å, $b = 15.366(4)$ Å, $c = 18.869(4)$ Å, $\alpha = 90^\circ$, $\beta = 112.274(4)^\circ$, $\gamma = 90^\circ$, $V = 4012.9(16)$ Å³, $D_{\text{calc}} = 1.584$ Mg cm⁻³, $\mu = 0.416$ mm⁻¹, $Z = 4$, monoclinic, space group $P2_1/n$ (No. 14), $\lambda = 0.71073$ Å, $T = 100$ K, ω and φ scans, 34549 reflections collected, 9583 independent ($R_{\text{int}} = 0.0436$), 682 refined parameters, $R1/wR2$ ($I \geq 2\sigma(I)$) = 0.0495 / 0.0977 and $R1/wR2$ (all data) = 0.0627 / 0.1026, maximum (minimum) residual electron density 0.404 (-0.336) e Å⁻³, all hydrogen atoms were calculated and refined as riding atoms.

3.4.4 Synthesis of **5**[Br]₄ (C₁₈H₂₄N₈Br₄)

To a 25 mL round bottom flask was added 1,1'-methylene bis(imidazole) (0.74 g, 5.0 mmol) and 1,2 dibromoethane (0.86 mL, 10.0 mmol). The mixture was refluxed in butyl alcohol (5 mL) for 6 h. **5**[Br]₄ precipitated from the solution mixture as the reaction proceeded. The bromide salt was collected by vacuum filtration as a white solid. Yield: 1.43 g, 85%. Crystals were grown from water/acetonitrile as colorless plates. ¹H NMR (300 MHz, DMSO-d₆): δ 4.70 (s, 8H), 6.67 (s, 4H), 7.73 (s, 4H), 7.96 (s, 4H), 9.39 (s, 4H). ¹³C NMR (300 MHz, DMSO-d₆): δ 49.0 and 58.9 (CH₂), 123.2, 123.9, 139.1 (Aromatic). ESI/MS: m/z 641(M⁺ of C₁₈H₂₃N₈P₂F₁₂).

X-ray crystal structure analysis of **5**[Br]₄: formula C₁₈H₂₈Br₄N₈O, *M_w* = 692.12, colorless crystal 0.22 x 0.09 x 0.05 mm, *a* = 7.194(2) Å, *b* = 9.054(3) Å, *c* = 10.292(4) Å, α = 71.651(7)°, β = 82.477(16)°, γ = 75.925(9)°, *V* = 616.1(4) Å³, *D*_{calc} = 1.865 Mg cm⁻³, μ = 6.560 mm⁻¹, *Z* = 1, triclinic, space group *P*-1 (No. 2), λ = 0.71073 Å, *T* = 100 K, ω and φ scans, 5405 reflections collected, 2773 independent (*R*_{int}) 0.0289, 201 refined parameters, *R*₁/*wR*₂ (*I* ≥ 2σ(*I*)) = 0.0321 / 0.0756 and *R*₁/*wR*₂ (all data) = 0.0407 / 0.0798, maximum (minimum) residual electron density 1.213 (-0.469) e Å⁻³, all hydrogen atoms were calculated and refined as riding atoms.

3.4.5 Synthesis of **6**[Br]₄ (C₂₀H₂₈N₈Br₄) and **6**[PF₆]₄ (C₂₀H₂₈N₈P₄F₂₄)

To a 25 mL round bottom flask was added 1,1'-methylene bis(imidazole) (0.74 g, 5.0 mmol) and 1,3 dibromopropane (1.01 mL, 10.0 mmol). The mixture was refluxed in butyl alcohol (5 mL) for 2 h. The bromide salt was collected by vacuum filtration as a

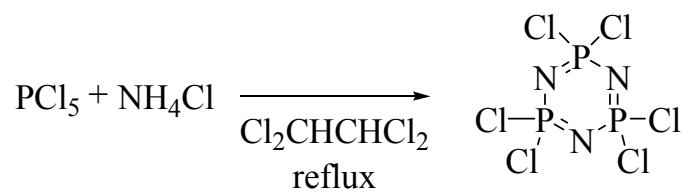
white solid. Yield: 2.63 g, 75%. Water and excess NH_4PF_6 were added, and $\mathbf{6}[\text{PF}_6]_4$ was collected as a white solid. Yield: 3.36 g, 70%. ^1H NMR (300 MHz, $\text{CD}_3\text{CN-d}_3$): δ 2.49 (t, 4H), 4.31 (t, 8H), 6.52 (s, 4H), 7.59 (s, 4H), 7.75 (s, 4H), 9.01 (s, 4H). ^{13}C NMR (300 MHz, $\text{CD}_3\text{CN-d}_3$): δ 29.5, 47.0, 59.0 (CH_2), 122.9, 123.9, 137.4 (Aromatic). ESI/MS: m/z 1105 (M of $\text{C}_{20}\text{H}_{28}\text{N}_8\text{P}_5\text{F}_{30}$).

X-ray crystal structure analysis of $\mathbf{6}[\text{PF}_6]_4$: formula $\text{C}_{24}\text{H}_{34}\text{F}_{24}\text{N}_{10}\text{P}_4$, $M_w = 1042.49$, colorless crystal 0.15 x 0.06 x 0.04 mm, $a = 9.028(11)$ Å, $b = 10.157(12)$ Å, $c = 12.096(14)$ Å, $\alpha = 101.59(2)^\circ$, $\beta = 109.423(19)^\circ$, $\gamma = 103.63(2)^\circ$, $V = 968(2)$ Å³, $D_{\text{calc}} = 1.788$ Mg cm⁻³, $\mu = 0.348$ mm⁻¹, $Z = 1$, triclinic, space group $P-1$ (No. 2), $\lambda = 0.71073$ Å, $T = 100$ K, ω and φ scans, 7051 reflections collected, 3401 independent (R_{int}) 0.0564, 336 refined parameters, $R1/wR2$ ($I \geq 2\sigma(I)$) = 0.0826 / 0.1806 and $R1/wR2$ (all data) = 0.01237/ 0.1954, maximum (minimum) residual electron density 0.623 (-0.367) e Å⁻³, all hydrogen atoms were calculated and refined as riding atoms.

CHAPTER IV
CYCLO AND POLYPHOSPHAZENES

4.1 Introduction

Phosphazenes denote a class of inorganic macrocyclic and polymeric molecules whose make up consists of formally unsaturated P-N bonds. The discovery of the first cyclophosphazene was over 160 years ago.¹⁰⁴ The simplest macrocyclic phosphazene is hexachlorocyclotriphosphazene, $[\text{NPCl}_2]_3$. The synthesis of this molecule is achieved by combining PCl_5 and NH_4Cl in *sym*-tetrachloroethane at reflux, shown in Equation 4-1.



Equation 4-1. Synthesis of hexachlorocyclotriphosphazene, $[\text{PCl}_2\text{N}]_3$.

In the late 1890's it was discovered that $[\text{NPCl}_2]_3$ could be converted into an “inorganic rubber” at high heat.¹⁰⁴ To this day the end groups of this high molecular weight polymer are not known and it has been proposed that the polymers may be large rings rather than linear chains.

4.2 Polyphosphazenes

There is a very fundamental difference in methodologies for creating structural diversity in inorganic polymers such as polyphosphazenes and classical organic polymers. The properties of polyphosphazenes are tailored by the substituents bonded to the phosphorus atoms of the polymer backbone. In contrast, organic polymers depend on different monomers, mixtures of monomers and polymerization conditions to alter chemical properties.¹⁰⁴

Polyphosphazenes are also much more flexible than traditional organic polymers.¹⁰⁵ The flexibility of the backbone of the polymer arises from the fact that only the phosphorus atoms are bonded to substituents. They also orient in such a way as to move the substituents as far apart as possible in a conformation known as *cis-trans* planar, Figure 4-1.¹⁰⁵ This helps to avoid steric interactions between the groups. The nitrogen atoms of the backbone are not appended and separate the phosphorus atoms. This also helps to limit steric interactions of side groups and allows for flexibility at the nitrogen. Rotation about the C-C bond of organic polymers is restricted by the fact that each carbon atom of the chain has some substituent attached.

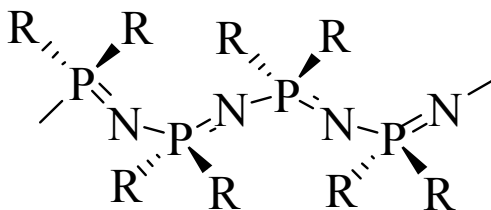
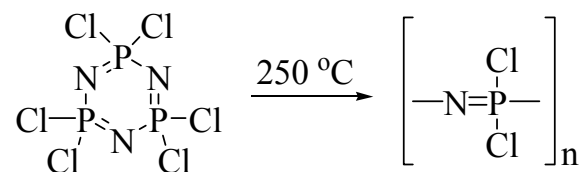


Figure 4-1. Illustration of *cis-trans* planar conformation of polyphosphazenes.

4.2.1 Polymerization of Cyclophosphazenes

The most common method for the synthesis of polyphosphazenes involves the ring opening polymerization (ROP) of $[\text{NPCl}_2]_3$. This reaction can be carried out by a variety of methods with varying results in yield and polymer weights. The polymers are typically tailored by substitution of the chlorides with organic substituents following ROP.

A polymer melt synthesis carried out in the absence of solvent is the simplest route for producing large amounts of polyphosphazene. When purified $[\text{NPCl}_2]_3$ is heated to 250 °C it produces a viscous clear liquid. Termination of heating prior to the melt reaching a viscosity where flow is no longer observed results in the isolation of organic solvent soluble uncrosslinked polyphosphazene, Equation 4-2. Unreacted $[\text{NPCl}_2]_3$ and cyclic oligomers can be removed by sublimation or by precipitation of the polymer from a solution in cyclohexane with heptane.¹⁰⁶



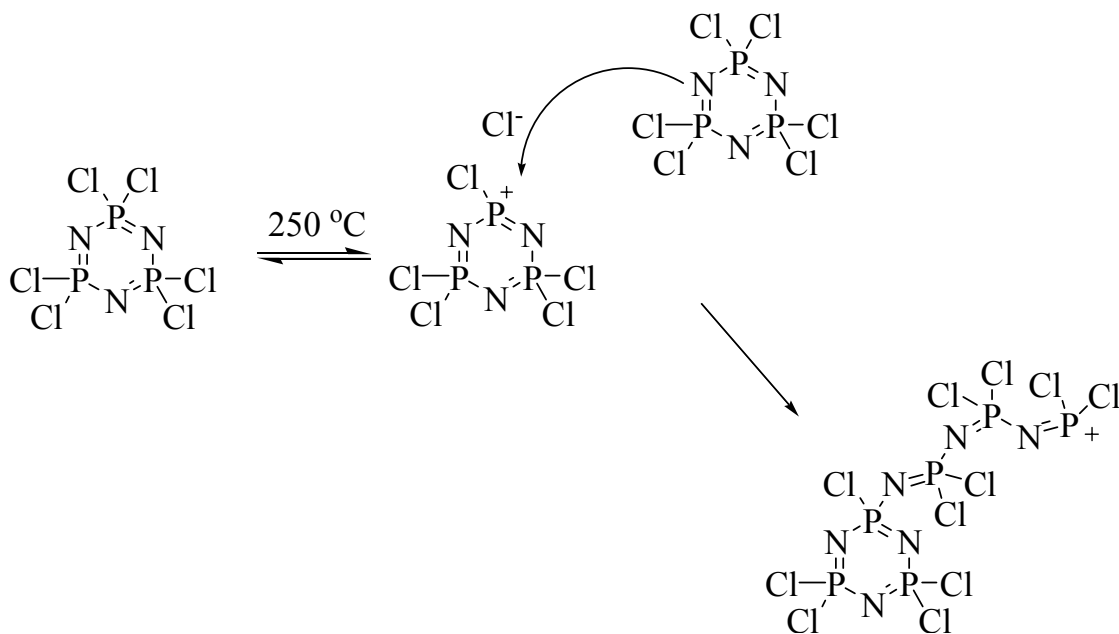
Equation 4-2. Synthesis of chloropolyphosphazene from $[\text{PCl}_2\text{N}]_3$.¹⁰⁶

Continual heating of the polymer melt until no viscous flow is observed results in the formation of crosslinked polyphosphazenes. The crosslinked polymer swells in organic solvents but is not soluble. At temperatures above 200°C under reduced pressures, chloropolyphosphazenes undergo depolymerization to form cyclic oligomers. The same result is observed when the polymer is heated above 350°C.

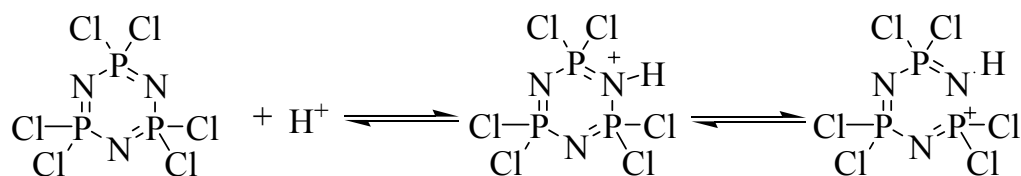
One major disadvantage of the polymer melt method is the high temperatures necessary to produce adequate yields of polyphosphazene. Melt temperatures below 250°C show a significant slowing of the rate polymerization with 230°C being the lower limit of reasonable temperatures. Solution state polymerizations can be conducted in solvents that are inert to reaction with $[\text{NPCl}_2]_n$. Suitable solvents include benzene, cyclohexane, and chlorobenzenes.¹⁰⁶ The use of solvents in the polymerization of phosphazenes tends to lower reaction temperatures and avoids crosslinking.

The most successful solution state polymerization of $[\text{NPCl}_2]_3$ was carried in 1,2,4-trichlorobenzene using BCl_3 as a polymerization initiator.^{107,108} Using BCl_3 in this manner is beneficial by providing reproducible results and eliminates crosslinking. However, the polymers isolated by this method are of lower molecular weight than by other means.¹⁰⁶

There are two major theories that explain the mechanism of ROP for $[\text{NPCl}_2]_3$. The first involves the ionization of one of the chlorides from the $[\text{NPCl}_2]_3$ ring to form a phosphonium cation. This cation then interacts with the lone pair of a nitrogen atom from an additional $[\text{NPCl}_2]_3$ ring which acts as a weak Lewis base. The attack of this nitrogen atom initiates ring opening and starts chain formation, Scheme 4-1. The reaction continues to progress in the same fashion yielding a polymer with a repeat unit of NPCl_2 . The second proposed mechanism for ROP involves the reaction of $[\text{NPCl}_2]_3$ with a source of H^+ . In this case a nitrogen atom of the $[\text{NPCl}_2]_3$ ring acts as base and becomes protonated and initiates ROP, Scheme 4-2. This mechanism is used to explain the necessity for traces of water to initiate ROP.¹⁰⁶



Scheme 4-1. Ionization mechanism for ROP of $[\text{NPCl}_2]_3$.¹⁰⁶



Scheme 4-2. Protonation mechanism for ROP of $[\text{NPCl}_2]_3$.¹⁰⁶

4.3 Bonding Structure of Cyclophosphazenes

The electronic structure of cyclophosphazenes is still not well understood despite their first isolation over a century and a half ago and the numerous chemical reactions and studies which have followed.¹⁰⁹ P-N bond lengths in cyclophosphazenes such as $[\text{NPCl}_2]_3$ are all equivalent and significantly shorter than expected for P-N single bonds. When the valence electrons of phosphorus, nitrogen (five each) and substituents are placed in two electron bonds a total of 12 nonbonded electrons remain, Figure 4-2. Six of these

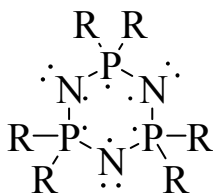


Figure 4-2. Pairing of electrons in $[\text{NPR}_2]_3$.¹⁰⁹

electrons are accounted for as lone pairs residing on the nitrogen atoms of the ring. These lone pairs are located in the plane of the ring in the sigma bond framework. There still remains a debate about the bonding structure of the final six electrons.

Two major theories have been used to explain the bonding structure of phosphazenes. The first theory explains the multiple bond character of the P-N bonds of phosphazenes through $d\pi$ - $p\pi$ bonding. The lone electrons of the nitrogen atoms are placed into the $2p_z$ orbitals and overlap with the $3d_{xz}$ orbitals of the phosphorus atoms. However, pairing of the orbitals in this fashion would cause a mismatch at no less than one of the phosphorus atoms as shown in Figure 4-3. The $3d_{yz}$ orbitals also have the appropriate symmetry to π -bond with the $2p_z$ orbitals. Similar contribution from both the $3d_{xz}$ and the $3d_{yz}$ orbitals would lead to nodes at each phosphorus atom. These nodes would allow for delocalization between the nitrogen and phosphorus atoms, but would eliminate any conjugation of the π orbitals.¹⁰⁹ This view of the P-N bonds in phosphazenes is known as the “island” bonding and is shown in Figure 4-4.

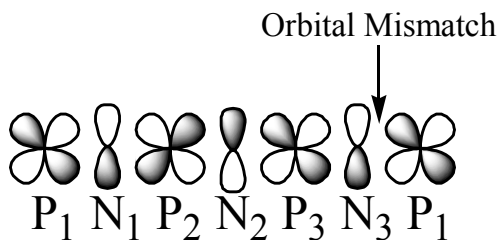


Figure 4-3. Depiction of the orbital mismatch in the $d\pi$ - $p\pi$ bonding structure of $[\text{NPR}_2]_3$.

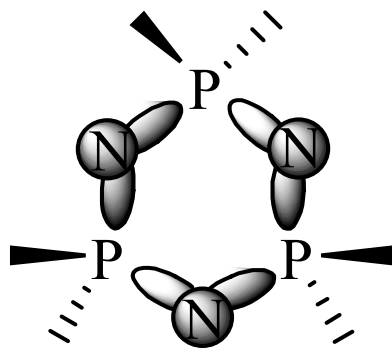


Figure 4-4. “Island” bonding in cyclophosphazenes.

The $d\pi$ - $p\pi$ bonding theory of phosphazenes has been brought into questions in the last decade. This is mainly due to the fact that the d-orbitals of the phosphorus atoms of phosphazenes are too high in energy to overlap with the p-orbitals of the nitrogen atoms.¹¹⁰ An alternative theory represents the electronic structure of phosphazenes in a zwitterionic manner as depicted in Figure 4-5. In this structure all of the non- σ electrons

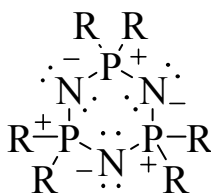


Figure 4-5. Zwitterionic structure of $[\text{NPR}_2]_3$.¹⁰⁹

are placed in the lone pair orbitals of the nitrogen atoms. This would ultimately lead to a negative charge on each of the nitrogen atoms and a positive charge on each of the phosphorus atoms. The fact that the resulting zwitterion would be unstable was pointed out in a review by Allcock.¹¹¹

The modern view of this theory takes into account that negative electron density from the nitrogen atoms can backbond to the σ^* orbitals of the phosphorus atoms and attached substituents. This phenomenon is known as negative hyperconjugation. The

overall view of the skeletal bonding of phosphazenes is now considered to involve σ and ionic-bonding as well as π -bonding which is induced by negative hyperconjugation.¹⁰⁹

4.4 Lewis Acid-Base Chemistry of $[\text{N}(\text{P}(\text{Cl})_2)_3]$

Lewis acids have been shown to catalyze the ROP of $[\text{N}(\text{P}(\text{Cl})_2)_3]$. It is believed that Lewis acids assist in the ionization of chloride from $[\text{N}(\text{P}(\text{Cl})_2)_3]$ and thus accelerate the rate of formation of the phosphonium cation responsible for initiating ROP.¹⁰⁶ Lewis acids such as BCl_3 , and AlCl_3 have been investigated for this purpose.^{107,108,112} Both BCl_3 and AlCl_3 have the ability to accept Cl^- to form BCl_4^- and AlCl_4^- . It has also been proposed that the formation of BCl_4^- as a counterion for the phosphonium ion generated during chain propagation aids in prevention of crosslinked polymers.¹⁰⁷

Two structures have been proposed for the reaction of Lewis acids with $[\text{N}(\text{P}(\text{Cl})_2)_3]$ and are shown in Figure 4-6. Structure **1** is the suggested intermediate in the BCl_3 catalyzed ROP of $[\text{N}(\text{P}(\text{Cl})_2)_3]$.^{107,108} Structure **2** is the proposed intermediate for the AlCl_3 catalyzed Friedel-Crafts substitution of $[\text{N}(\text{P}(\text{Cl})_2)_3]$.¹¹³ In order to better understand the Lewis acid-base chemistry of $[\text{N}(\text{P}(\text{Cl})_2)_3]$ and its effect on ROP, Tessier and coworkers prepared Lewis acid adducts of $[\text{N}(\text{P}(\text{Cl})_2)_3]$ with AlCl_3 , AlBr_3 , and GaCl_3 .¹¹⁴

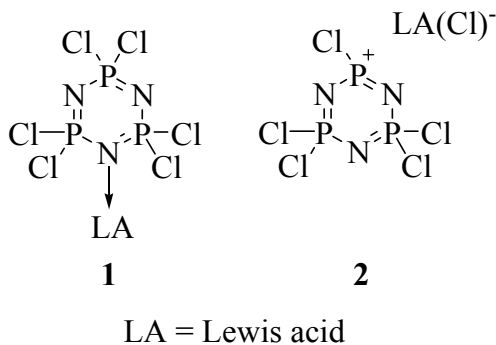
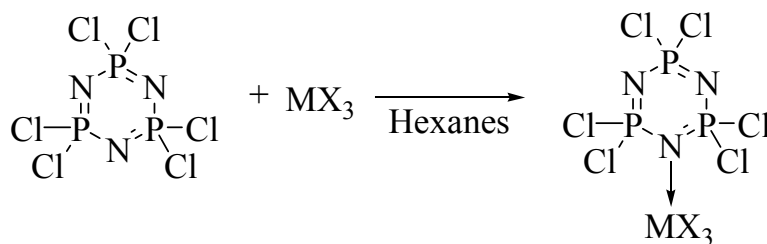


Figure 4-6. Proposed structures for the reaction of Lewis acids with $[\text{N}(\text{P}(\text{Cl})_2)_3]$.¹¹⁴

The reaction of AlCl_3 , AlBr_3 , and other Lewis acids with $[\text{NPCl}_2]_3$ have been previously reported.¹¹⁵⁻¹²⁰ No ^{31}P NMR or crystallographic data were reported for these compounds. The reaction of 1:1 $[\text{NPCl}_2]_3$ with AlCl_3 and GaCl_3 result in the formation of 1:1 adducts of $[\text{NPCl}_2]_3$ with the respective Lewis acids, Equation 4-3.¹¹⁴ Rigorous anaerobic conditions were used in the synthesis of both adducts. The ^{31}P NMR data for the resulting adducts was inconclusive as to structure, and showed only minor shifting from $[\text{NPCl}_2]_3$ with broad resonances. For this reason X-ray crystallography was an essential technique in identifying the exact chemical structures of the adducts.

Single crystals of both the AlCl_3 and the GaCl_3 adducts were isolated and their thermal ellipsoid plots are shown in Figures 4-7 and 4-8. The solid state structures are consistent with neutral adduct formation proposed by structure **1**. The most interesting feature of both structures is a lengthening of the P-N bonds associated with the nitrogen atom that is bonded to the Lewis acid. Typical P-N bond lengths in $[\text{NPCl}_2]_3$ average 1.58 Å while these bonds are more P-N single bond in nature with bond lengths averaging 1.66 Å (AlCl_3 adduct) and 1.64 Å (GaCl_3 adduct). The remaining P-N bond lengths remain within the normal observed range with averages of 1.57 Å (AlCl_3 adduct) and 1.58 Å (GaCl_3) adduct.



Equation 4-3. Synthesis of neutral $[\text{NPCl}_2]_3$ Lewis acid adducts.¹¹⁴

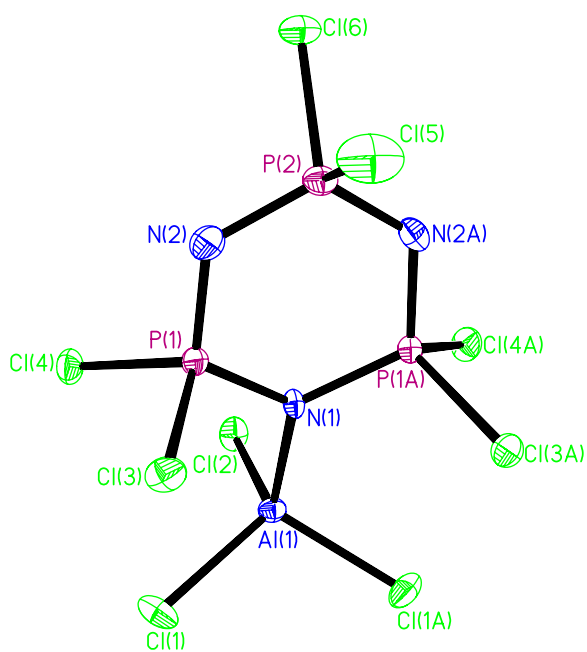


Figure 4-7. Thermal ellipsoid plot of the neutral adduct of AlCl_3 with $[\text{NPCl}_2]_3$.

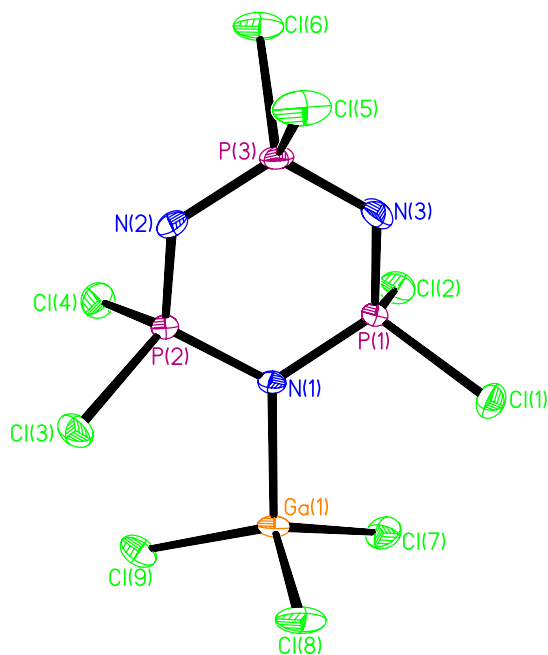


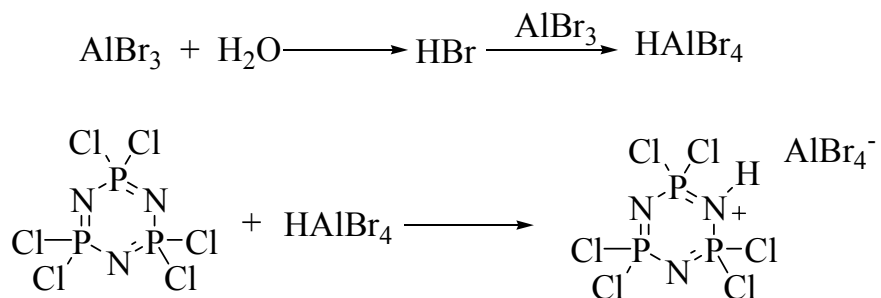
Figure 4-8. Thermal ellipsoid plot of the neutral adduct of GaCl_3 with $[\text{NPCl}_2]_3$.

Table 4-1

Comparison of bond lengths of neutral Lewis acid adducts with [NPCl ₂] ₃ .		
AlCl ₃ Adduct (Å)	GaCl ₃ Adduct(Å)	[NPCl ₂] ₃ (Å)
<u>Al-N</u>	<u>Ga-N</u>	
1.977(5)	2.049(3)	
1.978(5)	2.048(3)	
Avg. 1.978	Avg. 2.049	
<u>P-N long</u>	<u>P-N long</u>	
1.652(3)	1.640(3)	
1.657(3)	1.644(3)	
1.652(3)	1.648(3)	
1.657(3)	1.641(3)	
Avg. 1.652	Avg. 1.643	
<u>P-N short</u>	<u>P-N short</u>	<u>P-N</u>
1.567(4)	1.577(3)	1.5821(17)
1.569(4)	1.574(3)	1.5822(17)
1.569(4)	1.566(3)	1.5795(16)
1.565(4)	1.558(3)	1.5810(13)
1.572(4)	1.565(3)	1.5810(13)
1.572(4)	1.576(3)	
	1.578(3)	
	1.563(3)	
Avg. 1.57	Avg. 1.58	Avg. 1.58

Although [NPCl₂]₃ is known to be a poor Brønsted base protonated adducts have been isolated.¹²¹ In this case the reaction of Lewis acids AlBr₃ and SbCl₅ with [NPCl₂]₃ resulted in the formation of 1:1 protonated adducts with AlBr₄⁻ and SbCl₆⁻ counter ions. The formation of these protonated structures can be explained by traces of water present in the reaction, Scheme 4-3. Single crystals of both adducts were isolated and their thermal ellipsoid plots are shown in Figures 4-9 and 4-10. Like the neutral adducts discussed earlier the P-N bond lengths that flank the protonated nitrogen atom are single bond in character. The average P-N bond lengths are approximately 1.66 Å. The remaining P-N bond lengths are all in a range similar to those observed for [NPCl₂]₃. Further evidence for protonation can be found in the close N---Br (3.36 Å) and N---Cl

(3.27 Å) interactions. These distances suggest the existence of hydrogen bonding interactions in both structures. The ^1H NMR spectra also confirm the presence of H^+ .¹²¹



Scheme 4-3. Rationale for the formation of protonated $[\text{NPCl}_2]_3$ Lewis acid adducts.¹²¹

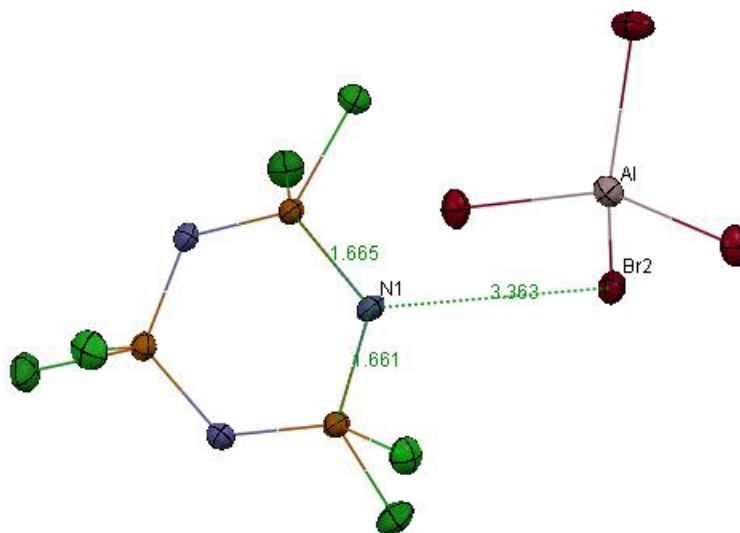


Figure 4-9. Thermal ellipsoid plot of $[\text{NPCl}_2]_3\text{H}^+ \text{AlBr}_4^-$ adduct.

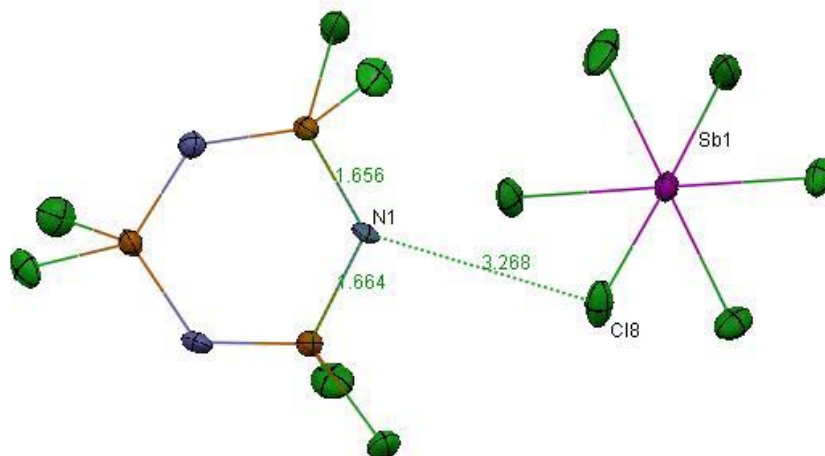


Figure 4-10. Thermal ellipsoid plot of $[\text{NPCl}_2]_3\text{H}^+ \text{SbCl}_6^-$ adduct.

Table 4-2

Comparison of bond lengths of Brønsted acid adducts with $[\text{NPCl}_2]_3$.

HAIBr ₄ Adduct (Å)	HSbCl ₆ Adduct (Å)	$[\text{NPCl}_2]_3$ (Å)
<u>N-Br</u>	<u>N-Cl</u>	
3.36	3.26	
<u>P-N long</u>	<u>P-N long</u>	
1.663(5)	1.656(5)	
1.664(5)	1.664(4)	
Avg. 1.64	Avg. 1.66	
<u>P-N short</u>	<u>P-N short</u>	<u>P-N</u>
1.553(5)	1.540(5)	1.5821(17)
1.555(5)	1.549(5)	1.5822(17)
1.585(5)	1.585(5)	1.5795(16)
1.590(5)	1.582(5)	1.5810(13)
		1.5810(13)
Avg. 1.57	Avg. 1.57	Avg. 1.58

All of the above crystallographically characterized Lewis acid and Brønsted acid adducts of $[\text{NPCl}_2]_3$ are all similar in two fundamental ways. Regardless of whether the adducts are neutral or protonated, all are shown to interact with one of the nitrogen atoms of the $[\text{NPCl}_2]_3$ ring. In this way they seem to support **1** as the structure formed in Lewis acid catalyzed ROP processes. The other feature is the lengthening of P-N bond lengths

directly associated with the nitrogen atom involved in adduct formation. This would seem to support that ring opening occurs by ionization of the P-N bond through the interaction of a nitrogen atom of the $[\text{N}(\text{PCl}_2)_3]$ ring acting as a Lewis or Brønsted base. However, the ROP takes place at temperatures higher than 200°C . The chemistry at these higher temperatures could be very different.

4.5 Experimental Section

4.5.1 General Considerations

Single crystals of Lewis and Brønsted acid adducts of $[\text{NPCI}_2]_3$ were provided by Dr. Amy Heston. Crystals were obtained by allowing the reaction flasks to rest undisturbed in the absence of light. Crystalline samples were removed from the reaction flasks in a glove box and placed into paratone oil on a glass slide. The slides were transferred in a desiccator wrapped in foil to avoid exposure to light. Single crystals were immediately mounted in a coating of paratone oil and data was collected in the dark.

4.5.2 X-ray Structure Determination Details

Data sets were collected on a Bruker Apex CCD diffractometer with graphite-monochromated Mo $K\alpha$ radiation ($\lambda = 0.71073 \text{ \AA}$). Unit cell determination was achieved by using reflections from three different orientations. An empirical absorption correction and other corrections were performed using multi-scan SADABS. Structure solution, refinement and modeling were accomplished using the Bruker SHELXTL package.⁸⁸ The structure was obtained by full-matrix least-squares refinement of F^2 and the selection of appropriate atoms from the generated difference map.

4.5.3 X-ray Details for $[\text{N}(\text{PCl}_2)_3] \cdot \text{AlCl}_3$

Formula: $\text{AlBr}_3\text{Cl}_6\text{N}_3\text{P}_3$, $M_w = 614.35$, colorless crystal 0.31 x 0.26 x 0.23 mm, $a = 10.9235(9) \text{ \AA}$, $b = 12.1204(10) \text{ \AA}$, $c = 12.1583(10) \text{ \AA}$, $\alpha = 90^\circ$, $\beta = 91.8480(2)^\circ$, $\gamma = 90^\circ$, $V = 1608.9(2) \text{ \AA}^3$, $D_{\text{calc}} = 2.536 \text{ Mg m}^{-3}$, $\mu = 8.847 \text{ mm}^{-1}$, $Z = 4$, monoclinic, space group $P2_1/m$ (No. 11), $\lambda = 0.71073 \text{ \AA}$, $T = 100 \text{ K}$, ω and φ scans, 14427 reflections collected, 4083 independent (R_{int}) 0.0388, 163 refined parameters, $R1/wR2 (I \geq 2\sigma(I)) = 0.0293 / 0.0574$ and $R1/wR2$ (all data) = 0.0371 / 0.0595, maximum (minimum) residual electron density 0.568 (-0.619) e \AA^{-3} .

4.5.4 X-ray Details for $[\text{N}(\text{PCl}_2)_3] \cdot \text{GaCl}_3$

Formula: $\text{Cl}_9\text{GaN}_3\text{P}_3$, $M_w = 523.71$, colorless crystal 0.28 x 0.15 x 0.04 mm, $a = 11.7624(11) \text{ \AA}$, $b = 10.7999(10) \text{ \AA}$, $c = 23.873(2) \text{ \AA}$, $\alpha = 90^\circ$, $\beta = 91.989(2)^\circ$, $\gamma = 90^\circ$, $V = 3030.8(5) \text{ \AA}^3$, $D_{\text{calc}} = 2.295 \text{ Mg m}^{-3}$, $\mu = 3.693 \text{ mm}^{-1}$, $Z = 8$, monoclinic, space group $P2_1/c$ (No. 14), $\lambda = 0.71073 \text{ \AA}$, $T = 100 \text{ K}$, ω and φ scans, 26454 reflections collected, 7291 independent (R_{int}) 0.0525, 289 refined parameters, $R1/wR2 (I \geq 2\sigma(I)) = 0.0405 / 0.0847$ and $R1/wR2$ (all data) = 0.0503 / 0.0882, maximum (minimum) residual electron density 1.056 (-0.541) e \AA^{-3} .

4.5.5 X-ray Details for $\text{H}[\text{NPCl}_2]_3^+\text{AlBr}_4^-$.

Formula: $\text{AlBr}_4\text{Cl}_6\text{N}_3\text{P}_3$, $M_w = 697.26$, colorless crystal $0.10 \times 0.06 \times 0.03$ mm, $a = 7.6721(9)$ Å, $b = 9.9263(12)$ Å, $c = 12.3245(14)$ Å, $\alpha = 84.643(2)^\circ$, $\beta = 85.055(2)^\circ$, $\gamma = 73.178(2)^\circ$, $V = 892.77(18)$ Å³, $D_{\text{calc}} = 2.583$ Mg m⁻³, $\mu = 10.121$ mm⁻¹, $Z = 2$, triclinic, space group $P-1$ (No. 2), $\lambda = 0.71073$ Å, $T = 100$ K, ω and φ scans, 7915 reflections collected, 4117 independent (R_{int}) 0.0248, 154 refined parameters, $R1/wR2$ ($I \geq 2\sigma(I)$) = 0.0342 / 0.0702 and $R1/wR2$ (all data) = 0.0461 / 0.0736, maximum (minimum) residual electron density 0.870 (-0.679) e Å⁻³.

4.5.6 X-ray Details for $\text{H}[\text{NPCl}_2]_3^+\text{SbCl}_6^-$.

Formula: $\text{Cl}_{12}\text{N}_3\text{P}_3\text{Sb}$, $M_w = 682.09$, colorless crystal $0.14 \times 0.10 \times 0.08$ mm, $a = 16.0656(17)$ Å, $b = 10.0854(11)$ Å, $c = 11.7766(12)$ Å, $\alpha = 90^\circ$, $\beta = 90^\circ$, $\gamma = 90^\circ$, $V = 1908.1(3)$ Å³, $D_{\text{calc}} = 2.374$ Mg m⁻³, $\mu = 3.363$ mm⁻¹, $Z = 4$, orthorhombic, space group $Pna2_1$ (No. 33), $\lambda = 0.71073$ Å, $T = 100$ K, ω and φ scans, 16343 reflections collected, 4572 independent (R_{int}) 0.0623, 172 refined parameters, $R1/wR2$ ($I \geq 2\sigma(I)$) = 0.0412 / 0.0802 and $R1/wR2$ (all data) = 0.0491 / 0.0824, maximum (minimum) residual electron density 0.644 (-0.708) e Å⁻³.

CHAPTER V

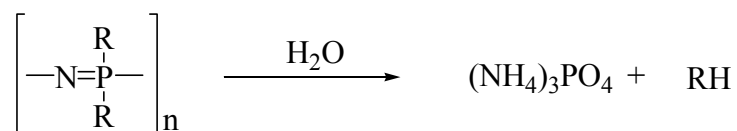
AN IMDAZOLE SUBSTITUTED CYCLOTRIPOSPHAZENE

5.1 Introduction

In the late 1890's Stokes discovered that when heated to high temperatures cyclophosphazenes of formula $[\text{NPCl}_2]_n$ form inorganic polymers. When subjected to moist environments phosphazenes of these types decompose to give ammonium phosphate and HCl.¹⁰⁴ It is this degradation pathway that makes phosphazenes of great interest for use as biodegradable medicinal carriers.¹²²

It can be envisioned that the chlorides of phosphazenes could be replaced with medicinal substituents that forms a P-R bond which is readily hydrolyzable. Upon hydrolysis the substituents would be released and the phosphazene support would degrade to harmless byproducts as shown in Equation 5-1.

Designed biodegradable phosphazene polymers with amino acid esters substituents have been described in the literature.¹²³



R = Medicinal Agent

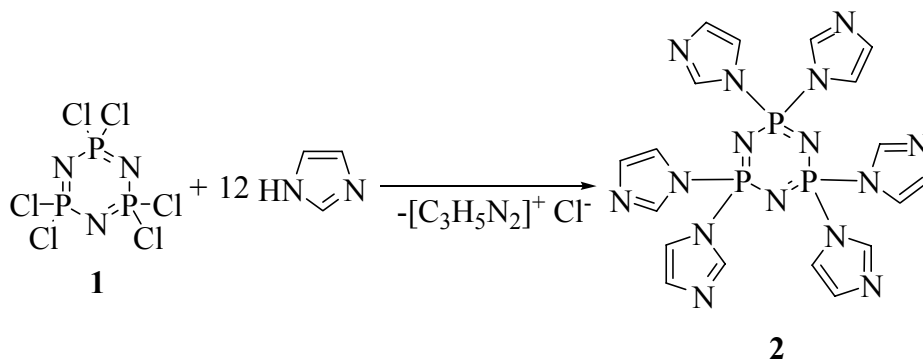
Equation 5-1. Hydrolysis of medicinally substituted phosphazene.

Biologically friendly substituents that have the ability to act as ligands to form transition metal complexes are also of interest. Transition metals have been used in medicine for ages. For example, silver is well known for its antimicrobial efficacy and gold complexes have long been used in the treatment of rheumatoid arthritis.^{27,33,124} For this reason, the synthesis of imidazole substituted cyclotriphosphazene was studied.

5.2 Synthesis of Hexakis(imidazolyl)cyclotriphosphazene

5.2.1 Initial Synthetic Approaches

Initial attempts to synthesize hexakis(imidazolyl)cyclotriphosphazene **2** were made using previously published procedures, Equation 5-2.¹²² Twelve equivalents of imidazole and one equivalent of hexachlorocyclotriphosphazene **1** were stirred for one hour in dry THF under nitrogen. The reaction was filtered under nitrogen and the solvent was removed to afford a white solid. The ³¹P NMR of the product does not correspond to that expected for **2** and is shown in Figure 5-1. Based on the doublet and triplet observed in the ³¹P NMR spectrum only five of the chlorides of **1** were substituted by imidazole resulting in the formation of **3**, structure depicted in Figure 5-2.



Equation 5-2. Synthesis of Hexakis(imidazolyl)cyclotriphosphazene.

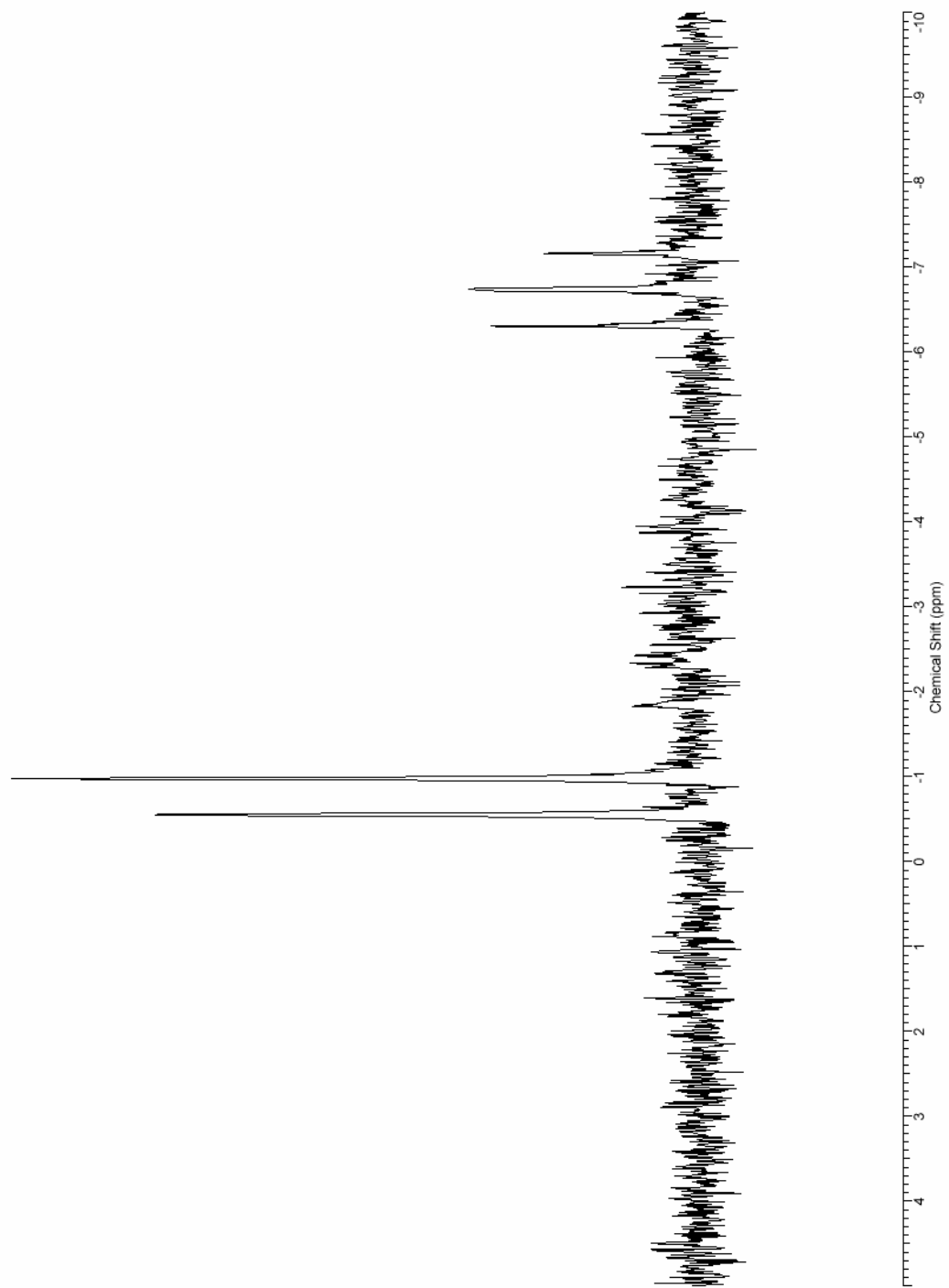
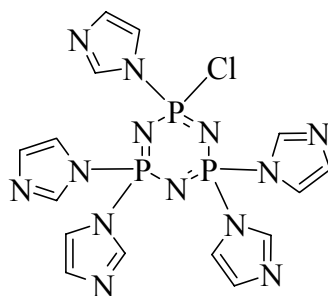


Figure 5-1. ^{31}P NMR spectrum of **3** in D_2O .



3

Figure 5-2. Penta substituted product of **1**.

The same reaction was repeated with a large excess of imidazole. Analysis of the recovered product by ^{31}P NMR revealed the isolation of a mixture of substituted products **2** and **3**, the spectrum of which is shown in Figure 5-3.

In an attempt to force the reaction to completion, **1** was refluxed in dry THF under nitrogen with excess imidazole. The ^{31}P NMR spectrum of the resulting products is shown in Figure 5-4. The spectrum shows a large number peaks which because of the complexity can only be attributed to the formation of multiple phosphazene oligomers.

Because the addition of large excess amounts of imidazole were unable to produce **2** as a single product and heating was shown to form oligomers the reaction was modified. Imidazole was reacted with potassium hydride in THF in order to increase its nucleophilicity. The addition of six equivalents of potassium imidazole with **1** in dry THF results in the precipitation of KCl, Scheme 5-1. After filtration and removal of the solvent a white solid was isolated. The ^{31}P NMR spectrum revealed the existence of substituted products **2** and **3**, shown in Figure 5-5. Integration of the peaks shows that the production

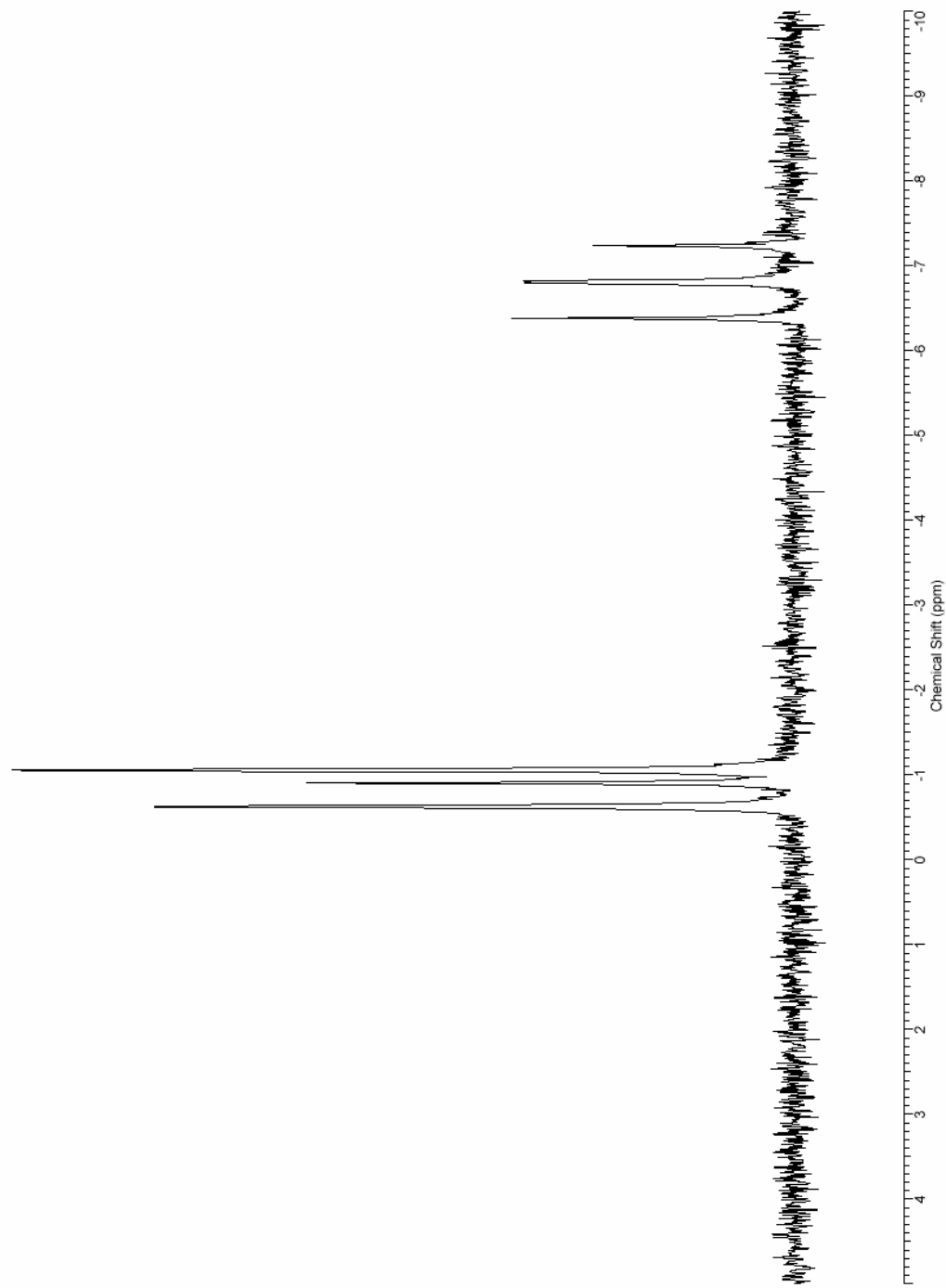


Figure 5-3. ^{31}P spectrum of a mixture of **2** and **3** in D_2O .

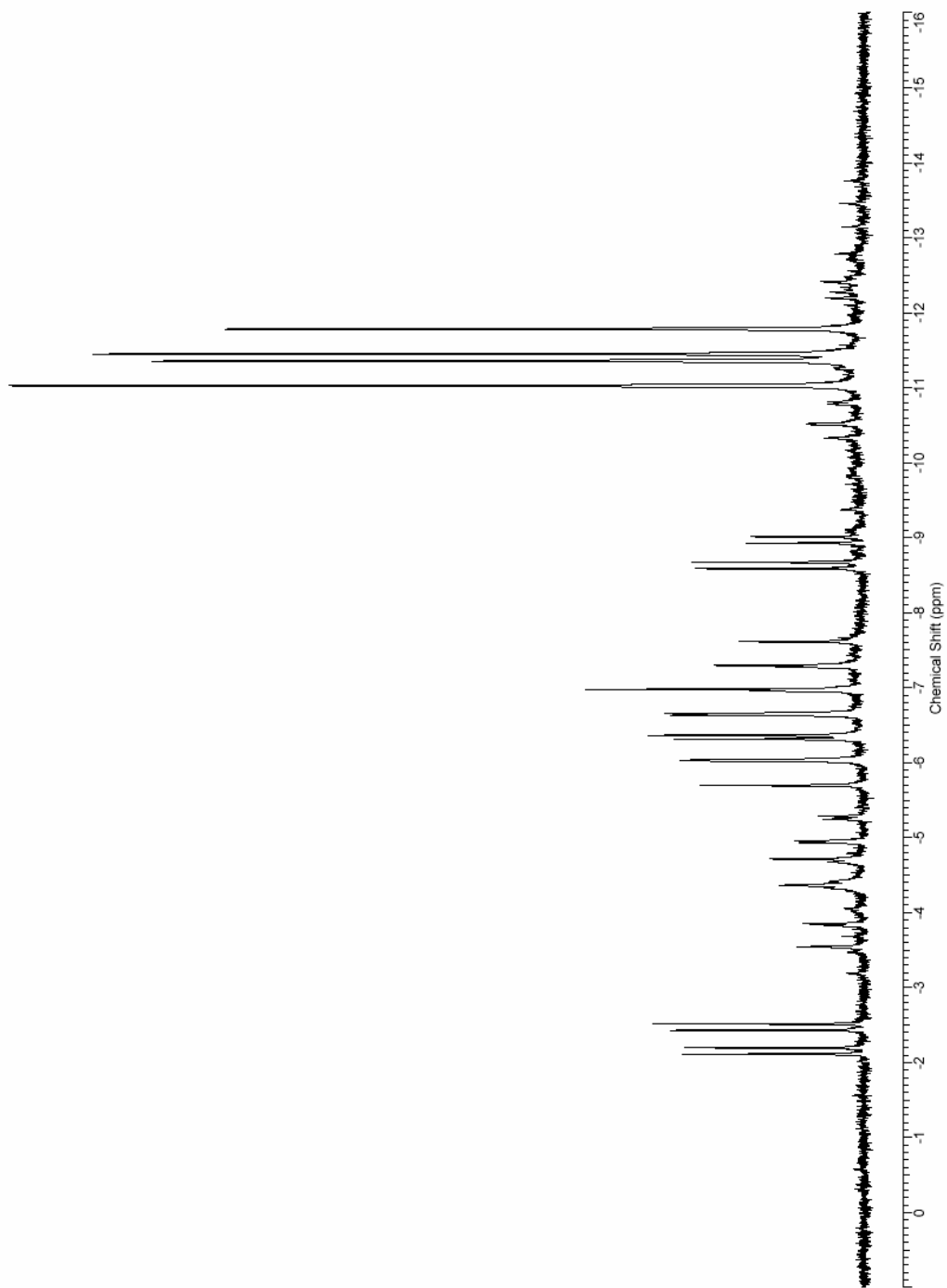
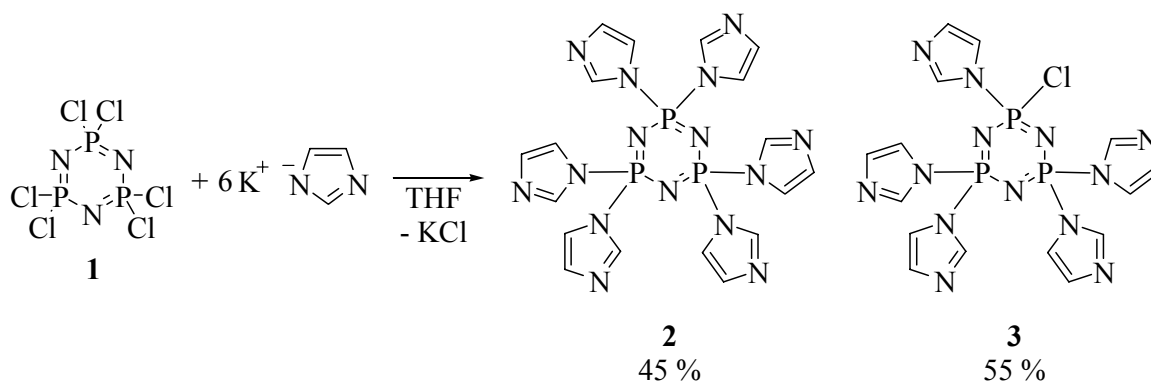


Figure 5-4. ^{31}P NMR spectrum of phosphazene oligomers in d_6 -DMSO.



Scheme 5-1. Reaction of six equivalents of potassium imidazole with **1**. The yield of **2** is about 45 % under these conditions. This procedure was repeated with seven and eight equivalents of potassium imidazole again resulting in mixtures of **2** and **3**. The percentage of **2** produced was increased in both cases.

5.2.2 Improved Synthetic Procedure

After numerous unsuccessful attempts to repeat the previously published procedure for the synthesis of hexakis(imidazolyl)cyclotriphosphazene **2**, several modifications were made to the reaction conditions. It was found that the use of excess imidazole, heating, and adjustment of the nucleophilicity of imidazole via the use of potassium imidazole were unable to produce **2** as a single product in high yield. In all previous attempts dry THF was used as the solvent. A series of solubility tests showed that imidazole hydrochloride, which is a byproduct of the reaction of imidazole with **1**, (Equation 5-2) is insoluble in dichloromethane. For this reason it was determined that dichloromethane may also be a suitable solvent for the substitution of **1** with imidazole.

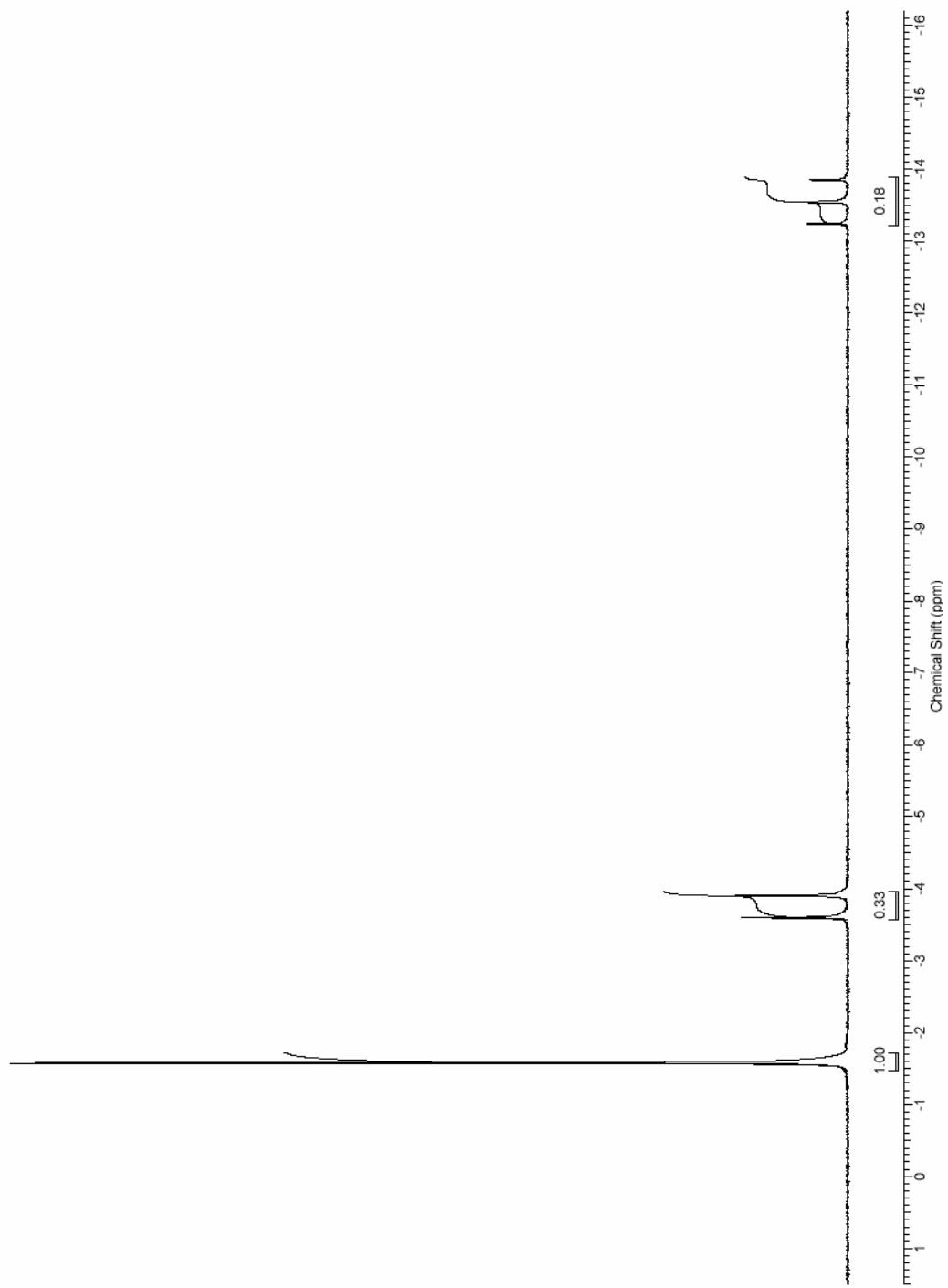


Figure 5-5. ^{31}P NMR spectrum of **2** and **3** in d_6 -DMSO. Isolated from the reaction of six equivalents of potassium imidazole with **1**.

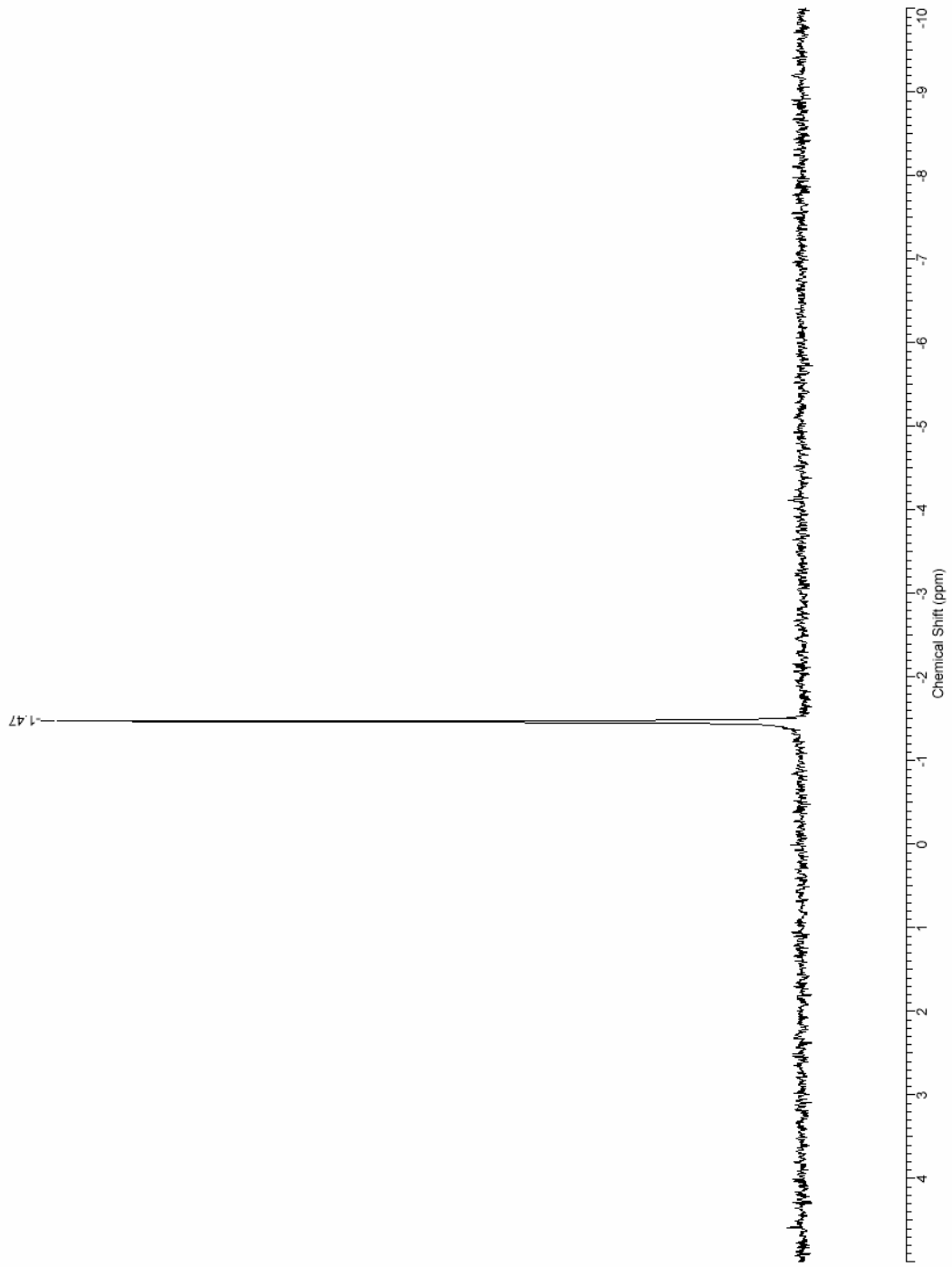


Figure 5-6. ^{31}P NMR spectrum of **2** in d_6 -DMSO.

The reaction of twelve equivalents of imidazole with **1** in dry dichloromethane under nitrogen results in the formation of **2** as a white solid in 87 % yield. The ^{31}P NMR spectrum shows a single resonance peak at -1.47 ppm corresponding to **2**, shown in Figure 5-6. No formation of the penta substituted phosphazene **3** was observed under these reaction conditions. The ^1H and ^{13}C NMR spectra are also consistent with the formation of **2** as the lone product. Substituted phosphazene **2** is stable in the solid form on the bench top for months with virtually no observed hydrolysis.

Single crystals of **2** suitable for X-ray diffraction studies were grown by slow evaporation from a concentrated sample in dichloromethane. The thermal ellipsoid plots of **2** are depicted in Figure 5-7. The asymmetric unit contains one full molecule of **2** and one dichloromethane solvent molecule. The P-N bonds of the phosphazene ring average 1.58 Å showing multiple bond character and are virtually identical to those observed in $[\text{NPCl}_2]_3$ **1**. P-N bond distances between the ring phosphorus atoms and the ring nitrogen atoms of the imidazole substituents average 1.68 Å. The ring shows some distortion from planarity. Dihedral angles of 7.1° at P(1) and 7.7° at N(1) were observed from the mean plane of the ring.

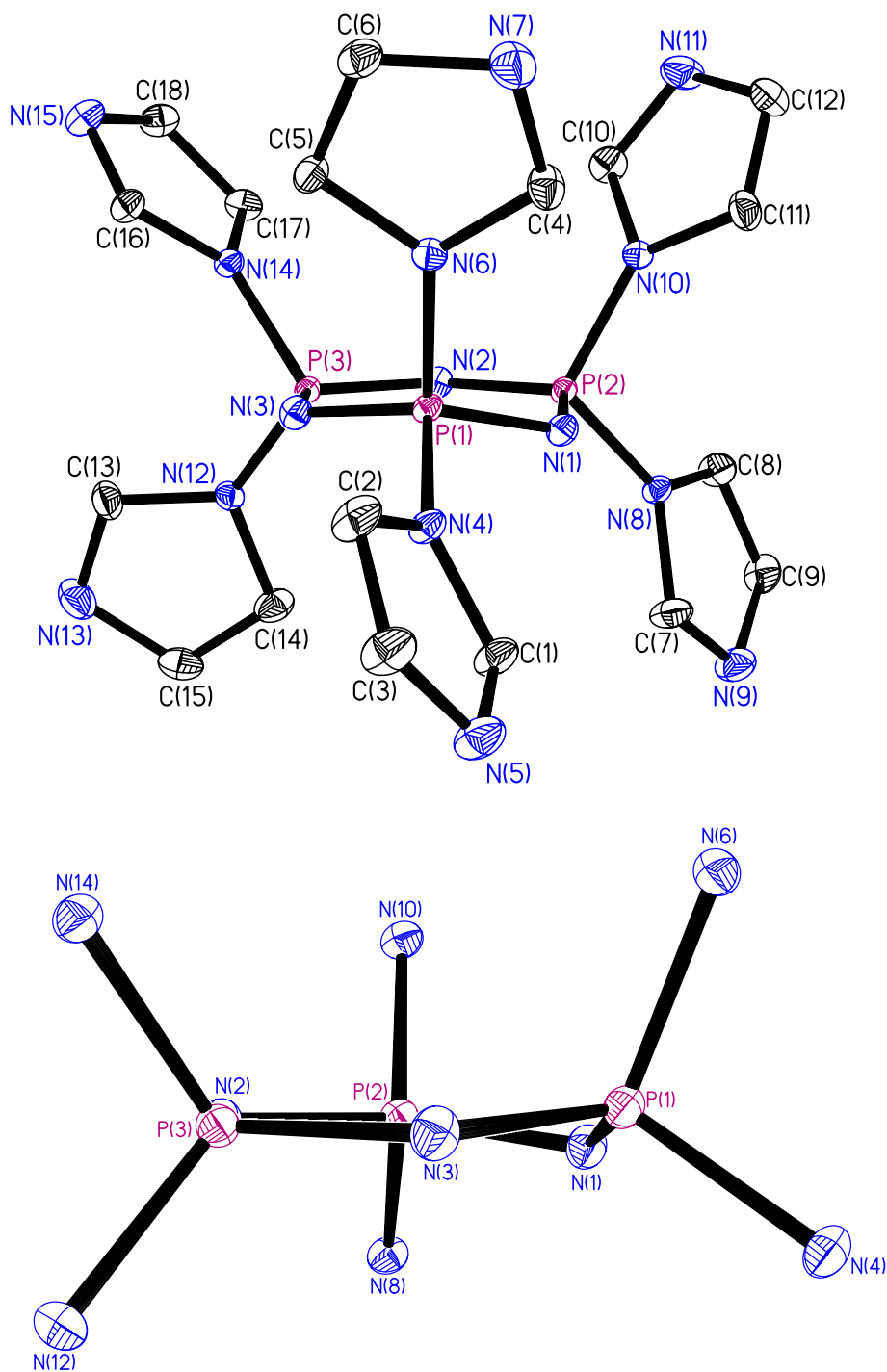


Figure 5-7. Top: thermal ellipsoid plot of **2** with hydrogen atoms removed for clarity and thermal ellipsoids shown at 50 % probability. Bottom: side view of the ring distortion of **2** with only the bonding nitrogen atoms of the imidazole rings shown. Thermal ellipsoids shown at 50 % probability.

5.3 Experimental Section

5.3.1 General Considerations

All reactions were performed under nitrogen using standard Schlenk techniques unless otherwise stated. Imidazole was dried on a vacuum line prior to use. Hexachlorocyclotriphosphazene was purchased from Aldrich and used without further purification. Dry dichloromethane was collected from a Pure Solv solvent purification system by Innovative Technology Inc. ^1H , ^{13}C , and ^{31}P NMR data were obtained using a Varian Gemini 300 MHz instrument. ^1H and ^{13}C NMR spectra were referenced to deuterated solvents and the ^{31}P NMR to an external 85 % phosphoric acid reference.

5.3.2 X-ray Structure Determination Details

Data sets were collected on a Bruker Apex CCD diffractometer with graphite-monochromated Mo $K\alpha$ radiation ($\lambda = 0.71073 \text{ \AA}$). Unit cell determination was achieved by using reflections from three different orientations. An empirical absorption correction and other corrections were performed using multi-scan SADABS. Structure solution, refinement and modeling were accomplished using the Bruker SHELXTL package.⁸⁸ The structure was obtained by full-matrix least-squares refinement of F^2 and the selection of appropriate atoms from the generated difference map.

5.3.3 Synthesis of **2** [NP(C₃H₃N₂)₂]₃

To an Schlenk flask was added dried imidazole (1.63 g, 24 mmol) and dichloromethane (60 mL). The flask was brought into the dry box and hexachlorocyclo-triphosphazene (0.69 g, 2 mmol) was added. The solution was stirred at room temperature for 2.5 hours and was then removed from the glove box. The reaction was opened to air and imidazole hydrochloride was removed by vacuum filtration. The dichloromethane was then removed via rotary evaporator to afford **2** as a white solid. Yield: 0.94 g, 87 %. Mp: 199-202 °C. ¹H NMR (300 MHz, *d*₆-DMSO): δ 7.22 (s, CH), 7.64 (s, CH), 8.19 (s, CH). ¹³C{¹H} NMR (75 MHz, *d*₆-DMSO): δ 119.1, 132.3, 138.9 (Aromatic). ³¹P NMR (*d*₆-DMSO): δ -1.47. ES-MS (m/z): calcd, 538.2 (M⁺ of C₁₈H₁₉N₁₅P₃).

X-ray crystal structure analysis of **2**: formula C₁₉H₂₀Cl₂N₁₅P₃, *M_w* = 622.31, colorless crystal 0.45 x 0.27 x 0.14 mm, *a* = 9.5339(8) Å, *b* = 15.6322(13) Å, *c* = 17.8162(15) Å, α = 90°, β = 90°, γ = 90°, *V* = 2655.3(4) Å³, *D*_{calc} = 1.557 Mg cm⁻³, μ = 0.469 mm⁻¹, *Z* = 4, orthorhombic, space group *P*2₁2₁2₁ (No. 19), λ = 0.71073 Å, *T* = 100 K, ω and φ scans, 23412 reflections collected, 6293 independent (*R*_{int}) 0.0338, 353 refined parameters, *R*₁/*wR*₂ (*I* ≥ 2σ(*I*)) = 0.0326 / 0.0744 and *R*₁/*wR*₂ (all data) = 0.0349 / 0.0755, maximum (minimum) residual electron density 0.425 (-0.268) e Å⁻³, all hydrogen atoms were calculated and refined as riding atoms.

BIBLIOGRAPHY

1. Öfele, K. *J. Organomet. Chem.* **1968**, *12*, 42.
2. Wanzlick, H.W.; Schönherr, H.J. *Angew. Chem. Int. Ed. Engl.* **1968**, *7*, 141.
3. Arduengo, A.J. III; Harlow, R.L.; Kline, M. *J. Am. Chem. Soc.* **1991**, *113*, 361.
4. Lappert, M.F. *J. Organomet. Chem.* **1975**, *100*, 139.
5. Lappert, M. F. *J. Organomet. Chem.* **1988**, *358*, 185.
6. Herrmann, W.A. *Angew. Chem. Int. Ed.* **2002**, *41*, 1290.
7. Bourissou, D.; Guerret, O.; Gabbaie, F.P.; Bertrand, G. *Chem. Rev.* **2000**, *100*, 39.
8. Herrmann, W.A.; Köcher, C. *Angew. Chem. Int. Ed. Engl.* **1997**, *36*, 2162.
9. Garrison, J.C.; Youngs, W.J. *Chem. Rev.* **2005**, *105*, 3978.
10. Lin, I.J.B.; Vasam, C.S. *Can. J. Chem.* **2005**, *83*, 812.
11. Crudden, C.M.; Allen, D.P. *Coord. Chem. Rev.* **2004**, *248*, 2247.
12. Peris, E.; Crabtree, R.H. *Coord. Chem. Rev.* **2004**, *248*, 2239.
13. Cavell, K.J.; McGuinness, D.S. *Coord. Chem. Rev.* **2004**, *248*, 671.
14. Deubel, D. V. *Organometallics* **2002**, *21*, 4303.
15. Abernethy, C. D.; Codd, G. M.; Spicer, M. D.; Taylor, M. K. *J. Am. Chem. Soc.* **2003**, *125*, 1128.
16. Termaten, A.T.; Schakel, M.; Ehlers, A.W.; Lutz, M.; Spek, A.L.; Lammertsma, K. *Chem. Eur. J.* **2003**, *9*, 3577.
17. Nemcsok, D.; Wichmann, K.; Frenking, G. *Organometallics* **2004**, *23*, 3640.

18. Lee, M.-T.; Hu, C.-H. *Organometallics* **2004**, *23*, 976.
19. Cavallo, L.; Correa, A.; Costabile, C.; Jacobsen, H. *J. Organomet. Chem.* **2005**, *690*, 5407.
20. Lee, C.-L.; Guo, W.-H.; Lee, M.-T.; Hu, C.-H. *J. Organomet. Chem.* **2005**, *690*, 5867.
21. Green, J.C.; Herbert, B.J. *Dalton* **2005**, 1214.
22. Anderson, C.J.; Welch, M.J. *Chem. Rev.* **1999**, *99*, 2219.
23. Arduengo, A.J.; Dias, H.V.R.; Calabrese, J.C.; Davidson, F. *Organometallics* **1993**, *12*, 3405.
24. Guerret, O.; Solé, S.; Gornitzka, H.; Teichert, M.; Trinquier, G.; Bertrand, G.J. *J. Am. Chem. Soc.* **1997**, *119*, 6668.
25. Wang, H.M.J.; Lin, I.J.B. *Organometallics* **1998**, *17*, 972.
26. Tulloch, A.A.D.; Danopoulos, A.A.; Winston, S.; Kleinhenz, S.; Eastham, G.J. *J. Chem. Soc., Dalton Trans.* **2000**, *24*, 4499.
27. Ellis, G.P.; Luscombe, D.K., Eds. *Progress in Medicinal Chemistry*; Elsevier Science **1994**, pp. 351-370.
28. White, R. J.; *Br. J. Nurs.*, **2002**, *15*, 3.
29. Russell, A. D.; Path, F. R.; Hugo, W. B.; *Prog. Med. Chem.*, **1994**, *31*, 351.
30. Albright, C. F.; Nachum, R.; Lechtman, M. D.; Electrolytic silver ion generator for water sterilization in Apollo spacecraft water systems. Apollo applications program. *NASA Contract Rep.*, **1967**, 133.
31. Conrand, A. H.; Tramp, C. R.; Long, C. J.; Wells, D. C.; Paulsen, A. Q.; Conrand, G. W.; *Aviat Space Environ Med.*, **1999**, *70*, 1096.
32. Berkow, R.; Fletcher, A.J., Eds. *The Merck Manual of Diagnosis and Therapy*, 6th ed., Merck Laboratories: Rahway, **1992**.
33. Melaiye, A.; Youngs, W.J. *Expert Opinion on Therapeutic Patents* **2005**, *15*(2), 125.
34. Feng, Q.L.; Wu, J.; Chen, G.Q. *J. Biomed. Mat Res.* **2000**, *52*, 662.

35. Garrison, J.C.; Simons, R.S.; Talley, J.M.; Wesdemiotis, C.; Tessier, C.A.; Youngs, W.J. *Organometallics* **2001**, *20*, 1276.
36. Melaiye, A.; Simons, R.S.; Milsted, A.; Pingitore, F.; Wesdemiotis, C.; Tessier, C.A.; Youngs, W.J. *J. Chem. Med.* **2004**, *47*, 973.
37. Garrison, J.C.; Tessier, C.A.; Youngs, W.J. *J. Organometallic Chem.* **2005**, *690*, 6008.
38. Ricketts, C.R.; Lowbury, E.J.L.; Lawrence, J.C.; Hall, M. *Br. Med. J.* **1970**, *1*, 444.
39. Melaiye, A. Synthesis and Antimicrobial Properties of Silver(I) N-Heterocyclic Carbene Complexes. Ph.D. Thesis, The University of Akron, Akron, OH, August **2005**.
40. Melaiye, A.; Sun, Z.; Hindi, K.; Milsted, A.; Ely, D.; Reneker, D.H.; Tessier, C.A.; Youngs, W.J. *J. Am. Chem. Soc.* **2005**, *127*, 2285.
41. Melaiye, A.; Sun, Z.; Seeyangnok, S.; Panzner, M.J.; Milsted, A.; Reneker, D.H.; Reddy, V.; Hull, D.H.; Kinder, J.D.; Tessier, C.A.; Youngs, W.J. *accepted Organometallics* **2006**.
42. Reneker D.H.; Yarin A.L.; Fong H.; Koombhongse S. *J. Appl. Phys.* **2000**, *87*, 4531.
43. Bognitzki, M.; Czado, W.; Frese, T.; Schaper, A.; Hellwig, M.; Steinhardt, M.; Greiner, A.; Wendorff, J. *Adv. Mater.* **2001**, *13*, 70.
44. Shin, Y.M.; Hohman, M.M.; Brenner, M.P.; Rutledge, G.C. *Polymer* **2001**, *42*, 9955.
45. Macdiarmid, A.G.; Jones, W.E. Jr.; Norris, I.D.; Gao, J.; Johnson, A.T.; Pinto, N.J.; Hone, J.; Han, B.; Ko, F.K.; Okuzaki, H.; Llaguno, M. *Synth. Met.* **2001**, *119*, 27.
46. Bognitzki, M.; Hou, H.; Ishaque, M.; Frese, T.; Hellwig, M.; Schwarte, C.; Schaper, A.; Wendorff, J. H.; Greiner, A. *Adv. Mater.* **2000**, *12(9)*, 637-640.
47. Bognitzki, M.; Frese, T.; Steinhardt, M.; Greiner, A.; Wendorff, J. *Polym. Eng. Sci.* **2001**, *41*, 982.
48. Fennessey, S.F.; Farris, R.J. *ANTEC*. **2003**, 3766.

49. Hu, X.; Tang, Y.; Gantzel, P.; Meyer, K. *Organometallics* **2003**, *22*, 612.
50. Kascatan-Nebioglu, A.; Panzner, M.J.; Tessier, C.A.; Youngs, W.J. *Coord. Chem. Rev.* Accepted.
51. Kascatan-Nebioglu, A.; Melaiye, A.; Hindi, K.; Durmus, S.; Panzner, M.J.; Hogue, L.A.; Mallett, R.J.; Hovis, C.E.; Coughenour, M.; Crosby, S.D.; Milsted, A.; Ely, D.L.; Tessier, C.A.; Cannon, C.L.; Youngs, W.J. *J. Med. Chem.* Accepted.
52. Berners-Price, S.J.; Johnson, R.K.; Giovenella A.J.; Faucette L.F.; Mirabelli, C.K.; Sadler, P.J. *J. Inorg. Biochem.* **1988**, *33*, 285.
53. Elsome, A.M.; Hamilton-Miller, J.M.T.; Brumfitt, W.; Nobble, W.C. *J. Antimicrob. Chemother.* **1996**, *37*, 911.
54. Novelli, F.; Recine, M.; Sparatore, F.; Juliano, C. *Farmaco* **1999**, *54*, 232.
55. Nomiya, K.; Noguchi, R.; Oda, M. *Inorg. Chim. Acta* **2000**, *298*, 24.
56. Nomiya, K.; Noguchi, R.; Ohsawa, K.; Tsuda, K.; Oda, M. *J. Inorg. Biochem.* **2000**, *78*, 363.
57. I. Özdemir, I.; Denizci, A.; Öztürk, H.T.; Çetinkaya, B. *Appl. Organometal. Chem.* **2004**, *18*, 318.
58. Barnard, P.J.; Baker, M.V.; Berners-Price, S.J.; Day, D.A. *J. Inorg. Biochem.* **2004**, *98*, 1642.
59. Schneider, S.K.; Herrmann, W.A.; Herdtweck, E. *Z. Anorg. Allg. Chem.* **2003**, *629*, 2363.
60. Ku, R.Z.; Huang, J.C.; Cho, J.Y.; Kiang, F.M.; Reddy, K.R.; Chen, Y.C.; Lee, K.J.; Lee, J.-H.; Lee, G.H.; Peng, S.M.; Liu, S.T. *Organometallics*, **1999**, *18*, 2145.
61. Lin, I.J.B.; Vasam, C.S. *Can. J. Chem.* **2005**, *83*, 812.
62. Shwarz, J.; Böhm, V.P.W.; Gardiner, M.G.; Grosche, M.; Herrmann, W.A.; Hieringer, W.; Raudaschl-Sieber, G. *Chem. Eur. J.* **2000**, *6*, 1773.
63. Herrmann, W.A. *Angew. Chem. Int. Ed.* **2002**, *41*, 1290.

64. Barnard, P.J.; Baker, M.V.; Berners-Price, S.J.; Skelton, B.W.; White, A.H. *Dalton Trans.* **2004**, 1038-1147.
65. Modica-Napolitano, J.S.; Aprile, J.R. *Adv. Drug Delivery Rev.* **2001**, *49*, 63.
66. Debatin, K.-M.; Poncet, D.; Kroemer, G. *Oncogene* **2002**, *21*, 8786.
67. Anderson, C.J.; Welch, M.J. *Chem. Rev.* **1999**, *99*, 2234.
68. Zweit, J. *Phys. Med. Biol.* **1996**, *41*, 1905.
69. Jurisson, S.S.; Ketring, A.R.; Volkert, W.A. *Transition Met. Chem.* **1997**, *22*, 315.
70. Poyatos, M.; Mas-Marza, E.; Mata, J.A.; Sanau, M.; Peris, E. *Eur. J. Inorg. Chem.* **2003**, *6*, 1215.
71. Poyatos, M.; Sanau, M.; Peris, E. *Inorg. Chem.* **2003**, *42*, 2572.
72. Poyatos, M.; Uriz, P.; Mata, J.A.; Claver, C.; Fernandez, E.; Peris, E. *Organometallics* **2003**, *22*, 1110.
73. Albrecht, M.; Crabtree, R.H.; Mata, J.; Peris, E. *Chem. Commun.* **2002**, *1*, 32.
74. Simons, R.S.; Custer, P.; Tessier, C.A.; Youngs, W.J. *Organometallics* **2003**, *22*, 1979.
75. Cotton, F.A., Ed. *Inorganic Synthesis*; McGraw-Hill Book Company **1972**, *13*, 90.
76. Herrmann, W.A.; Goossen, L.J.; Kocher, C.; Artus, G.J. *Angew. Chem. Int. Ed. Engl.* **1996**, *35*, 2805.
77. Quezada, C.A.; Garrison, J.C.; Tessier, C.A.; Youngs, W.J. *J. Organomet. Chem.* **2003**, *671*, 183.
78. Quezada, C.A.; Garrison, J.C.; Panzner, M.J.; Tessier, C.A.; Youngs, W.J. *Organometallics* **2004**, *23*, 4846.
79. Gavrilin, M.V.; Karpenya, L.I.; Ushakova, L.S.; Senchukoa, G.V.; Kompantseva, E.V. *Pharmaceutical Chem. J.* **2001**, *35*, 284.
80. Yu, L.J. *Agric. Food Chem.* **2003**, *51*, 2344.

81. Grany, G.A., Ed. *Synthetic Peptides a User's Guide*, 2nd ed.; Oxford University Press Inc.: New York, **2002**, Ch. 3.
82. Nyce, G. W.; Glauser, T.; Connor, E. F.; Mock, A.; Waymouth, R. M.; Hedrick, J. L. *J. Am. Chem. Soc.* **2003**, *125*, 3046.
83. Díez-Barra, E., *Heterocycles* **1992**, *34*, 1365.
84. Claramunt, R.M.; Elguero, J.; Meco, T. *J. Heterocyclic Chem.* **1983**, *20*, 1245.
85. Kascatan-Nebioglu, A.; Panzner, M.J.; Garrison, J.C.; Tessier, C.A.; Youngs, W.J. *Organometallics* **2004**, *23*, 1928.
86. Wanniarachchi, Y.A.; Khan, M.A.; Slaughter, L.M. *Organometallics*. **2004**, *23*, 5881.
87. Che, C.-M.; Tse, M.-C.; Chan, M.C.W.; Cheung, K.-K.; Phillips, D.L.; Leung, K.-H. *J. Am. Chem. Soc.* **2000**, *122*, 2464.
88. Sheldrick, G. M. SHELX97: Programs for Crystal Structural Analysis; University of Göttingen, Göttingen, Germany **1997**.
89. Garrison, J.C.; Panzner, M.J.; Tessier, C.A.; Youngs, W.J. *Synlett*. **2005**, *1*, 99.
90. Durmus, S.; Garrison, J. C.; Panzner, M. J.; Tessier, C. A.; Youngs, W. J. *Tetrahedron* **2005**, *61*, 97.
91. Baker, M. V.; Bosnich, M. J.; Williams, C. C.; Skelton, B. W.; White, A. H. *Aust. J. Chem.* **1999**, *52*, 823.
92. Alcalde, E.; Alvarez-Ru' a, C.; Garcia-Granda, S.; Garcia-Rodriquez, E.; Mesquida, N.; Pe' rez-Garcia, L. *J. Chem. Soc., Chem. Commun.* **1999**, 295.
93. Baker, M. V.; Bosnich, M. J.; Brown, D. H.; Byrne, L. T.; Hesler, V. J.; Skelton, B.W.; White, A. H.; Williams, C. C. *J. Org. Chem.* **2004**, *69*, 7640.
94. Alcalde, E.; Alemany, M.; Pérez-Garcia, L.; Rodriquez, M. *J. Chem. Soc., Chem. Commun.* **1995**, 1239.
95. Bitter, I.; Török, Z.; Csokai, V.; Grün, A.; Balázs, B.; Tóth, G.; Keserù, G. M.; Kovári, Z.; Czugler, M. *Eur. J. Org. Chem.* **2001**, 2861.
96. Harvey, J.D.; Ziegler, C.J. *Coord. Chem. Rev.* **2003**, *247*, 1.

97. Chmielewski, P.J.; Latos-Grazynski, L. *Coord. Chem. Rev.* **2005**, *249*, 2510.
98. Harvey, J.D.; Ziegler, C.J. *J. Inorg. Biochem.* **2006**, *100*, 869.
99. Rosa, A.; Ricciardi, G.; Rosi, M.; Sgamellotti, A.; Floriani, C. *J. Chem. Soc., Dalton Trans.* **1993**, 3759.
100. Hahn, F.E.; Langenhahn, V.; Van, D.L.; Tamm, M.; Wittenbecher, L.; Lügger, T. *Heteroat. Chem.* **2002**, *13*, 540.
101. Hahn, F.E.; Langenhahn, V.; Lügger, T.; Pape, T.; Van, D.L. *Angew. Chem. Int. Ed.* **2005**, *44*, 3759.
102. Sessler, J. L.; Mody, T. A.; Hemmi, G. W.; Lynch, V. *Inorg. Chem.* **1993**, *32*, 3175.
103. Chandler, C.J.; Deady, L.W.; Reiss, J.A. *J. Heterocycl. Chem.* **1981**, *18*, 599.
104. Allcock, H.R. In *Chemistry and Applications of Polyphosphazenes*, John Wiley & Sons, Inc.: New Jersey, **2003**, Chapter 1.
105. Allcock, H.R.; Mark, J.; West, R. "Polyphosphazenes" *Inorganic Polymers*, Prentice Hall: New York, **1992**, Chapter 3.
106. Allcock, H.R. In *Chemistry and Applications of Polyphosphazenes*, John Wiley & Sons, Inc.: New Jersey, **2003**, Chapter 5.
107. Sennett, M.S.; Hagnauer, G.L.; Singler, R.E.; Davies, G. *Macromolecules* **1986**, *19*, 959.
108. Potts, M.K.; Hagnauer, G.L.; Sennett, M.S.; Davies, G. *Macromolecules* **1989**, *22*, 4235.
109. Allcock, H.R. In *Chemistry and Applications of Polyphosphazenes*, John Wiley & Sons, Inc.: New Jersey, **2003**, Chapter 3.
110. Gilheany, D.G. *Chem. Rev.* **1994**, *94*, 1339.
111. Allcock, H.R. *Chem. Rev.* **1972**, *72*, 315.
112. Snyder; D.L., Stayer, J.; Mark L., Kang; J.W. *U.S. Patent* 4,123,503, **1978**.

113. Allcock, H.R. *Phosphorus-Nitrogen Compounds*; Academic: New York, **1972**, Chapters 4, 10-12.
114. Heston, A.J.; Panzner, M.J.; Youngs, W.J.; Tessier, C.A. *Inorg. Chem.* **2005**, *44*(19), 6518.
115. Coxon, G.E.; Sowerby, D.B. *J. Chem. Soc. A* **1969**, 3012.
116. Bodde, H.; Bach, H. *Chem. Ber.* **1942**, *75*, 215.
117. Goehring, M.; Hohenschutz, H.; Appel, R. *Z. Naturforsch.* **1954**, *9b*, 678.
118. Bode, H.; Bütow, K.; Lienau, G. *Chem. Ber.* **1948**, *81*, 547.
119. Kravchenko, E.A.; Levin, B.V.; Bananyarly, S.I.; Toktomatov, T.A. *Koord. Khim.* **1977**, *3*, 374.
120. Kandermirli, F. *Phosphorus, Sulfur, Silicon* **2003**, *178*, 2331.
121. Heston, A.J.; Panzner, M.J.; Youngs, W.J.; Tessier, C.A. *Phosphorus, Sulfur Silicon Relat. Elem.* **2004**, *179*(4-5), 831.
122. Allcock, H.R.; Fuller, T.J. *J. Am. Chem. Soc.* **1981**, *103*, 2250.
123. Hyde, M.; Schacht, E. In *Phosphazenes: A Worldwide Insight*; Gleria M., De Jaeger, R., Eds.; Nova Science Publishers, Inc.: New York, **2004**; 367.
124. *The Merck Manual of Diagnosis and Therapy*, 7th ed.; Berkow, R., Fletcher, A.J., Eds.; Merck Research Laboratories: Rahway, 419.

APPENDICES

APPENDIX A

SUPPLEMENTARY MATERIAL FOR THE X-RAY CRYSTAL STRUCTURE OF

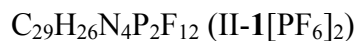


Table 1. Crystal data and structure refinement for 1[PF₆]₂.

Identification code	$C_{29}H_{26}F_{12}N_4P_2$	
Empirical formula	C29 H26 F12 N4 P2	
Formula weight	720.48	
Temperature	100(2) K	
Wavelength	0.71073 Å	
Crystal system	Monoclinic	
Space group	C2/c	
Unit cell dimensions	$a = 33.719(4)$ Å	$\alpha = 90^\circ$.
	$b = 5.9540(7)$ Å	$\beta = 97.050(2)^\circ$.
	$c = 14.3469(17)$ Å	$\gamma = 90^\circ$.
Volume	$2858.6(6)$ Å ³	
Z	4	
Density (calculated)	1.674 Mg/m ³	
Absorption coefficient	0.261 mm ⁻¹	
F(000)	1464	
Crystal size	0.28 x 0.20 x 0.07 mm ³	
Theta range for data collection	1.22 to 28.34°.	
Index ranges	$-44 \leq h \leq 44$, $-7 \leq k \leq 7$, $-19 \leq l \leq 19$	
Reflections collected	12206	
Independent reflections	3444 [R(int) = 0.0313]	
Completeness to theta = 28.34°	96.7 %	
Absorption correction	Semi-empirical from equivalents	
Max. and min. transmission	0.9820 and 0.9305	
Refinement method	Full-matrix least-squares on F ²	

Data / restraints / parameters	3444 / 0 / 213
Goodness-of-fit on F^2	1.148
Final R indices [$I > 2\sigma(I)$]	R1 = 0.0482, wR2 = 0.1202
R indices (all data)	R1 = 0.0603, wR2 = 0.1341
Largest diff. peak and hole	0.531 and -0.348 e.Å ⁻³

Table 2. Atomic coordinates ($\times 10^4$) and equivalent isotropic displacement parameters ($\text{Å}^2 \times 10^3$) for $1[\text{PF}_6]_2$. $U(\text{eq})$ is defined as one third of the trace of the orthogonalized U^{ij} tensor.

	x	y	z	U(eq)
P(1)	4193(1)	905(1)	8977(1)	15(1)
F(1)	4209(1)	1172(2)	7866(1)	26(1)
F(2)	4181(1)	3571(2)	9079(1)	26(1)
F(3)	4671(1)	963(2)	9151(1)	28(1)
F(4)	4214(1)	-1767(2)	8858(1)	26(1)
F(5)	3720(1)	831(2)	8809(1)	27(1)
F(6)	4184(1)	618(2)	10083(1)	24(1)
N(1)	4746(1)	3277(3)	1855(1)	15(1)
N(2)	4230(1)	5057(3)	1201(1)	15(1)
C(1)	5000	1847(5)	2500	15(1)
C(2)	4351(1)	3485(3)	1822(1)	15(1)
C(3)	4882(1)	4792(4)	1245(2)	20(1)
C(4)	4558(1)	5906(4)	837(2)	20(1)
C(5)	3813(1)	5786(4)	919(2)	18(1)
C(6)	3526(1)	4382(3)	1395(1)	15(1)
C(7)	3375(1)	2330(4)	986(1)	18(1)
C(8)	3142(1)	987(4)	1452(2)	18(1)
C(9)	3048(1)	1559(3)	2356(1)	15(1)
C(10)	2821(1)	131(4)	2881(2)	19(1)
C(11)	2743(1)	735(4)	3754(2)	21(1)
C(12)	2883(1)	2792(4)	4154(2)	21(1)
C(13)	3099(1)	4212(4)	3664(2)	19(1)
C(14)	3191(1)	3627(3)	2759(1)	15(1)

C(15) 3427(1) 5018(3) 2252(1) 16(1)

Table 3. Bond lengths [\AA] and angles [$^\circ$] for $\mathbf{1}[\text{PF}_6]_2$.

P(1)-F(5)	1.5834(14)
P(1)-F(2)	1.5945(14)
P(1)-F(6)	1.5999(13)
P(1)-F(3)	1.6011(14)
P(1)-F(4)	1.6032(14)
P(1)-F(1)	1.6101(13)
N(1)-C(2)	1.333(2)
N(1)-C(3)	1.374(3)
N(1)-C(1)	1.456(2)
N(2)-C(2)	1.322(3)
N(2)-C(4)	1.378(3)
N(2)-C(5)	1.479(2)
C(1)-N(1)#1	1.456(2)
C(3)-C(4)	1.349(3)
C(5)-C(6)	1.504(3)
C(6)-C(15)	1.366(3)
C(6)-C(7)	1.422(3)
C(7)-C(8)	1.353(3)
C(8)-C(9)	1.415(3)
C(9)-C(10)	1.419(3)
C(9)-C(14)	1.420(3)
C(10)-C(11)	1.360(3)
C(11)-C(12)	1.409(3)
C(12)-C(13)	1.365(3)
C(13)-C(14)	1.415(3)
C(14)-C(15)	1.411(3)
F(5)-P(1)-F(2)	90.32(7)
F(5)-P(1)-F(6)	90.44(7)
F(2)-P(1)-F(6)	90.68(7)

F(5)-P(1)-F(3)	179.60(8)
F(2)-P(1)-F(3)	90.04(7)
F(6)-P(1)-F(3)	89.40(7)
F(5)-P(1)-F(4)	90.71(7)
F(2)-P(1)-F(4)	178.51(8)
F(6)-P(1)-F(4)	90.38(7)
F(3)-P(1)-F(4)	88.93(7)
F(5)-P(1)-F(1)	90.35(7)
F(2)-P(1)-F(1)	89.83(7)
F(6)-P(1)-F(1)	179.06(8)
F(3)-P(1)-F(1)	89.81(7)
F(4)-P(1)-F(1)	89.09(7)
C(2)-N(1)-C(3)	109.09(17)
C(2)-N(1)-C(1)	125.69(15)
C(3)-N(1)-C(1)	124.93(16)
C(2)-N(2)-C(4)	108.60(17)
C(2)-N(2)-C(5)	126.67(17)
C(4)-N(2)-C(5)	124.72(17)
N(1)#1-C(1)-N(1)	108.4(2)
N(2)-C(2)-N(1)	108.33(17)
C(4)-C(3)-N(1)	106.45(18)
C(3)-C(4)-N(2)	107.51(18)
N(2)-C(5)-C(6)	110.82(16)
C(15)-C(6)-C(7)	119.64(18)
C(15)-C(6)-C(5)	119.71(19)
C(7)-C(6)-C(5)	120.54(18)
C(8)-C(7)-C(6)	120.26(19)
C(7)-C(8)-C(9)	121.39(19)
C(8)-C(9)-C(10)	122.62(19)
C(8)-C(9)-C(14)	118.52(18)
C(10)-C(9)-C(14)	118.85(19)
C(11)-C(10)-C(9)	120.5(2)
C(10)-C(11)-C(12)	120.77(19)
C(13)-C(12)-C(11)	120.1(2)
C(12)-C(13)-C(14)	120.7(2)

C(15)-C(14)-C(13)	122.01(19)
C(15)-C(14)-C(9)	119.02(18)
C(13)-C(14)-C(9)	118.95(19)
C(6)-C(15)-C(14)	121.10(19)

Symmetry transformations used to generate equivalent atoms:

#1 -x+1,y,-z+1/2

Table 4. Anisotropic displacement parameters ($\text{\AA}^2 \times 10^3$) for $1[\text{PF}_6]_2$. The anisotropic displacement factor exponent takes the form: $-2\pi^2 [h^2 a^{*2} U^{11} + \dots + 2 h k a^* b^* U^{12}]$

	U11	U22	U33	U23	U13	U12
P(1)	18(1)	11(1)	17(1)	0(1)	3(1)	1(1)
F(1)	36(1)	23(1)	19(1)	4(1)	7(1)	8(1)
F(2)	35(1)	12(1)	31(1)	-1(1)	6(1)	0(1)
F(3)	18(1)	32(1)	36(1)	0(1)	3(1)	2(1)
F(4)	44(1)	11(1)	24(1)	-1(1)	2(1)	3(1)
F(5)	19(1)	30(1)	31(1)	-1(1)	2(1)	-3(1)
F(6)	33(1)	23(1)	17(1)	0(1)	4(1)	3(1)
N(1)	13(1)	16(1)	15(1)	1(1)	1(1)	-1(1)
N(2)	15(1)	14(1)	15(1)	1(1)	4(1)	-1(1)
C(1)	12(1)	15(1)	18(1)	0	1(1)	0
C(2)	16(1)	15(1)	16(1)	1(1)	2(1)	-2(1)
C(3)	18(1)	24(1)	20(1)	4(1)	6(1)	-3(1)
C(4)	19(1)	21(1)	20(1)	6(1)	6(1)	-4(1)
C(5)	16(1)	21(1)	17(1)	6(1)	2(1)	2(1)
C(6)	12(1)	16(1)	17(1)	3(1)	0(1)	2(1)
C(7)	17(1)	19(1)	16(1)	-3(1)	2(1)	3(1)
C(8)	16(1)	16(1)	22(1)	-5(1)	1(1)	1(1)
C(9)	12(1)	14(1)	19(1)	0(1)	0(1)	2(1)
C(10)	15(1)	14(1)	26(1)	1(1)	2(1)	1(1)
C(11)	17(1)	22(1)	25(1)	7(1)	7(1)	0(1)
C(12)	20(1)	26(1)	17(1)	0(1)	5(1)	2(1)
C(13)	17(1)	20(1)	19(1)	-3(1)	1(1)	-1(1)

C(14)	13(1)	15(1)	17(1)	1(1)	0(1)	2(1)
C(15)	15(1)	15(1)	18(1)	-1(1)	0(1)	1(1)

Table 5. Hydrogen coordinates ($\times 10^4$) and isotropic displacement parameters ($\text{\AA}^2 \times 10^3$) for $\mathbf{1}[\text{PF}_6]_2$.

	x	y	z	U(eq)
H(1A)	4833	874	2854	18
H(1B)	5167	874	2146	18
H(2)	4185	2647	2183	18
H(3)	5152	5011	1133	24
H(4)	4557	7064	381	23
H(5A)	3749	5649	229	22
H(5B)	3784	7384	1090	22
H(7)	3438	1899	384	21
H(8)	3040	-367	1166	22
H(10)	2723	-1258	2620	22
H(11)	2592	-241	4098	25
H(12)	2827	3190	4766	25
H(13)	3187	5610	3933	22
H(15)	3519	6420	2511	19

APPENDIX B

SUPPLEMENTARY MATERIAL FOR THE X-RAY CRYSTAL STRUCTURE OF



Table 1. Crystal data and structure refinement for 2[PF₆].

Identification code	$C_{62}H_{54}Ag_2F_{12}N_{10}P_2$	
Empirical formula	C62 H54 Ag2 F12 N10 P2	
Formula weight	1444.83	
Temperature	100(2) K	
Wavelength	0.71073 Å	
Crystal system	Monoclinic	
Space group	P2(1)/c	
Unit cell dimensions	$a = 14.6559(12)$ Å	$\alpha = 90^\circ$.
	$b = 19.6526(16)$ Å	$\beta = 96.132(2)^\circ$.
	$c = 20.5800(16)$ Å	$\gamma = 90^\circ$.
Volume	$5893.7(8)$ Å ³	
Z	4	
Density (calculated)	1.628 Mg/m ³	
Absorption coefficient	0.808 mm ⁻¹	
F(000)	2912	
Crystal size	0.22 x 0.16 x 0.09 mm ³	
Theta range for data collection	1.40 to 28.30°.	
Index ranges	$-19 \leq h \leq 19$, $-25 \leq k \leq 26$, $-27 \leq l \leq 27$	
Reflections collected	52254	
Independent reflections	14175 [R(int) = 0.0682]	
Completeness to theta = 26.30°	100.0 %	
Absorption correction	Semi-empirical from equivalents	
Max. and min. transmission	0.9309 and 0.8423	
Refinement method	Full-matrix least-squares on F ²	

Data / restraints / parameters	14175 / 0 / 795
Goodness-of-fit on F^2	1.079
Final R indices [$I > 2\sigma(I)$]	R1 = 0.0594, wR2 = 0.1089
R indices (all data)	R1 = 0.0888, wR2 = 0.1185
Largest diff. peak and hole	1.163 and -1.193 e.Å ⁻³

Table 2. Atomic coordinates ($\times 10^4$) and equivalent isotropic displacement parameters ($\text{Å}^2 \times 10^3$) for $2[\text{PF}_6]$. $U(\text{eq})$ is defined as one third of the trace of the orthogonalized U_{ij} tensor.

	x	y	z	U(eq)
Ag(1)	2333(1)	4510(1)	3212(1)	17(1)
Ag(2)	2767(1)	5025(1)	1780(1)	17(1)
P(1)	2866(1)	8477(1)	3877(1)	21(1)
P(2)	2095(1)	1046(1)	1149(1)	21(1)
F(1)	2490(2)	9147(1)	4183(2)	55(1)
F(2)	2303(2)	8027(1)	4344(1)	34(1)
F(3)	3722(2)	8465(2)	4426(1)	40(1)
F(4)	2011(2)	8475(2)	3328(1)	57(1)
F(5)	3438(2)	8919(1)	3411(1)	33(1)
F(6)	3241(2)	7806(1)	3565(1)	43(1)
F(7)	1835(2)	1751(1)	1453(2)	52(1)
F(8)	1453(2)	664(1)	1612(1)	35(1)
F(9)	2937(2)	978(2)	1698(2)	75(1)
F(10)	2738(2)	1437(1)	686(1)	35(1)
F(11)	1257(2)	1126(2)	600(1)	58(1)
F(12)	2362(3)	346(2)	848(2)	74(1)
N(1)	3316(2)	3156(2)	3607(2)	18(1)
N(2)	2687(2)	3071(2)	2629(2)	17(1)
N(3)	3057(2)	3452(2)	1587(2)	18(1)
N(4)	4063(2)	4033(2)	1157(2)	20(1)
N(5)	1029(2)	5473(2)	3856(2)	20(1)
N(6)	1997(2)	6073(2)	3415(2)	18(1)
N(7)	2338(2)	6460(2)	2364(2)	17(1)

N(8)	1821(2)	6374(2)	1360(2)	20(1)
N(9)	1514(3)	8588(3)	733(3)	50(1)
N(10)	6599(3)	5863(3)	689(2)	55(1)
C(1)	4740(3)	4311(2)	3967(2)	27(1)
C(2)	5059(3)	4958(2)	3966(2)	26(1)
C(3)	4574(3)	5486(2)	4245(2)	22(1)
C(4)	4882(3)	6176(2)	4236(2)	29(1)
C(5)	4370(3)	6677(2)	4497(2)	31(1)
C(6)	3563(3)	6512(2)	4774(2)	31(1)
C(7)	3280(3)	5856(2)	4804(2)	27(1)
C(8)	3770(3)	5333(2)	4539(2)	19(1)
C(9)	3476(3)	4640(2)	4549(2)	21(1)
C(10)	3940(3)	4140(2)	4264(2)	21(1)
C(11)	3624(3)	3413(2)	4271(2)	25(1)
C(12)	2846(3)	3523(2)	3128(2)	16(1)
C(13)	3440(3)	2488(2)	3418(2)	21(1)
C(14)	3046(3)	2435(2)	2795(2)	23(1)
C(15)	2317(3)	3264(2)	1972(2)	18(1)
C(16)	3338(3)	4101(2)	1517(2)	16(1)
C(17)	3583(3)	2990(2)	1279(2)	24(1)
C(18)	4219(3)	3355(2)	1010(2)	26(1)
C(19)	4570(3)	4598(2)	880(2)	23(1)
C(20)	4593(3)	5235(2)	1281(2)	21(1)
C(21)	4308(3)	5839(2)	994(2)	20(1)
C(22)	4327(3)	6457(2)	1357(2)	19(1)
C(23)	4010(3)	7080(2)	1075(2)	22(1)
C(24)	4006(3)	7652(2)	1448(2)	26(1)
C(25)	4322(3)	7642(2)	2115(2)	31(1)
C(26)	4644(3)	7049(2)	2403(2)	28(1)
C(27)	4661(3)	6442(2)	2030(2)	22(1)
C(28)	4975(3)	5814(2)	2313(2)	27(1)
C(29)	4945(3)	5235(2)	1951(2)	25(1)
C(30)	47(3)	4382(2)	3000(2)	25(1)
C(31)	-50(3)	3850(2)	2578(2)	25(1)
C(32)	238(3)	3182(2)	2784(2)	22(1)

C(33)	153(3)	2622(2)	2357(2)	27(1)
C(34)	450(3)	1993(2)	2571(2)	30(1)
C(35)	825(3)	1900(2)	3217(2)	32(1)
C(36)	909(3)	2425(2)	3641(2)	27(1)
C(37)	621(3)	3088(2)	3442(2)	21(1)
C(38)	712(3)	3659(2)	3864(2)	22(1)
C(39)	448(3)	4296(2)	3654(2)	22(1)
C(40)	541(3)	4894(2)	4115(2)	25(1)
C(41)	1729(3)	5423(2)	3481(2)	18(1)
C(42)	875(3)	6143(2)	4027(2)	23(1)
C(43)	1484(3)	6525(2)	3749(2)	22(1)
C(44)	2720(3)	6282(2)	3020(2)	18(1)
C(45)	2253(2)	6014(2)	1860(2)	18(1)
C(46)	1961(3)	7088(2)	2183(2)	20(1)
C(47)	1633(3)	7031(2)	1548(2)	20(1)
C(48)	1636(3)	6122(2)	681(2)	26(1)
C(49)	1208(3)	5428(2)	661(2)	20(1)
C(50)	1654(3)	4873(2)	450(2)	23(1)
C(51)	1256(3)	4205(2)	465(2)	22(1)
C(52)	1719(3)	3615(2)	284(2)	26(1)
C(53)	1341(3)	2990(2)	336(2)	31(1)
C(54)	460(3)	2916(3)	538(2)	36(1)
C(55)	-12(3)	3477(3)	710(2)	31(1)
C(56)	376(3)	4139(2)	690(2)	25(1)
C(57)	-74(3)	4724(2)	890(2)	26(1)
C(58)	327(3)	5347(2)	881(2)	23(1)
C(59)	1891(4)	8807(3)	1199(3)	38(1)
C(60)	2386(3)	9076(3)	1790(3)	43(1)
C(61)	6957(4)	5679(3)	1179(3)	38(1)
C(62)	7415(4)	5435(3)	1798(3)	43(1)

Table 3. Bond lengths [\AA] and angles [$^\circ$] for $2[\text{PF}_6]$.

Ag(1)-C(12)	2.095(4)
Ag(1)-C(41)	2.100(4)
Ag(1)-Ag(2)	3.2440(5)
Ag(2)-C(16)	2.095(4)
Ag(2)-C(45)	2.097(4)
P(1)-F(1)	1.584(3)
P(1)-F(6)	1.591(3)
P(1)-F(5)	1.595(3)
P(1)-F(4)	1.595(3)
P(1)-F(3)	1.597(3)
P(1)-F(2)	1.600(3)
P(2)-F(12)	1.574(3)
P(2)-F(7)	1.584(3)
P(2)-F(11)	1.585(3)
P(2)-F(9)	1.588(3)
P(2)-F(8)	1.598(3)
P(2)-F(10)	1.605(3)
N(1)-C(12)	1.350(5)
N(1)-C(13)	1.387(5)
N(1)-C(11)	1.481(5)
N(2)-C(12)	1.358(5)
N(2)-C(14)	1.385(5)
N(2)-C(15)	1.451(5)
N(3)-C(16)	1.352(5)
N(3)-C(17)	1.386(5)
N(3)-C(15)	1.459(5)
N(4)-C(16)	1.365(5)
N(4)-C(18)	1.390(5)
N(4)-C(19)	1.484(5)
N(5)-C(41)	1.353(5)
N(5)-C(42)	1.387(5)
N(5)-C(40)	1.472(5)
N(6)-C(41)	1.348(5)

N(6)-C(43)	1.391(5)
N(6)-C(44)	1.461(5)
N(7)-C(45)	1.354(5)
N(7)-C(46)	1.386(5)
N(7)-C(44)	1.449(5)
N(8)-C(45)	1.349(5)
N(8)-C(47)	1.383(5)
N(8)-C(48)	1.480(5)
N(9)-C(59)	1.139(7)
N(10)-C(61)	1.144(7)
C(1)-C(2)	1.356(6)
C(1)-C(10)	1.418(6)
C(2)-C(3)	1.414(6)
C(3)-C(8)	1.413(6)
C(3)-C(4)	1.429(6)
C(4)-C(5)	1.381(6)
C(5)-C(6)	1.405(7)
C(6)-C(7)	1.359(6)
C(7)-C(8)	1.397(6)
C(8)-C(9)	1.429(5)
C(9)-C(10)	1.362(6)
C(10)-C(11)	1.504(6)
C(13)-C(14)	1.354(6)
C(17)-C(18)	1.342(6)
C(19)-C(20)	1.498(6)
C(20)-C(21)	1.370(6)
C(20)-C(29)	1.419(6)
C(21)-C(22)	1.424(6)
C(22)-C(23)	1.412(5)
C(22)-C(27)	1.420(6)
C(23)-C(24)	1.361(6)
C(24)-C(25)	1.402(6)
C(25)-C(26)	1.368(6)
C(26)-C(27)	1.422(6)
C(27)-C(28)	1.420(6)

C(28)-C(29)	1.357(6)
C(30)-C(31)	1.356(6)
C(30)-C(39)	1.421(6)
C(31)-C(32)	1.429(6)
C(32)-C(33)	1.406(6)
C(32)-C(37)	1.421(6)
C(33)-C(34)	1.368(6)
C(34)-C(35)	1.395(6)
C(35)-C(36)	1.349(6)
C(36)-C(37)	1.417(6)
C(37)-C(38)	1.415(6)
C(38)-C(39)	1.367(6)
C(39)-C(40)	1.509(6)
C(42)-C(43)	1.341(6)
C(46)-C(47)	1.348(6)
C(48)-C(49)	1.501(6)
C(49)-C(50)	1.367(6)
C(49)-C(58)	1.422(6)
C(50)-C(51)	1.437(6)
C(51)-C(52)	1.413(6)
C(51)-C(56)	1.423(6)
C(52)-C(53)	1.357(6)
C(53)-C(54)	1.406(7)
C(54)-C(55)	1.368(7)
C(55)-C(56)	1.422(6)
C(56)-C(57)	1.408(6)
C(57)-C(58)	1.359(6)
C(59)-C(60)	1.448(8)
C(61)-C(62)	1.456(7)
C(12)-Ag(1)-C(41)	168.00(15)
C(12)-Ag(1)-Ag(2)	96.12(10)
C(41)-Ag(1)-Ag(2)	95.80(11)
C(16)-Ag(2)-C(45)	168.67(15)
C(16)-Ag(2)-Ag(1)	94.96(11)
C(45)-Ag(2)-Ag(1)	96.37(11)

F(1)-P(1)-F(6)	179.7(2)
F(1)-P(1)-F(5)	90.84(15)
F(6)-P(1)-F(5)	89.05(15)
F(1)-P(1)-F(4)	90.22(19)
F(6)-P(1)-F(4)	89.52(18)
F(5)-P(1)-F(4)	90.05(15)
F(1)-P(1)-F(3)	90.63(18)
F(6)-P(1)-F(3)	89.64(16)
F(5)-P(1)-F(3)	90.55(14)
F(4)-P(1)-F(3)	178.95(19)
F(1)-P(1)-F(2)	89.78(15)
F(6)-P(1)-F(2)	90.34(15)
F(5)-P(1)-F(2)	179.26(16)
F(4)-P(1)-F(2)	90.37(16)
F(3)-P(1)-F(2)	89.02(14)
F(12)-P(2)-F(7)	179.5(2)
F(12)-P(2)-F(11)	90.7(2)
F(7)-P(2)-F(11)	89.65(19)
F(12)-P(2)-F(9)	90.0(2)
F(7)-P(2)-F(9)	89.6(2)
F(11)-P(2)-F(9)	179.1(2)
F(12)-P(2)-F(8)	90.63(16)
F(7)-P(2)-F(8)	89.59(15)
F(11)-P(2)-F(8)	90.58(15)
F(9)-P(2)-F(8)	89.91(16)
F(12)-P(2)-F(10)	89.94(16)
F(7)-P(2)-F(10)	89.84(15)
F(11)-P(2)-F(10)	89.40(15)
F(9)-P(2)-F(10)	90.11(16)
F(8)-P(2)-F(10)	179.43(16)
C(12)-N(1)-C(13)	111.9(3)
C(12)-N(1)-C(11)	125.0(3)
C(13)-N(1)-C(11)	123.0(3)
C(12)-N(2)-C(14)	112.0(3)
C(12)-N(2)-C(15)	123.4(3)

C(14)-N(2)-C(15)	124.0(3)
C(16)-N(3)-C(17)	112.2(3)
C(16)-N(3)-C(15)	123.4(3)
C(17)-N(3)-C(15)	124.3(3)
C(16)-N(4)-C(18)	111.6(3)
C(16)-N(4)-C(19)	125.9(3)
C(18)-N(4)-C(19)	122.2(3)
C(41)-N(5)-C(42)	111.6(4)
C(41)-N(5)-C(40)	125.3(3)
C(42)-N(5)-C(40)	122.9(3)
C(41)-N(6)-C(43)	112.2(3)
C(41)-N(6)-C(44)	123.9(3)
C(43)-N(6)-C(44)	123.9(3)
C(45)-N(7)-C(46)	111.6(3)
C(45)-N(7)-C(44)	123.6(3)
C(46)-N(7)-C(44)	124.7(3)
C(45)-N(8)-C(47)	111.5(3)
C(45)-N(8)-C(48)	124.6(3)
C(47)-N(8)-C(48)	123.7(3)
C(2)-C(1)-C(10)	121.5(4)
C(1)-C(2)-C(3)	120.0(4)
C(8)-C(3)-C(2)	119.7(4)
C(8)-C(3)-C(4)	119.2(4)
C(2)-C(3)-C(4)	121.1(4)
C(5)-C(4)-C(3)	119.0(4)
C(4)-C(5)-C(6)	120.7(4)
C(7)-C(6)-C(5)	120.7(4)
C(6)-C(7)-C(8)	120.6(4)
C(7)-C(8)-C(3)	119.7(4)
C(7)-C(8)-C(9)	121.8(4)
C(3)-C(8)-C(9)	118.5(4)
C(10)-C(9)-C(8)	121.0(4)
C(9)-C(10)-C(1)	119.3(4)
C(9)-C(10)-C(11)	120.8(4)
C(1)-C(10)-C(11)	119.9(4)

N(1)-C(11)-C(10)	112.3(3)
N(1)-C(12)-N(2)	103.7(3)
N(1)-C(12)-Ag(1)	126.4(3)
N(2)-C(12)-Ag(1)	129.4(3)
C(14)-C(13)-N(1)	106.4(4)
C(13)-C(14)-N(2)	106.1(4)
N(2)-C(15)-N(3)	110.4(3)
N(3)-C(16)-N(4)	103.2(3)
N(3)-C(16)-Ag(2)	131.0(3)
N(4)-C(16)-Ag(2)	125.5(3)
C(18)-C(17)-N(3)	106.4(4)
C(17)-C(18)-N(4)	106.5(4)
N(4)-C(19)-C(20)	113.4(3)
C(21)-C(20)-C(29)	118.8(4)
C(21)-C(20)-C(19)	119.8(4)
C(29)-C(20)-C(19)	121.3(4)
C(20)-C(21)-C(22)	121.6(4)
C(23)-C(22)-C(27)	118.8(4)
C(23)-C(22)-C(21)	122.5(4)
C(27)-C(22)-C(21)	118.7(4)
C(24)-C(23)-C(22)	120.4(4)
C(23)-C(24)-C(25)	121.4(4)
C(26)-C(25)-C(24)	119.9(4)
C(25)-C(26)-C(27)	120.4(4)
C(22)-C(27)-C(28)	118.8(4)
C(22)-C(27)-C(26)	119.1(4)
C(28)-C(27)-C(26)	122.1(4)
C(29)-C(28)-C(27)	120.8(4)
C(28)-C(29)-C(20)	121.3(4)
C(31)-C(30)-C(39)	121.3(4)
C(30)-C(31)-C(32)	120.7(4)
C(33)-C(32)-C(37)	119.6(4)
C(33)-C(32)-C(31)	122.0(4)
C(37)-C(32)-C(31)	118.4(4)
C(34)-C(33)-C(32)	120.1(4)

C(33)-C(34)-C(35)	120.4(4)
C(36)-C(35)-C(34)	121.0(4)
C(35)-C(36)-C(37)	120.9(4)
C(38)-C(37)-C(36)	123.1(4)
C(38)-C(37)-C(32)	118.9(4)
C(36)-C(37)-C(32)	118.0(4)
C(39)-C(38)-C(37)	121.8(4)
C(38)-C(39)-C(30)	118.9(4)
C(38)-C(39)-C(40)	120.8(4)
C(30)-C(39)-C(40)	120.2(4)
N(5)-C(40)-C(39)	112.9(3)
N(6)-C(41)-N(5)	103.6(3)
N(6)-C(41)-Ag(1)	130.4(3)
N(5)-C(41)-Ag(1)	125.4(3)
C(43)-C(42)-N(5)	106.9(4)
C(42)-C(43)-N(6)	105.8(4)
N(7)-C(44)-N(6)	110.8(3)
N(8)-C(45)-N(7)	104.0(3)
N(8)-C(45)-Ag(2)	124.7(3)
N(7)-C(45)-Ag(2)	131.0(3)
C(47)-C(46)-N(7)	106.1(4)
C(46)-C(47)-N(8)	106.7(3)
N(8)-C(48)-C(49)	111.4(3)
C(50)-C(49)-C(58)	119.5(4)
C(50)-C(49)-C(48)	121.5(4)
C(58)-C(49)-C(48)	119.0(4)
C(49)-C(50)-C(51)	120.9(4)
C(52)-C(51)-C(56)	119.2(4)
C(52)-C(51)-C(50)	122.4(4)
C(56)-C(51)-C(50)	118.3(4)
C(53)-C(52)-C(51)	120.7(4)
C(52)-C(53)-C(54)	120.8(5)
C(55)-C(54)-C(53)	120.0(5)
C(54)-C(55)-C(56)	120.9(4)
C(57)-C(56)-C(55)	122.4(4)

C(57)-C(56)-C(51)	119.3(4)
C(55)-C(56)-C(51)	118.2(4)
C(58)-C(57)-C(56)	121.0(4)
C(57)-C(58)-C(49)	120.9(4)
N(9)-C(59)-C(60)	178.7(6)
N(10)-C(61)-C(62)	179.2(6)

Symmetry transformations used to generate equivalent atoms:

Table 4. Anisotropic displacement parameters ($\text{\AA}^2 \times 10^3$) for $2[\text{PF}_6]$. The anisotropic displacement factor exponent takes the form: $-2\pi^2 [h^2 a^{*2} U^{11} + \dots + 2 h k a^* b^* U^{12}]$

	U11	U22	U33	U23	U13	U12
Ag(1)	20(1)	14(1)	17(1)	-1(1)	2(1)	3(1)
Ag(2)	19(1)	14(1)	18(1)	-1(1)	1(1)	1(1)
P(1)	21(1)	19(1)	24(1)	-2(1)	2(1)	2(1)
P(2)	23(1)	19(1)	23(1)	-2(1)	5(1)	-1(1)
F(1)	91(3)	24(2)	59(2)	2(1)	41(2)	17(2)
F(2)	28(1)	36(2)	39(2)	8(1)	9(1)	-5(1)
F(3)	28(2)	63(2)	28(2)	4(1)	-5(1)	-15(1)
F(4)	27(2)	96(3)	44(2)	18(2)	-9(1)	2(2)
F(5)	40(2)	29(2)	31(2)	5(1)	9(1)	-5(1)
F(6)	65(2)	26(2)	41(2)	-11(1)	16(2)	4(1)
F(7)	87(2)	23(2)	54(2)	-13(1)	41(2)	-9(2)
F(8)	42(2)	30(2)	35(2)	2(1)	17(1)	-6(1)
F(9)	29(2)	140(4)	53(2)	36(2)	-8(2)	-3(2)
F(10)	35(2)	35(2)	38(2)	-1(1)	18(1)	-9(1)
F(11)	37(2)	98(3)	37(2)	15(2)	-11(1)	-23(2)
F(12)	133(3)	23(2)	79(3)	-3(2)	76(2)	7(2)
N(1)	23(2)	15(2)	15(2)	0(1)	-1(1)	2(1)
N(2)	16(2)	17(2)	17(2)	-1(1)	1(1)	1(1)
N(3)	14(2)	18(2)	20(2)	-1(1)	0(1)	-1(1)
N(4)	21(2)	14(2)	25(2)	-5(2)	6(2)	0(1)

N(5)	23(2)	19(2)	18(2)	-2(2)	2(1)	3(2)
N(6)	18(2)	16(2)	19(2)	-1(1)	-2(1)	4(1)
N(7)	14(2)	15(2)	21(2)	3(1)	1(1)	4(1)
N(8)	19(2)	19(2)	23(2)	3(2)	2(1)	-1(1)
N(9)	48(3)	51(3)	56(3)	13(3)	23(3)	3(2)
N(10)	44(3)	70(4)	52(3)	3(3)	17(2)	-12(3)
C(1)	29(2)	33(3)	16(2)	0(2)	-6(2)	10(2)
C(2)	21(2)	36(3)	20(2)	1(2)	0(2)	1(2)
C(3)	22(2)	23(2)	17(2)	3(2)	-9(2)	2(2)
C(4)	28(2)	30(3)	26(2)	5(2)	-9(2)	-6(2)
C(5)	40(3)	15(2)	34(3)	4(2)	-20(2)	-6(2)
C(6)	40(3)	19(2)	31(3)	-4(2)	-11(2)	7(2)
C(7)	30(2)	26(2)	23(2)	-5(2)	-8(2)	3(2)
C(8)	21(2)	20(2)	14(2)	1(2)	-8(2)	-1(2)
C(9)	26(2)	19(2)	18(2)	2(2)	-1(2)	-4(2)
C(10)	33(2)	14(2)	14(2)	1(2)	-10(2)	2(2)
C(11)	42(3)	18(2)	16(2)	1(2)	-2(2)	0(2)
C(12)	23(2)	10(2)	15(2)	0(2)	4(2)	-3(2)
C(13)	22(2)	14(2)	28(2)	1(2)	4(2)	1(2)
C(14)	23(2)	16(2)	28(2)	-2(2)	2(2)	-1(2)
C(15)	19(2)	15(2)	20(2)	-2(2)	-2(2)	-4(2)
C(16)	17(2)	13(2)	17(2)	-2(2)	-3(2)	1(2)
C(17)	28(2)	16(2)	30(2)	-2(2)	6(2)	0(2)
C(18)	29(2)	18(2)	34(3)	-3(2)	13(2)	4(2)
C(19)	24(2)	19(2)	27(2)	1(2)	7(2)	-4(2)
C(20)	17(2)	17(2)	29(2)	3(2)	6(2)	-2(2)
C(21)	16(2)	22(2)	23(2)	3(2)	6(2)	-1(2)
C(22)	16(2)	19(2)	23(2)	4(2)	5(2)	-7(2)
C(23)	20(2)	20(2)	25(2)	8(2)	3(2)	2(2)
C(24)	23(2)	18(2)	38(3)	3(2)	7(2)	-3(2)
C(25)	26(2)	29(3)	37(3)	-4(2)	7(2)	-5(2)
C(26)	25(2)	31(3)	29(2)	-1(2)	3(2)	-11(2)
C(27)	17(2)	25(2)	26(2)	3(2)	3(2)	-7(2)
C(28)	23(2)	33(3)	23(2)	6(2)	-3(2)	-11(2)
C(29)	23(2)	20(2)	30(2)	9(2)	-4(2)	-4(2)

C(30)	21(2)	23(2)	31(2)	11(2)	1(2)	0(2)
C(31)	23(2)	26(2)	24(2)	6(2)	-4(2)	-4(2)
C(32)	17(2)	24(2)	24(2)	9(2)	3(2)	-5(2)
C(33)	24(2)	33(3)	25(2)	-1(2)	8(2)	-10(2)
C(34)	28(2)	26(3)	40(3)	-8(2)	16(2)	-6(2)
C(35)	32(3)	24(2)	44(3)	4(2)	16(2)	3(2)
C(36)	27(2)	29(3)	23(2)	11(2)	3(2)	2(2)
C(37)	19(2)	22(2)	23(2)	6(2)	6(2)	-3(2)
C(38)	20(2)	27(2)	21(2)	9(2)	3(2)	3(2)
C(39)	19(2)	24(2)	23(2)	5(2)	6(2)	0(2)
C(40)	29(2)	23(2)	23(2)	4(2)	7(2)	2(2)
C(41)	17(2)	21(2)	14(2)	0(2)	0(2)	5(2)
C(42)	25(2)	20(2)	25(2)	-5(2)	2(2)	10(2)
C(43)	27(2)	17(2)	22(2)	-2(2)	-1(2)	7(2)
C(44)	17(2)	19(2)	17(2)	1(2)	1(2)	2(2)
C(45)	10(2)	24(2)	21(2)	3(2)	2(2)	2(2)
C(46)	20(2)	15(2)	25(2)	0(2)	5(2)	0(2)
C(47)	18(2)	15(2)	28(2)	8(2)	4(2)	3(2)
C(48)	32(2)	25(2)	18(2)	2(2)	-2(2)	-4(2)
C(49)	22(2)	26(2)	12(2)	3(2)	-4(2)	-2(2)
C(50)	19(2)	34(3)	16(2)	2(2)	-2(2)	2(2)
C(51)	23(2)	25(2)	16(2)	1(2)	-5(2)	-1(2)
C(52)	30(2)	34(3)	13(2)	1(2)	-4(2)	3(2)
C(53)	41(3)	30(3)	21(2)	-3(2)	-4(2)	5(2)
C(54)	46(3)	33(3)	26(3)	7(2)	-6(2)	-12(2)
C(55)	23(2)	47(3)	22(2)	10(2)	-5(2)	-11(2)
C(56)	23(2)	34(3)	16(2)	3(2)	-6(2)	3(2)
C(57)	20(2)	37(3)	22(2)	6(2)	-1(2)	0(2)
C(58)	21(2)	27(2)	19(2)	2(2)	-5(2)	2(2)
C(59)	36(3)	30(3)	51(4)	15(3)	23(3)	6(2)
C(60)	36(3)	35(3)	57(4)	5(3)	6(3)	7(2)
C(61)	38(3)	31(3)	48(3)	-6(3)	18(3)	-7(2)
C(62)	42(3)	35(3)	52(3)	-9(3)	9(3)	-11(2)

Table 5. Hydrogen coordinates ($\times 10^4$) and isotropic displacement parameters ($\text{\AA}^2 \times 10^3$) for $2[\text{PF}_6]$.

	x	y	z	U(eq)
H(1)	5060	3963	3765	32
H(2)	5608	5057	3778	31
H(4)	5431	6288	4052	35
H(5)	4566	7137	4489	37
H(6)	3212	6864	4943	37
H(7)	2744	5751	5006	32
H(9)	2949	4526	4757	25
H(11A)	4133	3124	4469	30
H(11B)	3111	3376	4545	30
H(13)	3741	2136	3676	25
H(14)	3021	2042	2525	27
H(15A)	1892	3653	1993	22
H(15B)	1967	2878	1760	22
H(17)	3507	2510	1262	29
H(18)	4685	3184	767	32
H(19A)	4280	4700	434	28
H(19B)	5208	4449	843	28
H(21)	4093	5845	542	24
H(23)	3799	7100	623	26
H(24)	3785	8066	1252	31
H(25)	4312	8047	2367	37
H(26)	4858	7044	2855	34
H(28)	5208	5798	2762	32
H(29)	5165	4822	2150	30
H(30)	-156	4820	2854	30
H(31)	-313	3922	2142	30
H(33)	-110	2681	1918	33
H(34)	400	1618	2279	36
H(35)	1024	1459	3361	39

H(36)	1164	2349	4079	32
H(38)	963	3597	4305	27
H(40A)	-78	5045	4203	30
H(40B)	876	4748	4535	30
H(42)	424	6300	4290	28
H(43)	1552	7006	3775	27
H(44A)	3052	6678	3227	22
H(44B)	3165	5905	3001	22
H(46)	1939	7479	2452	24
H(47)	1332	7375	1281	24
H(48A)	2218	6104	478	31
H(48B)	1219	6443	424	31
H(50)	2235	4928	291	28
H(52)	2302	3657	124	31
H(53)	1676	2597	233	37
H(54)	193	2477	556	43
H(55)	-609	3424	844	38
H(57)	-667	4682	1032	32
H(58)	15	5733	1024	28
H(60A)	2457	8718	2124	64
H(60B)	2044	9458	1951	64
H(60C)	2993	9233	1696	64
H(62A)	7026	5099	1985	64
H(62B)	7526	5819	2100	64
H(62C)	8001	5225	1724	64

APPENDIX C

SUPPLEMENTARY MATERIAL FOR THE X-RAY CRYSTAL STRUCTURE OF

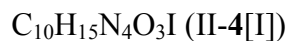


Table 1. Crystal data and structure refinement for 4[I].

Identification code	C ₁₀ H ₁₅ IN ₄ O ₃	
Empirical formula	C10 H15 I N4 O3	
Formula weight	366.16	
Temperature	100(2) K	
Wavelength	0.71073 Å	
Crystal system	Monoclinic	
Space group	P2(1)/c	
Unit cell dimensions	a = 15.0967(18) Å	α = 90°.
	b = 10.4071(13) Å	β = 104.119(2)°.
	c = 8.7080(10) Å	γ = 90°.
Volume	1326.8(3) Å ³	
Z	4	
Density (calculated)	1.833 Mg/m ³	
Absorption coefficient	2.421 mm ⁻¹	
F(000)	720	
Crystal size	0.37 x 0.29 x 0.19 mm ³	
Theta range for data collection	2.40 to 28.32°.	
Index ranges	-19 ≤ h ≤ 20, -13 ≤ k ≤ 13, -11 ≤ l ≤ 11	
Reflections collected	11589	
Independent reflections	3212 [R(int) = 0.0516]	
Completeness to theta = 28.32°	97.2 %	
Absorption correction	Semi-empirical from equivalents	
Max. and min. transmission	0.6299 and 0.3776	
Refinement method	Full-matrix least-squares on F ²	

Data / restraints / parameters	3212 / 0 / 167
Goodness-of-fit on F^2	1.072
Final R indices [$I > 2\sigma(I)$]	R1 = 0.0448, wR2 = 0.1071
R indices (all data)	R1 = 0.0565, wR2 = 0.1133
Largest diff. peak and hole	2.389 and -1.410 e.Å ⁻³

Table 2. Atomic coordinates ($\times 10^4$) and equivalent isotropic displacement parameters ($\text{Å}^2 \times 10^3$) for **4**[I]. $U(\text{eq})$ is defined as one third of the trace of the orthogonalized U_{ij} tensor.

	x	y	z	$U(\text{eq})$
I(1)	3556(1)	8841(1)	2002(1)	26(1)
O(1)	2634(2)	2538(3)	7505(3)	28(1)
O(2)	1341(2)	5429(3)	4932(3)	28(1)
O(3)	499(2)	5431(3)	8265(3)	26(1)
N(1)	1811(2)	6037(3)	11403(4)	20(1)
N(2)	3181(2)	5195(3)	12039(4)	20(1)
N(3)	3030(2)	3799(3)	9687(4)	22(1)
N(4)	1575(2)	3980(3)	7869(4)	22(1)
C(1)	2588(3)	6005(4)	12489(5)	21(1)
C(2)	2743(3)	4698(4)	10588(4)	21(1)
C(3)	2430(3)	3384(4)	8317(5)	23(1)
C(4)	1249(3)	4936(4)	8729(5)	22(1)
C(5)	1894(3)	5223(4)	10181(4)	21(1)
C(6)	1024(3)	6810(4)	11494(5)	25(1)
C(7)	4119(3)	5056(4)	12972(5)	31(1)
C(8)	3946(3)	3244(5)	10041(5)	33(1)
C(9)	973(3)	3577(4)	6338(5)	28(1)
C(10)	1297(3)	4065(4)	4948(5)	27(1)

Table 3. Bond lengths [\AA] and angles [$^\circ$] for **4**[I].

O(1)-C(3)	1.214(5)
O(2)-C(10)	1.420(5)
O(3)-C(4)	1.219(5)
N(1)-C(1)	1.316(5)
N(1)-C(5)	1.389(5)
N(1)-C(6)	1.453(5)
N(2)-C(1)	1.356(5)
N(2)-C(2)	1.376(5)
N(2)-C(7)	1.457(5)
N(3)-C(2)	1.357(5)
N(3)-C(3)	1.380(5)
N(3)-C(8)	1.462(5)
N(4)-C(3)	1.399(5)
N(4)-C(4)	1.405(5)
N(4)-C(9)	1.479(5)
C(2)-C(5)	1.359(5)
C(4)-C(5)	1.427(5)
C(9)-C(10)	1.501(6)
C(1)-N(1)-C(5)	107.7(3)
C(1)-N(1)-C(6)	124.9(3)
C(5)-N(1)-C(6)	127.4(3)
C(1)-N(2)-C(2)	107.2(3)
C(1)-N(2)-C(7)	121.4(3)
C(2)-N(2)-C(7)	131.2(3)
C(2)-N(3)-C(3)	118.8(3)
C(2)-N(3)-C(8)	124.7(3)
C(3)-N(3)-C(8)	116.5(3)
C(3)-N(4)-C(4)	125.8(3)
C(3)-N(4)-C(9)	116.6(3)
C(4)-N(4)-C(9)	117.6(3)
N(1)-C(1)-N(2)	110.1(3)

N(3)-C(2)-C(5)	122.7(3)
N(3)-C(2)-N(2)	129.7(3)
C(5)-C(2)-N(2)	107.5(3)
O(1)-C(3)-N(3)	121.6(4)
O(1)-C(3)-N(4)	120.5(4)
N(3)-C(3)-N(4)	117.9(3)
O(3)-C(4)-N(4)	122.7(4)
O(3)-C(4)-C(5)	125.7(4)
N(4)-C(4)-C(5)	111.6(3)
C(2)-C(5)-N(1)	107.5(3)
C(2)-C(5)-C(4)	122.9(4)
N(1)-C(5)-C(4)	129.6(4)
N(4)-C(9)-C(10)	112.5(3)
O(2)-C(10)-C(9)	111.8(3)

Symmetry transformations used to generate equivalent atoms:

Table 4. Anisotropic displacement parameters ($\text{\AA}^2 \times 10^3$) for **4**[I]. The anisotropic displacement factor exponent takes the form: $-2\pi^2 [h^2 a^{*2} U_{11} + \dots + 2 h k a^* b^* U_{12}]$.

	U11	U22	U33	U23	U13	U12
I(1)	22(1)	28(1)	28(1)	1(1)	4(1)	-2(1)
O(1)	35(2)	24(2)	27(2)	-3(1)	7(1)	7(1)
O(2)	27(2)	31(2)	26(2)	3(1)	5(1)	0(1)
O(3)	20(1)	29(2)	26(2)	1(1)	2(1)	2(1)
N(1)	20(2)	22(2)	20(2)	0(1)	7(1)	0(1)
N(2)	17(2)	22(2)	21(2)	1(1)	3(1)	-1(1)
N(3)	22(2)	24(2)	21(2)	1(1)	5(1)	3(1)
N(4)	24(2)	23(2)	18(2)	-1(1)	3(1)	-2(1)
C(1)	20(2)	23(2)	19(2)	-1(2)	5(2)	-3(2)
C(2)	24(2)	18(2)	19(2)	4(2)	5(2)	0(2)
C(3)	28(2)	17(2)	25(2)	5(2)	9(2)	0(2)

C(4)	27(2)	16(2)	24(2)	2(2)	6(2)	-5(2)
C(5)	22(2)	19(2)	23(2)	-1(2)	6(2)	-2(2)
C(6)	24(2)	26(2)	24(2)	3(2)	8(2)	6(2)
C(7)	23(2)	36(2)	31(2)	-5(2)	0(2)	6(2)
C(8)	29(2)	39(3)	27(2)	-4(2)	2(2)	14(2)
C(9)	31(2)	24(2)	25(2)	-6(2)	1(2)	-7(2)
C(10)	28(2)	30(2)	20(2)	-4(2)	-1(2)	3(2)

Table 5. Hydrogen coordinates ($\times 10^4$) and isotropic displacement parameters ($\text{\AA}^2 \times 10^3$) for 4[I].

	x	y	z	U(eq)
H(2)	1836	5673	5533	42
H(1)	2716	6481	13449	25
H(6A)	1157	7281	12499	37
H(6B)	495	6249	11433	37
H(6C)	888	7421	10612	37
H(7A)	4536	5440	12398	46
H(7B)	4263	4143	13154	46
H(7C)	4188	5493	13991	46
H(8A)	4383	3858	10663	49
H(8B)	4117	3053	9049	49
H(8C)	3954	2450	10648	49
H(9A)	348	3900	6266	33
H(9B)	946	2627	6297	33
H(10A)	1910	3708	4987	33
H(10B)	875	3764	3956	33

APPENDIX D

SUPPLEMENTARY MATERIAL FOR THE X-RAY CRYSTAL STRUCTURE OF
 $C_{12}H_{17}N_4O_5Ag$ (II-5)

Table 1. Crystal data and structure refinement for **5**.

Identification code	$C_{12}H_{17}AgN_4O_5$	
Empirical formula	C12 H17 Ag N4 O5	
Formula weight	405.17	
Temperature	100(2) K	
Wavelength	0.71073 Å	
Crystal system	Monoclinic	
Space group	C2/c	
Unit cell dimensions	a = 23.896(3) Å	$\alpha = 90^\circ$.
	b = 8.2797(11) Å	$\beta = 94.104(2)^\circ$.
	c = 14.8598(19) Å	$\gamma = 90^\circ$.
Volume	2932.5(7) Å ³	
Z	8	
Density (calculated)	1.835 Mg/m ³	
Absorption coefficient	1.405 mm ⁻¹	
F(000)	1632	
Crystal size	0.43 x 0.08 x 0.07 mm ³	
Theta range for data collection	1.71 to 28.34°.	
Index ranges	-31 ≤ h ≤ 31, -10 ≤ k ≤ 10, -19 ≤ l ≤ 19	
Reflections collected	12470	
Independent reflections	3512 [R(int) = 0.0494]	
Completeness to theta = 28.34°	96.3 %	
Absorption correction	Semi-empirical from equivalents	
Max. and min. transmission	0.9081 and 0.5834	
Refinement method	Full-matrix least-squares on F ²	

Data / restraints / parameters	3512 / 0 / 204
Goodness-of-fit on F^2	1.025
Final R indices [$I > 2\sigma(I)$]	R1 = 0.0447, wR2 = 0.0975
R indices (all data)	R1 = 0.0624, wR2 = 0.1061
Largest diff. peak and hole	1.335 and -0.794 e.Å ⁻³

Table 2. Atomic coordinates ($\times 10^4$) and equivalent isotropic displacement parameters ($\text{Å}^2 \times 10^3$) for **5**. $U(\text{eq})$ is defined as one third of the trace of the orthogonalized U_{ij} tensor.

	x	y	z	U(eq)
Ag(1)	-560(1)	4904(1)	526(1)	23(1)
O(1)	2207(1)	4522(3)	3582(2)	32(1)
O(2)	1216(1)	1138(3)	4867(2)	31(1)
O(3)	1051(1)	351(3)	2626(2)	26(1)
O(4)	-1314(1)	5299(3)	-284(2)	29(1)
O(5)	-1153(1)	7813(3)	189(2)	37(1)
N(1)	342(1)	2887(3)	1590(2)	19(1)
N(2)	532(1)	5451(4)	1741(2)	20(1)
N(3)	1427(1)	5193(3)	2693(2)	21(1)
N(4)	1604(1)	2472(3)	3165(2)	23(1)
C(1)	155(2)	4354(5)	1339(2)	22(1)
C(2)	956(2)	4625(4)	2213(2)	20(1)
C(3)	1774(2)	4102(4)	3178(3)	24(1)
C(4)	1152(2)	1810(4)	2634(2)	21(1)
C(5)	833(2)	3019(4)	2139(2)	19(1)
C(6)	95(2)	1370(4)	1236(3)	24(1)
C(7)	479(2)	7198(4)	1573(3)	29(1)
C(8)	1623(2)	6882(4)	2654(3)	30(1)
C(9)	1944(2)	1386(4)	3786(3)	26(1)
C(10)	1781(2)	1595(4)	4759(3)	26(1)
C(11)	-1436(2)	6797(5)	-265(3)	31(1)

C(12) -1956(2) 7309(7) -838(3) 51(1)

Table 3. Bond lengths [\AA] and angles [$^\circ$] for **5**.

Ag(1)-C(1)	2.072(4)
Ag(1)-O(4)	2.118(3)
Ag(1)-Ag(1)#1	3.1992(7)
O(1)-C(3)	1.210(4)
O(2)-C(10)	1.423(4)
O(2)-H(2)	0.8400
O(3)-C(4)	1.232(4)
O(4)-C(11)	1.274(5)
O(5)-C(11)	1.247(5)
N(1)-C(1)	1.338(5)
N(1)-C(5)	1.385(5)
N(1)-C(6)	1.469(4)
N(2)-C(2)	1.372(5)
N(2)-C(1)	1.384(5)
N(2)-C(7)	1.472(4)
N(3)-C(2)	1.372(5)
N(3)-C(3)	1.392(5)
N(3)-C(8)	1.477(4)
N(4)-C(4)	1.402(4)
N(4)-C(3)	1.409(4)
N(4)-C(9)	1.489(4)
C(2)-C(5)	1.364(5)
C(4)-C(5)	1.430(5)
C(6)-H(6A)	0.9800
C(6)-H(6B)	0.9800
C(6)-H(6C)	0.9800
C(7)-H(7A)	0.9800
C(7)-H(7B)	0.9800
C(7)-H(7C)	0.9800
C(8)-H(8A)	0.9800

C(8)-H(8B)	0.9800
C(8)-H(8C)	0.9800
C(9)-C(10)	1.533(5)
C(9)-H(9A)	0.9900
C(9)-H(9B)	0.9900
C(10)-H(10A)	0.9900
C(10)-H(10B)	0.9900
C(11)-C(12)	1.516(6)
C(12)-H(12A)	0.9800
C(12)-H(12B)	0.9800
C(12)-H(12C)	0.9800

C(1)-Ag(1)-O(4)	175.89(12)
C(1)-Ag(1)-Ag(1)#1	67.14(10)
O(4)-Ag(1)-Ag(1)#1	114.95(8)
C(10)-O(2)-H(2)	109.5
C(11)-O(4)-Ag(1)	109.0(3)
C(1)-N(1)-C(5)	110.1(3)
C(1)-N(1)-C(6)	124.0(3)
C(5)-N(1)-C(6)	125.5(3)
C(2)-N(2)-C(1)	109.1(3)
C(2)-N(2)-C(7)	128.9(3)
C(1)-N(2)-C(7)	121.8(3)
C(2)-N(3)-C(3)	118.9(3)
C(2)-N(3)-C(8)	123.7(3)
C(3)-N(3)-C(8)	117.1(3)
C(4)-N(4)-C(3)	126.3(3)
C(4)-N(4)-C(9)	118.5(3)
C(3)-N(4)-C(9)	115.2(3)
N(1)-C(1)-N(2)	106.3(3)
N(1)-C(1)-Ag(1)	127.4(3)
N(2)-C(1)-Ag(1)	126.3(3)
C(5)-C(2)-N(2)	107.4(3)
C(5)-C(2)-N(3)	122.7(3)
N(2)-C(2)-N(3)	130.0(3)

O(1)-C(3)-N(3)	121.8(3)
O(1)-C(3)-N(4)	121.2(3)
N(3)-C(3)-N(4)	117.0(3)
O(3)-C(4)-N(4)	122.1(3)
O(3)-C(4)-C(5)	125.8(3)
N(4)-C(4)-C(5)	112.1(3)
C(2)-C(5)-N(1)	107.0(3)
C(2)-C(5)-C(4)	122.5(3)
N(1)-C(5)-C(4)	130.2(3)
N(1)-C(6)-H(6A)	109.5
N(1)-C(6)-H(6B)	109.5
H(6A)-C(6)-H(6B)	109.5
N(1)-C(6)-H(6C)	109.5
H(6A)-C(6)-H(6C)	109.5
H(6B)-C(6)-H(6C)	109.5
N(2)-C(7)-H(7A)	109.5
N(2)-C(7)-H(7B)	109.5
H(7A)-C(7)-H(7B)	109.5
N(2)-C(7)-H(7C)	109.5
H(7A)-C(7)-H(7C)	109.5
H(7B)-C(7)-H(7C)	109.5
N(3)-C(8)-H(8A)	109.5
N(3)-C(8)-H(8B)	109.5
H(8A)-C(8)-H(8B)	109.5
N(3)-C(8)-H(8C)	109.5
H(8A)-C(8)-H(8C)	109.5
H(8B)-C(8)-H(8C)	109.5
N(4)-C(9)-C(10)	110.6(3)
N(4)-C(9)-H(9A)	109.5
C(10)-C(9)-H(9A)	109.5
N(4)-C(9)-H(9B)	109.5
C(10)-C(9)-H(9B)	109.5
H(9A)-C(9)-H(9B)	108.1
O(2)-C(10)-C(9)	112.6(3)
O(2)-C(10)-H(10A)	109.1

C(9)-C(10)-H(10A)	109.1
O(2)-C(10)-H(10B)	109.1
C(9)-C(10)-H(10B)	109.1
H(10A)-C(10)-H(10B)	107.8
O(5)-C(11)-O(4)	123.5(4)
O(5)-C(11)-C(12)	120.4(4)
O(4)-C(11)-C(12)	116.1(4)
C(11)-C(12)-H(12A)	109.5
C(11)-C(12)-H(12B)	109.5
H(12A)-C(12)-H(12B)	109.5
C(11)-C(12)-H(12C)	109.5
H(12A)-C(12)-H(12C)	109.5
H(12B)-C(12)-H(12C)	109.5

Symmetry transformations used to generate equivalent atoms:

#1 -x,-y+1,-z

Table 4. Anisotropic displacement parameters ($\text{\AA}^2 \times 10^3$) for **5**. The anisotropic displacement factor exponent takes the form: $-2\pi^2 [h^2 a^{*2} U_{11} + \dots + 2 h k a^* b^* U_{12}]$

	U11	U22	U33	U23	U13	U12
Ag(1)	24(1)	23(1)	22(1)	2(1)	-5(1)	3(1)
O(1)	28(2)	24(1)	41(2)	5(1)	-17(1)	-6(1)
O(2)	29(2)	29(2)	33(2)	0(1)	-4(1)	-1(1)
O(3)	31(2)	16(1)	30(2)	1(1)	-8(1)	-2(1)
O(4)	24(2)	32(2)	29(2)	3(1)	-5(1)	2(1)
O(5)	43(2)	31(2)	34(2)	-3(1)	-5(1)	12(1)
N(1)	20(2)	17(1)	20(2)	-1(1)	-5(1)	0(1)
N(2)	25(2)	16(1)	18(2)	0(1)	-2(1)	3(1)
N(3)	23(2)	16(1)	25(2)	0(1)	-4(1)	-2(1)
N(4)	23(2)	16(1)	27(2)	2(1)	-8(1)	-1(1)
C(1)	25(2)	23(2)	17(2)	0(2)	0(2)	3(2)
C(2)	24(2)	18(2)	19(2)	-2(1)	-1(2)	3(1)
C(3)	23(2)	20(2)	28(2)	2(2)	-7(2)	-4(2)

C(4)	20(2)	19(2)	23(2)	-2(2)	-2(2)	-1(1)
C(5)	20(2)	17(2)	18(2)	-3(1)	-5(1)	-1(1)
C(6)	27(2)	18(2)	27(2)	-1(2)	-5(2)	-2(2)
C(7)	36(2)	15(2)	32(2)	0(2)	-10(2)	4(2)
C(8)	33(2)	15(2)	41(3)	3(2)	-9(2)	-5(2)
C(9)	23(2)	18(2)	34(2)	3(2)	-11(2)	2(2)
C(10)	26(2)	20(2)	30(2)	2(2)	-13(2)	1(2)
C(11)	28(2)	39(2)	25(2)	6(2)	5(2)	12(2)
C(12)	36(3)	83(4)	35(3)	6(3)	0(2)	34(3)

Table 5. Hydrogen coordinates ($\times 10^4$) and isotropic displacement parameters ($\text{\AA}^2 \times 10^3$) for **5**.

	x	y	z	U(eq)
H(2)	1190	126	4862	46
H(6A)	-269	1593	914	36
H(6B)	44	628	1737	36
H(6C)	346	877	820	36
H(7A)	544	7784	2144	43
H(7B)	101	7439	1307	43
H(7C)	757	7535	1156	43
H(8A)	1590	7257	2026	46
H(8B)	2016	6943	2889	46
H(8C)	1392	7566	3019	46
H(9A)	2347	1637	3755	31
H(9B)	1883	250	3596	31
H(10A)	2034	932	5165	31
H(10B)	1834	2739	4939	31
H(12A)	-2277	7339	-464	77
H(12B)	-2030	6535	-1331	77
H(12C)	-1897	8386	-1088	77

APPENDIX E

SUPPLEMENTARY MATERIAL FOR THE X-RAY CRYSTAL STRUCTURE OF



Table 1. Crystal data and structure refinement for $3[\text{PF}_6]_2$.

Identification code	$\text{C}_{21}\text{H}_{18}\text{N}_6 \cdot 2(\text{P}_1\text{F}_6) \cdot 4(\text{C}_2\text{H}_6\text{SO})$	
Empirical formula	C ₂₉ H ₄₂ N ₆ O ₄ S ₄ P ₂ F ₁₂	
Formula weight	956.87	
Temperature	100(2) K	
Wavelength	0.71073 Å	
Crystal system	Monoclinic	
Space group	P 2(1)/n	
Unit cell dimensions	$a = 14.956(3) \text{ \AA}$	$\alpha = 90^\circ$.
	$b = 15.366(4) \text{ \AA}$	$\beta = 112.274(4)^\circ$.
	$c = 18.869(4) \text{ \AA}$	$\gamma = 90^\circ$.
Volume	$4012.9(16) \text{ \AA}^3$	
Z	4	
Density (calculated)	1.584 Mg/m ³	
Absorption coefficient	0.416 mm ⁻¹	
F(000)	1968	
Crystal size	0.41 x 0.13 x 0.06 mm ³	
Theta range for data collection	1.49 to 28.32°.	
Index ranges	$-19 \leq h \leq 19, -20 \leq k \leq 20, -25 \leq l \leq 25$	
Reflections collected	34549	
Independent reflections	9583 [R(int) = 0.0436]	
Completeness to theta = 28.32°	95.8 %	
Absorption correction	Semi-empirical from equivalents	
Max. and min. transmission	0.9755 and 0.8480	
Refinement method	Full-matrix least-squares on F ²	

Data / restraints / parameters	9583 / 0 / 682
Goodness-of-fit on F^2	1.135
Final R indices [$I > 2\sigma(I)$]	R1 = 0.0495, wR2 = 0.0977
R indices (all data)	R1 = 0.0627, wR2 = 0.1026
Largest diff. peak and hole	0.404 and -0.336 e.Å ⁻³

Table 2. Atomic coordinates ($\times 10^4$) and equivalent isotropic displacement parameters ($\text{Å}^2 \times 10^3$) for $3[\text{PF}_6]_2$. $U(\text{eq})$ is defined as one third of the trace of the orthogonalized U_{ij} tensor.

	x	y	z	U(eq)
S(1)	4304(1)	3761(1)	5709(1)	22(1)
S(2)	752(1)	9640(1)	2086(1)	18(1)
S(3)	4253(1)	9300(1)	2413(1)	23(1)
S(4)	8297(1)	6947(1)	2090(1)	21(1)
P(1)	8233(1)	5030(1)	3869(1)	21(1)
P(2)	2199(1)	6711(1)	1827(1)	17(1)
F(1)	9319(1)	5156(1)	3952(1)	40(1)
F(2)	7939(1)	4783(1)	2996(1)	48(1)
F(3)	8028(1)	6041(1)	3659(1)	42(1)
F(4)	8539(1)	5280(1)	4758(1)	33(1)
F(5)	8453(1)	4028(1)	4103(1)	34(1)
F(6)	7154(1)	4903(1)	3813(1)	52(1)
F(7)	2849(1)	6332(1)	1390(1)	29(1)
F(8)	2662(1)	7651(1)	1850(1)	34(1)
F(9)	1366(1)	6938(1)	1018(1)	28(1)
F(10)	1735(1)	5767(1)	1798(1)	28(1)
F(11)	3035(1)	6483(1)	2632(1)	28(1)
F(12)	1545(1)	7084(1)	2256(1)	32(1)
O(1)	5035(1)	3326(1)	5458(1)	31(1)
O(2)	1361(1)	9264(1)	2855(1)	21(1)
O(3)	4665(1)	8965(1)	3219(1)	28(1)
O(4)	9008(1)	7581(1)	2609(1)	27(1)
N(1)	9157(1)	1672(1)	5031(1)	14(1)

N(2)	7931(1)	232(1)	4589(1)	14(1)
N(3)	6328(1)	202(1)	4985(1)	16(1)
N(4)	6451(1)	1301(1)	5719(1)	15(1)
N(5)	7482(1)	2524(1)	6096(1)	15(1)
N(6)	8671(1)	2993(1)	5828(1)	15(1)
C(1)	9725(2)	2359(1)	5209(1)	15(1)
C(2)	10482(2)	2497(2)	4951(1)	20(1)
C(3)	10642(2)	1886(2)	4492(1)	19(1)
C(4)	10050(2)	1142(2)	4277(1)	17(1)
C(5)	10177(2)	492(2)	3779(1)	20(1)
C(6)	9581(2)	-192(2)	3559(1)	20(1)
C(7)	8808(2)	-297(2)	3822(1)	17(1)
C(8)	8170(2)	-1011(2)	3587(1)	20(1)
C(9)	7441(2)	-1082(2)	3848(1)	20(1)
C(10)	7353(2)	-448(1)	4353(1)	16(1)
C(11)	8658(2)	315(1)	4325(1)	14(1)
C(12)	9301(2)	1060(1)	4562(1)	14(1)
C(13)	6573(2)	-586(2)	4667(1)	18(1)
C(14)	5521(2)	719(2)	4631(1)	18(1)
C(15)	5599(2)	1410(2)	5090(1)	19(1)
C(16)	6879(2)	570(1)	5636(1)	16(1)
C(17)	6880(2)	1934(2)	6330(1)	17(1)
C(18)	7184(2)	3297(2)	5700(1)	19(1)
C(19)	7928(2)	3589(2)	5533(1)	19(1)
C(20)	8387(2)	2358(2)	6167(1)	16(1)
C(21)	9604(2)	3037(2)	5751(1)	18(1)
C(22)	4449(2)	3288(2)	6607(2)	29(1)
C(23)	3164(2)	3278(2)	5156(2)	28(1)
C(24)	-63(2)	8798(2)	1582(2)	27(1)
C(25)	1488(2)	9628(2)	1529(2)	25(1)
C(26)	4777(3)	8655(2)	1884(2)	39(1)
C(27)	4880(2)	10286(2)	2406(2)	31(1)
C(28)	8087(2)	7293(2)	1134(1)	22(1)

C(29) 7150(2) 7253(2) 2102(2) 26(1)

Table 3. Bond lengths [\AA] and angles [$^\circ$] for $\mathbf{3}[\text{PF}_6]_2$.

S(1)-O(1)	1.5024(17)
S(1)-C(22)	1.780(3)
S(1)-C(23)	1.788(3)
S(2)-O(2)	1.5056(16)
S(2)-C(24)	1.785(3)
S(2)-C(25)	1.786(2)
S(3)-O(3)	1.4993(18)
S(3)-C(27)	1.784(3)
S(3)-C(26)	1.785(3)
S(4)-O(4)	1.5004(18)
S(4)-C(29)	1.786(3)
S(4)-C(28)	1.789(2)
P(1)-F(2)	1.5829(17)
P(1)-F(1)	1.5847(16)
P(1)-F(6)	1.5887(17)
P(1)-F(5)	1.6015(16)
P(1)-F(3)	1.6038(17)
P(1)-F(4)	1.6080(15)
P(2)-F(12)	1.5944(15)
P(2)-F(8)	1.5960(16)
P(2)-F(11)	1.5987(15)
P(2)-F(10)	1.5994(15)
P(2)-F(9)	1.6008(15)
P(2)-F(7)	1.6035(14)
N(1)-C(1)	1.315(3)
N(1)-C(12)	1.363(3)
N(2)-C(10)	1.321(3)
N(2)-C(11)	1.362(3)
N(3)-C(16)	1.320(3)
N(3)-C(14)	1.387(3)

N(3)-C(13)	1.459(3)
N(4)-C(16)	1.330(3)
N(4)-C(15)	1.383(3)
N(4)-C(17)	1.459(3)
N(5)-C(20)	1.332(3)
N(5)-C(18)	1.384(3)
N(5)-C(17)	1.460(3)
N(6)-C(20)	1.323(3)
N(6)-C(19)	1.384(3)
N(6)-C(21)	1.458(3)
C(1)-C(2)	1.409(3)
C(1)-C(21)	1.517(3)
C(2)-C(3)	1.358(3)
C(3)-C(4)	1.409(3)
C(4)-C(12)	1.419(3)
C(4)-C(5)	1.431(3)
C(5)-C(6)	1.339(3)
C(6)-C(7)	1.429(3)
C(7)-C(8)	1.410(3)
C(7)-C(11)	1.413(3)
C(8)-C(9)	1.360(3)
C(9)-C(10)	1.403(3)
C(10)-C(13)	1.511(3)
C(11)-C(12)	1.452(3)
C(14)-C(15)	1.346(3)
C(18)-C(19)	1.344(3)
O(1)-S(1)-C(22)	106.11(13)
O(1)-S(1)-C(23)	106.15(12)
C(22)-S(1)-C(23)	97.54(14)
O(2)-S(2)-C(24)	106.12(12)
O(2)-S(2)-C(25)	106.34(11)
C(24)-S(2)-C(25)	97.35(13)
O(3)-S(3)-C(27)	106.51(13)
O(3)-S(3)-C(26)	106.15(14)

C(27)-S(3)-C(26)	97.13(15)
O(4)-S(4)-C(29)	105.53(11)
O(4)-S(4)-C(28)	106.00(11)
C(29)-S(4)-C(28)	97.61(12)
F(2)-P(1)-F(1)	90.03(10)
F(2)-P(1)-F(6)	91.53(10)
F(1)-P(1)-F(6)	178.38(11)
F(2)-P(1)-F(5)	90.14(9)
F(1)-P(1)-F(5)	89.67(9)
F(6)-P(1)-F(5)	89.91(10)
F(2)-P(1)-F(3)	91.31(9)
F(1)-P(1)-F(3)	89.91(10)
F(6)-P(1)-F(3)	90.47(10)
F(5)-P(1)-F(3)	178.49(10)
F(2)-P(1)-F(4)	179.60(11)
F(1)-P(1)-F(4)	89.60(9)
F(6)-P(1)-F(4)	88.83(10)
F(5)-P(1)-F(4)	89.71(8)
F(3)-P(1)-F(4)	88.84(8)
F(12)-P(2)-F(8)	90.28(9)
F(12)-P(2)-F(11)	90.33(8)
F(8)-P(2)-F(11)	89.85(8)
F(12)-P(2)-F(10)	90.11(8)
F(8)-P(2)-F(10)	179.55(9)
F(11)-P(2)-F(10)	90.36(8)
F(12)-P(2)-F(9)	90.03(8)
F(8)-P(2)-F(9)	90.06(8)
F(11)-P(2)-F(9)	179.63(9)
F(10)-P(2)-F(9)	89.72(8)
F(12)-P(2)-F(7)	179.54(9)
F(8)-P(2)-F(7)	90.03(9)
F(11)-P(2)-F(7)	90.01(8)
F(10)-P(2)-F(7)	89.58(8)
F(9)-P(2)-F(7)	89.63(8)
C(1)-N(1)-C(12)	118.28(18)

C(10)-N(2)-C(11)	117.52(18)
C(16)-N(3)-C(14)	108.93(19)
C(16)-N(3)-C(13)	125.03(19)
C(14)-N(3)-C(13)	125.89(19)
C(16)-N(4)-C(15)	109.26(19)
C(16)-N(4)-C(17)	124.62(19)
C(15)-N(4)-C(17)	125.71(19)
C(20)-N(5)-C(18)	109.04(18)
C(20)-N(5)-C(17)	124.73(19)
C(18)-N(5)-C(17)	125.95(19)
C(20)-N(6)-C(19)	108.97(18)
C(20)-N(6)-C(21)	125.34(19)
C(19)-N(6)-C(21)	125.66(19)
N(1)-C(1)-C(2)	123.9(2)
N(1)-C(1)-C(21)	119.56(19)
C(2)-C(1)-C(21)	116.48(19)
C(3)-C(2)-C(1)	118.4(2)
C(2)-C(3)-C(4)	120.1(2)
C(3)-C(4)-C(12)	117.6(2)
C(3)-C(4)-C(5)	122.0(2)
C(12)-C(4)-C(5)	120.4(2)
C(6)-C(5)-C(4)	120.8(2)
C(5)-C(6)-C(7)	120.8(2)
C(8)-C(7)-C(11)	118.0(2)
C(8)-C(7)-C(6)	121.2(2)
C(11)-C(7)-C(6)	120.8(2)
C(9)-C(8)-C(7)	119.1(2)
C(8)-C(9)-C(10)	119.0(2)
N(2)-C(10)-C(9)	124.1(2)
N(2)-C(10)-C(13)	118.91(19)
C(9)-C(10)-C(13)	116.97(19)
N(2)-C(11)-C(7)	122.3(2)
N(2)-C(11)-C(12)	119.27(19)
C(7)-C(11)-C(12)	118.44(19)
N(1)-C(12)-C(4)	121.76(19)

N(1)-C(12)-C(11)	119.60(18)
C(4)-C(12)-C(11)	118.61(19)
N(3)-C(13)-C(10)	113.33(18)
C(15)-C(14)-N(3)	107.1(2)
C(14)-C(15)-N(4)	106.4(2)
N(3)-C(16)-N(4)	108.21(19)
N(4)-C(17)-N(5)	108.17(17)
C(19)-C(18)-N(5)	106.7(2)
C(18)-C(19)-N(6)	107.2(2)
N(6)-C(20)-N(5)	108.13(19)
N(6)-C(21)-C(1)	113.42(18)

Symmetry transformations used to generate equivalent atoms:

Table 4. Anisotropic displacement parameters ($\text{\AA}^2 \times 10^3$) for $3[\text{PF}_6]_2$. The anisotropic displacement factor exponent takes the form: $-2\pi^2 [h^2 a^{*2} U^{11} + \dots + 2 h k a^* b^* U^{12}]$

	U11	U22	U33	U23	U13	U12
S(1)	19(1)	21(1)	28(1)	-2(1)	13(1)	-1(1)
S(2)	17(1)	18(1)	18(1)	0(1)	7(1)	1(1)
S(3)	20(1)	30(1)	19(1)	0(1)	9(1)	-4(1)
S(4)	22(1)	21(1)	19(1)	1(1)	7(1)	3(1)
P(1)	24(1)	22(1)	19(1)	-3(1)	11(1)	-5(1)
P(2)	16(1)	19(1)	15(1)	-1(1)	6(1)	1(1)
F(1)	35(1)	39(1)	59(1)	-14(1)	31(1)	-15(1)
F(2)	66(1)	52(1)	21(1)	-9(1)	11(1)	-7(1)
F(3)	67(1)	28(1)	35(1)	10(1)	23(1)	9(1)
F(4)	53(1)	27(1)	23(1)	-3(1)	18(1)	-1(1)
F(5)	49(1)	21(1)	39(1)	-3(1)	26(1)	-4(1)
F(6)	25(1)	58(1)	76(1)	-13(1)	23(1)	-8(1)
F(7)	23(1)	39(1)	31(1)	-4(1)	18(1)	1(1)
F(8)	37(1)	23(1)	36(1)	1(1)	6(1)	-7(1)
F(9)	24(1)	38(1)	17(1)	0(1)	2(1)	3(1)
F(10)	29(1)	25(1)	33(1)	-2(1)	16(1)	-6(1)

F(11)	27(1)	31(1)	20(1)	1(1)	2(1)	5(1)
F(12)	31(1)	43(1)	24(1)	-6(1)	13(1)	12(1)
O(1)	22(1)	40(1)	37(1)	-5(1)	17(1)	4(1)
O(2)	22(1)	25(1)	16(1)	1(1)	6(1)	-1(1)
O(3)	30(1)	37(1)	18(1)	2(1)	10(1)	-8(1)
O(4)	21(1)	40(1)	18(1)	-3(1)	4(1)	-3(1)
N(1)	14(1)	17(1)	12(1)	2(1)	4(1)	1(1)
N(2)	15(1)	17(1)	11(1)	0(1)	5(1)	1(1)
N(3)	16(1)	19(1)	14(1)	-1(1)	8(1)	-3(1)
N(4)	15(1)	19(1)	13(1)	1(1)	7(1)	-1(1)
N(5)	17(1)	17(1)	14(1)	-2(1)	9(1)	0(1)
N(6)	16(1)	18(1)	11(1)	-3(1)	6(1)	-3(1)
C(1)	14(1)	19(1)	12(1)	1(1)	4(1)	1(1)
C(2)	16(1)	22(1)	22(1)	-1(1)	8(1)	-3(1)
C(3)	14(1)	28(1)	19(1)	5(1)	10(1)	0(1)
C(4)	15(1)	23(1)	14(1)	3(1)	5(1)	3(1)
C(5)	17(1)	27(1)	19(1)	2(1)	12(1)	3(1)
C(6)	22(1)	26(1)	15(1)	-2(1)	10(1)	5(1)
C(7)	18(1)	20(1)	13(1)	2(1)	5(1)	3(1)
C(8)	26(1)	19(1)	16(1)	-4(1)	9(1)	1(1)
C(9)	23(1)	19(1)	18(1)	-3(1)	7(1)	-5(1)
C(10)	15(1)	19(1)	13(1)	3(1)	4(1)	0(1)
C(11)	14(1)	18(1)	12(1)	2(1)	5(1)	2(1)
C(12)	13(1)	18(1)	11(1)	2(1)	4(1)	3(1)
C(13)	20(1)	17(1)	18(1)	-3(1)	9(1)	-4(1)
C(14)	13(1)	26(1)	15(1)	2(1)	5(1)	-2(1)
C(15)	15(1)	24(1)	19(1)	3(1)	9(1)	2(1)
C(16)	14(1)	18(1)	16(1)	2(1)	7(1)	0(1)
C(17)	18(1)	21(1)	16(1)	-1(1)	11(1)	-1(1)
C(18)	21(1)	20(1)	19(1)	0(1)	11(1)	4(1)
C(19)	23(1)	18(1)	17(1)	0(1)	10(1)	1(1)
C(20)	17(1)	18(1)	13(1)	-1(1)	7(1)	0(1)
C(21)	14(1)	21(1)	20(1)	-3(1)	8(1)	-5(1)
C(22)	30(2)	28(2)	30(1)	0(1)	14(1)	-6(1)
C(23)	21(1)	33(2)	32(2)	-7(1)	13(1)	-3(1)

C(24)	22(1)	28(1)	28(1)	-1(1)	4(1)	-4(1)
C(25)	26(1)	29(1)	23(1)	1(1)	13(1)	0(1)
C(26)	62(2)	31(2)	34(2)	-6(1)	29(2)	-2(2)
C(27)	40(2)	27(1)	35(2)	-1(1)	25(1)	-2(1)
C(28)	18(1)	31(1)	19(1)	-5(1)	8(1)	-5(1)
C(29)	20(1)	38(2)	20(1)	-5(1)	8(1)	-5(1)

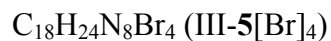
Table 5. Hydrogen coordinates ($\times 10^4$) and isotropic displacement parameters ($\text{\AA}^2 \times 10^3$) for $\mathbf{3}[\text{PF}_6]_2$.

	x	y	z	U(eq)
H(2)	10839(18)	3029(17)	5097(14)	22(7)
H(3)	11129(19)	1936(17)	4319(15)	25(7)
H(5)	10647(18)	579(15)	3574(14)	17(6)
H(6)	9674(17)	-634(16)	3233(14)	16(6)
H(8)	8270(16)	-1414(15)	3251(13)	12(6)
H(9)	7009(19)	-1538(18)	3700(15)	26(7)
H(13A)	6764(19)	-1002(17)	5053(15)	23(7)
H(13B)	6015(19)	-785(17)	4286(15)	22(7)
H(14)	5058(18)	557(16)	4177(15)	19(6)
H(15)	5225(17)	1896(16)	5048(13)	14(6)
H(16)	7427(16)	356(14)	5985(13)	6(5)
H(17A)	7278(18)	1614(16)	6786(15)	19(6)
H(17B)	6407(16)	2262(14)	6396(12)	6(5)
H(18)	6580(20)	3498(17)	5608(15)	24(7)
H(19)	7987(18)	4079(17)	5266(14)	19(6)
H(20)	8730(20)	1873(18)	6405(16)	29(7)
H(21A)	10082(19)	2970(17)	6242(16)	24(7)
H(21B)	9656(17)	3600(17)	5572(14)	17(6)
H(22A)	4437(19)	2687(19)	6557(15)	28(7)
H(22B)	5070(20)	3474(18)	6973(16)	31(8)
H(22C)	3980(20)	3505(17)	6752(15)	26(7)

H(23A)	3210(20)	2660(20)	5203(17)	38(8)
H(23B)	2980(20)	3487(19)	4627(18)	39(8)
H(23C)	2700(20)	3490(20)	5337(18)	47(9)
H(24A)	278(19)	8289(18)	1594(14)	22(7)
H(24B)	-470(20)	8669(19)	1859(17)	39(8)
H(24C)	-420(20)	9016(18)	1107(17)	30(7)
H(25A)	1730(19)	9048(19)	1549(15)	24(7)
H(25B)	1960(20)	10025(19)	1744(16)	29(7)
H(25C)	1100(20)	9815(18)	1022(16)	29(7)
H(26A)	5460(30)	8670(20)	2150(19)	48(10)
H(26B)	4530(20)	8070(20)	1884(17)	40(8)
H(26C)	4550(20)	8870(20)	1364(19)	44(9)
H(27A)	5540(20)	10195(19)	2639(17)	34(8)
H(27B)	4660(20)	10700(20)	2654(17)	38(8)
H(27C)	4710(20)	10448(19)	1887(18)	39(8)
H(28A)	7859(19)	7901(18)	1088(15)	25(7)
H(28B)	8650(20)	7234(17)	1048(14)	23(7)
H(28C)	7613(19)	6922(17)	804(15)	24(7)
H(29A)	7000(20)	7880(20)	1962(17)	39(8)
H(29B)	7194(18)	7129(16)	2599(16)	21(7)
H(29C)	6670(20)	6881(18)	1745(16)	31(7)

APPENDIX F

SUPPLEMENTARY MATERIAL FOR THE X-RAY CRYSTAL STRUCTURE OF

Table 1. Crystal data and structure refinement for **5**[Br]₄.

Identification code	C ₁₈ H ₂₆ Br ₄ N ₈ ·H ₂ O	
Empirical formula	C18 H28 Br4 N8 O	
Formula weight	692.12	
Temperature	100(2) K	
Wavelength	0.71073 Å	
Crystal system	Triclinic	
Space group	P-1	
Unit cell dimensions	a = 7.194(2) Å	α = 71.651(7)°.
	b = 9.054(3) Å	β = 82.477(16)°.
	c = 10.292(4) Å	γ = 75.925(9)°.
Volume	616.1(4) Å ³	
Z	1	
Density (calculated)	1.865 Mg/m ³	
Absorption coefficient	6.560 mm ⁻¹	
F(000)	340	
Crystal size	0.22 x 0.09 x 0.05 mm ³	
Theta range for data collection	2.09 to 27.60°.	
Index ranges	-9 ≤ h ≤ 9, -11 ≤ k ≤ 11, -13 ≤ l ≤ 13	
Reflections collected	5405	
Independent reflections	2773 [R(int) = 0.0289]	
Completeness to theta = 27.60°	96.6 %	
Absorption correction	Semi-empirical from equivalents	
Max. and min. transmission	0.7351 and 0.3263	
Refinement method	Full-matrix least-squares on F ²	
Data / restraints / parameters	2773 / 0 / 201	

Goodness-of-fit on F^2	1.054
Final R indices [$I > 2\sigma(I)$]	$R1 = 0.0321$, $wR2 = 0.0756$
R indices (all data)	$R1 = 0.0407$, $wR2 = 0.0798$
Largest diff. peak and hole	1.213 and $-0.469 \text{ e.}\text{\AA}^{-3}$

Table 2. Atomic coordinates ($\times 10^4$) and equivalent isotropic displacement parameters ($\text{\AA}^2 \times 10^3$) for $5[\text{Br}]_4$. $U(\text{eq})$ is defined as one third of the trace of the orthogonalized U_{ij} tensor.

	x	y	z	$U(\text{eq})$
Br(1)	2782(1)	8216(1)	288(1)	18(1)
Br(2)	1379(1)	7354(1)	5107(1)	18(1)
O	3409(4)	5128(3)	3047(3)	24(1)
N(1)	1869(4)	3308(3)	-1443(3)	15(1)
N(2)	2188(4)	2910(3)	694(3)	15(1)
N(3)	3882(4)	1104(3)	2674(3)	16(1)
N(4)	6024(4)	-1067(3)	3308(3)	16(1)
C(1)	1330(5)	3141(4)	-2715(3)	20(1)
C(2)	2358(5)	4655(4)	-1334(3)	17(1)
C(3)	2557(5)	4405(4)	6(3)	18(1)
C(4)	1772(4)	2280(4)	-216(3)	16(1)
C(5)	2095(5)	2189(4)	2181(3)	20(1)
C(6)	5337(5)	1475(4)	3196(3)	17(1)
C(7)	6669(5)	117(4)	3599(3)	17(1)
C(8)	4348(5)	-437(4)	2748(3)	17(1)
C(9)	6960(5)	-2761(4)	3676(3)	18(1)

Table 3. Bond lengths [\AA] and angles [$^\circ$] for **5**[Br]₄.

N(1)-C(4)	1.317(4)
N(1)-C(2)	1.388(4)
N(1)-C(1)	1.474(4)
N(2)-C(4)	1.336(4)
N(2)-C(3)	1.388(4)
N(2)-C(5)	1.462(4)
N(3)-C(8)	1.333(4)
N(3)-C(6)	1.390(4)
N(3)-C(5)	1.455(4)
N(4)-C(8)	1.323(4)
N(4)-C(7)	1.392(4)
N(4)-C(9)	1.466(4)
C(1)-C(9)#1	1.517(5)
C(2)-C(3)	1.347(4)
C(6)-C(7)	1.346(5)
C(9)-C(1)#1	1.517(5)
<hr/>	
C(4)-N(1)-C(2)	109.5(3)
C(4)-N(1)-C(1)	125.3(3)
C(2)-N(1)-C(1)	124.8(3)
C(4)-N(2)-C(3)	108.9(3)
C(4)-N(2)-C(5)	124.9(3)
C(3)-N(2)-C(5)	125.9(3)
C(8)-N(3)-C(6)	108.9(3)
C(8)-N(3)-C(5)	125.0(3)
C(6)-N(3)-C(5)	126.1(3)
C(8)-N(4)-C(7)	108.8(3)
C(8)-N(4)-C(9)	125.5(3)
C(7)-N(4)-C(9)	125.5(3)
N(1)-C(1)-C(9)#1	113.3(3)
C(3)-C(2)-N(1)	106.8(3)
C(2)-C(3)-N(2)	106.7(3)

N(1)-C(4)-N(2)	108.1(3)
N(3)-C(5)-N(2)	112.7(3)
C(7)-C(6)-N(3)	106.7(3)
C(6)-C(7)-N(4)	107.1(3)
N(4)-C(8)-N(3)	108.5(3)
N(4)-C(9)-C(1)#1	113.2(3)

Symmetry transformations used to generate equivalent atoms:

#1 -x+1,-y,-z

Table 4. Anisotropic displacement parameters ($\text{\AA}^2 \times 10^3$) for $5[\text{Br}]_4$. The anisotropic displacement factor exponent takes the form: $-2\pi^2 [h^2 a^{*2} U^{11} + \dots + 2 h k a^* b^* U^{12}]$

	U11	U22	U33	U23	U13	U12
Br(1)	21(1)	15(1)	16(1)	-4(1)	0(1)	-4(1)
Br(2)	21(1)	22(1)	14(1)	-6(1)	0(1)	-7(1)
O	31(1)	18(1)	17(1)	-2(1)	0(1)	0(1)
N(1)	17(1)	14(1)	14(1)	-5(1)	-1(1)	-2(1)
N(2)	17(1)	13(1)	15(1)	-3(1)	-1(1)	-3(1)
N(3)	17(1)	17(1)	10(1)	-2(1)	1(1)	-2(1)
N(4)	20(1)	17(1)	11(1)	-4(1)	0(1)	-5(1)
C(1)	21(2)	21(2)	19(2)	-10(1)	-7(1)	-1(2)
C(2)	17(2)	15(2)	20(2)	-3(1)	-2(1)	-3(1)
C(3)	21(2)	17(2)	20(2)	-9(1)	-2(1)	-4(1)
C(4)	16(2)	11(2)	19(2)	-4(1)	-3(1)	-1(1)
C(5)	18(2)	24(2)	14(2)	-4(1)	1(1)	0(1)
C(6)	24(2)	16(2)	11(1)	-3(1)	1(1)	-8(1)
C(7)	19(2)	21(2)	12(1)	-5(1)	3(1)	-8(1)
C(8)	21(2)	19(2)	11(1)	-5(1)	2(1)	-7(1)
C(9)	27(2)	13(2)	12(2)	-2(1)	-2(1)	-4(1)

Table 5. Hydrogen coordinates ($\times 10^4$) and isotropic displacement parameters ($\text{\AA}^2 \times 10^3$) for $5[\text{Br}]_4$.

	x	y	z	U(eq)
H(2)	2530(50)	5500(40)	-2110(40)	20(9)
H(3)	2890(50)	4990(40)	490(30)	13(8)
H(4)	1440(50)	1170(40)	0(40)	25(10)
H(6)	5300(50)	2450(40)	3260(40)	19(9)
H(7)	8020(60)	-10(50)	3880(40)	37(11)
H(8)	3530(60)	-950(50)	2450(40)	35(11)
H(10)	3170(50)	5880(50)	2440(40)	22(11)
H(11)	2910(60)	5560(50)	3560(50)	36(14)
H(1A)	530(60)	2340(50)	-2440(40)	28(10)
H(5A)	1160(50)	1640(40)	2420(40)	21(10)
H(9A)	5950(50)	-3360(40)	3750(30)	17(9)
H(1B)	550(50)	4210(50)	-3210(40)	26(10)
H(5B)	1870(40)	3030(40)	2670(30)	14(9)
H(9B)	7380(50)	-3010(50)	4570(40)	33(11)

APPENDIX G

SUPPLEMENTARY MATERIAL FOR THE X-RAY CRYSTAL STRUCTURE OF

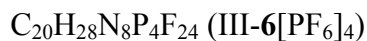


Table 1. Crystal data and structure refinement for **6**[PF₆]₄.

Identification code	$C_{20}H_{28}N_8, 4(PF_6) \cdot 2(CH_3CN)$	
Empirical formula	C ₂₄ H ₃₄ F ₂₄ N ₁₀ P ₄	
Formula weight	1042.49	
Temperature	100(2) K	
Wavelength	0.71073 Å	
Crystal system	Triclinic	
Space group	P-1	
Unit cell dimensions	a = 9.028(11) Å	α = 101.59(2)°.
	b = 10.157(12) Å	β = 109.423(19)°.
	c = 12.096(14) Å	γ = 103.63(2)°.
Volume	968(2) Å ³	
Z	1	
Density (calculated)	1.788 Mg/m ³	
Absorption coefficient	0.348 mm ⁻¹	
F(000)	524	
Crystal size	0.15 x 0.06 x 0.04 mm ³	
Theta range for data collection	1.87 to 24.99°.	
Index ranges	-10 ≤ h ≤ 10, -12 ≤ k ≤ 12, -14 ≤ l ≤ 14	
Reflections collected	7051	
Independent reflections	3401 [R(int) = 0.0564]	
Completeness to theta = 24.99°	99.7 %	
Absorption correction	Semi-empirical from equivalents	
Max. and min. transmission	0.9862 and 0.9497	
Refinement method	Full-matrix least-squares on F ²	
Data / restraints / parameters	3401 / 0 / 336	

Goodness-of-fit on F ²	1.118
Final R indices [I>2sigma(I)]	R1 = 0.0826, wR2 = 0.1806
R indices (all data)	R1 = 0.1237, wR2 = 0.1954
Largest diff. peak and hole	0.623 and -0.367 e.Å ⁻³

Table 2. Atomic coordinates ($\times 10^4$) and equivalent isotropic displacement parameters ($\text{\AA}^2 \times 10^3$) for $\mathbf{6}[\text{PF}_6]_4$. $U(\text{eq})$ is defined as one third of the trace of the orthogonalized U_{ij} tensor.

	x	y	z	U(eq)
P(1)	2305(2)	6182(2)	3601(2)	31(1)
P(2)	2846(2)	483(2)	7912(1)	33(1)
F(1A)	2820(13)	5054(9)	2832(11)	66(3)
F(1B)	3030(40)	6720(30)	2720(30)	171(13)
F(2A)	3823(9)	6238(11)	4819(7)	61(3)
F(2B)	3689(17)	7451(16)	4627(18)	117(7)
F(3A)	1834(13)	7275(10)	4409(12)	80(4)
F(3B)	1650(20)	5810(20)	4588(15)	83(5)
F(4A)	873(9)	6132(15)	2427(9)	82(5)
F(4B)	786(15)	4871(14)	2647(16)	109(8)
F(5A)	1102(10)	4931(10)	3786(12)	54(3)
F(5B)	3371(13)	5170(12)	3720(16)	55(5)
F(6A)	3544(12)	7360(11)	3439(13)	57(4)
F(6B)	1128(14)	7134(11)	3402(16)	56(4)
F(7)	2185(5)	-1205(4)	7617(4)	57(1)
F(8)	4243(5)	330(6)	7419(4)	85(2)
F(9)	4066(5)	644(4)	9264(3)	56(1)
F(10)	1464(4)	601(4)	8406(3)	43(1)
F(11)	1635(4)	341(4)	6562(3)	40(1)
F(12)	3496(5)	2144(4)	8199(3)	64(1)
N(1)	7448(6)	8993(5)	7550(4)	28(1)
N(2)	8216(6)	8442(5)	6070(4)	27(1)
N(3)	6094(6)	4399(5)	2414(4)	27(1)
N(4)	4028(6)	2459(5)	1591(4)	30(1)

N(5)	9728(8)	2039(6)	175(5)	49(2)
C(1)	7039(8)	8965(6)	8612(5)	33(1)
C(2)	8102(7)	8136(6)	7049(5)	31(1)
C(3)	7164(8)	9907(6)	6858(6)	36(2)
C(4)	7629(7)	9552(6)	5933(6)	34(1)
C(5)	8696(7)	7618(6)	5187(5)	30(1)
C(6)	7162(6)	6502(6)	4175(5)	26(1)
C(7)	7614(7)	5525(6)	3316(5)	29(1)
C(8)	5533(7)	3117(6)	2500(5)	28(1)
C(9)	4967(7)	4562(6)	1425(5)	33(1)
C(10)	3667(8)	3336(6)	894(5)	36(2)
C(11)	8891(9)	2691(7)	129(6)	44(2)
C(12)	7757(10)	3528(10)	22(9)	87(3)

Table 3. Bond lengths [\AA] and angles [$^\circ$] for $6[\text{PF}_6]_4$.

P(1)-F(2B)	1.526(12)
P(1)-F(6A)	1.527(9)
P(1)-F(1B)	1.551(17)
P(1)-F(4A)	1.552(7)
P(1)-F(3A)	1.559(8)
P(1)-F(5B)	1.562(9)
P(1)-F(4B)	1.566(10)
P(1)-F(3B)	1.570(11)
P(1)-F(5A)	1.571(7)
P(1)-F(1A)	1.583(8)
P(1)-F(6B)	1.590(9)
P(1)-F(2A)	1.625(7)
P(2)-F(10)	1.569(4)
P(2)-F(12)	1.573(4)
P(2)-F(9)	1.589(4)
P(2)-F(11)	1.590(4)
P(2)-F(8)	1.590(5)
P(2)-F(7)	1.598(4)
N(1)-C(2)	1.320(7)

N(1)-C(3)	1.381(7)
N(1)-C(1)	1.454(7)
N(2)-C(2)	1.312(7)
N(2)-C(4)	1.371(7)
N(2)-C(5)	1.465(7)
N(3)-C(8)	1.320(7)
N(3)-C(9)	1.358(7)
N(3)-C(7)	1.464(7)
N(4)-C(8)	1.336(7)
N(4)-C(10)	1.366(7)
N(4)-C(1)#1	1.458(7)
N(5)-C(11)	1.112(8)
C(1)-N(4)#1	1.458(7)
C(3)-C(4)	1.335(8)
C(5)-C(6)	1.509(8)
C(6)-C(7)	1.512(8)
C(9)-C(10)	1.353(8)
C(11)-C(12)	1.468(11)

F(2B)-P(1)-F(6A)	53.8(8)
F(2B)-P(1)-F(1B)	86.4(14)
F(6A)-P(1)-F(1B)	32.9(12)
F(2B)-P(1)-F(4A)	130.3(10)
F(6A)-P(1)-F(4A)	91.6(6)
F(1B)-P(1)-F(4A)	70.1(12)
F(2B)-P(1)-F(3A)	61.0(7)
F(6A)-P(1)-F(3A)	92.3(6)
F(1B)-P(1)-F(3A)	116.1(10)
F(4A)-P(1)-F(3A)	90.4(7)
F(2B)-P(1)-F(5B)	94.1(8)
F(6A)-P(1)-F(5B)	96.0(6)
F(1B)-P(1)-F(5B)	89.6(9)
F(4A)-P(1)-F(5B)	127.4(8)
F(3A)-P(1)-F(5B)	140.8(7)
F(2B)-P(1)-F(4B)	173.7(11)

F(6A)-P(1)-F(4B)	132.0(10)
F(1B)-P(1)-F(4B)	99.6(17)
F(4A)-P(1)-F(4B)	51.3(7)
F(3A)-P(1)-F(4B)	114.1(7)
F(5B)-P(1)-F(4B)	88.0(7)
F(2B)-P(1)-F(3B)	88.0(12)
F(6A)-P(1)-F(3B)	141.1(9)
F(1B)-P(1)-F(3B)	173.6(13)
F(4A)-P(1)-F(3B)	111.5(6)
F(3A)-P(1)-F(3B)	58.2(7)
F(5B)-P(1)-F(3B)	93.9(7)
F(4B)-P(1)-F(3B)	85.9(10)
F(2B)-P(1)-F(5A)	125.7(10)
F(6A)-P(1)-F(5A)	177.0(5)
F(1B)-P(1)-F(5A)	146.9(14)
F(4A)-P(1)-F(5A)	90.6(5)
F(3A)-P(1)-F(5A)	89.8(5)
F(5B)-P(1)-F(5A)	81.1(5)
F(4B)-P(1)-F(5A)	48.8(8)
F(3B)-P(1)-F(5A)	39.2(6)
F(2B)-P(1)-F(1A)	117.9(7)
F(6A)-P(1)-F(1A)	88.7(6)
F(1B)-P(1)-F(1A)	65.7(10)
F(4A)-P(1)-F(1A)	91.9(7)
F(3A)-P(1)-F(1A)	177.5(7)
F(5B)-P(1)-F(1A)	36.7(5)
F(4B)-P(1)-F(1A)	66.8(6)
F(3B)-P(1)-F(1A)	119.9(7)
F(5A)-P(1)-F(1A)	89.2(5)
F(2B)-P(1)-F(6B)	89.6(8)
F(6A)-P(1)-F(6B)	85.8(5)
F(1B)-P(1)-F(6B)	90.2(9)
F(4A)-P(1)-F(6B)	49.1(6)
F(3A)-P(1)-F(6B)	42.1(5)
F(5B)-P(1)-F(6B)	176.3(8)

F(4B)-P(1)-F(6B)	88.4(6)
F(3B)-P(1)-F(6B)	86.7(6)
F(5A)-P(1)-F(6B)	97.2(5)
F(1A)-P(1)-F(6B)	140.3(8)
F(2B)-P(1)-F(2A)	49.6(7)
F(6A)-P(1)-F(2A)	87.7(5)
F(1B)-P(1)-F(2A)	109.0(12)
F(4A)-P(1)-F(2A)	179.1(4)
F(3A)-P(1)-F(2A)	90.2(6)
F(5B)-P(1)-F(2A)	52.1(6)
F(4B)-P(1)-F(2A)	129.0(8)
F(3B)-P(1)-F(2A)	69.4(6)
F(5A)-P(1)-F(2A)	90.1(5)
F(1A)-P(1)-F(2A)	87.5(6)
F(6B)-P(1)-F(2A)	131.4(7)
F(10)-P(2)-F(12)	90.6(2)
F(10)-P(2)-F(9)	89.1(2)
F(12)-P(2)-F(9)	89.6(2)
F(10)-P(2)-F(11)	91.0(2)
F(12)-P(2)-F(11)	89.7(2)
F(9)-P(2)-F(11)	179.3(2)
F(10)-P(2)-F(8)	178.7(3)
F(12)-P(2)-F(8)	90.6(3)
F(9)-P(2)-F(8)	90.4(3)
F(11)-P(2)-F(8)	89.5(2)
F(10)-P(2)-F(7)	89.5(2)
F(12)-P(2)-F(7)	179.8(2)
F(9)-P(2)-F(7)	90.5(2)
F(11)-P(2)-F(7)	90.1(2)
F(8)-P(2)-F(7)	89.3(3)
C(2)-N(1)-C(3)	107.7(5)
C(2)-N(1)-C(1)	126.8(5)
C(3)-N(1)-C(1)	125.5(5)
C(2)-N(2)-C(4)	108.8(5)
C(2)-N(2)-C(5)	125.3(5)

C(4)-N(2)-C(5)	125.5(5)
C(8)-N(3)-C(9)	109.6(5)
C(8)-N(3)-C(7)	125.2(5)
C(9)-N(3)-C(7)	124.9(5)
C(8)-N(4)-C(10)	109.0(5)
C(8)-N(4)-C(1)#1	124.9(5)
C(10)-N(4)-C(1)#1	126.1(5)
N(1)-C(1)-N(4)#1	109.4(4)
N(2)-C(2)-N(1)	109.2(5)
C(4)-C(3)-N(1)	107.4(5)
C(3)-C(4)-N(2)	106.9(5)
N(2)-C(5)-C(6)	109.4(5)
C(5)-C(6)-C(7)	111.1(5)
N(3)-C(7)-C(6)	108.8(4)
N(3)-C(8)-N(4)	107.6(5)
C(10)-C(9)-N(3)	107.1(5)
C(9)-C(10)-N(4)	106.6(5)
N(5)-C(11)-C(12)	178.0(8)

Symmetry transformations used to generate equivalent atoms:

#1 -x+1,-y+1,-z+1

Table 4. Anisotropic displacement parameters ($\text{\AA}^2 \times 10^3$) for $\mathbf{6}[\text{PF}_6]_4$. The anisotropic displacement factor exponent takes the form: $-2\pi^2 [h^2 a^{*2} U^{11} + \dots + 2 h k a^* b^* U^{12}]$

	U11	U22	U33	U23	U13	U12
P(1)	30(1)	28(1)	43(1)	15(1)	19(1)	14(1)
P(2)	30(1)	43(1)	24(1)	11(1)	10(1)	9(1)
F(1A)	71(7)	48(5)	82(7)	-3(5)	44(6)	22(5)
F(1B)	270(30)	280(30)	240(30)	240(20)	240(30)	250(30)
F(2A)	48(5)	103(9)	40(5)	40(5)	15(4)	29(5)
F(2B)	72(9)	82(11)	130(15)	-24(10)	1(9)	10(8)
F(3A)	81(7)	65(6)	92(9)	-8(6)	45(7)	34(5)
F(3B)	96(11)	132(15)	89(11)	73(10)	70(10)	77(11)

F(4A)	43(5)	150(13)	61(6)	70(8)	9(4)	31(6)
F(4B)	71(8)	59(9)	111(14)	-45(9)	-33(8)	28(6)
F(5A)	39(5)	52(6)	93(10)	44(6)	35(6)	18(4)
F(5B)	37(6)	51(7)	106(14)	49(9)	35(8)	34(5)
F(6A)	34(4)	51(6)	118(12)	58(7)	42(6)	23(4)
F(6B)	52(7)	44(7)	105(13)	45(8)	49(8)	32(6)
F(7)	85(3)	42(2)	47(2)	10(2)	23(2)	31(2)
F(8)	53(3)	159(5)	61(3)	38(3)	39(2)	39(3)
F(9)	47(2)	85(3)	30(2)	20(2)	5(2)	22(2)
F(10)	40(2)	50(2)	33(2)	7(2)	16(2)	10(2)
F(11)	40(2)	44(2)	23(2)	9(2)	7(2)	4(2)
F(12)	79(3)	40(2)	34(2)	13(2)	-1(2)	-18(2)
N(1)	37(3)	19(2)	23(3)	4(2)	12(2)	5(2)
N(2)	33(3)	23(2)	23(3)	6(2)	12(2)	4(2)
N(3)	28(3)	24(3)	28(3)	4(2)	15(2)	6(2)
N(4)	43(3)	18(2)	23(3)	4(2)	12(2)	3(2)
N(5)	62(4)	37(3)	46(4)	10(3)	25(3)	11(3)
C(1)	46(4)	24(3)	22(3)	0(2)	15(3)	2(3)
C(2)	38(3)	25(3)	24(3)	5(3)	10(3)	2(3)
C(3)	47(4)	26(3)	47(4)	18(3)	26(3)	18(3)
C(4)	45(4)	28(3)	36(4)	17(3)	19(3)	11(3)
C(5)	33(3)	31(3)	24(3)	8(3)	12(3)	9(3)
C(6)	21(3)	28(3)	25(3)	5(2)	6(2)	7(2)
C(7)	27(3)	28(3)	31(3)	10(3)	9(3)	9(3)
C(8)	33(3)	26(3)	27(3)	5(3)	14(3)	11(3)
C(9)	40(3)	26(3)	23(3)	6(2)	7(3)	5(3)
C(10)	43(4)	35(3)	22(3)	9(3)	10(3)	3(3)
C(11)	43(4)	33(4)	44(4)	-6(3)	18(3)	4(3)
C(12)	51(5)	102(7)	83(7)	-22(5)	14(5)	40(5)

Table 5. Hydrogen coordinates ($\times 10^4$) and isotropic displacement parameters ($\text{\AA}^2 \times 10^3$) for $6[\text{PF}_6]_4$.

	x	y	z	U(eq)
H(1B)	6460	9661	8739	39
H(1A)	8070	9230	9359	39
H(2)	8437	7412	7349	38
H(3)	6720	10650	7013	43
H(4)	7565	9986	5299	41
H(5A)	9467	7156	5611	36
H(5B)	9275	8258	4833	36
H(6B)	6449	6973	3701	31
H(6A)	6520	5935	4541	31
H(7A)	8169	6071	2890	35
H(7B)	8391	5102	3792	35
H(8)	6097	2732	3101	34
H(9)	5072	5383	1156	39
H(10)	2692	3125	176	43
H(12A)	7392	3644	-801	131
H(12B)	8334	4466	643	131
H(12C)	6788	3034	154	131

APPENDIX H

SUPPLEMENTARY MATERIAL FOR THE X-RAY CRYSTAL STRUCTURE OF
 $[\text{NPCl}_2]_3 \cdot \text{AlCl}_3$ (IV)

Table 1. Crystal data and structure refinement for $[\text{NPCl}_2]_3 \cdot \text{AlCl}_3$.

Identification code	$\text{AlCl}_9^{15}\text{N}_3\text{P}_3$	
Empirical formula	$\text{Al Cl}_9^{15}\text{N}_3 \text{P}_3$	
Formula weight	480.97	
Temperature	100(2) K	
Wavelength	0.71073 Å	
Crystal system	Orthorhombic	
Space group	Pmn2(1)	
Unit cell dimensions	$a = 11.9974(11)$ Å	$\alpha = 90^\circ$.
	$b = 11.7111(11)$ Å	$\beta = 90^\circ$.
	$c = 10.7768(10)$ Å	$\gamma = 90^\circ$.
Volume	$1514.2(2)$ Å ³	
Z	4	
Density (calculated)	2.110 Mg/m ³	
Absorption coefficient	2.013 mm ⁻¹	
F(000)	928	
Crystal size	$0.11 \times 0.09 \times 0.05$ mm ³	
Theta range for data collection	1.74 to 28.26° .	
Index ranges	$-15 \leq h \leq 15, -14 \leq k \leq 15, -14 \leq l \leq 14$	
Reflections collected	13259	
Independent reflections	3798 [R(int) = 0.0368]	
Completeness to theta = 28.26°	98.8 %	
Absorption correction	Semi-empirical from equivalents	
Max. and min. transmission	0.9061 and 0.8138	
Refinement method	Full-matrix least-squares on F ²	
Data / restraints / parameters	3798 / 1 / 163	

Goodness-of-fit on F ²	1.275
Final R indices [I>2sigma(I)]	R1 = 0.0428, wR2 = 0.0874
R indices (all data)	R1 = 0.0446, wR2 = 0.0881
Absolute structure parameter	0.04(12)
Largest diff. peak and hole	0.737 and -0.445 e.Å ⁻³

Table 2. Atomic coordinates ($\times 10^4$) and equivalent isotropic displacement parameters ($\text{\AA}^2 \times 10^3$) for $[\text{N}(\text{PCl}_2)_3] \cdot \text{AlCl}_3$. U(eq) is defined as one third of the trace of the orthogonalized U^{ij} tensor.

	x	y	z	U(eq)
Cl(1)	1423(1)	1085(1)	10020(1)	23(1)
Cl(2)	0	3278(1)	8437(1)	18(1)
Cl(3)	1791(1)	-1046(1)	7716(1)	20(1)
Cl(4)	2270(1)	1491(1)	7015(1)	20(1)
Cl(5)	0	-1980(1)	4223(2)	37(1)
Cl(6)	0	415(1)	3007(1)	21(1)
Cl(7)	1442(1)	3007(1)	4368(1)	25(1)
Cl(8)	0	5354(1)	5650(2)	31(1)
Cl(9)	1830(1)	3773(1)	1301(1)	24(1)
Cl(10)	2241(1)	5671(1)	3277(1)	24(1)
Cl(11)	0	6326(1)	-1419(1)	32(1)
Cl(12)	0	8282(1)	503(1)	24(1)
P(1)	1177(1)	262(1)	6767(1)	13(1)
P(2)	0	-327(1)	4647(1)	15(1)
P(3)	1180(1)	5181(1)	1994(1)	14(1)
P(4)	0	6600(1)	387(1)	15(1)
Al(1)	0	1552(2)	8991(2)	13(1)
Al(2)	0	4036(2)	4315(2)	16(1)
N(1)	0	654(4)	7438(4)	11(1)
N(2)	1108(3)	-33(3)	5350(3)	21(1)
N(3)	0	4843(4)	2703(4)	13(1)
N(4)	1108(3)	6127(4)	971(4)	26(1)

Table 3. Bond lengths [\AA] and angles [$^\circ$] for $[\text{N}(\text{PCl}_2)_3 \cdot \text{AlCl}_3]$.

Cl(1)-Al(1)	2.1084(15)
Cl(2)-Al(1)	2.107(2)
Cl(3)-P(1)	1.9834(14)
Cl(4)-P(1)	1.9654(15)
Cl(5)-P(2)	1.989(2)
Cl(6)-P(2)	1.970(2)
Cl(7)-Al(2)	2.1088(15)
Cl(8)-Al(2)	2.110(2)
Cl(9)-P(3)	1.9713(15)
Cl(10)-P(3)	1.9642(15)
Cl(11)-P(4)	1.972(2)
Cl(12)-P(4)	1.974(2)
P(1)-N(2)	1.567(4)
P(1)-N(1)	1.652(3)
P(2)-N(2)#1	1.569(4)
P(2)-N(2)	1.569(4)
P(3)-N(4)	1.565(4)
P(3)-N(3)	1.657(3)
P(4)-N(4)	1.572(4)
P(4)-N(4)#1	1.572(4)
Al(1)-N(1)	1.977(5)
Al(1)-Cl(1)#1	2.1084(15)
Al(2)-N(3)	1.978(5)
Al(2)-Cl(7)#1	2.1088(15)
N(1)-P(1)#1	1.652(3)
N(3)-P(3)#1	1.657(3)
N(2)-P(1)-N(1)	116.3(2)
N(2)-P(1)-Cl(4)	109.19(15)
N(1)-P(1)-Cl(4)	107.86(15)
N(2)-P(1)-Cl(3)	110.62(15)
N(1)-P(1)-Cl(3)	107.87(17)
Cl(4)-P(1)-Cl(3)	104.35(7)

N(2)#1-P(2)-N(2)	115.9(3)
N(2)#1-P(2)-Cl(6)	109.67(15)
N(2)-P(2)-Cl(6)	109.67(15)
N(2)#1-P(2)-Cl(5)	108.95(15)
N(2)-P(2)-Cl(5)	108.95(15)
Cl(6)-P(2)-Cl(5)	102.88(10)
N(4)-P(3)-N(3)	116.5(2)
N(4)-P(3)-Cl(10)	108.97(17)
N(3)-P(3)-Cl(10)	107.41(17)
N(4)-P(3)-Cl(9)	110.29(17)
N(3)-P(3)-Cl(9)	108.19(18)
Cl(10)-P(3)-Cl(9)	104.76(7)
N(4)-P(4)-N(4)#1	115.6(3)
N(4)-P(4)-Cl(11)	109.75(17)
N(4)#1-P(4)-Cl(11)	109.75(17)
N(4)-P(4)-Cl(12)	109.02(17)
N(4)#1-P(4)-Cl(12)	109.02(17)
Cl(11)-P(4)-Cl(12)	103.01(9)
N(1)-Al(1)-Cl(2)	105.69(16)
N(1)-Al(1)-Cl(1)	107.90(9)
Cl(2)-Al(1)-Cl(1)	113.46(6)
N(1)-Al(1)-Cl(1)#1	107.90(9)
Cl(2)-Al(1)-Cl(1)#1	113.46(6)
Cl(1)-Al(1)-Cl(1)#1	108.15(10)
N(3)-Al(2)-Cl(7)#1	107.24(10)
N(3)-Al(2)-Cl(7)	107.24(10)
Cl(7)#1-Al(2)-Cl(7)	110.26(10)
N(3)-Al(2)-Cl(8)	104.42(17)
Cl(7)#1-Al(2)-Cl(8)	113.55(7)
Cl(7)-Al(2)-Cl(8)	113.55(7)
P(1)#1-N(1)-P(1)	117.5(3)
P(1)#1-N(1)-Al(1)	121.24(14)
P(1)-N(1)-Al(1)	121.24(14)
P(1)-N(2)-P(2)	124.3(2)
P(3)-N(3)-P(3)#1	117.4(3)

P(3)-N(3)-Al(2)	121.27(14)
P(3)#1-N(3)-Al(2)	121.27(14)
P(3)-N(4)-P(4)	125.3(2)

Symmetry transformations used to generate equivalent atoms:

#1 -x,y,z

Table 4. Anisotropic displacement parameters ($\text{\AA}^2 \times 10^3$) for $[\text{N}(\text{PCl}_2)_3] \cdot \text{AlCl}_3$. The anisotropic displacement factor exponent takes the form: $-2\pi^2 [h^2 a^{*2} U^{11} + \dots + 2 h k a^* b^* U^{12}]$

	U11	U22	U33	U23	U13	U12
Cl(1)	25(1)	24(1)	19(1)	-3(1)	-9(1)	8(1)
Cl(2)	17(1)	11(1)	26(1)	1(1)	0	0
Cl(3)	22(1)	17(1)	21(1)	5(1)	3(1)	7(1)
Cl(4)	14(1)	22(1)	24(1)	5(1)	-1(1)	-5(1)
Cl(5)	66(1)	15(1)	31(1)	-6(1)	0	0
Cl(6)	29(1)	22(1)	14(1)	2(1)	0	0
Cl(7)	27(1)	23(1)	26(1)	8(1)	-6(1)	4(1)
Cl(8)	59(1)	22(1)	12(1)	-3(1)	0	0
Cl(9)	25(1)	26(1)	22(1)	-2(1)	5(1)	7(1)
Cl(10)	21(1)	24(1)	28(1)	0(1)	-9(1)	-7(1)
Cl(11)	68(1)	18(1)	11(1)	1(1)	0	0
Cl(12)	38(1)	15(1)	18(1)	-1(1)	0	0
P(1)	11(1)	15(1)	13(1)	1(1)	0(1)	1(1)
P(2)	20(1)	13(1)	13(1)	-2(1)	0	0
P(3)	12(1)	17(1)	14(1)	4(1)	0(1)	0(1)
P(4)	18(1)	16(1)	11(1)	5(1)	0	0
Al(1)	15(1)	12(1)	12(1)	0(1)	0	0
Al(2)	25(1)	13(1)	10(1)	3(1)	0	0
N(1)	8(2)	10(2)	14(2)	-3(2)	0	0
N(2)	17(2)	28(2)	18(2)	-3(2)	4(2)	4(2)
N(3)	16(2)	14(2)	10(2)	6(2)	0	0
N(4)	16(2)	32(2)	30(2)	19(2)	5(2)	2(2)

APPENDIX I

SUPPLEMENTARY MATERIAL FOR THE X-RAY CRYSTAL STRUCTURE OF
[NPCl₂]₃ · GaCl₃ (IV)Table 1. Crystal data and structure refinement for [NPCl₂]₃ · GaCl₃.

Identification code	C₁₉GaN₃P₃	
Empirical formula	Cl ₁₉ Ga N ₃ P ₃	
Formula weight	523.71	
Temperature	100(2) K	
Wavelength	0.71073 Å	
Crystal system	Monoclinic	
Space group	P2(1)/c	
Unit cell dimensions	a = 11.7624(11) Å	α = 90°.
	b = 10.7999(10) Å	β = 91.989(2)°.
	c = 23.873(2) Å	γ = 90°.
Volume	3030.8(5) Å ³	
Z	8	
Density (calculated)	2.295 Mg/m ³	
Absorption coefficient	3.693 mm ⁻¹	
F(000)	2000	
Crystal size	0.28 x 0.15 x 0.04 mm ³	
Theta range for data collection	1.71 to 28.32°.	
Index ranges	-15 ≤ h ≤ 15, -13 ≤ k ≤ 14, -31 ≤ l ≤ 30	
Reflections collected	26454	
Independent reflections	7291 [R(int) = 0.0525]	
Completeness to theta = 28.32°	96.5 %	
Absorption correction	Semi-empirical from equivalents	
Max. and min. transmission	0.8663 and 0.4245	
Refinement method	Full-matrix least-squares on F ²	
Data / restraints / parameters	7291 / 0 / 289	

Goodness-of-fit on F ²	1.085
Final R indices [I>2sigma(I)]	R1 = 0.0405, wR2 = 0.0847
R indices (all data)	R1 = 0.0503, wR2 = 0.0882
Largest diff. peak and hole	1.056 and -0.541 e.Å ⁻³

Table 2. Atomic coordinates (x 10⁴) and equivalent isotropic displacement parameters (Å²x 10³) for [NPCl₂]₃ · GaCl₃. U(eq) is defined as one third of the trace of the orthogonalized U^{ij} tensor.

	x	y	z	U(eq)
Ga(1)	3404(1)	6116(1)	1184(1)	12(1)
Ga(2)	10958(1)	738(1)	1310(1)	15(1)
Cl(1)	9360(1)	1882(1)	2415(1)	22(1)
Cl(2)	11182(1)	3884(1)	2160(1)	26(1)
Cl(3)	9344(1)	1683(1)	142(1)	21(1)
Cl(4)	11120(1)	3790(1)	371(1)	24(1)
Cl(5)	6635(1)	4555(1)	1204(1)	29(1)
Cl(6)	8623(1)	6429(1)	1194(1)	26(1)
Cl(7)	12009(1)	775(1)	2061(1)	24(1)
Cl(8)	9624(1)	-616(1)	1308(1)	26(1)
Cl(9)	12002(1)	667(1)	589(1)	22(1)
Cl(10)	3486(1)	8017(1)	2357(1)	19(1)
Cl(11)	6024(1)	7392(1)	2151(1)	21(1)
Cl(12)	3533(1)	8149(1)	80(1)	16(1)
Cl(13)	6068(1)	7524(1)	366(1)	19(1)
Cl(14)	4567(1)	12132(1)	1289(1)	20(1)
Cl(15)	6950(1)	10890(1)	1345(1)	23(1)
Cl(16)	3898(1)	5034(1)	1907(1)	21(1)
Cl(17)	1675(1)	6746(1)	1178(1)	20(1)
Cl(18)	3868(1)	5118(1)	448(1)	20(1)
P(1)	9771(1)	3116(1)	1851(1)	15(1)
P(2)	9743(1)	3021(1)	669(1)	14(1)
P(3)	8312(1)	4629(1)	1218(1)	16(1)
P(4)	4706(1)	8334(1)	1835(1)	13(1)

P(5)	4740(1)	8418(1)	654(1)	12(1)
P(6)	5292(1)	10492(1)	1289(1)	13(1)
N(1)	10084(2)	2379(3)	1274(1)	14(1)
N(2)	8751(3)	3986(3)	673(1)	21(1)
N(3)	8793(3)	4084(3)	1792(1)	27(1)
N(4)	4340(2)	7715(2)	1228(1)	13(1)
N(5)	5017(2)	9831(3)	711(1)	15(1)
N(6)	4970(3)	9752(3)	1829(1)	18(1)

Table 3. Bond lengths [Å] and angles [°] for $[\text{N}(\text{PCl}_2)_3] \cdot \text{GaCl}_3$.

Ga(1)-N(4)	2.048(3)
Ga(1)-Cl(17)	2.1444(9)
Ga(1)-Cl(18)	2.1473(9)
Ga(1)-Cl(16)	2.1492(9)
Ga(2)-N(1)	2.049(3)
Ga(2)-Cl(7)	2.1425(10)
Ga(2)-Cl(8)	2.1451(10)
Ga(2)-Cl(9)	2.1505(10)
Cl(1)-P(1)	1.9658(13)
Cl(2)-P(1)	1.9744(13)
Cl(3)-P(2)	1.9618(12)
Cl(4)-P(2)	1.9741(13)
Cl(5)-P(3)	1.9733(13)
Cl(6)-P(3)	1.9795(13)
Cl(10)-P(4)	1.9631(13)
Cl(11)-P(4)	1.9811(12)
Cl(12)-P(5)	1.9601(12)
Cl(13)-P(5)	1.9803(12)
Cl(14)-P(6)	1.9660(12)
Cl(15)-P(6)	1.9963(13)
P(1)-N(3)	1.558(3)
P(1)-N(1)	1.644(3)
P(2)-N(2)	1.565(3)
P(2)-N(1)	1.640(3)

P(3)-N(2)	1.576(3)
P(3)-N(3)	1.578(3)
P(4)-N(6)	1.563(3)
P(4)-N(4)	1.641(3)
P(5)-N(5)	1.566(3)
P(5)-N(4)	1.648(3)
P(6)-N(6)	1.574(3)
P(6)-N(5)	1.577(3)

N(4)-Ga(1)-Cl(17)	103.93(8)
N(4)-Ga(1)-Cl(18)	108.28(8)
Cl(17)-Ga(1)-Cl(18)	114.94(4)
N(4)-Ga(1)-Cl(16)	106.73(8)
Cl(17)-Ga(1)-Cl(16)	114.06(4)
Cl(18)-Ga(1)-Cl(16)	108.36(4)
N(1)-Ga(2)-Cl(7)	107.04(8)
N(1)-Ga(2)-Cl(8)	102.95(9)
Cl(7)-Ga(2)-Cl(8)	114.52(4)
N(1)-Ga(2)-Cl(9)	107.27(8)
Cl(7)-Ga(2)-Cl(9)	109.98(4)
Cl(8)-Ga(2)-Cl(9)	114.33(4)
N(3)-P(1)-N(1)	115.81(16)
N(3)-P(1)-Cl(1)	108.60(14)
N(1)-P(1)-Cl(1)	108.23(11)
N(3)-P(1)-Cl(2)	111.11(15)
N(1)-P(1)-Cl(2)	107.82(12)
Cl(1)-P(1)-Cl(2)	104.65(6)
N(2)-P(2)-N(1)	115.81(16)
N(2)-P(2)-Cl(3)	109.44(13)
N(1)-P(2)-Cl(3)	107.42(11)
N(2)-P(2)-Cl(4)	110.07(13)
N(1)-P(2)-Cl(4)	108.44(11)
Cl(3)-P(2)-Cl(4)	105.09(6)
N(2)-P(3)-N(3)	115.75(16)
N(2)-P(3)-Cl(5)	108.93(13)

N(3)-P(3)-Cl(5)	109.10(14)
N(2)-P(3)-Cl(6)	110.03(13)
N(3)-P(3)-Cl(6)	109.28(14)
Cl(5)-P(3)-Cl(6)	102.98(6)
N(6)-P(4)-N(4)	115.86(15)
N(6)-P(4)-Cl(10)	109.10(12)
N(4)-P(4)-Cl(10)	108.33(11)
N(6)-P(4)-Cl(11)	110.77(13)
N(4)-P(4)-Cl(11)	107.76(11)
Cl(10)-P(4)-Cl(11)	104.38(6)
N(5)-P(5)-N(4)	116.24(15)
N(5)-P(5)-Cl(12)	110.36(12)
N(4)-P(5)-Cl(12)	106.95(11)
N(5)-P(5)-Cl(13)	109.94(12)
N(4)-P(5)-Cl(13)	108.39(11)
Cl(12)-P(5)-Cl(13)	104.23(5)
N(6)-P(6)-N(5)	116.03(15)
N(6)-P(6)-Cl(14)	109.87(12)
N(5)-P(6)-Cl(14)	109.40(12)
N(6)-P(6)-Cl(15)	108.45(13)
N(5)-P(6)-Cl(15)	109.09(12)
Cl(14)-P(6)-Cl(15)	103.22(5)
P(2)-N(1)-P(1)	118.60(17)
P(2)-N(1)-Ga(2)	120.62(16)
P(1)-N(1)-Ga(2)	120.70(16)
P(2)-N(2)-P(3)	124.3(2)
P(1)-N(3)-P(3)	124.8(2)
P(4)-N(4)-P(5)	118.20(17)
P(4)-N(4)-Ga(1)	120.84(16)
P(5)-N(4)-Ga(1)	120.96(15)
P(5)-N(5)-P(6)	123.52(18)
P(4)-N(6)-P(6)	124.01(19)

Symmetry transformations used to generate equivalent atoms:

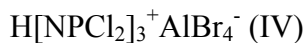
Table 4. Anisotropic displacement parameters ($\text{\AA}^2 \times 10^3$) for $\text{C}^{19}\text{GaN}_3\text{P}_3$. The anisotropic displacement factor exponent takes the form: $-2\pi^2 [h^2 a^{*2} U^{11} + \dots + 2 h k a^* b^* U^{12}]$

	U11	U22	U33	U23	U13	U12
Ga(1)	13(1)	9(1)	15(1)	1(1)	1(1)	0(1)
Ga(2)	13(1)	9(1)	21(1)	-1(1)	0(1)	2(1)
Cl(1)	25(1)	22(1)	19(1)	6(1)	6(1)	2(1)
Cl(2)	33(1)	18(1)	26(1)	-6(1)	-3(1)	-7(1)
Cl(3)	22(1)	20(1)	20(1)	-7(1)	-5(1)	3(1)
Cl(4)	26(1)	22(1)	25(1)	2(1)	8(1)	-7(1)
Cl(5)	17(1)	18(1)	54(1)	5(1)	6(1)	0(1)
Cl(6)	21(1)	12(1)	46(1)	-1(1)	1(1)	0(1)
Cl(7)	24(1)	24(1)	25(1)	4(1)	-6(1)	6(1)
Cl(8)	21(1)	11(1)	46(1)	-3(1)	5(1)	-3(1)
Cl(9)	17(1)	23(1)	27(1)	-8(1)	4(1)	2(1)
Cl(10)	23(1)	17(1)	17(1)	2(1)	6(1)	1(1)
Cl(11)	21(1)	20(1)	22(1)	-1(1)	-7(1)	5(1)
Cl(12)	18(1)	16(1)	15(1)	0(1)	-4(1)	-2(1)
Cl(13)	17(1)	18(1)	24(1)	-2(1)	6(1)	3(1)
Cl(14)	22(1)	10(1)	27(1)	-1(1)	1(1)	0(1)
Cl(15)	15(1)	26(1)	29(1)	-1(1)	-3(1)	-4(1)
Cl(16)	26(1)	15(1)	23(1)	7(1)	-4(1)	0(1)
Cl(17)	14(1)	23(1)	23(1)	1(1)	1(1)	3(1)
Cl(18)	23(1)	15(1)	23(1)	-6(1)	5(1)	-2(1)
P(1)	21(1)	11(1)	13(1)	-1(1)	2(1)	4(1)
P(2)	17(1)	11(1)	14(1)	0(1)	1(1)	2(1)
P(3)	17(1)	11(1)	21(1)	2(1)	2(1)	5(1)
P(4)	16(1)	11(1)	12(1)	1(1)	0(1)	1(1)
P(5)	13(1)	9(1)	13(1)	0(1)	0(1)	-1(1)
P(6)	15(1)	10(1)	16(1)	-1(1)	0(1)	-1(1)
N(1)	14(1)	11(1)	15(2)	0(1)	2(1)	4(1)
N(2)	29(2)	18(2)	16(2)	5(1)	-1(1)	12(1)
N(3)	38(2)	26(2)	17(2)	-3(1)	3(2)	19(2)

N(4)	16(1)	9(1)	14(1)	0(1)	0(1)	-2(1)
N(5)	20(2)	9(1)	15(2)	4(1)	1(1)	-4(1)
N(6)	26(2)	12(1)	15(2)	-1(1)	0(1)	-4(1)

APPENDIX J

SUPPLEMENTARY MATERIAL FOR THE X-RAY CRYSTAL STRUCTURE OF

Table 1. Crystal data and structure refinement for H[NPCl₂]₃⁺AlBr₄⁻.

Identification code	AlBr₄Cl₆¹⁵N₃P₃	
Empirical formula	Al Br ₄ Cl ₆ N ₃ P ₃	
Formula weight	697.26	
Temperature	100(2) K	
Wavelength	0.71073 Å	
Crystal system	Triclinic	
Space group	P-1	
Unit cell dimensions	a = 7.6721(9) Å	α = 84.643(2)°.
	b = 9.9263(12) Å	β = 85.055(2)°.
	c = 12.3245(14) Å	γ = 73.178(2)°.
Volume	892.77(18) Å ³	
Z	2	
Density (calculated)	2.583 Mg/m ³	
Absorption coefficient	10.212 mm ⁻¹	
F(000)	642	
Crystal size	0.10 x 0.06 x 0.03 mm ³	
Theta range for data collection	1.66 to 28.31°.	
Index ranges	-10 ≤ h ≤ 10, -13 ≤ k ≤ 13, -15 ≤ l ≤ 15	
Reflections collected	7915	
Independent reflections	4117 [R(int) = 0.0248]	
Completeness to theta = 28.31°	92.6 %	
Absorption correction	Semi-empirical from equivalents	
Max. and min. transmission	0.7493 and 0.5444	
Refinement method	Full-matrix least-squares on F ²	
Data / restraints / parameters	4117 / 0 / 154	

Goodness-of-fit on F^2	1.035
Final R indices [$I > 2\sigma(I)$]	$R1 = 0.0342$, $wR2 = 0.0702$
R indices (all data)	$R1 = 0.0461$, $wR2 = 0.0736$
Largest diff. peak and hole	0.870 and -0.679 e. \AA^{-3}

Table 2. Atomic coordinates ($\times 10^4$) and equivalent isotropic displacement parameters ($\text{\AA}^2 \times 10^3$) for $\text{H}[\text{NPCl}_2]_3^+ \text{AlBr}_4^-$. $U(\text{eq})$ is defined as one third of the trace of the orthogonalized U^{ij} tensor.

	x	y	z	$U(\text{eq})$
Br(1)	4731(1)	7444(1)	1621(1)	20(1)
Br(2)	3145(1)	5232(1)	3948(1)	17(1)
Br(3)	54(1)	8753(1)	3041(1)	23(1)
Br(4)	4267(1)	8495(1)	4509(1)	25(1)
Cl(1)	10382(2)	2342(1)	4072(1)	21(1)
Cl(2)	8570(1)	5441(1)	3219(1)	18(1)
Cl(3)	5435(2)	933(1)	2541(1)	22(1)
Cl(4)	4367(1)	3819(1)	1195(1)	22(1)
Cl(5)	11950(2)	709(1)	571(1)	24(1)
Cl(6)	9765(2)	3511(1)	-599(1)	24(1)
P(1)	9085(1)	3487(1)	2847(1)	14(1)
P(2)	6456(1)	2419(1)	1855(1)	14(1)
P(3)	9839(1)	2359(1)	804(1)	14(1)
Al	3049(2)	7509(1)	3260(1)	16(1)
N(1)	7065(5)	3177(4)	2848(3)	20(1)
N(2)	8064(5)	1848(4)	1008(3)	17(1)
N(3)	10191(5)	3234(4)	1731(3)	17(1)

Table 3. Bond lengths [\AA] and angles [$^\circ$] for $\text{H}[\text{NP}(\text{Cl}_2)_3]^+ \text{AlBr}_4^-$.

Br(1)-Al	2.2967(13)
Br(2)-Al	2.3212(14)
Br(3)-Al	2.2975(14)
Br(4)-Al	2.2942(13)
Cl(1)-P(1)	1.9610(15)
Cl(2)-P(1)	1.9549(15)
Cl(3)-P(2)	1.9562(15)
Cl(4)-P(2)	1.9710(15)
Cl(5)-P(3)	1.9652(15)
Cl(6)-P(3)	1.9774(15)
P(1)-N(3)	1.554(3)
P(1)-N(1)	1.665(3)
P(2)-N(2)	1.554(3)
P(2)-N(1)	1.661(4)
P(3)-N(2)	1.579(3)
P(3)-N(3)	1.583(3)
N(3)-P(1)-N(1)	112.25(18)
N(3)-P(1)-Cl(2)	111.79(14)
N(1)-P(1)-Cl(2)	105.91(14)
N(3)-P(1)-Cl(1)	113.12(15)
N(1)-P(1)-Cl(1)	108.08(14)
Cl(2)-P(1)-Cl(1)	105.18(6)
N(2)-P(2)-N(1)	112.46(18)
N(2)-P(2)-Cl(3)	112.28(14)
N(1)-P(2)-Cl(3)	107.33(14)
N(2)-P(2)-Cl(4)	112.89(14)
N(1)-P(2)-Cl(4)	107.05(14)
Cl(3)-P(2)-Cl(4)	104.31(7)
N(2)-P(3)-N(3)	115.26(18)
N(2)-P(3)-Cl(5)	108.73(14)
N(3)-P(3)-Cl(5)	110.30(14)
N(2)-P(3)-Cl(6)	110.01(14)

N(3)-P(3)-Cl(6)	108.35(14)
Cl(5)-P(3)-Cl(6)	103.54(7)
Br(4)-Al-Br(1)	110.01(5)
Br(4)-Al-Br(3)	110.48(5)
Br(1)-Al-Br(3)	110.62(5)
Br(4)-Al-Br(2)	107.44(5)
Br(1)-Al-Br(2)	109.91(5)
Br(3)-Al-Br(2)	108.30(5)
P(2)-N(1)-P(1)	123.6(2)
P(2)-N(2)-P(3)	125.6(2)
P(1)-N(3)-P(3)	126.2(2)

Symmetry transformations used to generate equivalent atoms:

Table 4. Anisotropic displacement parameters ($\text{\AA}^2 \times 10^3$) for $\text{H}[\text{NPCl}_2]_3^+ \text{AlBr}_4^-$. The anisotropic displacement factor exponent takes the form: $-2\pi^2 [h^2 a^{*2} U^{11} + \dots + 2 h k a^* b^* U^{12}]$

	U11	U22	U33	U23	U13	U12
Br(1)	20(1)	22(1)	16(1)	1(1)	2(1)	-2(1)
Br(2)	15(1)	15(1)	19(1)	0(1)	1(1)	-3(1)
Br(3)	18(1)	21(1)	23(1)	1(1)	-1(1)	2(1)
Br(4)	37(1)	27(1)	18(1)	-1(1)	-5(1)	-19(1)
Cl(1)	23(1)	21(1)	18(1)	3(1)	-4(1)	-4(1)
Cl(2)	20(1)	16(1)	19(1)	-3(1)	-2(1)	-5(1)
Cl(3)	22(1)	23(1)	25(1)	4(1)	-1(1)	-13(1)
Cl(4)	18(1)	22(1)	22(1)	0(1)	-3(1)	-2(1)
Cl(5)	18(1)	19(1)	33(1)	-5(1)	3(1)	0(1)
Cl(6)	32(1)	26(1)	15(1)	3(1)	0(1)	-10(1)
P(1)	13(1)	18(1)	13(1)	-2(1)	0(1)	-7(1)
P(2)	13(1)	17(1)	14(1)	-1(1)	-1(1)	-6(1)
P(3)	14(1)	16(1)	13(1)	-1(1)	1(1)	-4(1)
Al	17(1)	15(1)	14(1)	-1(1)	-2(1)	-3(1)
N(1)	15(2)	32(2)	18(2)	-7(2)	2(2)	-14(2)

N(2)	15(2)	20(2)	15(2)	-6(2)	0(1)	-6(2)
N(3)	14(2)	23(2)	17(2)	-5(2)	4(1)	-10(2)

APPENDIX K

SUPPLEMENTARY MATERIAL FOR THE X-RAY CRYSTAL STRUCTURE OF

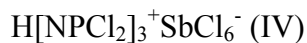


Table 1. Crystal data and structure refinement for $\text{H}[\text{NPCl}_2]_3^+\text{SbCl}_6^-$.

Identification code	Cl₁₂N₃P₃Sb	
Empirical formula	Cl ₁₂ N ₃ P ₃ Sb	
Formula weight	682.09	
Temperature	100(2) K	
Wavelength	0.71073 Å	
Crystal system	Orthorhombic	
Space group	Pna2(1)	
Unit cell dimensions	a = 16.0656(17) Å	α = 90°.
	b = 10.0854(11) Å	β = 90°.
	c = 11.7766(12) Å	γ = 90°.
Volume	1908.1(3) Å ³	
Z	4	
Density (calculated)	2.374 Mg/m ³	
Absorption coefficient	3.363 mm ⁻¹	
F(000)	1284	
Crystal size	0.14 x 0.10 x 0.08 mm ³	
Theta range for data collection	2.38 to 28.27°.	
Index ranges	-21 ≤ h ≤ 21, -12 ≤ k ≤ 13, -15 ≤ l ≤ 15	
Reflections collected	16343	
Independent reflections	4572 [R(int) = 0.0623]	
Completeness to theta = 28.27°	98.6 %	
Absorption correction	Semi-empirical from equivalents	
Max. and min. transmission	0.7747 and 0.6503	
Refinement method	Full-matrix least-squares on F ²	
Data / restraints / parameters	4572 / 1 / 172	

Goodness-of-fit on F^2	1.039
Final R indices [$I > 2\sigma(I)$]	$R1 = 0.0412$, $wR2 = 0.0802$
R indices (all data)	$R1 = 0.0491$, $wR2 = 0.0824$
Absolute structure parameter	0.51(2)
Largest diff. peak and hole	0.644 and -0.708 e. \AA^{-3}

Table 2. Atomic coordinates ($\times 10^4$) and equivalent isotropic displacement parameters ($\text{\AA}^2 \times 10^3$) for $\text{H}[\text{NPCl}_2]_3^+\text{SbCl}_6^-$. $U(\text{eq})$ is defined as one third of the trace of the orthogonalized U^{ij} tensor.

	x	y	z	$U(\text{eq})$
Sb(1)	632(1)	3053(1)	3772(1)	14(1)
Cl(1)	7405(1)	-183(2)	10976(1)	23(1)
Cl(2)	8798(1)	1914(2)	11174(1)	26(1)
Cl(3)	7335(1)	190(2)	6895(2)	27(1)
Cl(4)	8800(1)	2195(2)	6908(2)	23(1)
Cl(5)	5593(1)	2324(2)	9021(1)	26(1)
Cl(6)	6537(1)	5001(1)	9247(1)	22(1)
Cl(7)	479(1)	3993(2)	1963(1)	22(1)
Cl(8)	363(1)	901(2)	2977(2)	26(1)
Cl(9)	-809(1)	3365(2)	4082(1)	22(1)
Cl(10)	959(1)	5147(2)	4549(2)	28(1)
Cl(11)	2063(1)	2626(2)	3477(1)	22(1)
Cl(12)	736(1)	2052(2)	5583(2)	37(1)
P(1)	7823(1)	1431(2)	10267(1)	12(1)
P(2)	7822(1)	1638(2)	7780(1)	14(1)
P(3)	6724(1)	3087(1)	9115(1)	13(1)
N(1)	8167(3)	998(5)	8994(4)	15(1)
N(2)	7208(3)	2791(5)	7963(4)	17(1)
N(3)	7177(3)	2572(5)	10226(4)	16(1)

Table 3. Bond lengths [\AA] and angles [$^\circ$] for $\text{H}[\text{N}(\text{P}(\text{Cl}_2)_3]^+\text{SbCl}_6^-$.

Sb(1)-Cl(7)	2.3445(17)
Sb(1)-Cl(10)	2.3609(17)
Sb(1)-Cl(11)	2.3645(14)
Sb(1)-Cl(9)	2.3646(15)
Sb(1)-Cl(12)	2.3652(18)
Sb(1)-Cl(8)	2.4030(17)
Cl(1)-P(1)	1.949(2)
Cl(2)-P(1)	1.958(2)
Cl(3)-P(2)	1.956(2)
Cl(4)-P(2)	1.960(2)
Cl(5)-P(3)	1.976(2)
Cl(6)-P(3)	1.959(2)
P(1)-N(3)	1.549(5)
P(1)-N(1)	1.656(5)
P(2)-N(2)	1.540(5)
P(2)-N(1)	1.664(5)
P(3)-N(3)	1.585(5)
P(3)-N(2)	1.592(5)
Cl(7)-Sb(1)-Cl(10)	90.79(6)
Cl(7)-Sb(1)-Cl(11)	92.39(6)
Cl(10)-Sb(1)-Cl(11)	90.17(6)
Cl(7)-Sb(1)-Cl(9)	89.11(5)
Cl(10)-Sb(1)-Cl(9)	92.25(6)
Cl(11)-Sb(1)-Cl(9)	177.14(6)
Cl(7)-Sb(1)-Cl(12)	177.66(7)
Cl(10)-Sb(1)-Cl(12)	90.94(7)
Cl(11)-Sb(1)-Cl(12)	89.18(6)
Cl(9)-Sb(1)-Cl(12)	89.25(6)
Cl(7)-Sb(1)-Cl(8)	89.57(6)
Cl(10)-Sb(1)-Cl(8)	177.46(6)
Cl(11)-Sb(1)-Cl(8)	87.30(6)
Cl(9)-Sb(1)-Cl(8)	90.27(6)

Cl(12)-Sb(1)-Cl(8)	88.76(7)
N(3)-P(1)-N(1)	113.0(3)
N(3)-P(1)-Cl(1)	113.8(2)
N(1)-P(1)-Cl(1)	106.43(19)
N(3)-P(1)-Cl(2)	111.6(2)
N(1)-P(1)-Cl(2)	106.98(19)
Cl(1)-P(1)-Cl(2)	104.43(10)
N(2)-P(2)-N(1)	112.7(3)
N(2)-P(2)-Cl(3)	112.5(2)
N(1)-P(2)-Cl(3)	107.56(19)
N(2)-P(2)-Cl(4)	111.7(2)
N(1)-P(2)-Cl(4)	107.11(19)
Cl(3)-P(2)-Cl(4)	104.80(11)
N(3)-P(3)-N(2)	114.7(3)
N(3)-P(3)-Cl(6)	109.1(2)
N(2)-P(3)-Cl(6)	109.1(2)
N(3)-P(3)-Cl(5)	109.9(2)
N(2)-P(3)-Cl(5)	109.1(2)
Cl(6)-P(3)-Cl(5)	104.32(10)
P(1)-N(1)-P(2)	124.3(3)
P(2)-N(2)-P(3)	125.0(3)
P(1)-N(3)-P(3)	125.2(3)

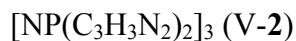
Symmetry transformations used to generate equivalent atoms:

Table 4. Anisotropic displacement parameters ($\text{\AA}^2 \times 10^3$) for $\text{H}[\text{NP}(\text{Cl}_2)_3]^+\text{SbCl}_6^-$. The anisotropic displacement factor exponent takes the form: $-2\pi^2 [h^2 a^{*2} U^{11} + \dots + 2 h k a^* b^* U^{12}]$

	U11	U22	U33	U23	U13	U12
Sb(1)	10(1)	16(1)	16(1)	1(1)	0(1)	2(1)
Cl(1)	24(1)	15(1)	29(1)	8(1)	10(1)	4(1)
Cl(2)	18(1)	36(1)	24(1)	-5(1)	-8(1)	-1(1)
Cl(3)	36(1)	24(1)	21(1)	-5(1)	-5(1)	-2(1)
Cl(4)	21(1)	26(1)	22(1)	7(1)	10(1)	4(1)
Cl(5)	17(1)	31(1)	30(1)	3(1)	-2(1)	-7(1)
Cl(6)	28(1)	10(1)	28(1)	1(1)	-3(1)	5(1)
Cl(7)	19(1)	31(1)	17(1)	5(1)	0(1)	-4(1)
Cl(8)	15(1)	16(1)	48(1)	-5(1)	-9(1)	1(1)
Cl(9)	14(1)	29(1)	23(1)	7(1)	2(1)	5(1)
Cl(10)	24(1)	26(1)	34(1)	-13(1)	-10(1)	8(1)
Cl(11)	9(1)	23(1)	32(1)	-6(1)	1(1)	1(1)
Cl(12)	26(1)	59(1)	27(1)	21(1)	0(1)	11(1)
P(1)	13(1)	13(1)	12(1)	2(1)	-1(1)	1(1)
P(2)	15(1)	14(1)	12(1)	2(1)	2(1)	2(1)
P(3)	12(1)	12(1)	15(1)	3(1)	-1(1)	2(1)
N(1)	19(2)	20(2)	8(3)	4(2)	-3(2)	7(2)
N(2)	19(3)	19(3)	11(3)	7(2)	0(2)	3(2)
N(3)	16(3)	14(3)	16(3)	3(2)	4(2)	2(2)

APPENDIX L

SUPPLEMENTARY MATERIAL FOR THE X-RAY CRYSTAL STRUCTURE OF

Table 1. Crystal data and structure refinement for **2**.

Identification code	[NP(C ₃ H ₃ N ₂) ₂] ₃ · CH ₂ Cl ₂	
Empirical formula	C ₁₉ H ₂₀ Cl ₂ N ₁₅ P ₃	
Formula weight	622.31	
Temperature	100(2) K	
Wavelength	0.71073 Å	
Crystal system	Orthorhombic	
Space group	P2(1)2(1)2(1)	
Unit cell dimensions	a = 9.5339(8) Å	α = 90°.
	b = 15.6322(13) Å	β = 90°.
	c = 17.8162(15) Å	γ = 90°.
Volume	2655.3(4) Å ³	
Z	4	
Density (calculated)	1.557 Mg/m ³	
Absorption coefficient	0.469 mm ⁻¹	
F(000)	1272	
Crystal size	0.45 x 0.27 x 0.14 mm ³	
Theta range for data collection	1.73 to 28.33°.	
Index ranges	-12 ≤ h ≤ 12, -20 ≤ k ≤ 20, -22 ≤ l ≤ 23	
Reflections collected	23412	
Independent reflections	6293 [R(int) = 0.0338]	
Completeness to theta = 28.33°	97.4 %	
Absorption correction	Semi-empirical from equivalents	
Max. and min. transmission	0.9373 and 0.8168	
Refinement method	Full-matrix least-squares on F ²	
Data / restraints / parameters	6293 / 0 / 353	

Goodness-of-fit on F^2	1.071
Final R indices [$I > 2\sigma(I)$]	$R1 = 0.0326$, $wR2 = 0.0744$
R indices (all data)	$R1 = 0.0349$, $wR2 = 0.0755$
Absolute structure parameter	0.04(5)
Largest diff. peak and hole	0.425 and -0.268 e.Å ⁻³

Table 2. Atomic coordinates ($\times 10^4$) and equivalent isotropic displacement parameters ($\text{Å}^2 \times 10^3$) for **2**. $U(\text{eq})$ is defined as one third of the trace of the orthogonalized U^{ij} tensor.

	x	y	z	$U(\text{eq})$
Cl(1)	8946(1)	5579(1)	332(1)	40(1)
Cl(2)	10477(1)	5073(1)	1674(1)	39(1)
P(1)	7589(1)	-853(1)	1043(1)	9(1)
P(2)	9607(1)	289(1)	630(1)	9(1)
P(3)	7109(1)	859(1)	1223(1)	9(1)
N(1)	8949(2)	-639(1)	569(1)	11(1)
N(2)	8625(2)	1045(1)	903(1)	11(1)
N(3)	6554(2)	-96(1)	1242(1)	11(1)
N(4)	6784(2)	-1645(1)	582(1)	11(1)
N(5)	6113(2)	-2489(1)	-360(1)	19(1)
N(6)	8031(2)	-1337(1)	1859(1)	11(1)
N(7)	9106(2)	-2226(1)	2642(1)	20(1)
N(8)	10296(2)	506(1)	-215(1)	11(1)
N(9)	10406(2)	602(1)	-1461(1)	19(1)
N(10)	11019(2)	256(1)	1191(1)	11(1)
N(11)	12581(2)	609(1)	2063(1)	21(1)
N(12)	5981(2)	1489(1)	756(1)	11(1)
N(13)	4009(2)	2184(1)	481(1)	22(1)
N(14)	6999(2)	1266(1)	2093(1)	11(1)
N(15)	6226(2)	1519(1)	3245(1)	17(1)
C(1)	6836(2)	-1812(1)	-179(1)	16(1)
C(2)	5941(2)	-2283(1)	887(1)	18(1)
C(3)	5549(2)	-2782(1)	308(1)	20(1)

C(4)	9139(2)	-1881(1)	1977(1)	15(1)
C(5)	7220(2)	-1367(1)	2512(1)	14(1)
C(6)	7890(2)	-1912(1)	2975(1)	16(1)
C(7)	9747(2)	259(1)	-896(1)	18(1)
C(8)	11389(2)	1064(1)	-384(1)	16(1)
C(9)	11441(2)	1105(1)	-1140(1)	18(1)
C(10)	11457(2)	854(1)	1711(1)	16(1)
C(11)	11969(2)	-419(1)	1241(1)	16(1)
C(12)	12900(2)	-187(1)	1770(1)	20(1)
C(13)	4741(2)	1833(1)	1012(1)	18(1)
C(14)	5981(2)	1635(1)	-16(1)	18(1)
C(15)	4788(2)	2058(1)	-167(1)	20(1)
C(16)	6116(2)	1015(1)	2667(1)	14(1)
C(17)	7690(2)	1994(1)	2346(1)	14(1)
C(18)	7207(2)	2129(1)	3047(1)	16(1)
C(19)	9148(3)	5742(2)	1304(1)	33(1)

Table 3. Bond lengths [\AA] and angles [$^\circ$] for **2**.

Cl(1)-C(19)	1.760(3)
Cl(2)-C(19)	1.771(3)
P(1)-N(3)	1.5818(17)
P(1)-N(1)	1.5828(16)
P(1)-N(4)	1.6719(16)
P(1)-N(6)	1.6926(17)
P(2)-N(1)	1.5842(16)
P(2)-N(2)	1.5844(16)
P(2)-N(10)	1.6765(16)
P(2)-N(8)	1.6779(16)
P(3)-N(2)	1.5815(17)
P(3)-N(3)	1.5845(16)
P(3)-N(14)	1.6775(16)
P(3)-N(12)	1.6794(17)
N(4)-C(1)	1.382(2)

N(4)-C(2)	1.391(3)
N(5)-C(1)	1.303(3)
N(5)-C(3)	1.383(3)
N(6)-C(4)	1.372(3)
N(6)-C(5)	1.397(2)
N(7)-C(4)	1.303(3)
N(7)-C(6)	1.392(3)
N(8)-C(7)	1.377(2)
N(8)-C(8)	1.391(3)
N(9)-C(7)	1.302(3)
N(9)-C(9)	1.384(3)
N(10)-C(10)	1.382(3)
N(10)-C(11)	1.393(2)
N(11)-C(10)	1.299(3)
N(11)-C(12)	1.383(3)
N(12)-C(13)	1.376(3)
N(12)-C(14)	1.394(2)
N(13)-C(13)	1.298(3)
N(13)-C(15)	1.387(3)
N(14)-C(16)	1.382(2)
N(14)-C(17)	1.391(2)
N(15)-C(16)	1.301(3)
N(15)-C(18)	1.382(3)
C(2)-C(3)	1.347(3)
C(5)-C(6)	1.348(3)
C(8)-C(9)	1.349(3)
C(11)-C(12)	1.345(3)
C(14)-C(15)	1.343(3)
C(17)-C(18)	1.347(3)
N(3)-P(1)-N(1)	118.21(9)
N(3)-P(1)-N(4)	112.19(9)
N(1)-P(1)-N(4)	105.70(8)
N(3)-P(1)-N(6)	107.28(9)
N(1)-P(1)-N(6)	110.40(9)

N(4)-P(1)-N(6)	101.87(8)
N(1)-P(2)-N(2)	118.04(9)
N(1)-P(2)-N(10)	109.33(8)
N(2)-P(2)-N(10)	108.34(8)
N(1)-P(2)-N(8)	106.19(8)
N(2)-P(2)-N(8)	110.82(8)
N(10)-P(2)-N(8)	103.09(8)
N(2)-P(3)-N(3)	119.10(9)
N(2)-P(3)-N(14)	108.71(9)
N(3)-P(3)-N(14)	108.44(8)
N(2)-P(3)-N(12)	107.37(9)
N(3)-P(3)-N(12)	110.46(9)
N(14)-P(3)-N(12)	101.27(8)
P(1)-N(1)-P(2)	118.79(10)
P(3)-N(2)-P(2)	120.91(10)
P(1)-N(3)-P(3)	119.46(10)
C(1)-N(4)-C(2)	105.55(16)
C(1)-N(4)-P(1)	127.27(14)
C(2)-N(4)-P(1)	127.17(14)
C(1)-N(5)-C(3)	105.18(17)
C(4)-N(6)-C(5)	106.21(16)
C(4)-N(6)-P(1)	126.84(14)
C(5)-N(6)-P(1)	126.27(14)
C(4)-N(7)-C(6)	105.17(17)
C(7)-N(8)-C(8)	105.66(16)
C(7)-N(8)-P(2)	125.83(14)
C(8)-N(8)-P(2)	127.89(14)
C(7)-N(9)-C(9)	105.03(17)
C(10)-N(10)-C(11)	105.81(16)
C(10)-N(10)-P(2)	128.46(14)
C(11)-N(10)-P(2)	125.68(14)
C(10)-N(11)-C(12)	105.38(18)
C(13)-N(12)-C(14)	105.32(17)
C(13)-N(12)-P(3)	127.90(14)
C(14)-N(12)-P(3)	125.77(14)

C(13)-N(13)-C(15)	105.00(19)
C(16)-N(14)-C(17)	106.22(16)
C(16)-N(14)-P(3)	127.95(14)
C(17)-N(14)-P(3)	125.50(14)
C(16)-N(15)-C(18)	105.61(17)
N(5)-C(1)-N(4)	112.16(18)
C(3)-C(2)-N(4)	106.06(17)
C(2)-C(3)-N(5)	111.05(19)
N(7)-C(4)-N(6)	112.12(18)
C(6)-C(5)-N(6)	105.55(18)
C(5)-C(6)-N(7)	110.92(18)
N(9)-C(7)-N(8)	112.42(18)
C(9)-C(8)-N(8)	105.87(18)
C(8)-C(9)-N(9)	111.02(18)
N(11)-C(10)-N(10)	111.92(19)
C(12)-C(11)-N(10)	105.68(18)
C(11)-C(12)-N(11)	111.20(19)
N(13)-C(13)-N(12)	112.63(19)
C(15)-C(14)-N(12)	106.10(19)
C(14)-C(15)-N(13)	110.94(19)
N(15)-C(16)-N(14)	111.50(18)
C(18)-C(17)-N(14)	105.52(18)
C(17)-C(18)-N(15)	111.14(18)
Cl(1)-C(19)-Cl(2)	111.03(14)

Symmetry transformations used to generate equivalent atoms:

Table 4. Anisotropic displacement parameters ($\text{\AA}^2 \times 10^3$) for **2**. The anisotropic displacement factor exponent takes the form: $-2\pi^2 [h^2 a^{*2} U^{11} + \dots + 2 h k a^* b^* U^{12}]$

	U11	U22	U33	U23	U13	U12
Cl(1)	44(1)	51(1)	25(1)	7(1)	-7(1)	-17(1)
Cl(2)	42(1)	40(1)	37(1)	0(1)	-9(1)	12(1)
P(1)	10(1)	9(1)	8(1)	-1(1)	1(1)	-1(1)
P(2)	9(1)	9(1)	8(1)	0(1)	1(1)	-1(1)
P(3)	9(1)	9(1)	8(1)	0(1)	0(1)	1(1)
N(1)	12(1)	10(1)	11(1)	-1(1)	1(1)	0(1)
N(2)	11(1)	10(1)	11(1)	0(1)	1(1)	0(1)
N(3)	11(1)	11(1)	12(1)	0(1)	1(1)	-2(1)
N(4)	13(1)	11(1)	10(1)	-2(1)	2(1)	-3(1)
N(5)	22(1)	20(1)	15(1)	-4(1)	2(1)	-7(1)
N(6)	11(1)	10(1)	11(1)	1(1)	0(1)	-1(1)
N(7)	19(1)	20(1)	21(1)	6(1)	1(1)	2(1)
N(8)	11(1)	12(1)	8(1)	0(1)	1(1)	-2(1)
N(9)	21(1)	25(1)	12(1)	2(1)	1(1)	-3(1)
N(10)	11(1)	13(1)	10(1)	-1(1)	-1(1)	0(1)
N(11)	19(1)	25(1)	18(1)	-2(1)	-6(1)	-2(1)
N(12)	11(1)	12(1)	11(1)	2(1)	-1(1)	1(1)
N(13)	16(1)	26(1)	24(1)	7(1)	-3(1)	3(1)
N(14)	12(1)	12(1)	10(1)	-1(1)	0(1)	1(1)
N(15)	22(1)	18(1)	13(1)	-2(1)	2(1)	-1(1)
C(1)	19(1)	19(1)	10(1)	-1(1)	3(1)	-4(1)
C(2)	22(1)	19(1)	13(1)	1(1)	6(1)	-10(1)
C(3)	24(1)	21(1)	17(1)	-4(1)	3(1)	-10(1)
C(4)	15(1)	13(1)	18(1)	3(1)	3(1)	3(1)
C(5)	14(1)	16(1)	11(1)	-1(1)	3(1)	0(1)
C(6)	18(1)	17(1)	12(1)	2(1)	2(1)	-3(1)
C(7)	20(1)	23(1)	11(1)	-2(1)	-2(1)	-7(1)
C(8)	15(1)	18(1)	15(1)	-1(1)	1(1)	-7(1)
C(9)	17(1)	20(1)	17(1)	4(1)	6(1)	-5(1)
C(10)	17(1)	13(1)	17(1)	-3(1)	-1(1)	-4(1)

C(11)	15(1)	15(1)	19(1)	1(1)	1(1)	5(1)
C(12)	15(1)	24(1)	21(1)	2(1)	-4(1)	3(1)
C(13)	13(1)	23(1)	19(1)	4(1)	1(1)	4(1)
C(14)	24(1)	18(1)	12(1)	3(1)	0(1)	3(1)
C(15)	23(1)	19(1)	17(1)	4(1)	-6(1)	-1(1)
C(16)	15(1)	14(1)	11(1)	1(1)	2(1)	-1(1)
C(17)	16(1)	11(1)	15(1)	1(1)	-3(1)	-3(1)
C(18)	22(1)	12(1)	14(1)	-2(1)	-2(1)	1(1)
C(19)	40(2)	36(1)	24(1)	3(1)	0(1)	10(1)

Table 5. Hydrogen coordinates ($\times 10^4$) and isotropic displacement parameters ($\text{\AA}^2 \times 10^3$) for **2**.

	x	y	z	U(eq)
H(1)	7340	-1473	-530	19
H(2)	5692	-2352	1399	21
H(3)	4963	-3271	352	24
H(4)	9848	-1994	1615	18
H(5)	6373	-1066	2608	16
H(6)	7575	-2061	3464	19
H(7)	8973	-120	-948	21
H(8)	11976	1356	-38	19
H(9)	12101	1434	-1416	22
H(10)	10992	1382	1801	19
H(11)	11961	-935	960	20
H(12)	13676	-526	1923	24
H(13)	4452	1815	1522	22
H(14)	6684	1468	-365	21
H(15)	4514	2246	-653	24
H(16)	5506	536	2643	16
H(17)	8360	2326	2081	17

H(18)	7503	2583	3363	19
H(19A)	8249	5620	1561	40
H(19B)	9393	6348	1399	40

APPENDIX M
ABBREVIATIONS AND ACCRONYMS

Å Angstrom	<i>c</i> crystallographic unit cell axis <i>c</i>
Anal. analysis	calcd. Calculated
α crystallographic unit-cell angle between axes <i>b</i> and <i>c</i>	<i>d</i> doublet (NMR spectra) lattice spacing (crystallographic)
β crystallographic unit-cell angle between axes <i>a</i> and <i>c</i>	DMF dimethylformamide DMSO dimethylsulfoxide
γ crystallographic unit-cell angle between axes <i>a</i> and <i>b</i>	ed edition Ed. editor
δ scale (NMR) ppm	ESI electro spray ionization
σ bond referring to bonding between sigma orbitals	et. al. and others <i>F</i> (000) scaling coefficient for structure
π bond referring to bonding between pi orbitals	factors Fc calculated structure factor
<i>a</i> crystallographic unit cell axis <i>a</i>	Fo observed structure factor
anal. Analysis	h hour
<i>b</i> crystallographic unit cell axis <i>b</i>	Hz hertz
C celcius	L general ligand

<i>J</i> nuclear spin-spin coupling	pp pages
constant through bonds	ppm parts per million
m multiplet	q quartet (spectral)
MeCN acetonitrile	R organic group
MeOH methanol	<i>R</i> , <i>R</i> residual based on Fo
min minutes	ROP ring opening polymerization
mL milliliter	RT room temperature
mmol millimole	s singlet (spectrum)
m/z mass-to-charge ratio	sat. saturated
Nap naphthalene	t triplet (spectrum)
<i>n</i> -Bu <i>n</i> -butyl	t _{1/2} half-life
NHC N-heterocyclic carbene	THF tetrahydrofuran
nm nanometer	U temperature factor
NMR nuclear magnetic resonance	unsat. unsaturated
p page	wR ₂ weighted residual based on I
Ph phenyl	